Computational homogenization for multi scale finite element simulation.

Carneiro Molina, Arturo Jose

CIVIL COMPUTATIONAL ENGINEERING CENTER
SCHOOL OF ENGINEERING
UNIVERSITY OF WALES SWANSEA

COMPUTATIONAL HOMOGENIZATION FOR MULTI SCALE FINITE ELEMENT SIMULATION

by

Arturo José Carneiro Molina

Ingeniero Industrial, MRes

Thesis submitted to the University of Wales
in candidature for the degree of Doctor of Philosophy

March 2007

Summary

This work presents a general formulation of small and large strain multiscale solid constitutive models based on the volume averaging of the microscopic strain (deformation gradient under large strain) and stress fields over a locally attached microstructure *Representative Volume Element* (RVE). Both elasto-plastic and hyperelastic behaviour are considered in the modelling of the RVE. A multiscale first-order computational homogenization method for modelling nonlinear deformation processes of evolving multi-phase materials is developed based on the Finite Element discretisation of both macro- and micro-structure. The approach consist of suitably imposing the macroscopic strain on the RVE and then computing the macroscopic stress as the volume average of the microscopic stress field obtained by solving numerically the local (initial) boundary value problem. In this context, the effective (homogenized) tangent modulus is obtained as a function of microstructure stiffness matrix which, in turn, depends upon the material properties and geometrical distribution of the micro-constituents in the RVE. The multiscale material presented here is restricted to two-dimensional problems, however we remark that the extension to three dimensions is trivial. The effectiveness of the proposed strategies is is demonstrated by means of numerical examples.

Acknowledgements

Firstly, I would like to thank to my supervisors *Prof. D. Perić* and *Dr. E. de Souza Neto* for their help and support. I would like to mention my PhD colleagues *M. Partovi* for his continuous discussions and *D. Speirs* for his help in the microanalysis. Also *J.L. Curiel* because we share passion for F.E. and a friendship for a long time. I would also like to thank *A. Gil* who has provided me with whenever needed. Secondly, I thank my family: mama (Manolita), papa (Pepe) and sister (M. Luisa) for their support from very far. They have always been there next to me. I would like to mentioned *Beverley* for her faith on me during this long and hard period of time.

The last moths of my PhD have been very hard. I would like to mention some friend as J.L. Padilla, Maria, Leon, Ricardo and Mauro. They have helped me in during this time in different ways. Also I want to say that someone has appear in my life, Alexandra. She has given me hope for a beautiful future together.

Contents

List of Figures

Chapter 1

Introduction

1.1 Multi-phase heterogeneous materials

The last several decades have seen an enormous developments in science and technology for heterogeneous materials. The heterogeneous nature of materials has a significant impact on the observed macroscopic behaviour of multi-phase materials. The degree of properties modification depends on the size, shape, spatial distribution and properties of micro constituents and their respective interfaces.

Examples of heterogeneous materials are: Alloy systems containing precipitates and pores, and polymer, ceramic or metal matrix composite materials. For instance, in reinforced composites, stiff and strong phase inclusions of glass, graphite, boron, or aluminium oxide, are added to epoxy resin, steel, titanium, or aluminium matrices to enhance strength, thermal expansion coefficient and wear resistance of structures. Also metal foams have received considerable attention in the last decade. The enhanced properties (e.g. a low weight, high energy absorbtion, etc) of these materials are primarily due to their foamed microstructure.

These functionally improved materials have found increasing utilization in aerospace, automotive, and other industries thus replacing some of traditional materials.

Determination of the macroscopic overall characteristic of the heterogeneous media is an essential problem in many engineering applications. The understanding of the relation between microstructural properties and the macroscopic behaviour is essential for the prediction of the performance of existing multi-phase materials. Moreover, it provides a designing tool for a microstructure such that the resulting macroscopic behaviour satisfy desired characteristics.

From economical point of view, performing straight forward experimental measures on a number of material samples of different sizes, for various geometrical and physical phase properties, volume fractions and loading paths is hardly a feasible task. Therefore, there is a clear need for modelling strategies that provide a better understanding of

micro-macro structure property relations in multi-phase heterogeneous materials. The last three decades have seen a development of improved analytical and numerical models for heterogeneous materials.

1.2 Modelling strategies for multi-phase materials

A transition from the microscopic properties to their macroscopic counterparts based on an averaging principles is termed homogenization.

The simplest method leading to homogenized modulus of heterogeneous material is based on the rule of mixture. This approach takes only one microstructural characteristic into consideration: the volume ratio of the heterogeneities.

A more sophisticated method is the effective medium approximation, as established by Eshelby [48] and further developed by Hashin [99], Mori and Tanaka [79] and more recent eg by Nan and Clarke [18]. Equivalent material properties are derived as a result of the analytical (or semi-analytical) solution of a boundary value problem for a spherical or ellipsoidal inclusion of one material in an infinite matrix of another material.

An extension of this method is the self-consistent approach, in which a particle of one phase is embedded into the effective material (the properties which are known a priori). We remark the work based on this method by Hill [73], Aktaa et al [33], González and Llorca [10], Dye et al [38], and Braccini and Wilkinson [61]. These strategies give a reasonable approximation for structures that possess some kind of geometrical regularity, however, they fail to describe the behaviour of clustered or dense micro-structures.

Although some work has been done on the extension of the self-consistent approach to non-linear cases, significantly more progress in estimating advanced properties of composites has been achieved by variational bounding methods (see [100]; [70]). The variational bounding methods are based on suitable variational (minimum energy) principles and provide upper and lower bounds for the overall properties of the composite.

Another approach is based on mathematical Asymptotic Expansion Homogenization (AEH) theory, documented in [49] , [26] and [78]. AEH is a perturbation technique based on the asymptotic series expansion in ε, a scale parameter, of a primary variable such as the displacement. The scale parameter is a ratio between the length scales, represented by the relation between micro heterogeneities size and a measure of macrostructure. It is represented by a very small positive number:

$$\varepsilon = \frac{l}{L} \ll 1 \tag{1.1}$$

see, e.g. [6], [50], [62] and [59]. The asymptotic homogenization technique gives effective overall properties plus local stress and strain values. However, the considerations are restricted to very simple microscopic geometries and simple material models, mostly at

small strains. It has been used by Ghosh et al [51], [52] in conjunction with a Voroni cell FE model.

The unit cell methods represent another way to approach the analysis of multi-phase materials. They appeared due to the complexity of microstructural mechanical and physical behaviour along with the developments of computational techniques. These approaches have been used in a large number of applications, see [1], [75], [80], [87] and [97]. The unit cell methods provide information on the local microstructural fields and effective material properties. These properties are generally determined by fitting the averaged microscopical stress-strain fields, resulting from the analysis of a Representative Volume Cell subjected to a certain loading path, based on a macroscopic closed-form phenomenological constitutive equations in a format established a priori. Within this approach we highlight the work of Moulinec and Suquet [37] using an alternative procedure based on Fourier series which avoids the meshing of complex microstructures by the FEM.

Once the constitutive behaviour becomes nonlinear, it is extremely difficult to make assumption on a suitable macroscopic constitutive format. We refer here to the work of Swan and co workers in [15], [16] and [17].

In conclusion, most of the homogenization techniques, mentioned so far, are not suitable for finite deformation or complex loading paths. They do not account for geometrical and physical changes in the microstructure.

In the FEM context, the use of a single FE capturing all microstructural details in a numerical solution of macroscopic BVP becomes impractical.

An alternative approach for homogenization of multi-phase heterogeneous materials, known as *Multi-Scale Computational Homogenization* or *Micro-Macro Modelling* has been gaining considerable popularity in the computational mechanics circles. Since the basic principles for the micro-macro modelling of heterogeneous materials were introduced (see [71], [50], [55], [51] and [32]), this technique has proved to be the most effective way to deal with arbitrary physically non-linear and time dependent material behaviour at micro-level. In the early development of the micro-macro modelling we emphasize the work od Guedes and Kikuchi [50] and Terada and Kikuchi [55].

A number of recent works deal with various approaches and techniques for the micro-macro simulation of heterogeneous materials. Among these we highlight the contributions by Miehe and coworkers in [42], [43] for analysis of polycrystalline materials and [13] with detailed algorithms for computation of the homogenized stress and overall modulus. A detailed two-scale kinematics linearization is given by Terada et al [57]. We also emphasize the work of Smit et al [94] and [95], and the work of Kouznetsova et al [23], [92], [29], [89], [67]. Furthermore, we mention the work based on an incremental variational formulation of the minimization of energy [81], [13], [11], [44], [12] and [14]. Some work also has been done to study the size of the RVE (Representative Volume Element) by Gusev [7], Terada et al [56], Partovi [63] and Gitman and co-workers [39] [34] [64] and [35].

The multiscale approach has made a great impact on other areas of computational

material modelling. In Pellegrino et al [84], van Rens et al [88] and Partovi [63] a methodology have proposed to compute macro homogenized yield surface evolution from the unit cell analysis. Multiscale analysis of composites has been performed by Carvelli et al [85], [86], and Taliercio et al [5], [3] and [4]. We also refer to work of Feyel [27], Michel et al [36], Bosso et al [83], and Ghosh and coworkers in [76] and [53]. Mejak has applied for imperfect bonding in [30] while Mercatoris and Massart have have used multiscale in [9] to model flexural behaviour of structures.

Multiscale approach has been used in conjuntion with meshfree methodology in [45]. In this context we also refer to Ibrahimbegovic et al [2] and Oñate [69].

The multiscale modelling techniques do not lead to closed-form overall constitutive equations. However, they compute the stress-deformation relationship at every macro point of interest by modelling of the microstructure RVE corresponding to the macroscopic point. The advantages of multiscale techniques are the following:

- They do not require constitutive assumptions on the macrolevel.
- They enable the incorporation of finite deformations and rotations at both micro and macro levels.
- They are suitable for nonlinear material behaviour.
- They provide the possibility to introduce detailed microstructural information, including geometrical and physical evolution, into the macroscopic analysis.
- Although we confine our study to the finite element method, they allow any modelling technique on the micro level.

The main disadvantage of multiscale techniques is a high computational cost. This concern however can be overcome partially by parallel computation (see [54]).

Despite of the high computational effort required, the numerical multiscale homogenization approach seems to be a versatile tool to establish micro-macro property structure relations in materials where the collective behaviour of an evolving multi-phase is not possible to predict by any other method. Furthermore, this micro-macro modelling technique is useful for verifying other homogenization methods or micro-mechanically based macroscopic constitutive models.

The computational multiscale homogenization technique developed in this work is built within a standard local continuum mechanics concept, where the response at macro material point depends only on the first gradient of the displacement field. There are two disadvantages for this approach. Firstly, although these techniques account for the volume fraction, distribution and morphology of the constituents, they can not take into account the effect of the absolute size of the microstructure. It is proven in [90] that this first-order approach gives a valid solution only if the size of the microstructure is much smaller than the size of the macroscale ($l_\mu \ll L_M$). Another difficulty arises from the

uniformity of the macro stress and strain fields. This approach is not appropriate for representing critical regions experiencing high gradients of solutions variables.

To overcome these problems Kouznetsova has developed second-order approach described in [90] (see also Kouznetsova et al [93] and [66]).

1.3 Scope and outline

The aim of this work consists in the development of a multiscale first-order computational F.E. homogenization method for modelling nonlinear deformation processes of evolving multi-phase materials. The approach consist of suitably imposing the macroscopic deformation on a microscopic cell (a *Representative Volume Element* or RVE for short) and then computing the macroscopic stress as the volume average of the microscopic stress field obtained numerically by the Finite Element Method. In this context, the effective (homogenized) tangent modulus is obtained as a function of microstructure stiffness matrix which, in turn, depends upon the material properties and geometrical distribution of the micro-constituents in the RVE. The multiscale material presented here is restricted to two-dimensional problems, however we remark that the extension to three dimensions is trivial.

In Chapter 2 a general description of continuum mechanics is given with the notions and terminology needed in this work. In Chapter 3 the Finite Element method is presented in the context of the nonlinear analysis. Chapter 4 gives the nonlinear material models used in the multiscale analysis considered in this work.

The following Chapters 5, 6, 7 and 8 develop a multiscale first-order approach. Such procedures are particularly attractive in the modelling of heterogeneous materials when the length-scale of heterogeneities is small compared to dimensions of the macroscopic body. Multiscale technique is introduced in Chapter 5 in the context of continuum small strain analysis and the basic principles of multiscale analysis are introduced. This approach follows the deformation-driven microstructure, which, in the case of small strain, means that the macroscopic small strain tensor is prescribed as an average over the microstructure unit cell RVE through the three classical constraints: Taylor constraint, Linear b.c. and Periodic b.c.

In the following Chapter 6 the Multiscale analysis in small strain is discretised by the standard Galerkin Finite Element discretization. Here the two main ingredients of the multiscale FE analysis are presented: The *stress update procedure* and the *overall tangent modulus* computation. Both are presented for the following constraints: a) the Taylor assumption, b) Linear displacement on the boundary condition (or Linear b.c. for short) and finally c) Periodic deformation and antiperiodic traction on the boundary (or Periodic b.c. for short).

Chapter 7 gives more complex multiscale continuum model, suitable for finite-large deformation analysis. For convenience, this chapter has been separated from Chapter 5.

Although the basic ideas are given for the small strain analysis, there are many important differences which are relevant for the large strain analysis.

The FE discretisation for large strain multiscale analysis is explained in Chapter 8. The *stress update procedure* and the *overall tangent modulus* computation are presented for the Taylor assumption, Linear b.c. and Periodic b.c.

To validate the formulations described previously, Chapter 9 gives numerical examples. The numerical tests have been performed for a material with voids. The quadratic rate of convergence obtained by a Newton-type solution method procedure confirms the success of the overall tangent moduli computation for the macroscale and the efficiency of solution procedure to update the stress at the microscale.

The code for computational homogenization has been implemented in an in-house program. This was based in a single scale program called Hyplas with main structure given in [22].

Chapter 2

Continuum mechanics

2.1 Introduction

Continuum mechanics is a building block for nonlinear F.E. analysis. The text by Malvern [60] has become a classic for it provides a lucid and comprehensive description of the field. Other text which has to be highlighted is Gurtin [65]. They have provided an initial and very important basis for this work. Bonet et al [40], Belytschko et al [96] and de Souza et al [22] follow mainly the description of the field orientated to nonlinear Finite Element analysis. They have also been essential in accomplishing this work successfully.

2.2 Outline

This chapter begins with a description of the kinematics (deformation and motion). Next the concepts of strain and stress in nonlinear continuum mechanics are described. The conservation equations, which are also termed balance equations, are derived next. They consist of the conservation of mass momentum and energy. The *equilibrium equation*, considered here as a special case of the momentum equation when the accelerations vanish, is derived in both the *spatial* and *material* domains. Then follows the derivation of the weak form of the equilibrium equation or *principle of virtual work* (PVW) equation. Finally, the Principle of Virtual Work is linearized as a basis for the Newton-Raphson solution method.

2.3 Kinematics: deformation and motion

Kinematics is the study of the motion and deformation without reference to the cause. This section provides Kinematic quantities and their notation that are used throughout this work.

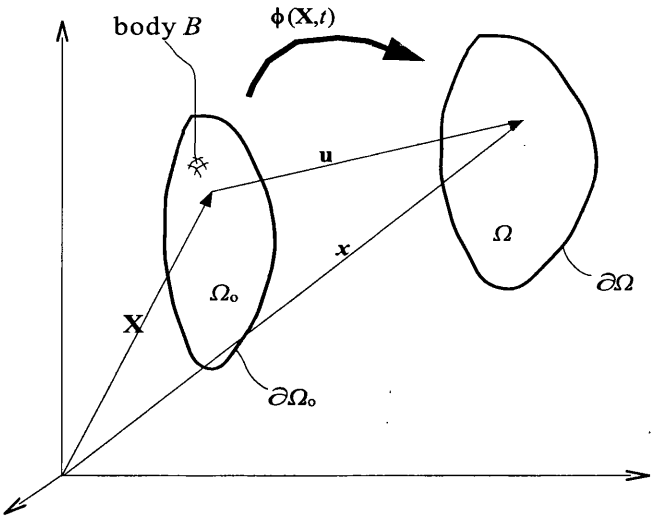

Figure 2.1: Initial (undeformed) and current (deformed) configurations of the body B; motion

2.3.1 Some definitions

Continuum mechanics is generally concerned with models of solids and fluids in which properties and response can be characterized by smooth functions of spatial variables.

Consider the evolution of a body B depicted in Figure 2.1. Initially at time $t = 0$ the body B occupies a region in the space denoted by Ω_0 which is termed the *initial configuration.* In describing the motion and deformation of the body B, a configuration, to which various equations are referred, is needed; it is called the *reference configuration.* In this work it is assumed that a initial configuration is used as reference or material configuration. The significance of the reference configuration lies in the fact that motion is defined with respect to this configuration. An *undeformed configuration* is also needed. Undeformed configuration is assumed to coincide with the initial configuration.

The body B occupies the region $\Omega(t)$ at time t. This domain is called the *current* or *spatial configuration* of the body; this will also be called the *deformed configuration.* The boundary of the domain is denoted by $\partial\Omega(t)$.

Although this work covers multiscale analysis related to two dimensional micro and macro models, for the purpose of general continuum mechanics described in this chapter, the dimension of the model is denoted by n_{sd}. Later in Chapter 3 in the context of finite element analysis the expressions are particularized for the two dimensional problems.

2.3.2 Eulerian and Lagrangian coordinates

The position vector of a material point, in the reference configuration, is given by $\mathbf{X}$,

$$\mathbf{X} = X_i \, \mathbf{e}_i \equiv \sum_{i=1}^{\mathrm{n_{sd}}} X_i \, \mathbf{e}_i \tag{2.1}$$

where X_i are the components of the position vector in the reference configuration and $\mathbf{e}_i$ are the unit base vectors of a Cartesian coordinate system; indicial notation have been used in the second expression of (2.1) and will be used throughout this work. The variable vector $\mathbf{X}$ does not change with time for a given material point; the variables $\mathbf{X}$ are called *material coordinates* or *Lagrangian coordinates* and provide labels for the material points.

The position of the points in the current configuration is given by

$$\boldsymbol{x} = x_i \, \mathbf{e}_i \equiv \sum_{i=1}^{\mathrm{n_{sd}}} x_i \, \mathbf{e}_i \tag{2.2}$$

where x_i are the components of the position vector in the current configuration. The components of the vector $\boldsymbol{x}$ give the spatial position and are denoted *spatial* or *Eulerian coordinates.*

2.3.3 Motion of a deformable body

Figure 2.1 shows the motion of the deformable body B. The *motion* of the body is described by

$$\boldsymbol{x} = \boldsymbol{\phi}(\mathbf{X}, t) \quad \text{or} \quad x_i = \phi_i(\mathbf{X}, t) \tag{2.3}$$

where $\boldsymbol{x}$ is the position of the material point $\mathbf{X}$ at time t. The function $\boldsymbol{\phi}(\mathbf{X}, t)$ defines a mapping between the initial or reference configuration and the current or deformed configuration.

2.3.4 Lagrangian description

Two approaches are used to describe the deformation and response of a continuum: the spatial or Eulerian and material or Lagrangian descriptions. In the Lagrangian approach the independent variables are the material coordinates X_i and time t. In solids mechanics, the stress generally depends on the deformation history, so the undeformed configuration must be specified. Therefore, the Lagrangian description is the most commonly used in the study of solid bodies. This approach has been used in this work.

2.3.5 Displacement, velocity and acceleration in material forms

The displacement of a material point $\mathbf{X}$ is given by the difference between its current configuration and its original position (see Figure 2.1), that is,

$$\mathbf{u}(\mathbf{X},t) \;=\; \boldsymbol{\phi}(\mathbf{X},t) - \boldsymbol{\phi}(\mathbf{X},0) \;=\; \boldsymbol{\phi}(\mathbf{X},t) - \mathbf{X} \;=\; \boldsymbol{x}(\mathbf{X},t) - \mathbf{X} \tag{2.4}$$

where $\mathbf{u}(\mathbf{X},t) = u_i\ \mathbf{e}_i$. Note different forms expressing the displacement field $\mathbf{u}$ in (2.4).

The velocity $\mathbf{v}(\mathbf{X},t)$ is the rate of change of the position vector for the material point, i.e. the time derivative with $\mathbf{X}$ held constant. It can be written in the following forms

$$\mathbf{v}(\mathbf{X},t) \;=\; \frac{\partial \boldsymbol{x}(\mathbf{X},t)}{\partial t} = \frac{\partial \boldsymbol{\phi}(\mathbf{X},t)}{\partial t} \;=\; \frac{\partial \mathbf{u}(\mathbf{X},t)}{\partial t} \;\equiv\; \dot{\mathbf{u}} \tag{2.5}$$

The above expression is termed the material form of the velocity. We note that time derivative with $\mathbf{X}$ held constant is called *material time derivative* (see [60] and [96] for further details).

The acceleration $\mathbf{a}(\mathbf{X},t)$ is the rate of change of velocity at material point, or in other words the material time derivative of the velocity. It can be expressed as

$$\mathbf{a}(\mathbf{X},t) \;=\; \frac{\partial \mathbf{v}(\mathbf{X},t)}{\partial t} = \frac{\partial^2 \mathbf{u}(\mathbf{X},t)}{\partial t^2} \;\equiv\; \dot{\mathbf{v}} \tag{2.6}$$

The above expression is denoted the material form of the acceleration.

2.3.6 Deformation gradient

The *deformation gradient* is defined by

$$\mathbf{F}(\mathbf{X},t) = \frac{\partial \boldsymbol{\phi}}{\partial \mathbf{X}} \equiv \frac{\partial \boldsymbol{x}}{\partial \mathbf{X}} \equiv \nabla_0 \boldsymbol{\phi} \quad \text{or} \quad F_{ij} = \frac{\partial \phi_i}{\partial X_j} \equiv \frac{\partial\, x_i}{\partial X_j} \tag{2.7}$$

In mathematical terminology $\mathbf{F}$ is the *Jacobian matrix* of the motion $\boldsymbol{\phi}(\mathbf{X},t)$. The operator ∇_0 is the *right gradient with respect to the material coordinates* $\mathbf{X}$ defined in [60]. In view of (2.4) the deformation gradient can be written as

$$\mathbf{F}(\mathbf{X},t) = \mathbf{I} + \nabla_0 \mathbf{u} \quad \text{or} \quad F_{ij} = \delta_{ij} + \frac{\partial u_i}{\partial X_j} \tag{2.8}$$

In terms of the spatial coordinates the deformation gradient $\mathbf{F}$ may be equivalently expressed

$$\mathbf{F}(\boldsymbol{x},t) = [\mathbf{I} - \nabla\mathbf{u}]^{-1} = [\mathbf{I} - \mathbf{H}]^{-1} \tag{2.9}$$

where ∇ is the *right gradient with respect to the spatial coordinates* $\boldsymbol{x}$ (see [60]) and $\mathbf{H}$ is the spatial gradient of the displacement given as

$$\mathbf{H} = \nabla\mathbf{u} \quad or \quad H_{ij} = \frac{\partial u_i}{\partial x_j} \tag{2.10}$$

If the infinitesimal vector $\mathrm{d}\mathbf{X}$ is considered in the reference configuration, then it follows from (2.7) that the corresponding vector $\mathrm{d}\boldsymbol{x}$ in the current configuration is given by

$$\mathrm{d}\boldsymbol{x} = \mathbf{F} \cdot \mathrm{d}\mathbf{X} \quad \text{or} \quad \mathrm{d}x_i = F_{ij}\, \mathrm{d}X_j \tag{2.11}$$

The deformation gradient is said to be a *two point* tensor.

The determinant of $\mathbf{F}$ is denoted by J and it is called the *Jacobian determinant* or the determinant of the deformation gradient

$$J = \det(\mathbf{F}) \tag{2.12}$$

The *Jacobian determinant* can be used to relate the integrals in the current and reference configurations

$$\int_{\Omega} f(\mathbf{x},t)\, d\Omega = \int_{\Omega_0} f(\boldsymbol{\phi}(\mathbf{X},t),t)\, J\, d\Omega_0 \tag{2.13}$$

The F.E. formulation is developed in the spatial form as will be shown in Chapter 3. Hence, the increment of the deformation gradient between two configurations as depicted in Figure 2.2 will prove useful. We could define the relation between the deformation gradient in the configuration Ω_n and Ω_{n+1} as

$$\mathbf{F}_{n+1} = \triangle\mathbf{F} \cdot \mathbf{F}_n \tag{2.14}$$

where $\triangle\mathbf{F}$ is the increment of the deformation gradient due to the motion of the body from the configuration Ω_n to Ω_{n+1}. The magnitude $\triangle\mathbf{F}$ can be expressed in spatial configuration as,

$$\triangle\mathbf{F} = [\mathbf{I} - \nabla\triangle\mathbf{u}]^{-1} = [\mathbf{I} - \triangle\mathbf{H}]^{-1} \tag{2.15}$$

where $\triangle\mathbf{u}$ is the increment of the displacement field due to the motion of the body from the configuration Ω_n to Ω_{n+1}

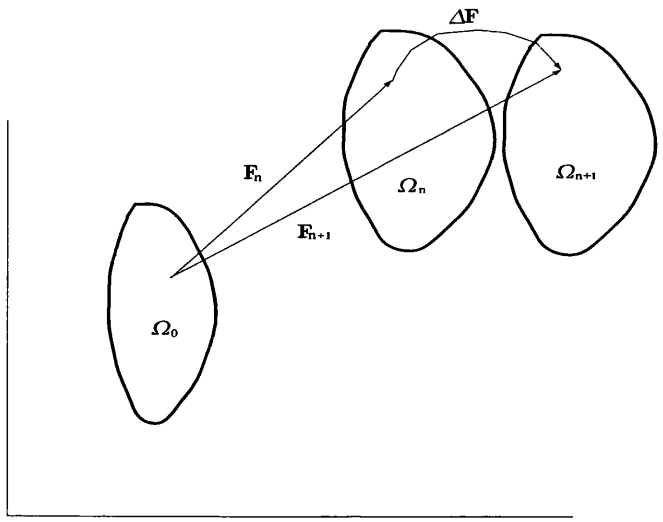

Figure 2.2: Incremental deformation gradient $\triangle\mathbf{F}$ between two configurations Ω_n and Ω_{n+1}

$$\triangle\mathbf{u} = \mathbf{u}_{n+1} - \mathbf{u}_n \tag{2.16}$$

and its spatial gradient has been defined following (2.10) as

$$\triangle\mathbf{H} = \nabla\triangle\mathbf{u} \quad or \quad \triangle H_{ij} = \frac{\partial\triangle u_i}{\partial x_j} \tag{2.17}$$

Isochoric/volumetric split of the deformation gradient

Any deformation can be locally decomposed into a purely *volumetric* deformation (or *pure contraction/dilatation*) followed by an *isochoric* (or *volume preserving*) deformation or viceversa. To see this note that the deformation gradient $\mathbf{F}$ can always be multiplicatively split as,

$$\mathbf{F} = \mathbf{F}_{iso} \cdot \mathbf{F}_v = \mathbf{F}_v \cdot \mathbf{F}_{iso} \tag{2.18}$$

where

$$\mathbf{F}_v \equiv J^{\frac{1}{3}}\,\mathbf{I} \tag{2.19}$$

is the *volumetric* component of $\mathbf{F}$ and

$$\mathbf{F}_{iso} \equiv J^{-\frac{1}{3}}\,\mathbf{F} \tag{2.20}$$

is the *isochoric* (*volume preserving*) component.

2.3.7 Right and Left Cauchy-Green deformation tensors

As a general measure of deformation the symmetric *right* and *left Cauchy-Green deformation tensor* are defined respectively as,

$$\mathbf{C} = \mathbf{F}^{\mathrm{T}} \cdot \mathbf{F} \tag{2.21}$$

and

$$\mathbf{B} = \mathbf{F} \cdot \mathbf{F}^{\mathrm{T}} \tag{2.22}$$

This tensor $\mathbf{C}$ relates the scalar product of the two spatial differential vectors $\mathrm{d}\boldsymbol{x}_1 \cdot \mathrm{d}\boldsymbol{x}_2$ with respect to the correspondent vector in the material configuration $\mathrm{d}\mathbf{X}_1$ and $\mathrm{d}\mathbf{X}_2$ in the following expression

$$\mathrm{d}\boldsymbol{x}_1 \cdot \mathrm{d}\boldsymbol{x}_1 = \mathrm{d}\mathbf{X}_1 \cdot \mathbf{C} \cdot \mathrm{d}\mathbf{X}_2 \,. \tag{2.23}$$

2.3.8 Polar decomposition

The deformation gradient $\mathbf{F}$ can be expressed as the product of the orthogonal rotation tensor $\mathbf{R}$ and the symmetric tensor $\mathbf{U}$ known as *right stretch tensor* or *material stretch tensor*

$$\mathbf{F} = \mathbf{R} \cdot \mathbf{U} \tag{2.24}$$

Inserting the above (2.24) into (2.11)

$$\mathrm{d}\boldsymbol{x} = \mathbf{R} \cdot (\mathbf{U} \cdot \mathrm{d}\mathbf{X}) \tag{2.25}$$

This shows that any motion of a body consists of a deformation which is represented by a mapping $\mathbf{U}$ followed by a rigid rotation $\mathbf{R}$.

To obtain this decomposition, consider the following relation between the right Cauchy-Green deformation tensor $\mathbf{C}$ and the right stretch tensor $\mathbf{U}$:

$$\mathbf{C} = \mathbf{F}^{\mathrm{T}} \cdot \mathbf{F} = (\mathbf{R} \cdot \mathbf{U})^{\mathrm{T}} \cdot \mathbf{R} \cdot \mathbf{U}) = \mathbf{U} \cdot \mathbf{U} \equiv \mathbf{U}^2 \tag{2.26}$$

Therefore, $\mathbf{U}$ is then extracted from the $\mathbf{C}$ using the relation obtained from the above

$$\mathbf{U} = \mathbf{C}^{\frac{1}{2}} \tag{2.27}$$

This fractional power of the matrix is defined in terms of its *spectral decomposition* (see [22] and [28]). The details of the derivation are left out of this work. Full explanation is given in [60] and [40].

2.4 Strain measures

A strain measure must vanish for any rigid body motion (in particular for rigid rotation). Different measures of strain and strain rates are used in continuum mechanics.

2.4.1 The Green strain tensor

The material Green strain tensor $\mathbf{E}$ is defined by considering the difference between the scalar product of the two infinitesimal vectors in the spatial and the reference configuration respectively as,

$$\frac{1}{2}(\mathrm{d}\boldsymbol{x}_1 \cdot \mathrm{d}\boldsymbol{x}_2 - \mathrm{d}\mathbf{X}_1 \cdot \mathrm{d}\mathbf{X}_2) = \mathrm{d}\mathbf{X}_1 \cdot \mathbf{E} \cdot \mathrm{d}\mathbf{X}_2; \quad \mathbf{E} = \frac{1}{2}(\mathbf{C} - \mathbf{I}) \tag{2.28}$$

The Green strain tensor can also be expressed in terms of displacement gradients by

$$\mathbf{E} = \frac{1}{2}\left(\nabla_0\mathbf{u} + (\nabla_0\mathbf{u})^{\mathrm{T}} + \nabla_0\mathbf{u} \cdot (\nabla_0\mathbf{u})^{\mathrm{T}} \right) \tag{2.29}$$

2.4.2 The small strain tensor

The *small strain tensor*[1] is defined as,

$$\boldsymbol{\epsilon} \equiv \nabla^s\mathbf{u} = \mathrm{sym}(\nabla\mathbf{u}) = \frac{1}{2}\left(\nabla\mathbf{u} + (\nabla\mathbf{u})^{\mathrm{T}} \right). \tag{2.30}$$

The tensor $\boldsymbol{\epsilon}$ is termed the small strain tensor because under small or infinitesimal deformation theory (where the displacement and displacement gradient are sufficiently small), the strain tensors (such as the Green strain (2.29)), can be approximated by the small strain tensor (2.30). Further details are given in [60]. It is important to keep in mind that

[1] In the definition of the small strain tensor the notation $\mathrm{sym}(\nabla *) = \nabla^s * = \frac{1}{2}(\nabla * + (\nabla *)^{\mathrm{T}})$ has been introduced for the symmetric operator over the gradient of any vector field $*$

the spatial displacement gradients $\nabla \mathbf{u}$ described in (2.30) can be identified as material gradients $\nabla_0 \mathbf{u}$ if the small strain theory conditions are applicable. We note this is not applicable in finite deformation theory.

By performing algebraic manipulations of (2.9), the spatial displacement gradient $\nabla \mathbf{u}$ is then expressed as function of the deformation gradient $\mathbf{F}$ as,

$$\nabla \mathbf{u} = \mathbf{I} - \mathbf{F}^{-1} \tag{2.31}$$

Inserting the above (2.31) into (2.30) the small strain tensor $\boldsymbol{\epsilon}$ can be expressed in terms of the deformation gradient $\mathbf{F}$ as,

$$\boldsymbol{\epsilon} = \mathbf{I} - \text{sym}(\mathbf{F}^{-1}) = \mathbf{I} - \frac{1}{2} \left(\mathbf{F}^{-1} + \mathbf{F}^{-\text{T}} \right). \tag{2.32}$$

2.4.3 The rate of deformation

The spatial field $\mathbf{L}$, defined as:

$$\mathbf{L} \equiv \nabla \mathbf{v} \tag{2.33}$$

is denoted the *velocity gradient.* The symmetric part of this tensor is called the *rate of deformation*

$$\mathbf{D} \equiv \text{sym}(\mathbf{L}) = \nabla^s \mathbf{v} = \frac{1}{2} \left(\nabla \mathbf{v} + (\nabla \mathbf{v})^{\text{T}} \right) = \frac{\partial \boldsymbol{\epsilon}}{\partial t}. \tag{2.34}$$

which also indicates that the rate-of-deformation $\mathbf{D}$ is the material time derivative of the small strain tensor $\boldsymbol{\epsilon}$.

2.5 Kinetics: stress and equilibrium

Kinetics theory is the science of the motion of a continuous body under external forces. Fundamentally, this involves developing measures for the internal stresses.

2.5.1 Stress measures

In nonlinear problems, various stress measures can be defined. Three measures of stress are considered here.

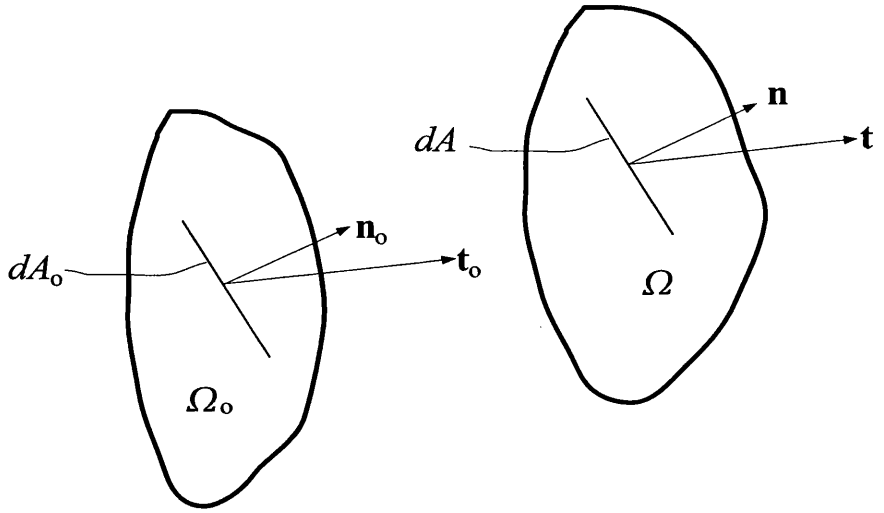

Figure 2.3: Stress vectors in both material Ω_0 and spatial Ω configurations

The Cauchy stress tensor

The Cauchy stress tensor $\boldsymbol{\sigma}$ is defined by the Cauchy's law

$$\boldsymbol{\sigma} \cdot \mathbf{n}\, \mathrm{d}A = \mathbf{t}\, \mathrm{d}A \tag{2.35}$$

where $\mathbf{t}$ is the traction vector (force per unit area) on the current surface, and $\mathbf{n}$ is normal vector to the current surface, both depicted in Figure 2.3. $\mathrm{d}A$ denotes an infinitesimal element of deformed area.

The Cauchy stress tensor is symmetric [98]. The Cauchy stress tensor is also referred to as the true stress.

The Kirchhoff stress tensor

Another stress measure frequently used is the Kirchhoff stress tensor $\boldsymbol{\tau}$ which is defined by

$$\boldsymbol{\tau} = J\, \boldsymbol{\sigma} \tag{2.36}$$

The Kirchhoff stress is defined similarly to the Cauchy stress, but is scaled with the determinant of the Jacobian J. For isochoric motion (or volume preserving deformation with $J = 1$) it becomes identical to the Cauchy stress.

The First Piola-Kirchhoff stress tensor

The definition of the First Piola-Kirchhoff stress tensor $\mathbf{P}$ is similar to that of the Cauchy stress except that it is expressed in terms of the area and normal of the reference surface, i.e. the undeformed surface,

$$\mathbf{P} \cdot \mathbf{n}_0 = \mathbf{t}_0 \tag{2.37}$$

Basic in the definition of the first Piola-Kirchhoff stress is the traction vector $\mathbf{t}_0$, which at the point of interest, measures the force that acts across the surface with normal $\mathbf{n}$ in the deformed configuration per unit of *reference* unit area. So that, the following relation relates $\mathbf{t}_0$ with the traction vector $\mathbf{t}$.

$$\mathrm{d}A\ \mathbf{t} = \mathrm{d}A_0\ \mathbf{t}_0 \tag{2.38}$$

where $\mathrm{d}A_0$ is the corresponding counterpart of $\mathrm{d}A$ in the undeformed configuration as can be observed in Figure 2.3 .

Using Nanson's relation (see [60])

$$\mathbf{n}\ \mathrm{d}A = J\,\mathbf{F}^{-\mathrm{T}} \cdot \mathbf{n}_0\ \mathrm{d}A_0, \tag{2.39}$$

the relation between the first Piola-Kirchhoff stress and the Cauchy stress tensors can be expressed as

$$\mathbf{P} = J\boldsymbol{\sigma} \cdot \mathbf{F}^{-\mathrm{T}} \tag{2.40}$$

The first Piola-Kirchhoff stress tensor is generally unsymmetric.

2.5.2 Conservation Equations

Mass Conservation

The mass $m(\Omega)$ of a material domain Ω is given by

$$m(\Omega) = \int_{\Omega} \rho(\mathbf{X}, t)\ \mathrm{d}\Omega \tag{2.41}$$

where $\rho(\mathbf{X}, t)$ is the density. Mass conservation requires that the mass of any material domain remains constant, since no material flows through the boundaries of a material domain. Therefore, the material time derivative of $m(\Omega)$ vanishes, i.e.

$$\frac{Dm}{Dt} = \frac{D}{Dt}\int_{\Omega} \rho \, \mathrm{d}\Omega = 0 \tag{2.42}$$

Applying Reynolds transport theorem (see [60] or [96]), to the above yields

$$\int_{\Omega} \Big(\frac{D\rho}{Dt} + \rho \, \mathrm{div}(\mathbf{v}) \Big) \mathrm{d}\Omega = 0 \tag{2.43}$$

Since the above holds for any subdomain Ω, it follows that

$$\frac{D\rho}{Dt} + \rho \, \mathrm{div}(\mathbf{v}) = 0 \tag{2.44}$$

The above is the *equation of mass conservation*, often called the *continuity equation.*

For the Lagrangian description, the mass conservation equation, (2.42), can be integrated in time to obtain an algebraic equation for the density:

$$\int_{\Omega} \rho \, \mathrm{d}\Omega = \text{constant} = \int_{\Omega_0} \rho_0 \, \mathrm{d}\Omega_0 \tag{2.45}$$

Transforming the left-hand side term to the reference domain by (2.13) gives

$$\int_{\Omega_0} (\rho \, J - \rho_0) \, \mathrm{d}\Omega_0 = 0 \tag{2.46}$$

Since the above equation holds for any subdomain, the following algebraic equation for mass conservation is obtained:

$$\rho(\mathbf{X}, t) \; J(\mathbf{X}, t) = \rho_0(\mathbf{X}, t) \quad \text{or} \quad \rho \, J = \rho_0 \tag{2.47}$$

Conservation of linear momentum

The equation emanating from the principle of linear momentum conservation is a key equation in nonlinear F.E. procedures. This principle is also called the momentum conservation principle or the balance of momentum principle.

Consider an arbitrary domain Ω with boundary $\partial\Omega$ subjected to a body force $\rho\mathbf{b}$ per unit mass and surface traction $\mathbf{t}$ per unit area. The total force is given by

$$\mathbf{f}(t) = \int_{\Omega} \rho \, \mathbf{b}(\boldsymbol{x}, t) \, \mathrm{d}V + \int_{\partial\Omega} \mathbf{t}(\boldsymbol{x}, t) \, \mathrm{d}A \tag{2.48}$$

The linear momentum is given by

$$\mathbf{p}(t) = \int_{\Omega} \rho \, \mathbf{v}(\boldsymbol{x}, t) \, \mathrm{d}V \tag{2.49}$$

where $\rho\mathbf{v}$ is the linear momentum per unit volume.

Newton's second law of motion for the continuum states that the material time derivative of the linear momentum equals the total force. Using (2.48) and (2.49), the momentum conservation principle gives

$$\frac{D\mathbf{p}}{Dt} = \mathbf{f} \;\Rightarrow\; \frac{D}{Dt}\int_{\Omega} \rho \, \mathbf{v} \, \mathrm{d}V = \int_{\Omega} \rho \, \mathbf{b}(\boldsymbol{x}, t) \, \mathrm{d}V + \int_{\partial\Omega} \mathbf{t}(\mathbf{x}, t) \, \mathrm{d}A \tag{2.50}$$

The above form is transformed by applying the Cauchy's law (2.35), the Gauss theorem and the Reynolds transport theorem to the following (see [60] for a details):

$$\int_{\Omega} \rho \, \frac{D\mathbf{v}}{Dt} \, \mathrm{d}V = \int_{\Omega} \rho \, \mathbf{b} \, \mathrm{d}V + \int_{\Omega} \nabla \cdot \boldsymbol{\sigma} \, \mathrm{d}V \tag{2.51}$$

Hence, all the terms can be grouped into the same integrand

$$\int_{\Omega} \left(\rho \, \frac{D\mathbf{v}}{Dt} - \rho \, \mathbf{b} - \nabla \cdot \boldsymbol{\sigma} \right) \mathrm{d}V = \mathbf{0} \tag{2.52}$$

Since (2.52) holds for any arbitrary domain, it can be stated

$$\rho \, \frac{D\mathbf{v}}{Dt} = \rho \, \mathbf{b} + \nabla \cdot \boldsymbol{\sigma} \tag{2.53}$$

This equation is called the *momentum equation* (also called the balance of linear momentum).

This form is applicable to both Lagrangian and Eulerian descriptions. In the Lagrangian descriptions, the dependent variables are assumed to be functions of the Lagrangian coordinates $\mathbf{X}$ and time t, therefore the momentum equation is

$$\rho(\mathbf{X}, t) \, \frac{\partial \mathbf{v}(\mathbf{X}, t)}{\partial t} = \rho(\mathbf{X}, t) \, \mathbf{b}(\mathbf{X}, t) + \operatorname{div} \boldsymbol{\sigma}(\boldsymbol{\phi}^{-1}(\boldsymbol{x}, t), t) \tag{2.54}$$

Note that the Cauchy stress $\boldsymbol{\sigma}$ must be expressed as a function of the Eulerian coordinates $\mathbf{x}$ through the inverse of the motion $\boldsymbol{\phi}^{-1}(\boldsymbol{x}, t), t)$ so that the spatial divergence of the stress field can be evaluated.

Although the previous form (2.54) is applicable in the Lagrangian description, the previous process of applying the second Newton's law can be followed from the beginning by taking integrals in the reference configuration. This results in the following form of the momentum equation

$$\rho_0 \frac{\partial \mathbf{v}(\mathbf{X}, t)}{\partial t} = \rho_0 \mathbf{b} + \nabla_0 \cdot \mathbf{P} \tag{2.55}$$

This is called the Lagrangian form of the momentum equation. Belytschko et al [96] give a detailed derivation regarding this form of the momentum equation.

Equilibrium equation

In the problems considered in this work, the loads are assumed applied very slowly and inertial forces are very small and can be neglected. In that case, the acceleration in the momentum equation can be dropped, resulting in

$$\text{div } \boldsymbol{\sigma} + \rho \mathbf{b} = \mathbf{0} \tag{2.56}$$

The above equation is called the *quasi-static equilibrium equation.* The problems to which the equilibrium equation is applicable are called *quasi-static problems.*

The material form of the equilibrium equation is

$$\text{div}_0 \mathbf{P} + \rho_0 \mathbf{b} = \mathbf{0} \tag{2.57}$$

where the inertia term has been removed from (2.55).

Conservation of angular momentum

The integral form of the conservation of angular momentum in the absence of distributed couples leads to the symmetry of the Cauchy stress tensor condition, as mentioned in Section 2.5.1. We refer to [60] and [28], for further details.

Conservation of energy

The first postulate of thermodynamics postulates the *conservation of energy.* In this work, only mechanical processes are considered in which the only source of energy is mechanical work. Therefore, the conservation of energy is mathematically expressed by the equation:

$$\rho\, \dot{e} = \boldsymbol{\sigma} \,:\, \mathbf{D} \tag{2.58}$$

where e is the internal energy per unit of mass. The Cauchy stress $\boldsymbol{\sigma}$ and the rate of deformation $\mathbf{D}$ are said to be *conjugate in power.*

2.6 Weak form of equilibrium. The Principle of Virtual Work (PVW)

In previous Section 2.5.2, the *strong* forms of the equilibrium equation have been stated in relations (2.56) and (2.57) in spatial and material forms, respectively.

In this Section the equilibrium equation in their correspondent *weak* (global or integral) form are established. The Finite Element formulations, developed later in Chapter 3, rely on the *weak* form of the equilibrium equation or *Principle of Virtual Work.*

Again the body B of the Figure 2.1 is considered. The body B occupies the region Ω_0 in its reference configuration with boundary $\partial\Omega_0$. In its spatial configuration the body occupies the region Ω with boundary $\partial\Omega$. the body is subjected to body forces $\mathbf{b}$ in its interior and surface traction $\mathbf{t}$ on its boundary.

Firstly we define the space for the test and trial functions:

The space of *test functions* is defined by:

$$\mathscr{U}_o = \{\, \delta\mathbf{u} \mid \delta\mathbf{u} \in C^0(\mathbf{X}),\ \delta\mathbf{u} = \mathbf{0} \text{ on } \partial\Omega_u \,\} \tag{2.59}$$

The selection of such a test function makes the integral over the kinematic boundary to vanish. The test function $\delta\mathbf{u}$ are also called *virtual displacement.*

The displacement *trial functions* are considered in the space given by

$$\mathscr{U} = \{\, \mathbf{u} \mid \mathbf{u} \in C^0(\mathbf{X}),\ \mathbf{u} = \overline{\mathbf{u}} \text{ on } \partial\Omega_u \,\} \tag{2.60}$$

where $\overline{\mathbf{u}}$ are the prescribed displacements on $\partial\Omega_u$. The space of displacement in $\mathscr{U}$ is called *kinematically admissible* displacements.

2.6.1 The spatial version of PVW

The spatial version of the principle of virtual work states: the body B body is in *equilibrium* if and only if its Cauchy stress field, $\boldsymbol{\sigma}$, satisfies the following equation

$$\int_{\Omega} [\ \boldsymbol{\sigma} : \delta\boldsymbol{\epsilon} - \mathbf{b} \cdot \delta\mathbf{u}\ ]\ \mathrm{d}V - \int_{\partial\Omega_t} \mathbf{t} \cdot \delta\mathbf{u}\ \mathrm{d}A = 0 \quad \forall\ \delta\mathbf{u} \in \mathscr{U}_0 \tag{2.61}$$

where $\delta\boldsymbol{\epsilon}$ is defined as,

$$\delta\boldsymbol{\epsilon} = \delta\nabla^s\mathbf{u} = \nabla^s(\delta\mathbf{u}) \tag{2.62}$$

The equivalence between the above weak form (2.61) and the strong from (2.56) is briefly described in [22] and [28], while a more detailed description is given in [96].

2.6.2 The material version of PVW

The virtual work equation can be equivalently expressed in the *reference* configuration of B. The corresponding material version is

$$\int_{\Omega_0} [\ \mathbf{P} : \delta\mathbf{F} - \mathbf{b} \cdot \delta\mathbf{u}\ ]\ \mathrm{d}V - \int_{\partial\Omega_{0t}} \mathbf{t}_0 \cdot \delta\mathbf{u}\ \mathrm{d}A = 0 \quad \forall\ \delta\mathbf{u} \in \mathscr{U}_0 \tag{2.63}$$

where $\delta\mathbf{F}$ is defined as,

$$\delta\mathbf{F} = \delta(\mathbf{I} + \nabla_0\mathbf{u}) = \delta\nabla_0\mathbf{u} = \nabla_0(\delta\mathbf{u}) \tag{2.64}$$

The equivalence between (2.63) and the strong form (2.57) is proven in [96].

2.6.3 The small strain version of PVW

Under small deformations, material and spatial configurations coincide and the virtual work equation reads simply:

$$\int_{\Omega_0} [\ \boldsymbol{\sigma} : \delta\boldsymbol{\epsilon} - \mathbf{b} \cdot \delta\mathbf{u}\ ]\ \mathrm{d}V - \int_{\partial\Omega_{0t}} \mathbf{t} \cdot \delta\mathbf{u}\ \mathrm{d}A = 0 \quad \forall\ \delta\mathbf{u} \in \mathscr{U}_0 \tag{2.65}$$

2.7 Introduction to the constitutive theory

In this Section, a brief description of the constitutive theory with internal variables is given, without details of any particular model, which is given in subsequent Chapter 4.

2.7.1 Thermodynamics with internal variables

This approach is based on the hypothesis that at any instant of a thermodynamical process, the thermodynamical state at a given point can be completely determined by the knowledge of a finite number of *state variables*. The thermodynamic state depends only on the *instantaneous* value of the state variables and not on their past history.

It is assumed that at any time t, the thermodynamic state at a point is determined by the following set of *state variables*:

$$\{ \mathbf{F},\ T,\ \mathbf{g},\ \boldsymbol{\alpha} \} \tag{2.66}$$

where $\mathbf{F}, T$ and $\mathbf{g}$ are the *instantaneous* values of the deformation gradient, temperature and the temperature gradient. Also

$$\boldsymbol{\alpha} = \{\alpha_k\} \tag{2.67}$$

is the set of *internal variables* containing, in general, entities of scalar, vectorial, and tensorial nature associated with dissipative mechanisms.

2.7.2 General constitutive law

The *specific free energy* is assumed to take the form

$$\psi = \psi(\mathbf{F}, T, \boldsymbol{\alpha}) \tag{2.68}$$

Only *purely mechanical* case is considered in this work. In this case, thermal effects are ignored, and therefore the specific free energy ψ remains function only of the deformation gradient $\mathbf{F}$ and the set of internal variables $\boldsymbol{\alpha}$

$$\psi = \psi(\mathbf{F}, \boldsymbol{\alpha}) \tag{2.69}$$

Without giving details, the mechanical constitutive equation takes the following form,

$$\mathbf{P} = \rho_0 \frac{\partial \psi}{\partial \mathbf{F}} \ \Rightarrow\ \mathbf{P} = \mathbf{P}(\mathbf{F}, \boldsymbol{\alpha}) \tag{2.70}$$

for the first Piola-Kirchhoff stress $\mathbf{P}$. Equivalent to (2.70) are the following constitutive relations for the Cauchy stress $\boldsymbol{\sigma}$ and the Kirchhoff stress $\boldsymbol{\tau}$:

$$\boldsymbol{\sigma} = \rho \frac{\partial \psi}{\partial \mathbf{F}} \cdot \mathbf{F}^{\mathrm{T}} \ \Rightarrow\ \boldsymbol{\sigma} = \boldsymbol{\sigma}(\mathbf{F}, \boldsymbol{\alpha}) \tag{2.71}$$

$$\boldsymbol{\tau} = \rho_0 \frac{\partial \psi}{\partial \mathbf{F}} \cdot \mathbf{F}^{\mathrm{T}} \;\Rightarrow\; \boldsymbol{\tau} = \boldsymbol{\tau}(\mathbf{F}, \boldsymbol{\alpha}) \tag{2.72}$$

In order to completely characterize the constitutive model complementary laws associated with dissipative mechanisms are required. In general it is assumed that the flux variables $\dot{\boldsymbol{\alpha}}$ are given functions of the state variables, so that the constitutive equations are postulated in the purely mechanical case as

$$\dot{\boldsymbol{\alpha}} = \dot{\boldsymbol{\alpha}}(\mathbf{F}, \boldsymbol{\alpha}) \tag{2.73}$$

Small strain case

In the infinitesimal strain case, the small strain tensor $\boldsymbol{\epsilon}$ replaces the deformation gradient. Therefore, the specific free energy has the following format

$$\psi = \psi(\boldsymbol{\epsilon}, \boldsymbol{\alpha}) \tag{2.74}$$

The set of constitutive equations is now defined as,

$$\boldsymbol{\sigma} = \rho \frac{\partial \psi}{\partial \boldsymbol{\epsilon}} \;\Rightarrow\; \boldsymbol{\sigma} = \boldsymbol{\sigma}(\boldsymbol{\epsilon}, \boldsymbol{\alpha}) \tag{2.75}$$

$$\dot{\boldsymbol{\alpha}} = \dot{\boldsymbol{\alpha}}(\boldsymbol{\epsilon}, \boldsymbol{\alpha}) \tag{2.76}$$

for the Cauchy stress $\boldsymbol{\sigma}$ and the rate of internal variables $\boldsymbol{\alpha}$.

2.8 Linearization of the virtual work

The virtual work representation of the equilibrium equations presented before in Section 2.6 is generally nonlinear. For a given material and loading conditions, its solution is given by a deformed configuration in a state of equilibrium. In order to obtain this equilibrium position using a Newton-Raphson iterative procedure, it is necessary to *linearize the equilibrium* equations using the general *directional derivative* procedure as explained in [40] and [22]. Linearization of the virtual work gives the *tangent modulus* that is a fundamental part in the assemblage of the tangent stiffness matrix, which is a crucial component of the implicit Finite Element solution procedure explained in the Chapter 3.

2.8.1 Material version. The material tangent modulus

The linearization of the virtual work, expressed previously in its material form in (2.63), is presented in this section. The problem is reduced to finding a kinematically admissible field $\mathbf{u}$ such that it satisfies:

$$G(\mathbf{u}, \delta\mathbf{u}) = 0 \quad \forall\, \delta\mathbf{u} \in \mathscr{U}_0 \tag{2.77}$$

where G is the *virtual work* defined as:

$$G(\mathbf{u}, \delta\mathbf{u}) \equiv \int_{\Omega_0} [\, \delta\mathbf{F} : \mathbf{P}(\mathbf{F}(\mathbf{u})) - \mathbf{b} \cdot \delta\mathbf{u} \,]\, \mathrm{d}V - \int_{\partial\Omega_{0t}} \mathbf{t}_0 \cdot \delta\mathbf{u}\, \mathrm{d}A \tag{2.78}$$

The dependence of G on the unknown displacement function $\mathbf{u}$ follows from the constitutive dependence of the stress tensor $\mathbf{P}$, given previously in (2.70), on the deformation gradient $\mathbf{F}$ which itself is a function of displacements as shown in (2.8). The virtual work (2.77) is linearized with respect to the unknown displacement $\mathbf{u}$ about the trial solution $\hat{\mathbf{u}}$. The linearized problem consist of finding the incremental displacement $\triangle\mathbf{u}$ such that:

$$L(\Delta\mathbf{u}, \delta\mathbf{u}) \equiv G(\hat{\mathbf{u}}, \delta\mathbf{u}) + DG(\hat{\mathbf{u}}, \delta\mathbf{u})[\triangle\mathbf{u}] = 0 \quad \forall\, \delta\mathbf{u} \in \mathscr{U}_0 \tag{2.79}$$

where L is the linearized virtual work and

$$DG(\hat{\mathbf{u}}, \delta\mathbf{u})[\triangle\mathbf{u}] = \left.\frac{\mathrm{d}}{\mathrm{d}\varepsilon}\right|_{\varepsilon=0} G(\hat{\mathbf{u}} + \varepsilon\triangle\mathbf{u}, \delta\mathbf{u}) \tag{2.80}$$

is the directional derivative of G at $\hat{\mathbf{u}}$ in the direction of $\triangle\mathbf{u}$.

Explicitly, the directional derivative of G is given by:

$$DG(\hat{\mathbf{u}}, \delta\mathbf{u})[\Delta\mathbf{u}] = \left.\frac{\mathrm{d}}{\mathrm{d}\varepsilon}\right|_{\varepsilon=0} \int_{\Omega_0} \delta\mathbf{F} : \mathbf{P}(\mathbf{F}(\varepsilon))\, \mathrm{d}V = \int_{\Omega_0} \left.\frac{\mathrm{d}}{\mathrm{d}\varepsilon}\right|_{\varepsilon=0} [\, \delta\mathbf{F} : \mathbf{P}(\mathbf{F}(\varepsilon)) \,]\, \mathrm{d}V \tag{2.81}$$

where $\mathbf{F}(\varepsilon)$ has been defined as:

$$\mathbf{F}(\varepsilon) = \mathbf{I} + \nabla_0(\hat{\mathbf{u}} + \varepsilon\triangle\mathbf{u}) = \hat{\mathbf{F}} + \varepsilon\, \nabla_0\triangle\mathbf{u} \tag{2.82}$$

with

$$\hat{\mathbf{F}} = \mathbf{I} + \nabla_0\hat{\mathbf{u}} \tag{2.83}$$

denoting the deformation gradient corresponding to displacement $\hat{\mathbf{u}}$.

The only term in (2.81) which depends on ε is $\mathbf{P}$. By applying the chain rule to compute the derivative with respect of ε leads to the well-known *material tangent modulus* as shown in the following:

$$\left.\frac{\mathrm{d}}{\mathrm{d}\varepsilon}\right|_{\varepsilon=0} \mathbf{P}(\mathbf{F}(\varepsilon)) = \left.\frac{\partial \mathbf{P}}{\partial \mathbf{F}}\right|_{\mathbf{F}=\hat{\mathbf{F}}} : \left.\frac{\partial \mathbf{F}}{\partial \varepsilon}\right|_{\varepsilon=0} = \boldsymbol{\mathcal{C}}^{PF} : \nabla_0 \triangle \mathbf{u} \tag{2.84}$$

where $\boldsymbol{\mathcal{C}}^{PF}$ is the above mentioned material tangent modulus for deformation gradient $\hat{\mathbf{F}}$

$$\boldsymbol{\mathcal{C}}^{PF} \equiv \left.\frac{\partial \mathbf{P}}{\partial \mathbf{F}}\right|_{\mathbf{F}=\hat{\mathbf{F}}} \tag{2.85}$$

By inserting the expression (2.84) into the directional derivative (2.81) leads to the final expression of directional derivative

$$DG(\hat{\mathbf{u}}, \delta\mathbf{u})[\Delta\mathbf{u}] = \int_{\Omega_0} \delta\mathbf{F} : \boldsymbol{\mathcal{C}}^{PF} : \nabla_0 \triangle \mathbf{u} \, \mathrm{d}V \tag{2.86}$$

Finally, by inserting (2.86) into the linearized problem (2.79) gives

$$G(\hat{\mathbf{u}}, \delta\mathbf{u}) + \int_{\Omega_0} \delta\mathbf{F} : \boldsymbol{\mathcal{C}}^{PF} : \nabla_0 \triangle \mathbf{u} \, \mathrm{d}V = 0 \quad \forall \, \delta\mathbf{u} \in \mathscr{U}_0 \tag{2.87}$$

This represents the linearized problem in the material formulation.

2.8.2 Spatial version. The spatial tangent modulus

The linearization of the virtual work in spatial form (2.61) is going to be determined based on the previously linearized material (2.87). The virtual work functional is defined in its spatial form by:

$$G(\mathbf{u}, \delta\mathbf{u}) \equiv \int_{\Omega} [\, \delta\boldsymbol{\epsilon} : \boldsymbol{\sigma}(\mathbf{F}(\mathbf{u})) - \mathbf{b} \cdot \delta\mathbf{u} \,] \, \mathrm{d}V - \int_{\partial\Omega_t} \mathbf{t} \cdot \delta\mathbf{u} \, \mathrm{d}A \tag{2.88}$$

The dependence of the Cauchy stress tensor $\boldsymbol{\sigma}$ with respect to the deformation gradient $\mathbf{F}$ is given by the constitutive equation (2.71).

To computation of the directional derivative is based on the equivalence between the material (2.78) and spatial virtual work (2.88). Thus, the directional derivative can be computed from the material expression previously determined in (2.86) with the help of (2.13) and the relation between gradients

$$\nabla_0 \mathbf{f} = \nabla \mathbf{f} \cdot \mathbf{F} \tag{2.89}$$

where $\mathbf{f}$ represents any vector field. Therefore the directional derivative (2.86) is computed in its spatial form as

$$DG(\hat{\mathbf{u}}, \delta\mathbf{u})[\Delta\mathbf{u}] = \int_\Omega \delta\mathbf{H} \cdot \mathbf{F} : \frac{1}{J}\, \boldsymbol{\mathcal{C}}^{PF} : \triangle\mathbf{H} \cdot \mathbf{F}\, \mathrm{d}V \tag{2.90}$$

where the previous expression for the spatial gradient of the displacement increment (2.17) has been used. The following transformation has been used to obtain (2.90)

$$\delta\mathbf{F} \equiv \nabla_0(\delta\mathbf{u}) = \nabla\delta\mathbf{u} \cdot \mathbf{F} = \delta\nabla\mathbf{u} \cdot \mathbf{F} = \delta\mathbf{H} \cdot \mathbf{F} \tag{2.91}$$

The variation of the spatial gradient of the displacement is denoted as,

$$\delta\mathbf{H} = \delta\nabla\mathbf{u} = \nabla\delta\mathbf{u} \tag{2.92}$$

By re-grouping terms of the above integrand (2.90), the directional derivative may be equivalently written as:

$$DG(\hat{\mathbf{u}}, \delta\mathbf{u})[\Delta\mathbf{u}] = \int_\Omega \delta\mathbf{H} : \boldsymbol{\mathcal{A}} : \triangle\mathbf{H}\, \mathrm{d}V \tag{2.93}$$

where $\boldsymbol{\mathcal{A}}$ denotes the *spatial tangent modulus*, defined in index notation by:

$$\mathcal{A}_{ijkl} = \frac{1}{J}\, F_{jp}\, \mathcal{C}^{PF}_{ipkq}\, F_{lq} \tag{2.94}$$

Following [22], the spatial tangent modulus $\boldsymbol{\mathcal{A}}$ can be also expressed in the following form:

$$\mathcal{A}_{ijkl} = \frac{1}{J}\frac{\partial \tau_{ij}}{\partial F_{km}} F_{lm} - \sigma_{il}\delta_{jk} \tag{2.95}$$

This equation (2.95) in index form, is also presented in tensorial notation by

$$\boldsymbol{\mathcal{A}} = \frac{1}{J}\boldsymbol{\mathcal{D}}^{\tau\mathrm{F}} \diamond \mathbf{F} - \boldsymbol{\sigma} \star \mathbf{I} \tag{2.96}$$

where $\diamond$ and $\star$ are symbolic operators with index form given above in (2.95). The modulus $\boldsymbol{\mathcal{D}}^{\tau\mathrm{F}}$ relates the variations Kirchhoff stress $\boldsymbol{\tau}$ and deformation gradient tensor $\mathbf{F}$ in a form

$$\mathcal{D}^{\tau \mathrm{F}} \equiv \frac{\partial \boldsymbol{\tau}}{\partial \mathbf{F}} \tag{2.97}$$

Hence, the linearized problem in its spatial form is given by

$$G(\hat{\mathbf{u}}, \delta\mathbf{u}) + \int_{\Omega} \delta\mathbf{H} : \boldsymbol{\mathcal{A}} : \triangle\mathbf{H} \, \mathrm{d}V = 0 \quad \forall \, \delta\mathbf{u} \in \mathscr{U}_0 \tag{2.98}$$

where $G(\hat{\mathbf{u}}, \delta\mathbf{u})$ is given by (2.88).

2.8.3 Small strain version. The tangent modulus

Considering the simplest case of small deformations and strains, for which the principle of virtual work has been presented in (2.63), the virtual work functional becomes

$$G = \int_{\Omega_0} [\, \delta\boldsymbol{\epsilon} : \boldsymbol{\sigma}(\boldsymbol{\epsilon}(\mathbf{u})) - \mathbf{b} \cdot \delta\mathbf{u} \,] \, \mathrm{d}V - \int_{\partial\Omega_{0t}} \mathbf{t} \cdot \delta\mathbf{u} \, \mathrm{d}A \tag{2.99}$$

where the Cauchy stress tensor $\boldsymbol{\sigma}$ is function of the small strain tensor $\boldsymbol{\epsilon}$ as mentioned in (2.75).

The directional derivative, for the infinitesimal strain, takes the following form

$$DG(\hat{\mathbf{u}}, \delta\mathbf{u})[\Delta\mathbf{u}] = \frac{\mathrm{d}}{\mathrm{d}\varepsilon}\bigg|_{\varepsilon=0} \int_{\Omega_0} \delta\boldsymbol{\epsilon} : \boldsymbol{\sigma}(\boldsymbol{\epsilon}(\varepsilon)) \, \mathrm{d}V = \int_{\Omega_0} \frac{\mathrm{d}}{\mathrm{d}\varepsilon}\bigg|_{\varepsilon=0} [\, \delta\boldsymbol{\epsilon} : \boldsymbol{\sigma}(\boldsymbol{\epsilon}(\varepsilon)) \,] \, \mathrm{d}V \tag{2.100}$$

where $\boldsymbol{\epsilon}(\varepsilon)$ has been defined as

$$\boldsymbol{\epsilon}(\varepsilon) = \nabla^s(\hat{\mathbf{u}} + \varepsilon\triangle\mathbf{u}) = \hat{\boldsymbol{\epsilon}} + \varepsilon \, \nabla^s\triangle\mathbf{u} \tag{2.101}$$

with

$$\hat{\boldsymbol{\epsilon}} = \nabla^s(\hat{\mathbf{u}}) \tag{2.102}$$

denoting the strain tensor field at $\hat{\mathbf{u}}$.

Straightforward application of the chain rule to $\boldsymbol{\sigma}$ in (2.100) yields

$$DG(\hat{\mathbf{u}}, \delta\mathbf{u})[\Delta\mathbf{u}] = \int_{\Omega_0} \delta\boldsymbol{\epsilon} : \boldsymbol{\mathcal{C}} : \nabla^s\triangle\mathbf{u} \, \mathrm{d}V \tag{2.103}$$

where $\boldsymbol{\mathcal{C}}$ is, in the small strain case, the *small strain tangent modulus* for the strain $\hat{\boldsymbol{\epsilon}}$ given as

$$\boldsymbol{\mathcal{C}} \equiv \left.\frac{\partial \boldsymbol{\sigma}}{\partial \boldsymbol{\epsilon}}\right|_{\boldsymbol{\epsilon}=\hat{\boldsymbol{\epsilon}}} \tag{2.104}$$

Hence, the linearized virtual work in small strain analysis is given by

$$G(\hat{\mathbf{u}}, \delta\mathbf{u}) + \int_{\Omega_0} \delta\boldsymbol{\epsilon} : \boldsymbol{\mathcal{C}} : \nabla^s \triangle\mathbf{u} \ \mathrm{d}V = 0 \quad \forall\, \delta\mathbf{u} \in \mathscr{U}_0 \tag{2.105}$$

where G is given by (2.99).

2.8.4 Newton-Raphson solution algorithm

The principle of virtual work has been presented in Section 2.6 in terms of the virtual displacement as,

$$G(\mathbf{u}, \delta\mathbf{u}) = 0 \quad \forall\, \delta\mathbf{u} \in \mathscr{U}_0 \tag{2.106}$$

Considering a trial solution $\hat{\mathbf{u}}$, the above equation has been linearized in Section 2.8, in the direction of an increment $\triangle\mathbf{u}$ at $\hat{\mathbf{u}}$ as,

$$G(\hat{\mathbf{u}}, \delta\mathbf{u}) + DG(\hat{\mathbf{u}}, \delta\mathbf{u})[\triangle\mathbf{u}] = 0 \quad \forall\, \delta\mathbf{u} \in \mathscr{U}_0 \tag{2.107}$$

The directional derivative represents the change in the internal forces due to increment $\triangle\mathbf{u}$ (assuming that external forces are constant). In the context of F.E. analysis, the directional derivative of the virtual work equation will be the source of the tangent matrix.

2.9 Conclusions

In this chapter, a general description of the continuum mechanics has been described, as it is essential for nonlinear F.E. analysis given in Chapter 3. Discrete forms of the equilibrium equations and its linearization will be given in the next Chapter 3. Furthermore, the general continuum mechanics description of this chapter will be used in subsequent Chapters 5 and 7 to describe the theory of continuum multiscale analysis for small and large strain, respectively.

Chapter 3

Finite Element Method

3.1 Introduction

In this chapter a general F.E. formulation is given. More details about the F.E. Method are given in [25], [96], [40], [58].

The equilibrium equations and their corresponding linearizations have been established in terms of a material or spatial description in Chapter 2. Either of these descriptions can be used to derive the discretized equilibrium equations and their corresponding matrix forms. Irrespective of which configuration is used, the resulting quantities will be identical.

3.1.1 Outline

This chapter is divided as follows: Firstly, an introduction to the Finite Element Method in given in Section 3.2. Secondly, kinematics are discretised. Then, the derivation of the discretized equilibrium equation and its linearization are accomplished in the spatial form in Sections 3.2.2 and 3.2.3, respectively. This is due to their simplicity; They are also used in spatial form in the multiscale discrete analysis for large strains in Chapter 8. Moreover, the derivation for the case of small strain analysis is given. This will be used in Chapter 6 for multiscale discrete analysis in small strains.

Having discretized the governing equations, expressions for the nodal forces and stiffness matrices are developed. The Newton-Raphson solution technique is introduced together with line search enhancement in Section 3.2.4.

So far, we have developed the formulation for a generic $n_{sd}-$space. In this work the simulation is performed in two dimensional space, therefore detailed formulation is developed in 2D.

3.2 The Finite Element Method

In this section, the Finite Element equations for the spatial configuration are developed by means of the principle of virtual work (PVW). For this purpose the current domain Ω is subdivided into n_{elem} finite elements where each element occupies the space Ω_e $e = 1 \cdots \mathrm{n}_{elem}$. Therefore, the union of the elements comprises the total discretized domain, $\Omega = \cup_e \Omega_e$.

3.2.1 Discretized kinematics

Element Coordinates

The discretization is established in the initial configuration using isoparametric elements to interpolate the initial geometry in terms of the coordinates $\mathbf{X}_I$ defining the initial position of the element nodes as,

$$\mathbf{X}(\boldsymbol{\xi}) = \sum_{I=1}^{\mathrm{n}_{node}} N_I(\boldsymbol{\xi})\, \mathbf{X}_I \tag{3.1}$$

where $N_I(\boldsymbol{\xi})$ is the *standard shape function* (or *interpolation function*) associated to each node I of the element. The parent coordinates in 2D are then $\boldsymbol{\xi} = [\xi, \eta]$ (see [82] and [68] for additional details) and n_{node} denotes the number of nodes per element. This can also be expressed in global form by

$$\mathbf{X}(\boldsymbol{\xi}) = \mathbb{N}\, \mathbf{X}^e \tag{3.2}$$

with the element interpolation matrix defined as,

$$\mathbb{N} = [\, \mathbb{N}_1 \cdots \mathbb{N}_{\mathrm{n}_{node}}] \tag{3.3}$$

given in terms of the node interpolation matrices in which

$$\mathbb{N}_I = \begin{bmatrix} N_I & 0 \\ 0 & N_I \end{bmatrix} \tag{3.4}$$

represents diagonal matrix for the node I. In addition, the element nodal material coordinate vector $\mathbf{X}^e$ of (3.2) is given as

$$\mathbf{X}^e = \begin{bmatrix} \mathbf{X}_1 \\ \vdots \\ \mathbf{X}_{\mathrm{n}_{node}} \end{bmatrix} \tag{3.5}$$

Motion and displacement

The subsequent *motion* is described in terms of the current position $\mathbf{x}_I$ of the nodal particles as,

$$\mathbf{x}(\boldsymbol{\xi}, t) = \sum_{I=1}^{\mathrm{n}_{node}} N_I(\boldsymbol{\xi})\ \mathbf{x}_I(t) = \mathbb{N}\ \mathbf{x}^e \tag{3.6}$$

with notation defined in (3.2). The element nodal spatial coordinate vector $\mathbf{x}^e$ takes the same form as their material counterpart $\mathbf{X}^e$. The displacement field is also interpolated as,

$$\mathbf{u}(\boldsymbol{\xi}, t) = \sum_{I=1}^{\mathrm{n}_{node}} N_I(\boldsymbol{\xi})\ \mathbf{u}_I(t) = \mathbb{N}\ \mathbf{u}^e \tag{3.7}$$

where $\mathbf{u}_I$ are the nodal displacement and $\mathbf{u}^e$ is the element nodal displacement vector. In the same way the virtual displacement field is defined as

$$\delta\mathbf{u}(\boldsymbol{\xi}, t) = \sum_{I=1}^{\mathrm{n}_{node}} N_I(\boldsymbol{\xi})\ \delta\mathbf{u}_I(t) = \mathbb{N}\ \delta\mathbf{u}^e \tag{3.8}$$

The deformation gradient

The deformation gradient tensor $\mathbf{F}$ in 2D, defined in (2.7), is re-cast in the matrix-vector notation as,

$$\mathbf{F} = \begin{bmatrix} F_{11} \\ F_{21} \\ F_{12} \\ F_{22} \end{bmatrix} \tag{3.9}$$

Similarly the displacement spatial gradient (2.10) can be written in a corresponding manner as,

$$\mathbf{H} = \begin{bmatrix} H_{11} \\ H_{21} \\ H_{12} \\ H_{22} \end{bmatrix} \tag{3.10}$$

In index form the displacement spatial gradient $\mathbf{H}$ is obtained as follows

$$H_{ij} = \frac{\partial u_i}{\partial x_j} = \sum_{I=1}^{\mathrm{n}_{node}} \frac{\partial N_I \; u_{Ii}}{\partial x_j} = \sum_{I=1}^{\mathrm{n}_{node}} N_{I,j} \; u_{Ii} \tag{3.11}$$

The displacement spatial gradient can be computed in matrix form as,

$$\mathbf{H} = \sum_{I=1}^{\mathrm{n}_{node}} \mathbb{G}_I \; \mathbf{u}_I = \mathbb{G} \; \mathbf{u}^e \tag{3.12}$$

where $\mathbb{G}$ is the *element discrete spatial gradient operator* defined as

$$\mathbb{G} = [\; \mathbb{G}_1 \cdots \mathbb{G}_{\mathrm{n}_{node}}] \tag{3.13}$$

The node discrete gradient operator $\mathbb{G}_I$ takes the following form for plane stress and plane strain analysis:

$$\mathbb{G}_I = \begin{bmatrix} N_{I,1} & 0 \\ 0 & N_{I,1} \\ N_{I,2} & 0 \\ 0 & N_{I,2} \end{bmatrix} \tag{3.14}$$

Hence, the increment displacement spatial gradient $\triangle\mathbf{H}$ can computed in the same matrix vector form as,

$$\triangle\mathbf{H} = \mathbb{G} \; \triangle\mathbf{u}^e \tag{3.15}$$

Once $\triangle\mathbf{H}$ is computed, the increment of the deformation gradient $\triangle\mathbf{F}$ is calculated using (2.15) in the tensorial form. Then the updated deformation gradient is simply computed in tensorial form by (2.14).

The computation of the spatial derivatives of the shape functions are obtained as,

$$N_{I,j} = \frac{\partial N_I}{\partial x_j} = \frac{\partial N_I}{\partial \xi_k}\frac{\partial \xi_k}{\partial x_j} = \frac{\partial N_I}{\partial \xi_k}(F^{\xi}_{kj})^{-1} \quad \text{or} \quad N_{I,\mathbf{x}} = N_{I,\boldsymbol{\xi}} \; \mathbf{x}^{-1}_{,\boldsymbol{\xi}} = N_{I,\boldsymbol{\xi}} \; \mathbf{F}^{-1}_{\xi} \tag{3.16}$$

The matrix $\partial x_i/\partial \xi_j$ is the Jacobian of the map between the current configuration of the element and the standard isoparametric domain as is depicted in Figure 3.1. Two symbols have been used for the matrix $\mathbf{x}_{,\boldsymbol{\xi}}$ and $\mathbf{F}_{\xi}$, where $F^{\xi}_{ij} = \partial x_i/\partial \xi_j$. The second symbol is used to indicate that the Jacobian with respect to the standard element coordinates can be viewed as a deformation gradient with respect to the standard configuration. In 2D space

$$\mathbf{x}_{,\boldsymbol{\xi}}(\boldsymbol{\xi}, t) \equiv \mathbf{F}_{\xi}(\boldsymbol{\xi}, t) = \begin{bmatrix} x_{\xi} & x_{\eta} \\ y_{\xi} & y_{\eta} \end{bmatrix} \tag{3.17}$$

This can be computed from (3.6) by taking derivative respect to the isoparametric coordinates $\boldsymbol{\xi}$ as,

$$\mathbf{x}_{,\boldsymbol{\xi}}(\boldsymbol{\xi}, t) = \sum_{I=1}^{\mathrm{n}_{node}} N_{I,\boldsymbol{\xi}}(\boldsymbol{\xi})\ \mathbf{x}_I(t) \tag{3.18}$$

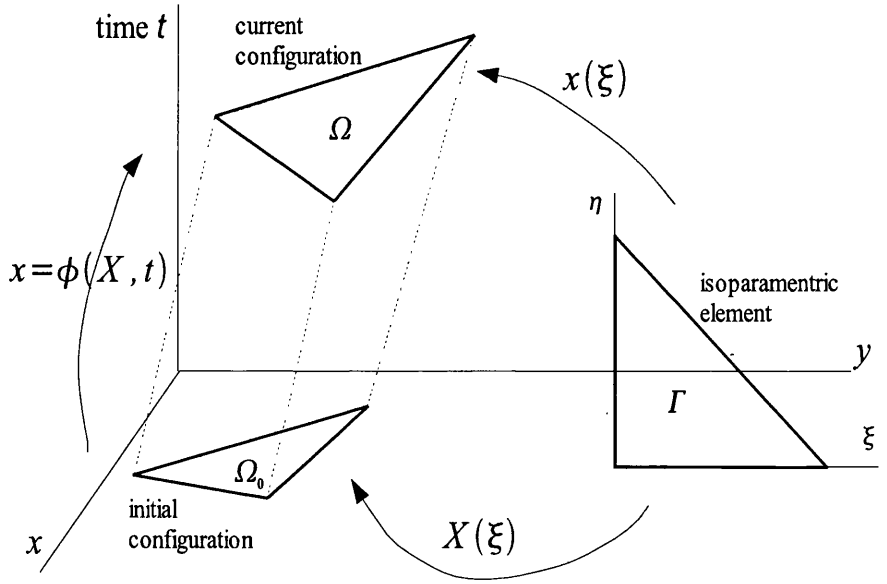

Figure 3.1: Initial Ω_0 and current Ω configurations of an element and their mapping to the isoparametric element Γ

The small strain tensor

The small strain tensor $\boldsymbol{\epsilon}$ is defined in matrix form for 2D analysis by

$$\boldsymbol{\epsilon} = [\epsilon_{11}, \epsilon_{22}, \gamma_{12}]^{\mathrm{T}} \tag{3.19}$$

where $\gamma_{12} = 2\epsilon_{12}$ is the shear deformation or distortional angle. The small strain $\boldsymbol{\epsilon}$ is computed in matrix form as

$$\boldsymbol{\epsilon} = \sum_{I=1}^{\mathrm{n}_{node}} \mathbb{B}_I \, \mathbf{u}_I = \mathbb{B} \, \mathbf{u}^e \tag{3.20}$$

where $\mathbb{B}$ is the *element discrete symmetric gradient operator* (or global strain-displacement operator) defined as,

$$\mathbb{B} = [\, \mathbb{B}_1 \cdots \mathbb{B}_{\mathrm{n}_{node}}] \tag{3.21}$$

The node discrete symmetric gradient operator $\mathbb{B}_I$ takes the following form for plane stress and plane strain analysis:

$$\mathbb{B}_I = \begin{bmatrix} N_{I,1} & 0 \\ 0 & N_{I,2} \\ N_{I,2} & N_{I,1} \end{bmatrix} \tag{3.22}$$

3.2.2 Discretized equilibrium equations

Discretized equilibrium in spatial configuration

The discretized equilibrium equations are developed in this section in the matrix-vector notation. To achieve this requires a reinterpretation of the symmetric Cauchy stress tensor as a vector comprising three independent components (2D) as,

$$\boldsymbol{\sigma} = [\sigma_{11}, \sigma_{22}, \sigma_{12}]^{\mathrm{T}} \tag{3.23}$$

In order to obtain the discretized spatial equilibrium equations given in Section 2.6, we rewrite the spatial virtual work (2.61) in a matrix form taking into consideration that the domain Ω has been discretized in the standard Finite Element analysis as,

$$G(\mathbf{u}, \delta\mathbf{u}) \equiv \int_{\Omega} [\, \delta\boldsymbol{\epsilon}^{\mathrm{T}} \boldsymbol{\sigma}(\mathbf{F}) - \delta\mathbf{u}^{\mathrm{T}} \mathbf{b} \,] \, \mathrm{d}V - \int_{\partial\Omega_t} \delta\mathbf{u}^{\mathrm{T}} \mathbf{t} \, \mathrm{d}A = 0 \tag{3.24}$$

where the discrete body Ω was divided in a number of finite elements Ω_e as,

$$\Omega = \bigcup_{e=1}^{\mathrm{n}_{elem}} \Omega_e$$

The Cauchy stress $\boldsymbol{\sigma}$ depends on the deformation gradient $\mathbf{F}$ as previously expressed in (2.71). Making substitutions in the virtual strain vector $\delta\boldsymbol{\epsilon}$ and the virtual displacement vector $\delta\mathbf{u}$ in terms of the *nodal virtual displacement global vector* $\delta\mathbf{u}^g$ the above discretized form (3.24) finally is rearranged in the form

$$G(\mathbf{u}^g, \delta\mathbf{u}^g) \equiv \delta\mathbf{u}^{g\mathrm{T}}\{\int_\Omega [\ \mathbb{B}^{g\mathrm{T}}\boldsymbol{\sigma} - \mathbb{N}^{g\mathrm{T}}\mathbf{b}\ ]\ \mathrm{d}V - \int_{\partial\Omega_t} \mathbb{N}^{g\mathrm{T}}\mathbf{t}\ \mathrm{d}A\} = 0 \tag{3.25}$$

where the global vector $\delta\mathbf{u}^g$ takes the form

$$\delta\mathbf{u}^g = \begin{bmatrix} \delta\mathbf{u}_1 \\ \vdots \\ \delta\mathbf{u}_{\mathrm{n}_{poin}} \end{bmatrix} \tag{3.26}$$

and n_{poin} denotes the *total number of nodes* in the discretized domain Ω. The *global matrix of shape functions* or *global interpolation matrix* $\mathbb{N}^g$ and the *global strain-displacement matrix* $\mathbb{B}^g$ are defined as,

$$\mathbb{N}^g = [\ \mathbb{N}^g_1 \cdots \mathbb{N}^g_{\mathrm{n}_{poin}}] \tag{3.27}$$

$$\mathbb{B}^g = [\ \mathbb{B}^g_1 \cdots \mathbb{B}^g_{\mathrm{n}_{poin}}] \tag{3.28}$$

where each $\mathbb{N}^g_I\ \forall\ I = 1 \cdots \mathrm{n}_{poin}$ is the the global node interpolation matrix expressed as,

$$\mathbb{N}^g_I = \begin{bmatrix} N^g_I & 0 \\ 0 & N^g_I \end{bmatrix} \tag{3.29}$$

where N^g_I denotes the *global shape function* associated with the global node I (see [68] and [22] for more information).

For convenience, the *internal* $\mathbf{F}^{int}$ and *external global force vectors* $\mathbf{F}^{ext}$ are defined respectively as follows

$$\mathbf{F}^{int} = \int_\Omega \mathbb{B}^{g\mathrm{T}}\boldsymbol{\sigma}\ \mathrm{d}V \tag{3.30}$$

$$\mathbf{F}^{ext} = \int_\Omega \mathbb{N}^{g\mathrm{T}}\mathbf{b}\ \mathrm{d}V + \int_{\partial\Omega_t} \mathbb{N}^{g\mathrm{T}}\mathbf{t}\ \mathrm{d}A \tag{3.31}$$

The *residual* or *out of balance force vector* $\mathbf{R}$ is defined as the difference between the internal and external global force vectors as,

$$\mathbf{R}(\mathbf{u}^g) \equiv \mathbf{F}^{int}(\mathbf{u}^g) \; - \; \mathbf{F}^{ext} \tag{3.32}$$

After the previous definition of the residual force vector $\mathbf{R}$, the discretized virtual work equation (3.24) can be re-written as,

$$G(\mathbf{u}^g, \delta\mathbf{u}^g) \equiv \delta\mathbf{u}^{g\mathrm{T}} \; \mathbf{R} = 0 \tag{3.33}$$

Since the virtual work (3.33) must be satisfied for any arbitrary virtual nodal displacements $\delta\mathbf{u}^g$ which satisfies $\mathscr{U}_o$, the *discretized nonlinear equilibrium equations* are obtained as,

$$\mathbf{R} \equiv \mathbf{F}^{int}(\mathbf{u}^g) \; - \; \mathbf{F}^{ext} = \mathbf{0} \tag{3.34}$$

In actual finite element computations, the above global force vectors $\mathbf{F}^{int}$ and $\mathbf{F}^{ext}$ are obtained as the assemblies:

$$\mathbf{F}^{int} = \mathsf{A}_{e=1}^{n_{elem}} \; \mathbf{f}_e^{int} \tag{3.35}$$

$$\mathbf{F}^{ext} = \mathsf{A}_{e=1}^{n_{elem}} \; \mathbf{f}_e^{ext} \tag{3.36}$$

of the *element* vectors:

$$\mathbf{f}_e^{int} = \int_{\Omega_e} \mathbb{B}^{\mathrm{T}} \boldsymbol{\sigma} \; dv \tag{3.37}$$

$$\mathbf{f}_e^{ext} = \int_{\Omega_e} \mathbb{N}^{\mathrm{T}} \mathbf{b} \; \mathrm{d}V + \int_{\partial\Omega_e^t} \mathbb{N}^{\mathrm{T}} \mathbf{t} \; \mathrm{d}A \tag{3.38}$$

where A is the *finite element assembly operator* [68] [82]. These element force vectors are usually computed by numerical integration. In the context of Finite Element computation, the most commonly used is the Gaussian quadrature, so that the element force vectors are finally computed as,

$$\mathbf{f}_e^{int} = \sum_{igp=1}^{n_{gaussp}} \omega_{igp} \; \mathbb{B}_{igp}^{\mathrm{T}} \; \boldsymbol{\sigma}_{igp} \; J_{\xi\, igp} \tag{3.39}$$

$$\mathbf{f}_e^{ext} = \sum_{igp=1}^{n_{gaussp}} \omega_i \; \mathbb{N}_{igp}^{\mathrm{T}} \; \mathbf{b}_{igp} \; J_{\xi\, igp} \; + \sum_{igp=1}^{n_{gaussb}} \omega_{igp}^b \; \mathbb{N}_{igp}^{\mathrm{T}} \; \mathbf{t}_{igp} \; J_{\xi\, igp}^b \tag{3.40}$$

where the Gaussian quadrature has been applied with n_{gaussp} and n_{gaussb} points for integrals, respectively, over the element domain Ω_e and the relevant portion of its boundary $\partial\Omega_e^t$. $J_{\xi\, i_{gp}} = J_\xi(\boldsymbol{\xi}_{i_{gp}})$ is the determinant of the *Jacobian* of the transformation $\mathbf{x} : \Gamma \rightarrow \Omega_e$ that maps the standard parent element domain Γ onto the current element domain Ω_e. $\omega_{i_{gp}}$ is the corresponding *weight* at the general Gauss point i_{gp}. Note that $\boldsymbol{\xi}_{i_{gp}}$ is a *position* (coordinates) of the Gauss point in the standard parent element domain Γ. More details are provided in [68], [22].

Discretised equilibrium in small strain

The small strain discretized equilibrium equations are developed in the similar way. The small strain version of the equilibrium equation (2.65) can be written in a matrix form as,

$$G(\mathbf{u}, \delta\mathbf{u}) \equiv \int_{\Omega_0} [\ \delta\boldsymbol{\epsilon}^{\mathrm{T}}\boldsymbol{\sigma}(\boldsymbol{\epsilon}) - \delta\mathbf{u}^{\mathrm{T}}\mathbf{b}\ ]\ \mathrm{d}V - \int_{\partial\Omega_{0t}} \delta\mathbf{u}^{\mathrm{T}}\mathbf{t}\ \mathrm{d}A = 0 \tag{3.41}$$

The rest of the procedure is similar to the spatial version of the discretised equation. However, two issues are important to take into consideration: Firstly, the Cauchy stress $\boldsymbol{\sigma}$ is a function of the small strain $\boldsymbol{\epsilon}$ as indicated in (2.75). Secondly, in small strain expressions all the derivatives of the shape functions are referred to the material or undeformed configuration. Finally, the final discretized nonlinear equilibrium equations are similar to (3.34), with the forces computed following the same procedure.

3.2.3 Discretization of the linearized equilibrium equations

Equation (3.34) represents a set of nonlinear equilibrium equations with the current nodal displacements as unknowns. The solution of these equations is achieved by using a Newton-Raphson iterative procedure, which involves the discretization of the linearized equilibrium equations given in Section 2.8. There we recall the linearized equilibrium equation (2.107)

$$G(\hat{\mathbf{u}}, \delta\mathbf{u}) + DG(\hat{\mathbf{u}}, \delta\mathbf{u})[\triangle\mathbf{u}] = 0 \tag{3.42}$$

where G in its spatial form has been previously discretized in Section 3.2.2, using the matrix-vector notation. The directional derivative $DG(\hat{\mathbf{u}}, \delta\mathbf{u})[\triangle\mathbf{u}]$ must be computed explicitly in order to perform the iterative procedure.

Discretisation of directional derivative on the spatial configuration

The directional derivative DG has previously been derived in its continuum spatial form (2.93). In order to compute directional derivative DG in its discrete form, the matrix-

vector expressions for $\delta\mathbf{H}$ and $\triangle\mathbf{H}$ (described in the Section 3.2.1) are used. Although they have been developed before in element form, they are recalled again as,

$$\delta\mathbf{H} = \mathbb{G}^g \; \delta\mathbf{u}^g \tag{3.43}$$

$$\triangle\mathbf{H} = \mathbb{G}^g \; \triangle\mathbf{u}^g \tag{3.44}$$

where $\mathbb{G}^g$ is the *global discrete spatial gradient operator* given by:

$$\mathbb{G} = [\; \mathbb{G}_1 \cdots \mathbb{G}_{\mathrm{n}_{poin}}] \tag{3.45}$$

Therefore, the directional derivative is rearranged in matrix form as,

$$DG(\hat{\mathbf{u}}, \delta\mathbf{u})[\Delta\mathbf{u}] = \int_\Omega \delta\mathbf{H}^{\mathrm{T}} \boldsymbol{\mathcal{A}} \; \triangle\mathbf{H} \; \mathrm{d}V \tag{3.46}$$

where $\boldsymbol{\mathcal{A}}$ is the matrix form of the fourth order tensor (2.96) which represents the spatial tangent modulus. Inserting (3.43) and (3.44) into (3.46), the directional derivative is now expressed as:

$$DG(\hat{\mathbf{u}}, \delta\mathbf{u})[\Delta\mathbf{u}] = \delta\mathbf{u}^{g\mathrm{T}} \underbrace{\{\int_\Omega \mathbb{G}^{g\mathrm{T}} \boldsymbol{\mathcal{A}} \; \mathbb{G}^g \; \mathrm{d}V\}}_{\mathbf{K}_\mathrm{T}} \; \triangle\mathbf{u}^g \tag{3.47}$$

At this stage, the *global tangent stiffness matrix* is defined as,

$$\mathbf{K}_\mathrm{T} = \int_\Omega \mathbb{G}^{g\mathrm{T}} \boldsymbol{\mathcal{A}} \; \mathbb{G}^g \; \mathrm{d}V \tag{3.48}$$

Therefore, the directional derivative is re-written in terms of the global stiffness matrix as follows

$$DG(\hat{\mathbf{u}}, \delta\mathbf{u})[\Delta\mathbf{u}] = \delta\mathbf{u}^{g\mathrm{T}} \; \mathbf{K}_\mathrm{T} \; \triangle\mathbf{u}^g \tag{3.49}$$

Although we have defined in the above expression (3.48) the global stiffness matrix $\mathbf{K}_\mathrm{T}$ in a compact global form, this matrix is normally computed by the standard F.E. assemblage of the *element stiffnesses* $\mathbf{K}_e$ as

$$\mathbf{K}_\mathrm{T} = \mathsf{A}_{e=1}^{\mathrm{n}_{elem}} \mathbf{K}_e \tag{3.50}$$

where the element stiffness matrix $\mathbf{K}_e$ is represented in the following form:

$$\mathbf{K}_e = \int_{\Omega_e} \mathbb{G}^{\mathrm{T}} \boldsymbol{\mathcal{A}}\, \mathbb{G}\, \mathrm{d}V \tag{3.51}$$

The element stiffness matrices $\mathbf{K}_e$ are computed by numerical integration Gaussian quadrature as,

$$\mathbf{K}_e = \sum_{i_{gp}=1}^{n_{gaussp}} \omega_{i_{gp}} \mathbb{G}_{i_{gp}}^{\mathrm{T}} \boldsymbol{\mathcal{A}}_{i_{gp}}\, \mathbb{G}_{i_{gp}}\, J_{\xi\, i_{gp}} \tag{3.52}$$

where $J_{\xi\, i_{gp}} = J_\xi(\boldsymbol{\xi}_{i_{gp}})$ is the determinant of the *Jacobian* of the transformation $\boldsymbol{x} : \Gamma \rightarrow \Omega_e$ that maps the standard isoparametric element domain Γ onto the current or deformed element domain Ω_e (see Figure 3.1).

Discretization of directional derivative in small strain analysis

The procedure is identical to the previous one for spatial configuration. The directional derivative DG has previously been derived in its continuum small strain form (2.103). In order to compute directional derivative DG in its discrete form, the matrix-vector expressions for $\delta\boldsymbol{\epsilon}$ and $\nabla^s \triangle\mathbf{u}$ are used as,

$$\delta\boldsymbol{\epsilon} = \mathbb{B}^g\, \delta\mathbf{u}^g \tag{3.53}$$

$$\nabla^s \triangle\mathbf{u} = \mathbb{B}^g\, \triangle\mathbf{u}^g \tag{3.54}$$

where $\mathbb{B}^g$ is the *global strain-displacement operator* defined in (3.28). Hence, the directional derivative is rearranged in matrix form as,

$$DG(\hat{\mathbf{u}}, \delta\mathbf{u})[\Delta\mathbf{u}] = \int_{\Omega} \delta\boldsymbol{\epsilon}^{\mathrm{T}} \boldsymbol{\mathcal{C}}\, \nabla^s \triangle\mathbf{u}\, \mathrm{d}V \tag{3.55}$$

where $\boldsymbol{\mathcal{C}}$ is the matrix form of the fourth order tensor (2.104) which represents the small strain tangent modulus. Inserting (3.53) and (3.54) into (3.55), the directional derivative is now expressed as:

$$DG(\hat{\mathbf{u}}, \delta\mathbf{u})[\Delta\mathbf{u}] = \delta\mathbf{u}^{g\mathrm{T}} \underbrace{\{ \int_{\Omega} \mathbb{B}^{g\mathrm{T}} \boldsymbol{\mathcal{C}}\, \mathbb{B}^g\, \mathrm{d}V \}}_{\mathbf{K}_{\mathrm{T}}}\, \triangle\mathbf{u}^g \tag{3.56}$$

The *global tangent stiffness matrix* for small strain case is defined as,

$$\mathbf{K}_{\mathrm{T}} = \int_{\Omega_0} \mathbb{B}^{g\mathrm{T}} \boldsymbol{\mathcal{C}}\, \mathbb{B}^{g}\, \mathrm{d}V \tag{3.57}$$

Therefore, the directional derivative is re-written in terms of the global stiffness matrix as follows

$$DG(\hat{\mathbf{u}}, \delta\mathbf{u})[\Delta\mathbf{u}] = \delta\mathbf{u}^{g\mathrm{T}}\, \mathbf{K}_{\mathrm{T}}\, \triangle\mathbf{u}^{g} \tag{3.58}$$

The global stiffness matrix $\mathbf{K}_{\mathrm{T}}$ is normally computed again by Finite Element assemblage from *element stiffness matrices* $\mathbf{K}_e$. The element stiffness matrix at small strains remains as,

$$\mathbf{K}_e = \int_{\Omega_{0e}} \mathbb{B}^{\mathrm{T}} \boldsymbol{\mathcal{C}}\, \mathbb{B}\, \mathrm{d}V \tag{3.59}$$

To accomplish the computation of $\mathbf{K}_e$ by numerical integration Gaussian quadrature the element stifness matrix reads as,

$$\mathbf{K}_e = \sum_{i_{gp}=1}^{n_{gaussp}} \omega_{i_{gp}} \mathbb{G}^{\mathrm{T}}_{i_{gp}} \boldsymbol{\mathcal{A}}_{i_{gp}}\, \mathbb{G}_{i_{gp}}\, J^0_{\xi\, i_{gp}} \tag{3.60}$$

where $J^0_{\xi\, i_{gp}} = J^0_{\xi}(\boldsymbol{\xi}_{i_{gp}})$ is the determinant of the *Jacobian* of the transformation $\mathbf{X} : \Gamma \rightarrow \Omega_{0e}$ that maps the standard isoparametric element domain Γ onto the reference or initial element domain Ω_{0e} (see Figure 3.1), since the analysis is performed at small strains.

3.2.4 Newton-Raphson iteration and solution procedure

Newton-Raphson solution algorithm

In Section 3.2.2 it was shown that the equilibrium equation was discretized as $G(\mathbf{u}^g, \delta\mathbf{u}^g) = \delta\mathbf{u}^{g\mathrm{T}}\, \mathbf{R}$ in (3.33), whereas the linearized virtual work term is expressed in terms of the tangent matrix as $DG(\hat{\mathbf{u}}, \delta\mathbf{u})[\Delta\mathbf{u}] = \delta\mathbf{u}^{g\mathrm{T}}\, \mathbf{K}_{\mathrm{T}}\, \triangle\mathbf{u}^{g}$ in (3.49). Consequently the Newton-Raphson equation $G(\mathbf{u}^g, \delta\mathbf{u}^g) + DG(\hat{\mathbf{u}}, \delta\mathbf{u})[\Delta\mathbf{u}] = 0$ given in equation (2.107) is expressed in discretized form as,

$$\delta\mathbf{u}^{g\mathrm{T}}\, \mathbf{K}_{\mathrm{T}}\, \triangle\mathbf{u}^{g} = -\delta\mathbf{u}^{g\mathrm{T}}\, \mathbf{R} \tag{3.61}$$

Since the nodal virtual displacement are arbitrary, a *discretized Newton-Raphson scheme* is formulated as,

$$\mathbf{K}_{\mathrm{T}} \triangle \mathbf{u}^g = -\mathbf{R}(\mathbf{u}_k^g); \quad \mathbf{u}_{k+1}^g = \mathbf{u}_k^g + \triangle \mathbf{u}^g \tag{3.62}$$

The external load $\mathbf{F}^{ext}$ is practically applied in a series of increments. Typically, the more increments taken, the easier it becomes to find a converged solution.

An outline of the solution algorithm is depicted [40] and a more detailed scheme is given into [22].

REMARK: The tangent stiffness matrix can also be found directly as,

$$\mathbf{K}_{\mathrm{T}} = \frac{\partial \mathbf{R}}{\partial \mathbf{u}^g} \tag{3.63}$$

Line search method

The Newton-Raphson process discussed above is generally capable of reaching the convergence of equilibrium equations in a small number of iterations. Nevertheless, during the course of complex deformation processes, situations may occur where the straight forward application of the Newton-Raphson method becomes insufficient. A technique used to improve the convergence rate is the *line search method.* This technique consists of interpreting the increment displacement vector $\triangle \mathbf{u}^g$ obtained from (3.62) as an optimal direction towards the solution but allowing the magnitude of step to be controlled by a parameter ς as,

$$\mathbf{u}_{k+1}^g = \mathbf{u}_k^g + \varsigma \triangle \mathbf{u}^g \tag{3.64}$$

Details of this technique applied to perform numerical examples in Chapter 9 are given in [40].

3.3 Conclusions

In this chapter a general discrete formulation of Finite Element analysis has been given. It is going to be used to derive the expressions of the discrete Finite Element Multiscale analysis in subsequent Chapters 6 and 8 for small and large strain analysis, respectively. We note that the overall tangent modulus for the macroscale is obtained from the stiffness matrix of the corresponding microstructure.

A detailed description of the material models used during this work is given in Chapter 4. Stress is given as a function of the deformation and set of internal variables are described. Also the tangent relation stress-strain for different materials models are illustrated. Those material models, described in Chapter 4, govern the microstructural behavior within the numerical tests performed in Chapter 9.

Chapter 4

Constitutive Models

4.1 Introduction

In mathematical description of material behaviour, the response of the material is characterized by a constitutive equation which gives the stress as a function of the deformation history.

The constitutive equations written in terms of the functionals of history of deformation gradient $\mathbf{F}$, temperature T and temperature gradient $\mathbf{g}$ (see [22] for more information) have no practical utility in modelling real materials undergoing real thermodynamical process. Therefore, it is necessary simplifications.

An effective alternative theory to the general description based on history functionals is the adoption of the so-called *thermodynamics with internal variables* introduced previously in Section 2.7.1. The stress is now a function of the instantaneous deformation and a set of internal variables. In this chapter material models are outlined in order to give form to those relations between stress and deformation and internal variables.

For each material model the two most relevant components of the Finite Element implementation are explained:

- The *state update procedure*, where the stresses are computed for a given state of deformation. The stress computed by such procedure is used to assemble the *elemental internal force vector.*
- The computation of the corresponding *tangent modulus*, which is used in the assemblage of the *element tangent stiffness matrix.*

Firstly, the simplest material model known as *linear elastic* material model under *small strain is introduced.*

Next, we consider nonlinear elasticity presenting the most common constitutive elastic model at *finite strain* regime known as the *hyperelastic* constitutive model. Hyperelasticity, or Green elasticity, is path-independent and fully reversible, and also, the stress is derived from strain (or stored) energy potential. Neo-Hookean model is outlined as the simplest model of this *rubber-like response.*

Finally, in the context of *small strains* elasto-plasticity is introduced as an example of path-dependent material. The simplest von Mises elasto-plastic model is outlined.

4.2 Linear elasticity in small strain

The simplest example of application of the finite element method is the isotropic *linear elasticity*, in which the Cauchy stress tensor $\boldsymbol{\sigma}$ is a linear function of the small strain tensor $\boldsymbol{\epsilon}$, i.e.,

$$\boldsymbol{\sigma} = \boldsymbol{\mathcal{C}} : \boldsymbol{\epsilon} \tag{4.1}$$

where $\boldsymbol{\mathcal{C}}$ is the small strain tangent modulus given in (2.104), which in the case of isotropic elasticity material, takes the form

$$\boldsymbol{\mathcal{C}} = 2G\,(\boldsymbol{\mathcal{I}} - \frac{1}{3}\mathbf{I}\otimes\mathbf{I}) + K\,\mathbf{I}\otimes\mathbf{I} \tag{4.2}$$

where G and K are respectively, the *shear* and *bulk modulus.* $\mathbf{I}$ is the second order identity and $\boldsymbol{\mathcal{I}}$ is the identity operator in the space of symmetric second order tensors, given in component form as

$$\mathcal{I}_{ijkl} = \frac{1}{2}(\delta_{ik}\delta_{jl} + \delta_{il}\delta_{jk}) \tag{4.3}$$

In this simplest example, the load can be applied in one single step and the displacement field is attained in one single Newton iteration. The tangent modulus computation is given in (4.2) and the stress computation follows from (4.1) as,

$$\boldsymbol{\sigma} = 2G\,\boldsymbol{\epsilon}_d + K\epsilon_v\,\mathbf{I} \tag{4.4}$$

where $\boldsymbol{\epsilon}_d$ is the deviatoric component of the elastic strain $\boldsymbol{\epsilon}$ and $\epsilon_v \equiv tr[\boldsymbol{\epsilon}]$ is the volumetric elastic strain.

4.3 Finite strain Hyperelasticity

In this section, a more general elastic constitutive relations for finite strain hyperelasticity are presented. We note that elastic materials for which work is independent of the load path and is fully reversible, are said to be *hyperelastic* (or Green elastic) materials. Hyperelastic materials are characterized by the existence of a stored (or strain) energy function that acts as a potential. This function is identified with the specific free-energy function ψ that takes the form:

$$\psi = \psi(\mathbf{F}) \tag{4.5}$$

Functions of this form are a particular case of the general potential (2.69) defined in Section 2.7.2 which include the description of dissipative materials (with internal variables). Hyperelastic models are *non-dissipative* and, therefore, do not require the consideration of internal variables. From the above equation (4.5) the *first Piola-Kirchhoff* stress tensor is obtained as,

$$\mathbf{P}(\mathbf{F}) = \rho_0 \frac{\partial \psi}{\partial \mathbf{F}} \tag{4.6}$$

where ρ_0 is the reference density (2.47). The stress depends solely on the *current* deformation and it is not affected by the deformation history. The fee-energy function completely defines a hyperelastic model. Following (2.71) and (2.72) the *Cauchy* and *Kirchhoff* stress tensors are then, respectively, given as

$$\boldsymbol{\sigma}(\mathbf{F}) = \rho \frac{\partial \psi}{\partial \mathbf{F}} \cdot \mathbf{F}^{\mathrm{T}} \tag{4.7}$$

and

$$\boldsymbol{\tau}(\mathbf{F}) = \rho_0 \frac{\partial \psi}{\partial \mathbf{F}} \cdot \mathbf{F}^{\mathrm{T}} \tag{4.8}$$

4.3.1 Isotropic hyperelastic materials

It can be shown (Malvern [60]) that the stored strain energy (potential) ψ for an hyperelastic material which is *isotropic* with respect to the initial configuration, can be written as a function of the principal invariants $(I_1(\mathbf{B}), I_2(\mathbf{B}), I_3(\mathbf{B}))$ of the left Cauchy-Green deformation tensor $\mathbf{B}$ (2.22). Thus,

$$\psi = \psi(\mathbf{F}) = \psi(\mathbf{B}) = \psi(I_1, I_2, I_3) \tag{4.9}$$

where

$$I_1 \equiv tr[\mathbf{B}], \quad I_2 \equiv \frac{1}{2}\{I_1^2 - tr[\mathbf{B}^2]\}, \quad I_3 \equiv \det(\mathbf{B}) \tag{4.10}$$

The Kirchhoff stress is an isotropic tensor valued function of $\mathbf{B}$ given from (4.8) by a simple manipulation as,

$$\boldsymbol{\tau}(\mathbf{B}) = 2\rho_0 \frac{\partial \psi}{\partial \mathbf{B}} \cdot \mathbf{B} \tag{4.11}$$

In the following Section, the Neo-Hookean material model is presented as an example of hyperelastic isotropic material.

4.3.2 Neo-Hookean model

The Neo-Hookean material model represents an extension of the isotropic linear law (Hooke's law) to large deformations (see [8]). The stored strain-energy function for a regularized (compressible) Neo-Hookean material can be written as

$$\rho_0 \psi(I_1^*, J) = \frac{1}{2}G(I_1^* - 3) + \frac{1}{2}K(\ln J)^2 \tag{4.12}$$

where $I_1^* = tr[\mathbf{B}_{iso}]$ is the first invariant of the isochoric left Cauchy-Green deformation tensor:

$$\mathbf{B}_{iso} \equiv \mathbf{F}_{iso} \cdot \mathbf{F}_{iso}^{\mathrm{T}} = J^{-\frac{2}{3}}\mathbf{B} \tag{4.13}$$

with $\mathbf{F}_{iso}$ being the isochoric component of the deformation gradient defined in (2.20). K is the *logarithmic bulk modulus* which relates the hydrostatic pressure to the purely volumetric component of the deformation gradient, and G is the *shear modulus*.

The stress constitutive function

The constitutive function for the Kirchhoff stress of the regularized Neo-Hookean material is obtained by using the strain energy function (4.12) in the potential relation (4.11). Since Neo-Hookean model has been defined in terms of the principal invariants, the chain rule is applied giving

$$\frac{\partial \psi}{\partial \mathbf{B}} = \frac{\partial \psi}{\partial I_1^*}\frac{\partial I_1^*}{\partial \mathbf{B}_{iso}} : \frac{\partial \mathbf{B}_{iso}}{\partial \mathbf{B}} + \frac{\partial \psi}{\partial J}\frac{\partial J}{\partial \mathbf{B}}. \tag{4.14}$$

The final expression for the Kirchhoff stress, for the Neo-Hookean compressible material, is obtained in compact form as,

$$\boldsymbol{\tau} = G\,\mathbf{B}^{d}_{iso} + K(\ln J)\,\mathbf{I} \tag{4.15}$$

where $\mathbf{B}^{d}_{iso} \equiv \mathrm{dev}[\mathbf{B}_{iso}]$ is the deviatoric part of the isochoric left Cauchy-Green deformation tensor $\mathbf{B}_{iso}$.

The spatial tangent modulus

Under isotropy, stress $\boldsymbol{\tau}$ can be expressed as a function of $\mathbf{B}$ only. The spatial elasticity tensor $\boldsymbol{\mathcal{A}}$ defined in (2.96) , is equivalently expressed as,

$$\boldsymbol{\mathcal{A}} = \frac{2}{J}\boldsymbol{\mathcal{D}}^{\tau\mathrm{B}} \cdot \mathbf{B} - \boldsymbol{\sigma} \star \mathbf{I} \tag{4.16}$$

where the modulus $\boldsymbol{\mathcal{D}}^{\tau\mathrm{B}}$ is defined as

$$\boldsymbol{\mathcal{D}}^{\tau\mathrm{B}} \equiv \frac{\partial \boldsymbol{\tau}}{\partial \mathbf{B}}. \tag{4.17}$$

The above tensorial notation for the spatial tangent operator for isotropic material on (4.16) is written in index form as follows:

$$\mathcal{A}_{ijkl} = \frac{2}{J}\frac{\partial \tau_{ij}}{\partial B_{km}} B_{ml} - \sigma_{il}\delta_{jk} \tag{4.18}$$

It should be noted that the only term in (4.16) that depends on the particular material model is the fourth order tensor $\boldsymbol{\mathcal{D}}^{\tau\mathrm{B}}$. In what follows, the expression for $\boldsymbol{\mathcal{D}}^{\tau\mathrm{B}}$ is derived for the Neo-Hookean constitutive model.

Tangent operator for regularized Neo-Hookean model

To obtain a compact representation of the spatial elasticity for the compressible Neo-Hookean model, the expression (4.15) for the Kirchhoff stress is differentiated to give the following:

$$\frac{\partial \boldsymbol{\tau}}{\partial \mathbf{B}} = G\,\frac{\partial \mathbf{B}_{iso}}{\partial \mathbf{B}} - \frac{1}{3}\,\mathbf{I} \otimes \frac{\partial\, \mathrm{tr}[\mathbf{B}_{iso}]}{\partial \mathbf{B}} + K\,\mathbf{I} \otimes \frac{\partial \ln J}{\partial \mathbf{B}} \tag{4.19}$$

Further mathematical derivation is needed to reach the final form of $\boldsymbol{\mathcal{D}}^{\tau\mathrm{B}}$. First, we note that

$$\frac{\partial \mathbf{B}_{iso}}{\partial \mathbf{B}} = J^{-\frac{2}{3}}(\boldsymbol{\mathcal{I}} - \frac{1}{3}\mathbf{B}\otimes\mathbf{B}^{-1}) \tag{4.20}$$

$$\frac{\partial \operatorname{tr}[\mathbf{B}_{iso}]}{\partial \mathbf{B}} = J^{-\frac{2}{3}}\boldsymbol{\mathcal{I}} - \frac{1}{3}\operatorname{tr}[\mathbf{B}_{iso}]\mathbf{B}^{-1} \tag{4.21}$$

$$\frac{\partial \ln J}{\partial \mathbf{B}} = \frac{1}{J}\frac{\partial J}{\partial \mathbf{B}} = \frac{1}{2}\mathbf{B}^{-1} \tag{4.22}$$

Finally, $\boldsymbol{\mathcal{D}}^{\tau \mathrm{B}}$ is written as,

$$\boldsymbol{\mathcal{D}}^{\tau \mathrm{B}} \equiv \frac{\partial \boldsymbol{\tau}}{\partial \mathbf{B}} = G\,\boldsymbol{\mathcal{D}}_{ev} : (J^{-\frac{2}{3}}\boldsymbol{\mathcal{I}} - \frac{1}{3}\mathbf{B}\otimes\mathbf{B}^{-1}) + \frac{1}{2}K\,\mathbf{I}\otimes\mathbf{B}^{-1} \tag{4.23}$$

where the fourth order tensor $\boldsymbol{\mathcal{D}}_{ev}$ is the *deviatoric projection operator* in the space of the symmetric tensors:

$$\boldsymbol{\mathcal{D}}_{ev} = \boldsymbol{\mathcal{I}} - \frac{1}{3}\mathbf{I}\otimes\mathbf{I} \tag{4.24}$$

The expression $\boldsymbol{\mathcal{D}}^{\tau \mathrm{B}} \cdot \mathbf{B}$ which appears the first on the left hand side from the general spatial tangent operator for isotropic material (4.23) is computed for Neo-Hookean model as,

$$\boldsymbol{\mathcal{D}}^{\tau \mathrm{B}} \cdot \mathbf{B} = G\,\boldsymbol{\mathcal{D}}_{ev} \cdot \mathbf{B}_{iso} - \frac{1}{3}\boldsymbol{\tau}_d \otimes \mathbf{I} + \frac{1}{2}K\,\mathbf{I}\otimes\mathbf{I} \tag{4.25}$$

By inserting (4.25) into (4.16) the spatial tangent operator for the Neo-Hookean model is obtained.

4.4 Path dependent materials in small strain

4.4.1 Introduction

When the stress tensor is no longer a function of the instantaneous value of the infinitesimal strain only, the constitutive equation of the material model is *path-dependent.* This means that the stress tensor depends on the history of strains to which the solid has been subjected. It was explained in Section 2.7.1 that this kind of material is conventionally described with internal variables. For instance, in small strain the rate constitutive function is given by the set (2.75), (2.76). An example of path dependent-material is the elasto-plastic material which is described in the following section.

4.4.2 The incremental constitutive function

The implementation of the constitutive relation in the F.E. code requires a procedure for the evaluation of the stress for a given deformation (or increment of deformation from previous state). This was a straightforward function evaluation for hyperelasticity as explained in previous Section 4.3.2. In the case of the path-dependent materials it requires an integration of the rate form of the constitutive equations. The algorithm for integration of the rate form of the constitutive relation is called a *stress update algorithm* or *constitutive integration algorithm.*

In general, algorithms for integration of the rate constitutive equations are obtained by adopting some kind of time (or pseudotime) discretisation along with some hypothesis on the deformation path between adjacent time stations. Within the context of purely mechanical theory, considering the time increment $[\,t_n\,,\,t_{n+1}\,]$ and the given set $\boldsymbol{\alpha}_n$ of internal variables at t_n, the strain tensor $\boldsymbol{\epsilon}_{n+1}$ at time t_{n+1} must determine the stress $\boldsymbol{\sigma}_{n+1}$ uniquely through the integration algorithm. Such algorithm defines an approximate *incremental constitutive function*, $\hat{\boldsymbol{\sigma}}$, for the stress tensor:

$$\boldsymbol{\sigma}_{n+1} = \hat{\boldsymbol{\sigma}}(\boldsymbol{\alpha}_n\,,\boldsymbol{\epsilon}_{n+1}) \tag{4.26}$$

whose outcome, must tend to the exact solution of the actual evolution problem with vanishingly small strain increments. The numerical constitutive law is nonlinear in general and *path-independent* within one increment. That is, within each increment $\boldsymbol{\sigma}_{n+1}$ is a function of $\boldsymbol{\epsilon}_{n+1}$ alone since the argument $\boldsymbol{\alpha}_n$ is constant within the time step $[\,t_n\,,\,t_{n+1}\,]$. This make (4.26) analogous to a nonlinear elastic law within each time step.

The integration algorithm also defines an incremental constitutive function for the internal variables of the model as,

$$\boldsymbol{\alpha}_{n+1} = \hat{\boldsymbol{\alpha}}(\boldsymbol{\alpha}_n\,,\boldsymbol{\epsilon}_{n+1}). \tag{4.27}$$

In the context of elasto-plasticity, procedures such as elastic predictor/return mapping algorithm, later discussed in Section 4.6.2, provide a concrete example of numerical integration scheme for path dependent constitutive law.

4.4.3 The consistent tangent modulus

The *consistent tangent modulus* or *algorithmic modulus* that is associated with the constitutive integration algorithm, and therefore, is used in the development of the *stiffness matrix*, is presented. The consistent tangent operator is the derivative of the incremental constitutive function (4.26), therefore

$$\hat{\mathcal{C}} = \frac{\partial \hat{\sigma}}{\partial \epsilon_{n+1}}. \tag{4.28}$$

The generally implicit function (4.26) is typically defined by the integration algorithm for the rate constitutive equations of the model. The concept of the linearization of the incremental constitutive function was formalized by Simo & Taylor [46] in the context of elasto-plasticity. It is remarked that the full Newton-Raphson procedure, applied to solve the nonlinear F.E. equations (3.34), relies on the consistent tangent operator to reach the quadratic rate of convergence expected of the solution scheme.

4.5 The mathematical theory of plasticity

Materials for which permanent strains are developed upon loading are called plastic materials. Many materials exhibit elastic behaviour up to the so-called *yield stress*. The elasto-plastic materials are further classified as *rate-independent* elasto-plastic materials, where the stress is independent of the strain rate, and *rate-dependent* elasto plastic materials (or elasto-viscoplastic materials) in which the stress depends on the strain rate. In particular the theory outlined here is restricted to the materials (and conditions) for which the permanent deformations do not depend on the rate of application of loads or rate-independent plasticity.

The present section reviews very briefly the mathematical theory of plasticity. For more comprehensive treatment of the theory of plasticity reference [72] is recommended while reference [41] is recommended for more advanced treatment of the subject. The theory presented here is restricted to small strains and provides the basis for the numerical simulation of the behaviour of elasto-plastic solid discussed in Section 4.6.

4.5.1 General elasto-plastic constitutive model

A well-known mathematical model for uniaxial tension experiment has been described in [47] and [22]. The one-dimensional equations contain the basic ingredients of the general elasto-plastic constitutive model presented in the following:

- The elasto-plastic *strain decomposition*: $\boldsymbol{\epsilon} = \boldsymbol{\epsilon}^e + \boldsymbol{\epsilon}^p$
- An *elastic law*: $\boldsymbol{\sigma} = \boldsymbol{\mathcal{C}}^e : \boldsymbol{\epsilon}^e = \boldsymbol{\mathcal{C}}^e : (\boldsymbol{\epsilon} - \boldsymbol{\epsilon}^p)$
- A *yield criterion*, stated with the help of a yield function: $f(\boldsymbol{\sigma}, \boldsymbol{\alpha}) \leq 0$
- A plastic flow rule defining the evolution of the plastic straining: $\dot{\boldsymbol{\epsilon}}^p = \dot{\gamma}\,\mathbf{N}$
- A hardening law, characterising the evolution of the yield limit: $\dot{\boldsymbol{\alpha}} = \dot{\gamma}\,\mathbf{H}$

Additive decomposition of the strain tensor

The strain tensor, $\boldsymbol{\epsilon}$, is split into a sum of an elastic component, $\boldsymbol{\epsilon}^e$, and a plastic component, $\boldsymbol{\epsilon}^p$, as

$$\boldsymbol{\epsilon} = \boldsymbol{\epsilon}^e + \boldsymbol{\epsilon}^p \,. \tag{4.29}$$

The tensors $\boldsymbol{\epsilon}^e$ and $\boldsymbol{\epsilon}^p$ are known, respectively, as the *elastic strain tensor* and *plastic strain tensor*. In rate form (4.29) can also be expressed as,

$$\dot{\boldsymbol{\epsilon}} = \dot{\boldsymbol{\epsilon}}^e + \dot{\boldsymbol{\epsilon}}^p \,. \tag{4.30}$$

The elastic law

This work is focussed on materials whose elastic behaviour is linear and isotropic as described in Section 4.2. In this case, the general elastic law is given by:

$$\boldsymbol{\sigma} = \boldsymbol{\mathcal{C}}^e : \boldsymbol{\epsilon}^e = 2\,G\,\boldsymbol{\epsilon}^e_d + K\epsilon^e_v\,\mathbf{I} \tag{4.31}$$

where $\boldsymbol{\mathcal{C}}^e$ is the standard isotropic elasticity tensor given in (4.2) and G and K are the shear and bulk modulus, respectively. The tensor $\boldsymbol{\epsilon}^e_d$ is the deviatoric component of the elastic strain and the scalar $\epsilon^e_v \equiv \mathrm{tr}[\boldsymbol{\epsilon}^e]$ is the volumetric elastic strain.

The yield criterion and the yield surface

The yield criterion can be express as follows: The *yield function* f is negative when only elastic deformations are possible, and reach zero value when plastic flow is imminent. This concept is obtained by stating that the plastic flow may occur when

$$f(\boldsymbol{\sigma}, \boldsymbol{\alpha}) = 0 \,. \tag{4.32}$$

The yield function f defines the *elastic domain* as the following set of stresses

$$\mathbb{E} = \{\boldsymbol{\sigma} | f(\boldsymbol{\sigma}, \boldsymbol{\alpha}) < 0\} \,. \tag{4.33}$$

Admissible stress must lie either in the elastic domain or on its boundary. The set of *plastically admissible stress* is then defined as,

$$\bar{\mathbb{E}} = \{\boldsymbol{\sigma} | f(\boldsymbol{\sigma}, \boldsymbol{\alpha}) \leq 0\} \,. \tag{4.34}$$

The yield locus, i.e., the set of stresses for which plastic yielding may occur, is the boundary of the elastic domain, where $f(\boldsymbol{\sigma}, \boldsymbol{\alpha}) = 0$. The yield locus in this case is represented by a hypersurface in the space of stresses. This hypersurface is termed the *yield surface* and is defined as

$$\mathbb{Y} = \{\boldsymbol{\sigma} \mid f(\boldsymbol{\sigma}, \boldsymbol{\alpha}) = 0\}\,. \tag{4.35}$$

Therefore, any admissible stress must satisfy the restriction:

$$f(\boldsymbol{\sigma}, \boldsymbol{\alpha}) \leq 0 \tag{4.36}$$

The plastic flow rule

The complete characterization of the general plasticity model requires the definition of the evolutions laws for the internal variables, i.e.variables associated with the dissipative phenomena. In the present case, the internal variables are the plastic strain tensor $\boldsymbol{\epsilon}^p$ and the set $\boldsymbol{\alpha}$ of hardening variables.

The *plastic flow rule* is postulated as,

$$\dot{\boldsymbol{\epsilon}}^p = \dot{\gamma}\,\mathbf{N} \tag{4.37}$$

where the scalar $\dot{\gamma}$ is called the *plastic multiplier*. The plastic multiplier is *non-negative*,

$$\dot{\gamma} \geq 0\,, \tag{4.38}$$

and it satisfies the *complementary condition*:

$$f\,\dot{\gamma} = 0\,. \tag{4.39}$$

The tensor $\mathbf{N}$ included in (4.37) defines the flow direction

$$\mathbf{N} = \mathbf{N}(\boldsymbol{\sigma}, \boldsymbol{\alpha}) \tag{4.40}$$

where $\boldsymbol{\alpha}$ is the *hardening thermodynamical force.*

The hardening law

The phenomenon known as *hardening* consists of an evolution of the yield stress that accompanies the evolution of the plastic strain. It can be incorporated into the general

elasto-plastic model by simply assuming an evolution for the hardening variables as,

$$\dot{\boldsymbol{\alpha}} = \dot{\gamma}\,\mathbf{H} \tag{4.41}$$

where $\mathbf{H}$ is the *generalised hardening modulus* which defines the evolution of the hardening variables

$$\mathbf{H} = \mathbf{H}(\boldsymbol{\sigma}, \boldsymbol{\alpha})\,. \tag{4.42}$$

In this work it is assumed that the material follows the *associative plastic model*, which means that the plastic flow rule and the hardening law are defined in terms of *flow* or *plastic potential*. Moreover, it is assumed that the flow potential coincides with the yield function f; therefore, the flow vector is obtained as,

$$\mathbf{N} = \frac{\partial f}{\partial \boldsymbol{\sigma}} \tag{4.43}$$

and the hardening modulus is

$$\mathbf{H} = -\frac{\partial f}{\partial \boldsymbol{\alpha}}\,. \tag{4.44}$$

4.5.2 The von Mises model

A special case of the general case presented above is the von Mises J_2 flow model based on a von Mises yield surface. This model is specially useful for metal plasticity, for it was firstly developed in [91]. For a thorough discussion about this model see [41]. The key assumption of this model is that the plastic flow in metals is unaffected by pressure.

The von Mises yield criterion

It states that "*plastic yielding begins when the J_2 invariant of the deviatoric stress reaches a critical value*"; therefore, the yield function for the von Mises criterion can be formulated as,

$$f(\boldsymbol{\sigma}, \alpha) = q(\boldsymbol{\sigma}) - \sigma_y(\alpha)\,, \tag{4.45}$$

where σ_y is the uniaxial yield stress (see [41]), and

$$q(\boldsymbol{\sigma}) \equiv \sqrt{3\,J_2(\boldsymbol{s})} \tag{4.46}$$

is termed the *von Mises effective or equivalent stress.* The equivalent stress depends only on the deviatoric part of the Cauchy or true stress $\boldsymbol{s} = \boldsymbol{\sigma}_d = \text{dev}[\boldsymbol{\sigma}]$. The deviatoric stress $\boldsymbol{s}$ is a traceless tensor, hence the effective stress (4.46) can be computed using the definition for the second invariant given in (4.10) as follows

$$q(\boldsymbol{\sigma}) = \sqrt{\tfrac{3}{2}\boldsymbol{s} : \boldsymbol{s}} = \sqrt{\frac{3}{2}}\,\|\boldsymbol{s}\|\,. \tag{4.47}$$

The Prandtl-Reuss flow rule for von Mises model

The Prandtl-Reuss plasticity law is the flow rule obtained by taking the von Mises yield function (4.45) as a flow potential. The corresponding flow vector is given as,

$$\mathbf{N} \equiv \frac{\partial}{\partial \boldsymbol{\sigma}}[\sqrt{3\,J_2(\boldsymbol{s})}] = \sqrt{\frac{3}{2}}\frac{\boldsymbol{s}}{\|\boldsymbol{s}\|}\,. \tag{4.48}$$

4.5.3 Hardening law

Hardening is characterised by the dependence of the yield stress level upon the history of the plastic straining to which the body has been subjected. Hardening is represented by changes in the hardening thermodynamical force $\boldsymbol{\alpha}$, during plastic yielding.

Perfect plasticity

A material model is said to be *perfectly plastic* if no hardening is allowed, that is, the yield stress level does not depend in any way on the degree of plastification. In this case, the the yield surface remains fixed regardless of any deformation process the material may suffer.

Isotropic Hardening

A model is said to have isotropic hardening if the evolution of the yielding surface is such that, at any stage of hardening, it corresponds to an uniform (isotropic) expansion of the initial yield surface, without translation.

The suitable choice of the set $\boldsymbol{\alpha}$ of hardening internal variables, must obviously depend on the specific characteristic of the material considered. In treatment of isotropic hardening, the set $\boldsymbol{\alpha}$ is identified with a single *scalar* variable α, which determines the size of the yield surface. One of the most popular approaches, followed in this work, is the *strain hardening* model.

In strain hardening models, the *effective plastic strain*, $\bar{\epsilon}^p$ is chosen as the internal variable α associates with isotropic hardening. The effective plastic strain is defined as,

$$\bar{\epsilon}^p \equiv \int_0^t \sqrt{\frac{2}{3}\dot{\boldsymbol{\epsilon}}^p : \dot{\boldsymbol{\epsilon}}^p}\, \mathrm{d}t = \int_0^t \sqrt{\frac{2}{3}}\, \|\dot{\boldsymbol{\epsilon}}^p\|\, \mathrm{d}t\,, \tag{4.49}$$

The variable $\bar{\epsilon}^p$ is also known as the *generalised* or *accumulated* plastic strain and its evolution law is given by:

$$\dot{\bar{\epsilon}}^p = \sqrt{\frac{2}{3}\dot{\boldsymbol{\epsilon}}^p : \dot{\boldsymbol{\epsilon}}^p} = \sqrt{\frac{2}{3}}\, \|\dot{\boldsymbol{\epsilon}}^p\|\,. \tag{4.50}$$

The effect of the hardening variable, on the size of the yield surface, is introduced by making the yield stress dependent on $\bar{\epsilon}^p$. For instance, in the von Mises criterion the uniaxial yield stress is given as

$$\sigma_y = \sigma_y(\bar{\epsilon}^p)\,. \tag{4.51}$$

The function (4.51) defines the so-called *hardening curve*. If the yield stress σ_y is a linear function of the effective plastic strain $\bar{\epsilon}^p$, the model is said to be *linear hardening*.

4.6 F.E. in small strain plasticity

4.6.1 Introduction

In the previous Section 4.5, the mathematical theory of plasticity has been reviewed. This section describes the numerical/computational procedures necessary for the general framework of Chapter 3. The methodology presented in this section is firstly derived for the general plasticity model introduced in Section 4.5. Finally the von Mises model with isotropic-linear hardening is briefly described as it has been used in the numerical examples in Chapter 9. For further details about the F.E. implementation in plasticity we recommend references [24] and [22].

4.6.2 The general operator split algorithm for elasto-plasticity

In this Section an algorithm for numerical integration of the elasto-plastic constitutive equations is derived. Due to the additive structure of the total strain rate (4.30), the original value problem of elasto-plasticity is split into a sequence of two subproblems, the *elastic predictor* and the *plastic corrector*, as described below.

Firstly, we solve the *elastic predictor* problem, in which the material is assumed to behave purely elastically between times t_n and t_{n+1}, with the internal variables $\boldsymbol{\alpha}$ *frozen* during the time interval $[t_n, t_{n+1}]$.

The solution of the elastic predictor at time t_{n+1}, denoted by $\boldsymbol{\epsilon}^{e\,trial}_{n+1}$, $\boldsymbol{\epsilon}^{p\,trial}_{n+1}$ and $\boldsymbol{\alpha}^{e\,trial}_{n+1}$, define the so-called *elastic trial state.* The next step in the elasto-plastic operator split algorithm consist of taking the elastic trial state as initial condition for the plastic corrector problem.

Finally, the solution obtained from the plastic corrector at t_{n+1}, denoted

$$\{\boldsymbol{\sigma}_{n+1}, \boldsymbol{\epsilon}^{e}_{n+1}, \boldsymbol{\epsilon}^{p}_{n+1}, \boldsymbol{\alpha}_{n+1}\}$$

is an approximation to the solution of the actual elasto-plastic initial value problem at t_{n+1}. The solution to each of the split subproblems is discussed in the following:

Elastic Predictor

The *elastic trial state* at t_{n+1}, is given by:

$$\boldsymbol{\epsilon}^{e\,trial}_{n+1} = \boldsymbol{\epsilon}^{e}_{n} + \triangle\boldsymbol{\epsilon} \tag{4.52}$$

$$\boldsymbol{\epsilon}^{p\,trial}_{n+1} = \boldsymbol{\epsilon}^{p}_{n} \tag{4.53}$$

$$\boldsymbol{\alpha}^{trial}_{n+1} = \boldsymbol{\alpha}_{n} \tag{4.54}$$

where $\triangle\boldsymbol{\epsilon}$ is the prescribed increment of total displacement within the interval $[t_n, t_{n+1}]$. The associated *elastic trial stress* is computed following the constitutive elastic law for linear elastic material given in (4.1) as,

$$\boldsymbol{\sigma}^{trial}_{n+1} = \boldsymbol{\mathcal{C}}^{e} : \boldsymbol{\epsilon}^{e\,trial}_{n+1}\,. \tag{4.55}$$

Now admissibility check is performed, using the trial yield function. If the elastic state lies inside the elastic domain (or on its boundary) $f^{trial}_{n+1} \equiv f(\boldsymbol{\sigma}^{trial}_{n+1}, \boldsymbol{\alpha}^{trial}_{n+1}) \leq 0$, the trial state is the solution, otherwise, $f^{trial}_{n+1} \equiv f(\boldsymbol{\sigma}^{trial}_{n+1}, \boldsymbol{\alpha}^{trial}_{n+1}) > 0$ and plastic corrector is necessary.

Plastic corrector. The return mapping

One possibility to integrate the plastic corrector equations consist of adopting a *fully implicit backward Euler scheme* to discretise it. The implicit backward Euler discretisation reduces the problem to the following system of nonlinear equations:

$$\boldsymbol{\epsilon}^e_{n+1} = \boldsymbol{\epsilon}^{e\,trial}_{n+1} - \triangle\gamma\,\mathbf{N}_{n+1} = \boldsymbol{\epsilon}^e_n + \triangle\boldsymbol{\epsilon} - \triangle\gamma\,\mathbf{N}_{n+1} \tag{4.56}$$

$$\boldsymbol{\epsilon}^p_{n+1} = \boldsymbol{\epsilon}^{p\,trial}_{n+1} + \triangle\gamma\,\mathbf{N}_{n+1} = \boldsymbol{\epsilon}^p_n + \triangle\gamma\,\mathbf{N}_{n+1} \tag{4.57}$$

$$\boldsymbol{\alpha}_{n+1} = \boldsymbol{\alpha}^{trial}_{n+1} + \triangle\gamma\,\mathbf{H}_{n+1} = \boldsymbol{\alpha}_n + \triangle\gamma\,\mathbf{H}_{n+1} \tag{4.58}$$

$$\triangle\gamma \geq 0 \quad f_{n+1} \leq 0 \quad \triangle\gamma\, f_{n+1} = 0 \tag{4.59}$$

where $f_{n+1} = f(\boldsymbol{\sigma}_{n+1}, \boldsymbol{\alpha}_{n+1})$ with

$$\boldsymbol{\sigma}_{n+1} = \boldsymbol{\mathcal{C}}^e : \boldsymbol{\epsilon}^e_{n+1} = \boldsymbol{\sigma}^{trial}_{n+1} - \triangle\gamma\ \boldsymbol{\mathcal{C}}^e : \mathbf{N}_{n+1}\,. \tag{4.60}$$

and

$$\mathbf{N}_{n+1} = \frac{\partial f}{\partial \boldsymbol{\sigma}_{n+1}} \quad , \quad \mathbf{H}_{n+1} = -\frac{\partial f}{\partial \boldsymbol{\alpha}_{n+1}}\,. \tag{4.61}$$

If the elastic trial state lies outside the elastic domain $f(\boldsymbol{\sigma}^{trial}_{n+1}, \boldsymbol{\alpha}^{trial}_{n+1}) > 0$, i.e. the elastic trial states violates admissibility. The system to be solved consists of (4.56), (4.58) and $f(\boldsymbol{\sigma}_{n+1}, \boldsymbol{\alpha}_{n+1}) = 0$, where the *incremental plastic multiplier* $\triangle\gamma$ is required to be strictly positive, $\triangle\gamma > 0$. Once the system is solved, the plastic strain can be updated a posteriori by means of (4.57).

For a detailed account of the return mapping algorithm, its graphical interpretation and solution see [47] and [22].

4.6.3 Integration algorithm for the von Mises model with isotropic hardening

In this section, the fully implicit return mapping algorithm, explained in previous Section 4.6.2, is particularised for the von Mises model described in Section 4.5.2.

Elastic Predictor

Given the increment of strain $\triangle\boldsymbol{\epsilon}$, corresponding to the (pseudo-) time increment $[t_n, t_{n+1}]$, and given the state variables $\{\boldsymbol{\epsilon}^e_n, \bar{\epsilon}^p_n\}$ at t_n, the elastic trial strain and trial accumulated plastic strain at t_{n+1}, are given by:

$$\boldsymbol{\epsilon}^{e\,trial}_{n+1} = \boldsymbol{\epsilon}^e_n + \triangle\boldsymbol{\epsilon} \tag{4.62}$$

$$\bar{\epsilon}^{p\,trial}_{n+1} = \bar{\epsilon}^{p}_{n}\,. \tag{4.63}$$

The corresponding elastic trial stress is computed as:

$$\boldsymbol{\sigma}^{trial}_{n+1} = \boldsymbol{\mathcal{C}}^{e} : \boldsymbol{\epsilon}^{e\,trial}_{n+1}\,, \tag{4.64}$$

or, equivalently, by applying the hydrostatic/deviatoric decomposition,

$$\boldsymbol{s}^{trial}_{n+1} = 2G\,\boldsymbol{\epsilon}^{e\,trial}_{d\,n+1} \qquad \text{and} \qquad p^{trial}_{n+1} = K\,\epsilon^{e\,trial}_{v\,n+1}\,, \tag{4.65}$$

where $\boldsymbol{s}$ is the deviatoric stress and p the hydrostatic pressure. The trial yield stress is simply

$$\sigma^{trial}_{y\,n+1} = \sigma_y(\bar{\epsilon}^{p}_{n}) = \sigma_{y\,n}. \tag{4.66}$$

Having computed the elastic trial state, the next step in the algorithm is to check whether $\boldsymbol{\sigma}^{trial}_{n+1}$ lies inside or outside of the trial yield surface:

- If $\boldsymbol{\sigma}^{trial}_{n+1}$ lies inside the trial surface, i.e., if $f(\boldsymbol{\sigma}^{trial}_{n+1}, \sigma_{y\,n}) \leq 0$, then the process within the interval $[t_n, t_{n+1}]$ is purely elastic and the elastic trial state itself is the solution to the integration problem.
- Otherwise, the process is elasto-plastic within the time step $[t_n, t_{n+1}]$ and the *return mapping* procedure described below has to be applied.

Plastic corrector

In the present case, the direct specialisation of the general fully implicit return mapping equations to the von Mises model gives the set of nonlinear equations:

$$\boldsymbol{\epsilon}^{e}_{n+1} = \boldsymbol{\epsilon}^{e\,trial}_{n+1} - \triangle\gamma\sqrt{\frac{3}{2}}\frac{\boldsymbol{s}_{n+1}}{\|\boldsymbol{s}_{n+1}\|} = \boldsymbol{\epsilon}^{e}_{n} + \triangle\boldsymbol{\epsilon} - \triangle\gamma\sqrt{\frac{3}{2}}\frac{\boldsymbol{s}_{n+1}}{\|\boldsymbol{s}_{n+1}\|} \tag{4.67}$$

$$\bar{\epsilon}^{p}_{n+1} = \bar{\epsilon}^{p}_{n} + \triangle\gamma \tag{4.68}$$

$$q_{n+1} - \sigma_y(\bar{\epsilon}^{p}_{n+1}) = 0 \tag{4.69}$$

where $q_{n+1} = \sqrt{3J_2(\boldsymbol{s}_{n+1})}$. This set has to be solved for $\boldsymbol{\epsilon}^{e}_{n+1}$, $\bar{\epsilon}^{p}_{n+1}$ and $\triangle\gamma$. The deviatoric stress $\boldsymbol{s}_{n+1}$ is given as,

$$\boldsymbol{s}_{n+1} = \boldsymbol{s}_{n+1}(\boldsymbol{\epsilon}^e_{n+1}) = 2\,G\,\mathrm{dev}[\boldsymbol{\epsilon}^e_{n+1}]\,. \tag{4.70}$$

After the solution of the above system, the plastic strain tensor can be updated according to the following equation:

$$\boldsymbol{\epsilon}^p_{n+1} = \boldsymbol{\epsilon}^p_n + \triangle\gamma\sqrt{\frac{3}{2}}\frac{\boldsymbol{s}_{n+1}}{\|\boldsymbol{s}_{n+1}\|}\,. \tag{4.71}$$

It is remarked that the above system can be substantially simplified. In fact, the return mapping von Mises model can be reduced to a *single* nonlinear equation having the incremental plastic multiplier $\triangle\gamma$ as the only variable.

Upon the system (4.67) - (4.69), it should be noted that the von Mises flow vector is *purely deviatoric*, so that the deviatoric/volumetric split of (4.67) gives:

$$\epsilon^e_{v\,n+1} = \epsilon^{e\,trial}_{v\,n+1} \tag{4.72}$$

$$\boldsymbol{\epsilon}^e_{d\,n+1} = \boldsymbol{\epsilon}^{e\,trial}_{d\,n+1} - \triangle\gamma\sqrt{\frac{3}{2}}\frac{\boldsymbol{s}_{n+1}}{\|\boldsymbol{s}_{n+1}\|} \tag{4.73}$$

Equivalently, in terms of the stresses,

$$p_{n+1} = p^{trial}_{n+1} \tag{4.74}$$

$$\boldsymbol{s}_{n+1} = \boldsymbol{s}^{trial}_{n+1} - \triangle\gamma\,2\,G\sqrt{\frac{3}{2}}\frac{\boldsymbol{s}_{n+1}}{\|\boldsymbol{s}_{n+1}\|} \tag{4.75}$$

that is the return mapping affects only the deviatoric stress component. The hydrostatic stress, p_{n+1} has the value computed in the elastic predictor stage, and it can be eliminated from the system of equations. After further simplifications given in [22], the system of equations for the return mapping von Mises model is reduced to the following *scalar*(generally nonlinear) equation having the incremental plastic multiplier, $\triangle\gamma$, as the only unknown:

$$q^{trial}_{n+1} - 3\,G\,\triangle\gamma - \sigma_y(\bar{\epsilon}^p_n + \triangle\gamma) = 0\,. \tag{4.76}$$

The above equation is then solved by the Newton-Raphson method. Once it is solved, with $\triangle\gamma$ at hand, the state variables are updated as follows:

$$\boldsymbol{s}_{n+1} = \left(1 - \frac{\triangle\gamma\, 3\, G}{q^{trial}_{n+1}}\right) \boldsymbol{s}^{trial}_{n+1} \tag{4.77}$$

$$\boldsymbol{\sigma}_{n+1} = \boldsymbol{s}_{n+1} + p^{trial}_{n+1}\, \mathbf{I} \tag{4.78}$$

$$\boldsymbol{\epsilon}^{e}_{n+1} = \boldsymbol{\mathcal{C}}^{e-1} : \boldsymbol{\sigma}_{n+1} = \frac{1}{2\, G}\, \boldsymbol{s}_{n+1} + \frac{1}{3}\, \boldsymbol{\epsilon}^{e\, trial}_{v\, n+1} \tag{4.79}$$

$$\bar{\epsilon}^{p}_{n+1} = \bar{\epsilon}^{p}_{n} + \triangle\gamma \tag{4.80}$$

The plastic strain tensor is updated by means of (4.71).

It should be noted that the only source of nonlinearity in the von Mises return mapping equation (4.76) is the *hardening curve*, defined by the given function $\sigma_y = \sigma_y(\bar{\epsilon}^p)$. For *linear hardening* materials, this function is linear and is expressed by

$$\sigma_y(\bar{\epsilon}^p) = \sigma_0 + H\, \bar{\epsilon}^p\,, \tag{4.81}$$

where σ_0 is the initial yield stress of the virgin material and H is the (constant) hardening slope. In such case, (4.76) reads as,

$$q^{trial}_{n+1} - 3\, G\, \triangle\gamma - [\sigma_0 + (\bar{\epsilon}^p_n + \triangle\gamma) H] = 0 \tag{4.82}$$

and the incremental plastic multiplier can be obtained in *closed form* as,

$$\triangle\gamma = \frac{f^{trial}}{3\, G + H}\,, \tag{4.83}$$

where f^{trial} is the yield function value at the elastic trial state.

4.6.4 The consistent tangent operator in elasto-plasticity

Introduction

In Section 4.4.3, the consistent tangent operator was introduced in general context of the path dependent materials as the one used in the computation of the element tangent stiffness. In this section the tangent operator is explained in the context of elasto-plastic materials. The von Mises elasto-plastic model with isotropic hardening is outlined now as a particularisation.

Consistent tangent operator

Elasto-plastic materials require in general some kind of numerical integration algorithm to update the stress tensor, as shown in Section 4.6.2. Basically, given the known internal variables set $\boldsymbol{\alpha}_n$ and the new prescribed total strain $\boldsymbol{\epsilon}_{n+1}$ as input, the general procedure, described in Section 4.6.2, will deliver the updated stress $\boldsymbol{\sigma}_{n+1}$ as the result of the application of the particular numerical algorithm. This defines an algorithmic constitutive function, $\hat{\boldsymbol{\sigma}}$ (4.26), for the Cauchy stress tensor:

$$\boldsymbol{\sigma}_{n+1} = \hat{\boldsymbol{\sigma}}(\boldsymbol{\alpha}_n\,, \boldsymbol{\epsilon}_{n+1}) \tag{4.84}$$

It should be noted that within a load increment $[t_n, t_{n+1}]$, the internal variable set $\boldsymbol{\alpha}_n$ (given as an argument of $\hat{\boldsymbol{\sigma}}$) is *constant*, therefore only the total strain $\boldsymbol{\epsilon}_{n+1}$, change during the global Newton iteration. In other words, within each load increment the Cauchy stress $\boldsymbol{\sigma}_{n+1}$ delivered by the integration algorithm is a function of the total strain tensor $\boldsymbol{\epsilon}_{n+1}$ *only*. This function $\hat{\boldsymbol{\sigma}}(\boldsymbol{\alpha}_n\,, \boldsymbol{\epsilon}_{n+1})$, with $\boldsymbol{\alpha}_n$ fixed, defines a stress/strain relation equivalent to a nonlinear elastic law. The consistent tangent modulus is the derivative of this equivalent nonlinear law,

$$\hat{\boldsymbol{\mathcal{C}}} \equiv \frac{\mathrm{d}\hat{\boldsymbol{\sigma}}}{\mathrm{d}\boldsymbol{\epsilon}_{n+1}} = \left.\frac{\partial\hat{\boldsymbol{\sigma}}}{\partial\boldsymbol{\epsilon}_{n+1}}\right|_{\boldsymbol{\alpha}_n}. \tag{4.85}$$

It is worth remarking that, rather than the total strain $\boldsymbol{\epsilon}_{n+1}$, the *elastic trial strain* $\boldsymbol{\epsilon}_{n+1}^{e\,trial}$ is the actual input to the integration procedure. It can be seen in [22] that the following identity is valid

$$\hat{\boldsymbol{\mathcal{C}}} = \frac{\partial\hat{\boldsymbol{\sigma}}}{\partial\boldsymbol{\epsilon}_{n+1}} = \frac{\partial\hat{\boldsymbol{\sigma}}}{\partial\boldsymbol{\epsilon}_{n+1}^{e\,trial}}\,. \tag{4.86}$$

Crucial to the derivation of the elasto-plastic consistent tangent modulus is the fact that the Cauchy stress $\boldsymbol{\sigma}_{n+1}$ is defined *implicitly* through the corresponding nonlinear system. In others words, $\boldsymbol{\sigma}_{n+1}$ is an *implicit function* of the elastic trial strain $\boldsymbol{\epsilon}_{n+1}^{e\,trial}$. Thus, the consistent tangent operator $\hat{\boldsymbol{\mathcal{C}}}$ is simply the *derivative if the implicit function defined by the return mapping equations* and it is derived by following the standard procedure for differentiation of implicit functions.

The elasto-plastic consistent tangent modulus for the von Mises model with isotropic hardening

The implicit elastic predictor/return mapping algorithm for the von Mises model has been described in Section 4.6.3. In this section the elasto-plastic tangent operator consistent with the von Mises implicit return mapping is presented.

In view of the volumetric/deviatoric decoupling of the von Mises model, the tangent relations:

$$\frac{\mathrm{d}p_{n+1}}{\mathrm{d}\epsilon_{v\,n+1}^{e\,trial}} \quad \text{and} \quad \frac{\mathrm{d}\boldsymbol{s}_{n+1}}{\mathrm{d}\boldsymbol{\epsilon}_{d\,n+1}^{e\,trial}}, \tag{4.87}$$

respectively are derived first. The full consistent tangent operator is subsequently obtained by assembling the hydrostatic and deviatoric contributions.

The hydrostatic tangent relation

The constitutive function for the hydrostatic pressure, p_{n+1}, is an *explicit* function of the elastic trial volumetric strain, $\epsilon_{v\,n+1}^{e\,trial}$. It is given by combining (4.74) and (4.65) as,

$$p_{n+1} = K\,\epsilon_{v\,n+1}^{e\,trial}\,. \tag{4.88}$$

The tangent relation is therefore,

$$\frac{\mathrm{d}p_{n+1}}{\mathrm{d}\epsilon_{v\,n+1}^{e\,trial}} = K, \tag{4.89}$$

where K is the bulk modulus.

The deviatoric tangent relation

The constitutive function for the deviatoric stress, $\boldsymbol{s}_{n+1}$, is an *implicit* function of the elastic trial deviatoric strain, $\boldsymbol{\epsilon}_{d\,n+1}^{e\,trial}$:

$$\boldsymbol{s}_{n+1} = \hat{\boldsymbol{s}}(\boldsymbol{\epsilon}_{d\,n+1}^{e\,trial})\,. \tag{4.90}$$

The elastic trial von Mises effective stress is given by,

$$q_{n+1}^{trial} = q(\boldsymbol{s}_{n+1}^{trial}) = \sqrt{\tfrac{3}{2}\boldsymbol{s}_{n+1}^{trial} : \boldsymbol{s}_{n+1}^{trial}} = \sqrt{\frac{3}{2}}\,\|\boldsymbol{s}_{n+1}^{trial}\|\,. \tag{4.91}$$

Using the deviatoric elastic constitutive law (4.70), for the trial state, the above (4.91) is transformed as,

$$q_{n+1}^{trial} = 2\,G\,\sqrt{\tfrac{3}{2}\boldsymbol{\epsilon}_{d\,n+1}^{trial} : \boldsymbol{\epsilon}_{d\,n+1}^{trial}} = 2\,G\,\sqrt{\frac{3}{2}}\,\|\boldsymbol{\epsilon}_{d\,n+1}^{trial}\|\,. \tag{4.92}$$

By substituting (4.92) into the single equation of the return mapping for the von Mises elasto-plastic model, defined in (4.76), it follows

$$2\,G\sqrt{\frac{3}{2}}\,\|\boldsymbol{\epsilon}^{trial}_{dn+1}\| - 3\,G\,\triangle\gamma - \sigma_y(\bar{\epsilon}^p_n + \triangle\gamma) = 0\,. \tag{4.93}$$

The updated formula for the deviatoric stress given at (4.77) can also be changed using the above as,

$$\boldsymbol{s}_{n+1} = \left(1 - \frac{\triangle\gamma\,3\,G}{2\,G\sqrt{\frac{3}{2}}\,\|\boldsymbol{\epsilon}^{trial}_{dn+1}\|}\right)2\,G\,\boldsymbol{\epsilon}^{trial}_{dn+1} \tag{4.94}$$

For a given $\bar{\epsilon}^p_n$, equation (4.93) together with the algorithmic updated formula (4.94) define the deviatoric stress $\boldsymbol{s}_{n+1}$.

Once $\hat{\boldsymbol{s}}$ is defined by (4.93) and (4.94), the next step is its differentiation. Details of this step are skipped in this work, and the reader is referred to [46], [47] and [22] for full derivation. Hence, the deviatoric tangent relation consistent with the implicit return mapping of the von Mises model is given by,

$$\frac{\mathrm{d}\boldsymbol{s}_{n+1}}{\mathrm{d}\boldsymbol{\epsilon}^{e\,trial}_{dn+1}} = 2\,G\left(1 - \frac{\triangle\gamma\,3\,G}{q^{trial}_{n+1}}\right)\boldsymbol{\mathcal{I}} + 6\,G^2\left(\frac{\triangle\gamma}{q^{trial}_{n+1}} - \frac{1}{3\,G + H}\right)\bar{\mathbf{N}}_{n+1}\otimes\bar{\mathbf{N}}_{n+1} \tag{4.95}$$

where $\bar{\mathbf{N}}_{n+1}$ is the *unit* flow vector defined as,

$$\bar{\mathbf{N}}_{n+1} = \frac{\boldsymbol{s}^{trial}_{n+1}}{\|\boldsymbol{s}^{trial}_{n+1}\|}\,. \tag{4.96}$$

The full elasto-plastic consistent tangent

Having determined the hydrostatic and consistent tangents, the next step now is to assemble them into the full elasto-plastic tangent operator. In the integration algorithm, after the computation of the deviatoric stress, $\boldsymbol{s}_{n+1}$, and the hydrostatic pressure, p_{n+1}, the stress $\boldsymbol{\sigma}_{n+1}$ is evaluated as,

$$\boldsymbol{\sigma}_{n+1} = \boldsymbol{s}_{n+1} + p_{n+1}\mathbf{I}. \tag{4.97}$$

In terms of the algorithmic constitutive functions described above,

$$\boldsymbol{\sigma}_{n+1} = \hat{\boldsymbol{s}}(\boldsymbol{\epsilon}^{trial}_{dn+1}) + \hat{p}(\epsilon^{trial}_{vn+1})\mathbf{I}. \tag{4.98}$$

Differentiation of the above formula with a straightforward application of the chain rule gives

$$\frac{\mathrm{d}\boldsymbol{\sigma}_{n+1}}{\mathrm{d}\boldsymbol{\epsilon}^{e\,trial}_{n+1}} = \frac{\mathrm{d}\boldsymbol{s}_{n+1}}{\mathrm{d}\boldsymbol{\epsilon}^{e\,trial}_{d\,n+1}} : \frac{\mathrm{d}\boldsymbol{\epsilon}^{e\,trial}_{d\,n+1}}{\mathrm{d}\boldsymbol{\epsilon}^{e\,trial}_{n+1}} + \frac{\mathrm{d}p_{n+1}}{\mathrm{d}\epsilon^{trial}_{v\,n+1}}\mathbf{I}\otimes\frac{\mathrm{d}\epsilon^{e\,trial}_{v\,n+1}}{\mathrm{d}\boldsymbol{\epsilon}^{e\,trial}_{n+1}} \tag{4.99}$$

The derivatives of the deviatoric and volumetric elastic trial strain with respect to the elastic trial strain tensor, which appear in the above formula, can be easily determined by considering the definition of deviatoric and volumetric component of a generic strain tensor, $\boldsymbol{\epsilon}$:

$$\epsilon_v \equiv \mathrm{tr}[\boldsymbol{\epsilon}] = \mathbf{I} : \boldsymbol{\epsilon} \qquad \boldsymbol{\epsilon}_d \equiv \boldsymbol{\epsilon} - \frac{1}{3}\epsilon_v\mathbf{I} = [\boldsymbol{\mathcal{I}} - \frac{1}{3}\mathbf{I}\otimes\mathbf{I}] : \boldsymbol{\epsilon}\,. \tag{4.100}$$

From these relationships, it follows that:

$$\frac{\mathrm{d}\boldsymbol{\epsilon}^{e\,trial}_{d\,n+1}}{\mathrm{d}\boldsymbol{\epsilon}^{e\,trial}_{n+1}} = \boldsymbol{\mathcal{I}} - \frac{1}{3}\mathbf{I}\otimes\mathbf{I} \qquad \frac{\mathrm{d}\epsilon^{e\,trial}_{v\,n+1}}{\mathrm{d}\boldsymbol{\epsilon}^{e\,trial}_{n+1}} = \mathbf{I}\,. \tag{4.101}$$

Finally, substitution of the last two expressions, together with (4.95) and (4.89) into (4.99) results in the following formula for the elasto-plastic tangent operator consistent with the return mapping scheme for the von Mises model:

$$\hat{\boldsymbol{\mathcal{C}}} \equiv \frac{\mathrm{d}\boldsymbol{\sigma}_{n+1}}{\mathrm{d}\boldsymbol{\epsilon}^{e\,trial}_{n+1}} = 2\,G\left(1-\frac{\triangle\gamma\,3\,G}{q^{trial}_{n+1}}\right)[\boldsymbol{\mathcal{I}}-\frac{1}{3}\mathbf{I}\otimes\mathbf{I}]+6\,G^2\left(\frac{\triangle\gamma}{q^{trial}_{n+1}}-\frac{1}{3\,G+H}\right)\bar{\mathbf{N}}_{n+1}\otimes\bar{\mathbf{N}}_{n+1}+K\,\mathbf{I}\otimes\mathbf{I} \tag{4.102}$$

The use of the consistent tangent operator in the context of elasto-plastic model solved by the Newton-Raphson procedure was firstly introduced by Simo & Taylor [46]. The convergence of the Newton scheme relies on the use of the consistent tangent operator.

4.7 Conclusion

In this chapter the stress has been established as a function of the instantaneous deformation and a set of internal variables. In the following chapters the multiscale theory will be developed. The material models illustrated during this chapter govern the microstructural behaviour of the microstructures in the multiscale analysis performed in numerical examples in Chapter 9.

Chapter 5

Multiscale continuum model at small strains

5.1 Introduction

In this Chapter, a general continuum multiscale model at small strain is described. The Chapter 2 gives the continuum mechanics background related to this Chapter.

5.1.1 Outline

Firstly, a general multiscale continuum description is given. A strain-driven microstructure analysis is assumed, where the macroscopic strain is prescribed over the microstructure as an average. Then the basic microvariables and macrovariables are introduced. The Hill-Mandel principle or averaging theorem is given to link the scales. Finally, three classical conditions are given, to prescribe the macrostrain over the microstructure:

- Taylor assumption over the microstructure.
- Linear displacement on the boundary (Linear b.c.).
- Periodic displacement and antiperiodic traction on the boundary (Periodic b.c.).

5.2 Continuum macro and microscale

A homogenized macro-continuum with locally attached microstructures visualized in Figure 5.1 is considered. The microstructure $\mathbb{B} \subset \mathbb{R}^3$ is considered, with overall properties related to the macrocontinuum $\overline{\mathbb{B}} \subset \mathbb{R}^3$.

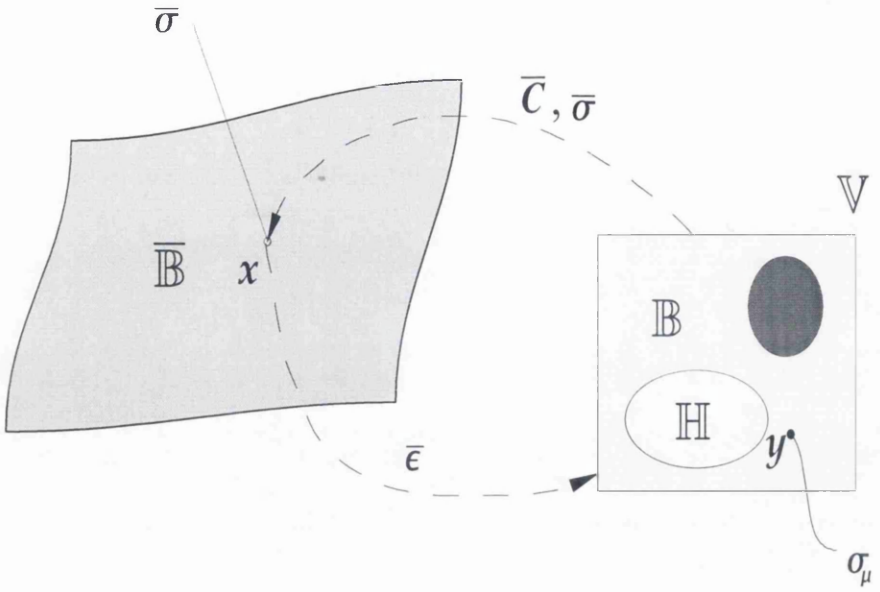

Figure 5.1: Micro to macro transition

A point $\boldsymbol{x} \in \overline{\mathbb{B}}$ of the homogenized macromedium $\overline{\mathbb{B}} \subset \mathbb{R}^3$ is represented as a microstructure $\mathbb{B} \subset \mathbb{R}^3$. The tensors $\overline{\boldsymbol{\sigma}}$ and $\boldsymbol{\sigma}_\mu$ denote the macro and micro Cauchy stress tensor at $\boldsymbol{x} \in \overline{\mathbb{B}}$ and $\boldsymbol{y} \in \mathbb{B}$, respectively. The Representative Volume Element (RVE) of the microstructure $\mathbb{V} \subset \mathbb{R}^3$ represents the part of the heterogeneous material consisting of the solid part $\mathbb{B}$ and the hole $\mathbb{H}$, i.e. $\mathbb{V} = \mathbb{B} \cup \mathbb{H}$ and $\partial\mathbb{B} = \partial\mathbb{V} \cup \partial\mathbb{H}$. It is assumed the traction field on the surface of the holes in the interior of RVE vanishes, i.e.

$$\mathbf{t}(\boldsymbol{y}, t) = \mathbf{0} \quad \text{at} \quad \boldsymbol{y} \in \partial\mathbb{H} \tag{5.1}$$

where $\mathbf{t} \equiv \boldsymbol{\sigma}_\mu \cdot \mathbf{n}$ on $\partial\mathbb{B}$ is the traction field vector on the surface with outward normal $\mathbf{n}$ at $\boldsymbol{y} \in \partial\mathbb{B}$.

5.3 Basic microvariables

First of all note that any arbitrary physically nonlinear and time-dependant material behaviour on the microlevel under small strains can be taken into consideration within this technique.

Microscopic strain tensor, $\boldsymbol{\epsilon}_\mu$, for small strain analysis, is defined as the symmetric part of the displacement gradient tensor as previously defined in (2.30) within the general continuum mechanics theory,

$$\boldsymbol{\epsilon}_\mu \equiv \text{sym}\{\nabla(\mathbf{u})\} \tag{5.2}$$

where $\mathbf{u}$ is the displacement field at a material point $\boldsymbol{y} \in \mathbb{B}$, considering $\mathbb{B}$ as the microstructure.

Microequilibrium state is assumed in the presence of the body forces $\mathbf{b}$ per unit of mass (2.56),

$$\mathrm{div}\boldsymbol{\sigma}_\mu + \rho\,\mathbf{b} = \mathbf{0} \quad \text{in } \mathbb{B} \tag{5.3}$$

where symmetric stress tensor $\boldsymbol{\sigma}_\mu$ is assumed to be related to the strain tensor $\boldsymbol{\epsilon}_\mu$ by some constitutive law, as defined in Chapter 4, for instance the following incremental constitutive law

$$\boldsymbol{\sigma}_\mu = \hat{\boldsymbol{\sigma}}_\mu(\boldsymbol{\epsilon}_\mu\ ;\boldsymbol{\alpha}\ ;\ \boldsymbol{y}) \quad \text{in } \mathbb{B} \tag{5.4}$$

where $\boldsymbol{\alpha}$ is the set of internal variables. The simplest example, elastic constitutive model

$$\boldsymbol{\sigma}_\mu = \frac{\partial\psi(\boldsymbol{\epsilon}_\mu\ ;\ \boldsymbol{y})}{\partial\boldsymbol{\epsilon}_\mu} \quad \text{in } \mathbb{B} \tag{5.5}$$

governed by a strain energy function ψ. Applying the Gauss theorem in (5.3) the global microequilibrium conditions are obtained

$$\int_{\partial\mathbb{B}} \mathbf{t}\ \mathrm{d}A + \int_{\mathbb{B}} \rho\,\mathbf{b}\ \mathrm{d}V = \mathbf{0} \quad \text{and} \quad \int_{\partial\mathbb{B}} \boldsymbol{y}\times\mathbf{t}\ \mathrm{d}A + \int_{\mathbb{B}} \boldsymbol{y}\times\rho\,\mathbf{b}\ \mathrm{d}V = \mathbf{0} \tag{5.6}$$

where $\mathbf{t} = \boldsymbol{\sigma}_\mu\cdot\mathbf{n}$ on $\partial\mathbb{B}$ denotes the traction field on the surface with outward normal $\mathbf{n}$ at $\boldsymbol{y}\in\partial\mathbb{B}$.

5.4 Basic macrovariables and averaging theorem

Within the described homogenization technique no constitutive assumptions have been assumed at the macrolevel.

5.4.1 Macrostress

Overall macrostress $\boldsymbol{\sigma}_{\mathrm{M}}$ of microstructure $\mathbb{B}$ is defined as average of the microstresses over the unit cell. Applying Gauss theorem and microquilibrium (5.3), $\boldsymbol{\sigma}_{\mathrm{M}}$ yields the expression

$$\boldsymbol{\sigma}_{\mathrm{M}} \equiv \overline{\boldsymbol{\sigma}} = \frac{1}{|\mathbb{V}|}\int_{\mathbb{V}} \boldsymbol{\sigma}_{\mu}\, \mathrm{d}V = \frac{1}{|\mathbb{V}|}\int_{\partial\mathbb{V}} \mathrm{sym}[\mathbf{t}\otimes\boldsymbol{y}]\, \mathrm{d}A + \frac{1}{|\mathbb{V}|}\int_{\mathbb{V}} \rho\, \mathrm{sym}[\mathbf{b}\otimes\boldsymbol{y}]\, \mathrm{d}V \quad (5.7)$$

in terms of the traction $\mathbf{t}$ at $\boldsymbol{y} \in \partial\mathbb{V}$ and body force vector field $\mathbf{b}$ at $\boldsymbol{y} \in \mathbb{V}$. We refer to the Appendix A.1 for further details of the proof of expression (5.7)

5.4.2 Macrostrain

By applying Green's Lemma, in similar way, overall macrostrain $\overline{\boldsymbol{\epsilon}}$ is defined,

$$\overline{\boldsymbol{\epsilon}} \equiv \frac{1}{|\mathbb{V}|}\int_{\mathbb{V}} \boldsymbol{\epsilon}_{\mu}\, \mathrm{d}V = \cdots = \frac{1}{|\mathbb{V}|}\int_{\partial\mathbb{V}} \mathrm{sym}[\mathbf{u}\otimes\mathbf{n}]\, \mathrm{d}A \quad (5.8)$$

in terms of the displacement $\mathbf{u}$ at $\boldsymbol{y} \in \partial\mathbb{V}$. We refer to the Appendix B.1 for further details of the proof of expression (5.8)

5.4.3 Overall tangent modulus

Overall Tangent Modulus $\overline{\boldsymbol{\mathcal{C}}}$ for small strain analysis, defined previously at (2.104), relates the variations of overall macrostress $\overline{\boldsymbol{\sigma}}$ and the macrostrain $\overline{\boldsymbol{\epsilon}}$ in a form

$$\overline{\boldsymbol{\mathcal{C}}} \equiv \frac{\mathrm{d}\overline{\boldsymbol{\sigma}}}{\mathrm{d}\overline{\boldsymbol{\epsilon}}} \quad (5.9)$$

Overall Tangent Modulus $\overline{\boldsymbol{\mathcal{C}}}$ in elasticity yields the relation

$$\dot{\overline{\boldsymbol{\sigma}}} = \overline{\boldsymbol{\mathcal{C}}} : \dot{\overline{\boldsymbol{\epsilon}}} \quad (5.10)$$

The computation of these fourth-order tensors, in their discrete F.E. form, is one of the the main aims of this work.

5.4.4 The Hill-Mandel principle

The Hill-Mandel principle or averaging theorem [74], demands that macroscopic stress power must equal the volume average of the microscopic stress work power over the RVE correspondent to the macroscopic point $\boldsymbol{x}$, that is

$$\overline{\boldsymbol{\sigma}} : \dot{\overline{\boldsymbol{\epsilon}}} = \frac{1}{|\mathbb{V}|}\int_{\mathbb{V}} \boldsymbol{\sigma}_{\mu} : \dot{\boldsymbol{\epsilon}}_{\mu}\, \mathrm{d}V \quad (5.11)$$

Inserting (5.2) into the above (5.11), then integrating by parts the right hand side of (5.11) and finally applying microequlibrium (5.3), the averaging theorem can be expressed in the following form

$$\overline{\boldsymbol{\sigma}} : \dot{\overline{\boldsymbol{\epsilon}}} = \frac{1}{|\mathbb{V}|} \int_{\partial \mathbb{V}} \mathbf{t} \cdot \dot{\mathbf{u}} \, \mathrm{d}A + \frac{1}{|\mathbb{V}|} \int_{\mathbb{V}} \rho \mathbf{b} \cdot \dot{\mathbf{u}} \, \mathrm{d}V \tag{5.12}$$

5.5 Definition of the boundary condition for the microscale RVE

The boundary conditions for the displacement $\mathbf{u}$ and traction $\mathbf{t}$ at the microstruture, are chosen such that the averaging condition (5.11) is satisfied. Three classical types of boundary conditions are prescribed on the unit cell: (a) Taylor assumption over the RVE (b) Linear displacements on the boundary (or Linear b.c.) and (c) Periodic displacements and antiperiodic tractions on the boundary (or Periodic b.c.). A crucial aspect is the formulation in deformation-driven context, where the macroscopic strain $\overline{\boldsymbol{\epsilon}}$ is prescribed.

The displacement field is divided in two parts:

$$\mathbf{u}(\boldsymbol{y}) = \mathbf{u}^*(\boldsymbol{y}) + \widetilde{\mathbf{u}}(\boldsymbol{y}) = \overline{\boldsymbol{\epsilon}}\, \boldsymbol{y} + \widetilde{\mathbf{u}}(\boldsymbol{y}) \tag{5.13}$$

where $\mathbf{u}^*$ is the *Taylor displacement*, which defines a constant deformation $\overline{\boldsymbol{\epsilon}}$ over the unit cell as,

$$\mathbf{u}^* \equiv \overline{\boldsymbol{\epsilon}}\, \boldsymbol{y} \tag{5.14}$$

The component $\widetilde{\mathbf{u}}$ is known as *displacement fluctuation*, which is considered to be the unknown.

Insertion of the rate form of (5.13) into the averaging theorem (5.12) yields in the following new form of the Hill-Mandel principle

$$\frac{1}{|\mathbb{V}|} \int_{\partial \mathbb{V}} \mathbf{t} \cdot \dot{\widetilde{\mathbf{u}}} \, \mathrm{d}A + \frac{1}{|\mathbb{V}|} \int_{\mathbb{V}} \rho \mathbf{b} \cdot \dot{\widetilde{\mathbf{u}}} \, \mathrm{d}V = 0 \tag{5.15}$$

5.5.1 Taylor assumption

This model was firstly proposed by Taylor [31] and applied to metallic single crystals. The Taylor assumption defines a displacement field over the microstructure

$$\mathbf{u}(\boldsymbol{y}) = \overline{\boldsymbol{\epsilon}}\,\boldsymbol{y} \qquad \text{at } \boldsymbol{y} \in \mathbb{V} \tag{5.16}$$

with constant strain $\overline{\boldsymbol{\epsilon}}$ imposed on the whole unit cell RVE. An equivalent way to express this condition is to prescribe a zero displacement fluctuation over the whole unit cell

$$\widetilde{\mathbf{u}}(\boldsymbol{y}) = \mathbf{0} \qquad \text{at } \boldsymbol{y} \in \mathbb{V} \tag{5.17}$$

Insertion of the above condition into (5.15) proves that Taylor assumption satisfies the averaging theorem.

5.5.2 Linear displacements on the boundary of RVE

In this state, the definition of the linear deformation boundary constraint over the microstructure RVE shown in Figure 5.2, in terms of the macroscopic strain $\overline{\boldsymbol{\epsilon}}$, assumes the following form

$$\mathbf{u}(\boldsymbol{y}) = \overline{\boldsymbol{\epsilon}}\,\boldsymbol{y} \qquad \text{at } \boldsymbol{y} \in \partial\mathbb{V} \tag{5.18}$$

In another way the above can be expressed stating that this model defines zero displacement fluctuation over the boundary of the unit cell

$$\widetilde{\mathbf{u}}(\boldsymbol{y}) = \mathbf{0} \qquad \text{at } \boldsymbol{y} \in \partial\mathbb{V} \tag{5.19}$$

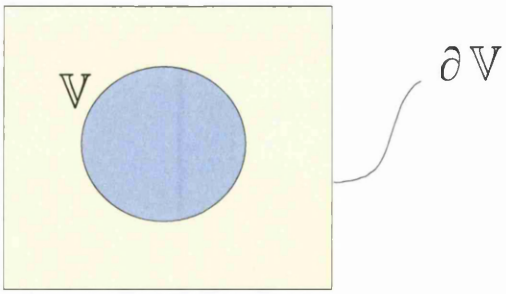

Figure 5.2: Microstructure for linear b.c.

This condition defines a linear deformation $\overline{\boldsymbol{\epsilon}}$ on the boundary $\partial\mathbb{V}$ of the RVE. Insertion of the above condition (5.19) into the new averaging condition form (5.15) confirms that this model satisfies the averaging theorem only when body force effect is negligible.

5.5.3 Periodic deformation and antiperiodic traction on the boundary of RVE

Another possibility consists of applying periodic deformation and antiperiodic traction on the boundary of the RVE $\partial\mathbb{V}$, which is represented by

$$\mathbf{u}(\boldsymbol{y}^+) - \mathbf{u}(\boldsymbol{y}^-) \;=\; \overline{\boldsymbol{\epsilon}}\,(\boldsymbol{y}^+ - \boldsymbol{y}^-) \tag{5.20}$$

$$\mathbf{t}(\boldsymbol{y}^+) = -\mathbf{t}(\boldsymbol{y}^-) \tag{5.21}$$

Taking into consideration the displacement field division (5.13), the periodic deformation condition above (5.20) can also be imposed by requiring that the displacement fluctuation on the boundary of RVE is periodic, hence

$$\widetilde{\mathbf{u}}(\boldsymbol{y}^+) \;=\; \widetilde{\mathbf{u}}(\boldsymbol{y}^-) \tag{5.22}$$

In order to apply these conditions the boundary of the unit cell is decomposed in two parts as indicated in Figure 5.3:. Thus $\partial\mathbb{V} = \partial\mathbb{V}^+ \cup \partial\mathbb{V}^-$ with outwards normals $\mathbf{n}^+ = -\mathbf{n}^-$ which are associated with the points $\boldsymbol{y}^+ \in \partial\mathbb{V}^+$ and $\boldsymbol{y}^- \in \partial\mathbb{V}^-$.

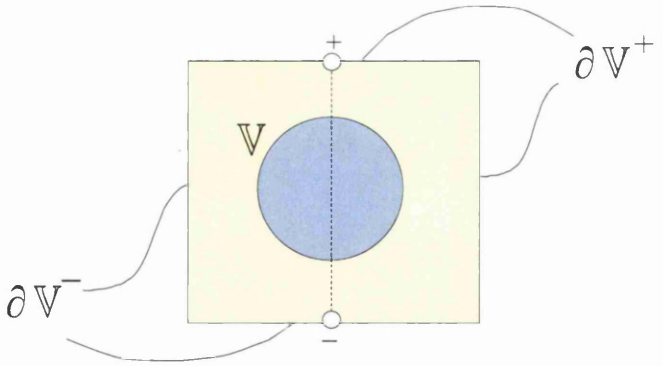

Figure 5.3: Microstructure for periodic b.c.

Body force is not taken into consideration, so that these conditions satisfy the averaging theorem. This can be proved easily by inserting periodic displacement fluctuation (5.22) and antiperiodic traction (5.21) into the new form of the averaging theorem (5.15).

5.6 Conclusions

In this chapter, the main ingredients of multiscale continuum homogenization of solids undergoing small strains have been given. The next Chapter 6 describes the multiscale discrete F.E. analysis, based on the formulation described in this chapter.

Chapter 6

Multiscale discretised model at small strains

6.1 Introduction

In this chapter, a general discretised multiscale F.E. model at small strain is described. The previous Chapter 5 gives the continuum mechanics background necessary for this chapter.

6.1.1 Outline

Firstly, a general multiscale F.E. description based on the F.E. discretisation is given. A strain-driven microstructure analysis is assumed, where the macroscopic strain at macro Gauss point level is prescribed over the discretised microstructure as an average. Secondly, the partition of the displacement field and a matrix F.E. notation are introduced. Then, a microequilibrium solution procedure is given for the microstructure with the consequent average macrostress and overall tangent modulus computation. Finally, those computations are particularised for Taylor assumption, Linear b.c. and Periodic b.c.

6.2 Discrete macro and microscale

A discrete model of the macro and microstructure is considered in Figure 6.1.

This work is focussed on deformation-driven microstructures where the value of the overall macroscopic deformation $\overline{\epsilon}$ is prescribed over the discretised RVE. This family of algorithms is considered to be more convenient in comparison with stress-driven microstructures [15].

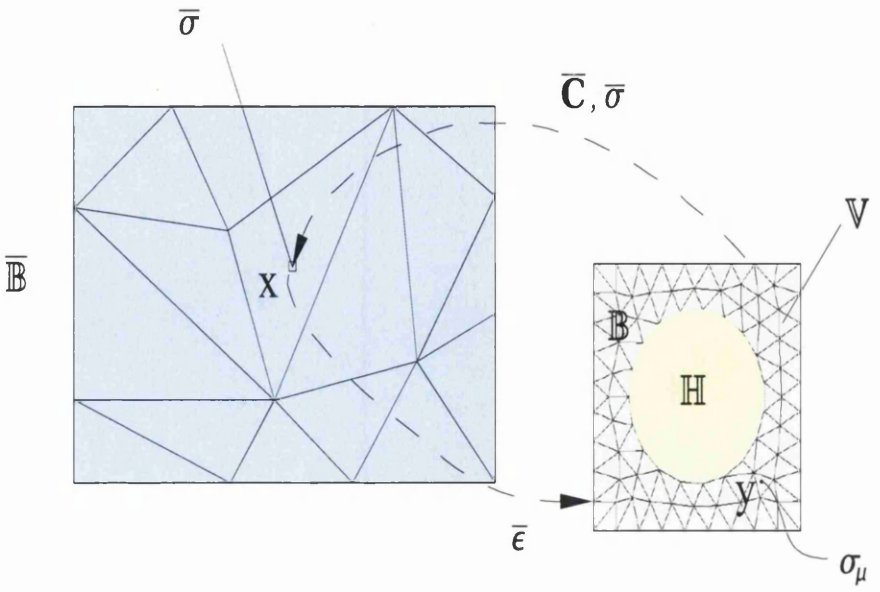

Figure 6.1: Micro to macro transition

The main idea of this procedure is based on F.E. discretisation. At every integration Gauss point of the macrostructure, a discrete RVE microstructure is considered as representation of the macro Gauss point.

Based on the Finite Elements discretisation of the microstructure, the goal is to develop a procedure for computing the overall tangent modulus $\overline{\mathcal{C}}$ and macroscopic average stress $\overline{\sigma}$ at each macroscopic integration point with locally attached microstructure.

6.3 Displacement field partition and matrix notation

Following Chapter 5, in which the continuum displacement field partition was established, the F.E. vector of global displacements is divided into two parts:

$$\mathbf{u} = \mathbf{u}^* + \widetilde{\mathbf{u}} \tag{6.1}$$

where the *Taylor displacement* $\mathbf{u}^*$ (previously defined in the continuum form (5.14)) is expressed in its discrete form as,

$$\mathbf{u}^*_j \equiv \overline{\boldsymbol{\epsilon}}\,\mathbf{y}_j \quad j = 1 \cdots n \tag{6.2}$$

for the n nodes of the microstructure RVE. The *displacement fluctuation* $\widetilde{\mathbf{u}}$ is the unknown for every free node of the discretised microstructure unit cell.

From now on, standard Finite Element matrix notation will be used, where the tensor

entities so far used, can be identified now in the form

$$\overline{\boldsymbol{\epsilon}} \equiv \left\{ \begin{array}{c} \overline{\varepsilon}_{11} \\ \overline{\varepsilon}_{22} \\ 2\,\overline{\varepsilon}_{12} \end{array} \right\} \quad \text{and} \quad \mathbf{u}_{\mathrm{j}} \equiv \left\{ \begin{array}{c} u_1 \\ u_2 \end{array} \right\}_{\mathrm{j}} \tag{6.3}$$

with $\overline{\boldsymbol{\epsilon}}$ as matrix representation of macrostrain tensor and $\mathbf{u}_{\mathrm{j}}$ is the displacement field at node j of the discretised unit cell $\mathbb{V}$. Moreover, the averaged stress field $\overline{\boldsymbol{\sigma}}$ and the force vector $\boldsymbol{f}_{\mathrm{j}}$ associated with the microcell node j, are also defined in this notation as follows,

$$\overline{\boldsymbol{\sigma}} \equiv \left\{ \begin{array}{c} \overline{\sigma}_{11} \\ \overline{\sigma}_{22} \\ \overline{\sigma}_{12} \end{array} \right\} \quad \text{and} \quad \boldsymbol{f}_{\mathrm{j}} \equiv \left\{ \begin{array}{c} f_1 \\ f_2 \end{array} \right\}_{\mathrm{j}} \tag{6.4}$$

The *Taylor displacement* $\mathbf{u}_{\mathrm{j}}^{*}$ of the node j is computed in the following matrix form

$$\mathbf{u}_{\mathrm{j}}^{*} = \mathbb{D}_{\mathrm{j}}^{\mathrm{T}}\,\overline{\boldsymbol{\epsilon}}\,, \quad \mathrm{j} = 1 \cdots \mathrm{n}. \tag{6.5}$$

where $\mathbb{D}_{\mathrm{j}}$ is the *coordinate matrix* at node j of the microstructure defined as (see [11])

$$\mathbb{D}_{\mathrm{j}} \equiv \frac{1}{2} \begin{bmatrix} 2\,y_1 & 0 \\ 0 & 2\,y_2 \\ y_2 & y_1 \end{bmatrix}_{\mathrm{j}} \tag{6.6}$$

6.4 Discretised micro-equilibrium state and solution procedure

The solution at macro level is independent on the solution technique used on the micro level. A Newton-Raphson solution has been adopted here following the development in [42] and [43].

Following a standard procedure, the *discrete boundary value problem*, given previously in (3.34), is recalled as follows. Find the *nodal displacements global vector* $\mathbf{u}$, such that

$$\mathbf{r}(\mathbf{u}) \equiv \mathbf{f}^{int}(\mathbf{u}) - \mathbf{f}^{ext} = \mathbf{0} \tag{6.7}$$

where $\mathbf{f}^{int}$ and $\mathbf{f}^{ext}$ are, respectively, the *internal* and *external global force vectors*, and the difference between them is the *residual* (or *out-of-balance force*) vector $\mathbf{r}$. These global vectors were defined in Chapter 3.

An iterative Newton-Raphson procedure for the solution of the non-linear microscopic equilibrium (6.7) is considered here. Each iteration determines the current fluctuation field assuming frozen macroscopic strain $\overline{\boldsymbol{\epsilon}}$. At the end of the procedure, when microequilibrium is reached, the averaged macroscopic stress over the microstructure RVE is updated.

6.4.1 Microstructure equilibrium solution

In this Section an iterative Newton-Raphson procedure for the solution of the Non-linear microscopic equilibrium (6.7) is developed. An iteration determines the current fluctuation field via the update

$$\widetilde{\mathbf{u}} \leftarrow \widetilde{\mathbf{u}} + \delta\widetilde{\mathbf{u}} \tag{6.8}$$

It is assumed that the microstructure RVE, corresponding to a macroscopic Gauss point in Figure 6.1 , has reached equilibrium at time step n. Therefore, all the state variable and stress of the microscopic RVE are known at that stage. The goal is to compute equilibrium at the time step $n+1$ with the incremental strain $\triangle\overline{\boldsymbol{\epsilon}}$ information passed from the macroscale from the global Newton-Raphson iteration to the microscale RVE. From the additive nature of the strain tensor it follows that

$$\overline{\boldsymbol{\epsilon}}_{n+1} = \overline{\boldsymbol{\epsilon}}_n + \triangle\overline{\boldsymbol{\epsilon}} \tag{6.9}$$

The F.E. discrete incremental boundary value problem for the microstructure RVE can be established as follows:

Given: The displacement vector $\mathbf{u}_n$, the stress field $\boldsymbol{\sigma}_n$, the set of internal variables $\boldsymbol{\alpha}_n$ at time step n and the incremental macrostrain $\triangle\overline{\boldsymbol{\epsilon}}$.

Find: The displacement vector $\mathbf{u}_{n+1}$, the stress field $\boldsymbol{\sigma}_{n+1}$ and the set of internal variables $\boldsymbol{\alpha}_{n+1}$ at time step $n+1$. In addition, the macroscopic stress $\overline{\boldsymbol{\sigma}}_{n+1}$ is computed, once the microstructure is in equilibrium using (6.21). $\overline{\boldsymbol{\sigma}}_{n+1}$ is returned back to the macroscale and is used as a macrostress at macro Gauss point level corresponding to the microstructure RVE computed.

The procedure differs depending on the boundary constraint applied over the microstructure RVE. Therefore, Linear and Periodic constraints have different particularizations of this procedure given later in Sections 6.7.5 and 6.8.5 respectively.

In the following, a Newton-Raphson method is used to find the equilibrium at the microstructure RVE at time step $n+1$ assuming the system is already in equilibrium at time step n. The general idea consists in taking the microstructure as frozen with macroscopic strain $\overline{\boldsymbol{\epsilon}} = \textit{constant}$. Therefore, the differential Taylor displacement is zero during the iteration $\mathrm{d}\mathbf{u}^* = \mathbf{0}$.

Before proceeding with the description of the scheme, we note that the incremental displacement field, $\triangle \mathbf{u} = \mathbf{u}_{n+1} - \mathbf{u}_n$, can be additively decomposed as,

$$\triangle \mathbf{u} = \triangle \mathbf{u}^* + \triangle \widetilde{\mathbf{u}} = \triangle \overline{\boldsymbol{\epsilon}}\, \mathbf{y} + \triangle \widetilde{\mathbf{u}} \tag{6.10}$$

due to the additive properties of the strain tensor $\overline{\boldsymbol{\epsilon}}$. The general solution procedure is described as follows:

1. The initial incremental displacement guess $\triangle \mathbf{u}^0$ is given as the incremental Taylor displacement,

$$\triangle \mathbf{u}^0 = \triangle \mathbf{u}^* = \triangle \overline{\boldsymbol{\epsilon}}\, \mathbf{y} \tag{6.11}$$

   In other words, the incremental macro strain $\triangle \overline{\boldsymbol{\epsilon}}$ is fully prescribed at the first pseudo step, so that, the Taylor displacement is fully prescribed as the initial guess. This means that the initial displacement guess at time step $n+1$, $\mathbf{u}^0_{n+1}$, is given by,

$$\mathbf{u}^0_{n+1} = \mathbf{u}_n + \triangle \mathbf{u}^0 \tag{6.12}$$

   Using the split displacement (6.1) at time step n, the initial guess displacement is then expressed as,

$$\mathbf{u}^0_{n+1} = \mathbf{u}^*_{n+1} + \widetilde{\mathbf{u}}_n \tag{6.13}$$

   In the above it can be observed that the incremental Taylor displacement $\triangle \mathbf{u}^*$ is prescribed entirely at the beginning of the procedure. Moreover, the initial displacement fluctuation is taken as the converged from the previous time step n. Hence,

$$\widetilde{\mathbf{u}}^0_{n+1} = \widetilde{\mathbf{u}}_n \tag{6.14}$$

   or in another words the incremental fluctuation is taken as zero value during the initial guess:

$$\triangle \widetilde{\mathbf{u}} = 0 \tag{6.15}$$

2. Computation of the internal forces $\mathbf{f}^{int}$. This is computed with the incremental displacement $\triangle \mathbf{u}$ and the set of state variables $\{\boldsymbol{\epsilon}_{n+1}, \boldsymbol{\alpha}_{n+1}\}$ at microscopic Gauss point level.

3. Check convergence $\|\mathbf{r}\| < \varepsilon_{tolerance}$. This residual force $\mathbf{r}$ depends on the boundary constraint applied on the RVE.

   - IF $\|\mathbf{r}\| < \varepsilon_{tolerance}$. EQUILIBRIUM. The solution is $\mathbf{u}^k_{n+1}$. END OF k ITERATION

- ELSE GO TO NEXT STEP

4. Computation of the incremental internal fluctuation. Let assume that the iterative fluctuation is divided in two parts,

$$\delta\widetilde{\mathbf{u}} = \left\{ \begin{array}{c} \delta\widetilde{\mathbf{u}}_r \\ \delta\widetilde{\mathbf{u}}_d \end{array} \right\} \tag{6.16}$$

where $\delta\widetilde{\mathbf{u}}_r$ are the independent d.o.f. and $\delta\widetilde{\mathbf{u}}_d$ are the dependent d.o.f. displacements of the microstructure. Therefore $\delta\widetilde{\mathbf{u}}_d$ is known once $\delta\widetilde{\mathbf{u}}_r$ is computed. They are different depending on the micro boundary constraint (Linear or Periodic b.c.). The Newton-Raphson iteration is defined by,

$$\mathbf{K}_r\ \delta\widetilde{\mathbf{u}}_r = -\mathbf{r} \quad \Rightarrow \quad \delta\widetilde{\mathbf{u}}_r = -\mathbf{K}_r^{-1}\ \mathbf{r} \tag{6.17}$$

where $\mathbf{r}$ is the residual force and $\mathbf{K}_r$ is the reduced matrix of the system. In Sections 6.7.5 and 6.8.5 particularisations for Linear and Periodic b.c. are given, respectively.

The updating of the incremental fluctuation is as follows

$$\triangle\widetilde{\mathbf{u}} \ \leftarrow \triangle\widetilde{\mathbf{u}} + \delta\widetilde{\mathbf{u}} \tag{6.18}$$

and also the incremental displacement

$$\triangle\mathbf{u} \ \leftarrow \triangle\mathbf{u} + \delta\widetilde{\mathbf{u}} \tag{6.19}$$

GO TO step 2.

Finally, when the microequilibrium is reached, the macro Cauchy stress $\overline{\boldsymbol{\sigma}}_{n+1}$ is computed from the value of the boundary forces. It is described in the discrete form in Section 6.5. This macro stress is used to compute the internal forces at the macro level.

6.5 General average stress and overall tangent modulus computation

6.5.1 Average stress computation

Assuming no body forces in the expression for the average stress (5.7), in the discrete setting, $\mathbf{t}\ \mathrm{d}A \rightarrow \boldsymbol{f}_{\mathrm{j}}^{ext}$, that is the infinitesimal force $\mathbf{t}\ \mathrm{d}A$ becomes the finite force $\boldsymbol{f}_{\mathrm{j}}^{ext}$ at nodal position $\mathbf{y}_{\mathrm{j}}$ on the boundary $\partial\mathbb{V}$. Therefore (5.7) degenerates into the discrete sum

$$\overline{\boldsymbol{\sigma}} = \frac{1}{|\mathbb{V}|} \sum_{j=1}^{n_b} \text{sym}[\boldsymbol{f}_j^{ext} \otimes \mathbf{y}_j] \tag{6.20}$$

where n_b is the number of nodes on the boundary $\partial\mathbb{V}$. Using matrix representation this expression becomes

$$\overline{\boldsymbol{\sigma}} = \frac{1}{|\mathbb{V}|} \sum_{j=1}^{n_b} \mathbb{D}_j \, \boldsymbol{f}_j^{ext} \tag{6.21}$$

where $\mathbb{D}_j$ is the coordinate matrix (6.6) evaluated at node j on the boundary of the discretised microstructure RVE $\partial\mathbb{V}$. The above expression can be rearranged in the following global expression

$$\overline{\boldsymbol{\sigma}} = \frac{1}{|\mathbb{V}|} \mathbb{D}_b \, \mathbf{f}_b^{ext} \,, \tag{6.22}$$

where $\mathbf{f}_b^{ext}$ is the external nodal force vector of the boundary nodes, and $\mathbb{D}_b$ is the *boundary coordinate matrix* defined by:

$$\mathbb{D}_b \equiv \left[\mathbb{D}_1^b \;\; \mathbb{D}_2^b \;\; \dots \;\; \mathbb{D}_{n_b}^b \right] \tag{6.23}$$

6.5.2 Overall tangent modulus computation

In the computational homogenization approach no explicit form of the constitutive behavior on the macro-level is assumed a priori, so that the tangent modulus has to be determined from the relations between variations of the macroscopic stress and variations of the macroscopic strain at the integration macro Gauss point of interest. This can be accomplished by numerical differentiation of the numerical macroscopic stress-strain relation, for instance, by using forward difference approximations as suggested in [43]. Another approach is to condense the microstructural stiffness matrix to the macroscopic matrix tangent modulus. This task is achieved by reducing the total RVE system of equations to the relation between the forces acting on the boundary $\partial\mathbb{V}$ and the displacement on the boundary. This procedure has been used in [92], [90], and also in [13], in combination of the Lagrange multiplier method to impose the boundary constraints.

A similar scheme has been used in this work that employs direct condensation to obtain a relation between the variation of the forces acting on the boundary $\partial\mathbb{V}$ and the variation of the Taylor displacement on the boundary nodes array $\mathrm{d}\mathbf{u}^*$ which depends linearly of the macroscopic strain variation $\mathrm{d}\overline{\boldsymbol{\epsilon}}$.

The total microstructural system of equations that gives the relation between the iterative nodal displacement $\mathrm{d}\mathbf{u}$ and iterative nodal external force vectors is

$$\mathbf{K}\ \mathrm{d}\mathbf{u} = \mathrm{d}\mathbf{f}^{ext}. \tag{6.24}$$

With the displacement partition (6.1) the system can be rearranged as follows

$$\mathbf{K}\ \mathrm{d}\mathbf{u} = \mathrm{d}\mathbf{f}^{ext} \ \Rightarrow\ \mathbf{K}\ \mathrm{d}\mathbf{u}^{*} + \mathbf{K}\ \mathrm{d}\widetilde{\mathbf{u}} = \mathrm{d}\mathbf{f}^{ext} \tag{6.25}$$

The boundary constraints are then applied to this system in the following sections to condense the system. This procedure gives the expression that relates the variation boundary external forces $\mathrm{d}\mathbf{f}_{\mathrm{b}}^{ext}$ against the variation of the Taylor displacement $\mathrm{d}\mathbf{u}^{*}$.

Finally, the overall tangent modulus $\overline{\boldsymbol{\mathcal{C}}}$ defined in (5.9), can be computed in its discretised F.E. matrix form, using previous averaged stress expression (6.22), in the following way

$$\overline{\boldsymbol{\mathcal{C}}} = \frac{\mathrm{d}\overline{\boldsymbol{\sigma}}}{\mathrm{d}\overline{\boldsymbol{\epsilon}}} = \frac{1}{|\mathbb{V}|}\,\mathbb{D}_{\mathrm{b}}\,\frac{\mathrm{d}\mathbf{f}_{\mathrm{b}}^{ext}}{\mathrm{d}\overline{\boldsymbol{\epsilon}}} \tag{6.26}$$

Particularisations of the computation of average macrostress and overall tangent modulus are given in the following sections of this chapter, for Taylor assumption, Linear b.c. and Periodic b.c.

6.6 Taylor assumption

Based on the above-mentioned notation the *global coordinate matrix* is defined for this assumption as

$$\mathbb{D}_{\mathrm{global}} \equiv \left[\ \mathbb{D}_1\ \ \mathbb{D}_2\ \ \ldots\ \ \mathbb{D}_{\mathrm{n}}\ \right] \tag{6.27}$$

composed of the coordinate matrices of every single node of the RV. Hence, using this matrix formulation, the Taylor displacement counterpart (6.5), can be expressed in the global form as

$$\mathbf{u}^{*} = \mathbb{D}_{\mathrm{global}}^{\mathrm{T}}\,\overline{\boldsymbol{\epsilon}} \tag{6.28}$$

In this assumption, zero displacement fluctuation is considered for every single node of the unit cell, therefore

$$\widetilde{\mathbf{u}}_{\mathrm{j}} = \mathbf{0} \quad \mathrm{j} = 1 \cdots \mathrm{n}$$

or in global notation

$$\widetilde{\mathbf{u}} = \mathbf{0} \tag{6.29}$$

6.6.1 Average stress and tangent modulus of Taylor assumption

In order to compute the average stress and homogenised tangent modulus for Taylor assumption, the rule of mixtures is used. Therefore the average stress is computed as,

$$\overline{\boldsymbol{\sigma}} = \frac{1}{|\mathbb{V}|}\sum_{i=1}^{n_c} v_i\,\boldsymbol{\sigma}_i \tag{6.30}$$

where n_c is the number of different phases and v_i is the volume of the phase i of the RVE. The stress in each phase $\boldsymbol{\sigma}_i$ is computed separately imposing the global macrostrain $\overline{\boldsymbol{\epsilon}}$.

The homogenised tangent modulus is also computed in the same way by

$$\overline{\boldsymbol{\mathcal{C}}} = \frac{1}{|\mathbb{V}|}\sum_{i=1}^{n_c} v_i\,\boldsymbol{\mathcal{C}}_i \tag{6.31}$$

where $\boldsymbol{\mathcal{C}}_i$ is the tangent modulus of phase i.

The Taylor-type approach has been used in [42], [43] for analysis of polycrystalline materials.

6.7 Discrete form of the linear displacements boundary condition

In view of the discrete formulation of the boundary conditions outlined in Section 5.5.2, the nodes of the mesh are partitioned into those on the surface $\partial\mathbb{V}$ of RVE and those in the interior of $\mathbb{V}$, see Figure 6.2. In this mesh $\mathrm{n_b}$ boundary nodes and $\mathrm{n_i}$ internal nodes are distinguished. The discrete form of this linear constraint was introduced in [20] and [21].

6.7.1 Partitioning of algebraic equations

Partitioning of the current nodal displacements and nodal forces are given as

$$\mathbf{u} = \left\{ \begin{array}{c} \mathbf{u}_\mathrm{i} \\ \mathbf{u}_\mathrm{b} \end{array} \right\} \quad \text{and} \quad \mathbf{f} = \left\{ \begin{array}{c} \mathbf{f}_\mathrm{i} \\ \mathbf{f}_\mathrm{b} \end{array} \right\} \tag{6.32}$$

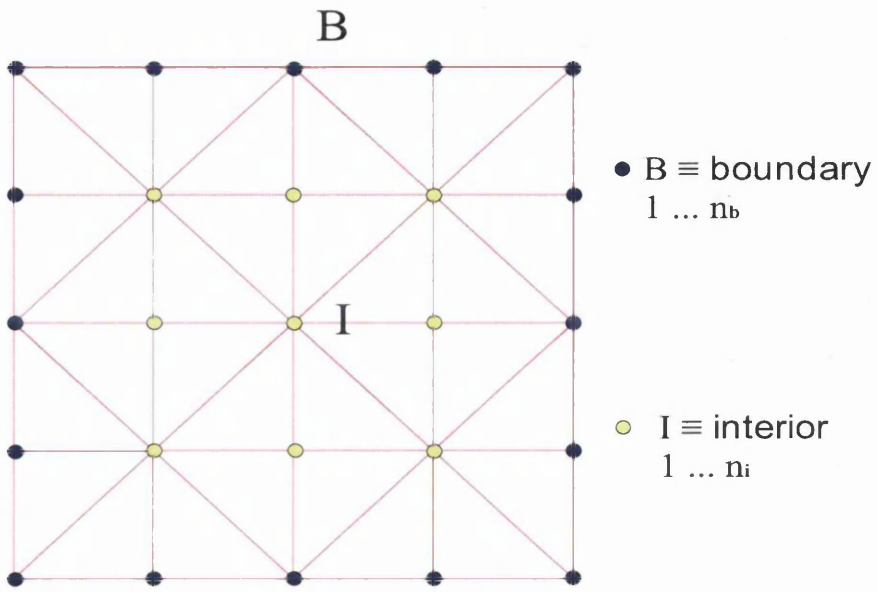

Figure 6.2: Mesh for linear displacement on the boundary

where the displacements $\mathbf{u}_i$ and $\mathbf{u}_b$ are gathered from $\mathbf{u}$, for the interior and boundary nodes, respectively (see Figure 6.2). Using these two vectors we obtain a new $\mathbf{u}$ rearranged as shown in (6.32).

In line with (6.32), the tangent stiffness matrix is rearranged as

$$\mathbf{K} = \frac{\mathrm{d}\mathbf{f}^{int}}{\mathrm{d}\mathbf{u}} = \begin{bmatrix} \mathbf{k}_{ii} & \mathbf{k}_{ib} \\ \mathbf{k}_{bi} & \mathbf{k}_{bb} \end{bmatrix} \tag{6.33}$$

comprising contributions associated with internal nodes and nodes on the surface of the RVE.

6.7.2 Linear displacement

At each node j of the boundary $\partial\mathbb{V}$ condition (5.19) induces the discrete constraint

$$\widetilde{\mathbf{u}}_j \;=\; \mathbf{0} \quad j \;=\; 1 \cdots n_b \tag{6.34}$$

These constraints can be represented as a global boundary displacement vector

$$\widetilde{\mathbf{u}}_b \;=\; \mathbf{0} \tag{6.35}$$

According to the matrix notation introduced in Section 6.3, we defined the *global coordinate matrix*

$$\mathbb{D}_{\text{global},l} \equiv \left[\mathbb{D}_{\text{i}} \quad \mathbb{D}_{\text{b},l} \right] \tag{6.36}$$

where $\mathbb{D}_{\text{i}}$ and $\mathbb{D}_{\text{b},l}$ are the *interior coordinate matrix* and the *boundary coordinate matrix*, respectively, given as

$$\mathbb{D}_{\text{i}} \equiv \left[\mathbb{D}^i_1 \quad \mathbb{D}^i_2 \quad \dots \quad \mathbb{D}^i_{\text{n}_\text{i}} \right] \quad \text{and} \quad \mathbb{D}_{\text{b},l} \equiv \left[\mathbb{D}^b_1 \quad \mathbb{D}^b_2 \quad \dots \quad \mathbb{D}^b_{\text{n}_\text{b}} \right]. \tag{6.37}$$

The matrices $\mathbb{D}_{\text{i}}$ and $\mathbb{D}_{\text{b},l}$ are defined in terms of node coordinate matrices (6.6) for the interior and boundary nodes, respectively. The Taylor displacement $\mathbf{u}^*$ previously defined in (6.28) for the Taylor assumption, is now represented

$$\mathbf{u}^* = \mathbb{D}^{\text{T}}_{\text{global},l}\, \overline{\boldsymbol{\epsilon}} \tag{6.38}$$

where $\mathbb{D}_{\text{global},l}$ is the global coordinate matrix (6.36) and $\overline{\boldsymbol{\epsilon}}$ is the matrix representation of the prescribed macroscopic strain (6.3). In this model the variation of the Taylor displacement vector $\mathrm{d}\mathbf{u}^*$ is represented as

$$\mathrm{d}\mathbf{u}^* = \mathbb{D}^{\text{T}}_{\text{global},l}\, \mathrm{d}\overline{\boldsymbol{\epsilon}} \tag{6.39}$$

that is, as a function of the variation of the macroscopic average strain vector $\mathrm{d}\overline{\boldsymbol{\epsilon}}$.

6.7.3 Average macro-stress of linear b.c.

For this model the average stress is computed based on the matrix expression for the average stress (6.22). Making use of the boundary coordinate matrix $\mathbb{D}_{\text{b},l}$ defined in (6.37) it can be rearranged in the following global expression

$$\overline{\boldsymbol{\sigma}} = \frac{1}{|\mathbb{V}|}\, \mathbb{D}_{\text{b},l}\, \mathbf{f}^{ext}_{\text{b}} \tag{6.40}$$

where $\mathbf{f}^{ext}_{\text{b}}$ is the external nodal force vector of the boundary nodes defined in the partition (6.32).

where $\mathbf{f}^{ext}_{\text{b}}$ is the external nodal force vector of the boundary nodes defined in the partition (6.32).

6.7.4 Overall tangent modulus of linear b.c.

Using partitioning of the algebraic equations (6.32) and (6.33), the system (6.24) can be rewritten

$$\begin{bmatrix} \mathbf{k}_{ii} & \mathbf{k}_{ib} \\ \mathbf{k}_{bi} & \mathbf{k}_{bb} \end{bmatrix} \begin{Bmatrix} \mathrm{d}\mathbf{u}_i \\ \mathrm{d}\mathbf{u}_b \end{Bmatrix} = \begin{Bmatrix} \mathrm{d}\mathbf{f}_i^{ext} \\ \mathrm{d}\mathbf{f}_b^{ext} \end{Bmatrix} \quad \equiv \quad \mathbf{K}\ \mathrm{d}\mathbf{u} = \mathrm{d}\mathbf{f}^{ext} \tag{6.41}$$

for the case when $\mathrm{d}\mathbf{f}_i^{ext} = \mathbf{0}$. The general procedure explained in Section 6.5.2 where the rearranged system (6.25) was obtained is followed, so that the system (6.41) is then rearranged as,

$$\Rightarrow\ \mathbf{K}\ \mathrm{d}\tilde{\mathbf{u}} = \mathrm{d}\mathbf{f}^{ext} - \mathbf{K}\ \mathrm{d}\mathbf{u}^* \tag{6.42}$$

where Taylor displacement variation $\mathrm{d}\mathbf{u}^*$ is given by (6.39) for the linear model. By introducing linear displacement constraint in discrete form (6.35) into system (6.42), internal nodal displacement fluctuation vector can be computed as,

$$\mathrm{d}\tilde{\mathbf{u}}_i \ = \ -\mathbf{k}_{ii}^{-1}\ \mathbf{K}_I\ \mathrm{d}\mathbf{u}^* \tag{6.43}$$

where $\mathbf{K}_I$ matrix is defined as

$$\mathbf{K}_I \equiv \left[\ \mathbf{k}_{ii} \quad \mathbf{k}_{ib}\ \right]. \tag{6.44}$$

From the system (6.42), the variation of external boundary force vector is calculated

$$\mathrm{d}\mathbf{f}_b^{ext} = \ \mathbf{k}_{bi}\ \mathrm{d}\tilde{\mathbf{u}}_i \ + \ \mathbf{K}_B\ \mathrm{d}\mathbf{u}^* \tag{6.45}$$

where $\mathbf{K}_B$ matrix is defined as

$$\mathbf{K}_B \equiv \left[\ \mathbf{k}_{bi} \quad \mathbf{k}_{bb}\ \right]. \tag{6.46}$$

Inserting (6.43) into (6.45), the $\mathrm{d}\mathbf{f}_b^{ext}$ vector is obtained

$$\mathrm{d}\mathbf{f}_b^{ext} = \ (\ \mathbf{K}_B \ - \ \mathbf{k}_{bi}\ \mathbf{k}_{ii}^{-1}\ \mathbf{K}_I\ )\ \mathrm{d}\mathbf{u}^* \tag{6.47}$$

in terms of the variation of the Taylor displacement $\mathrm{d}\mathbf{u}^*$. Compacting the right hand side of (6.47), the variation of the external boundary force vector is expressed as

$$\mathrm{d}\mathbf{f}_b^{ext} \ = \ \mathbf{K}_{\mathbf{lin}}^{\mathbf{B}}\ \mathrm{d}\mathbf{u}^* \tag{6.48}$$

where the *condensed linear stiffness matrix* $\mathbf{K}_{\mathbf{lin}}^{\mathbf{B}}$ is defined as follows,

$$\mathbf{K}_{\mathbf{lin}}^{\mathbf{B}} \ \equiv \ \mathbf{K}_B - \ \mathbf{k}_{bi}\ \mathbf{k}_{ii}^{-1}\ \mathbf{K}_I\,. \tag{6.49}$$

Finally, insertion of the variation of the Taylor displacement (6.39) for Linear model, into (6.48) identifies the boundary force vector

$$\mathrm{d}\mathbf{f}_{\mathrm{b}}^{ext} = \mathbf{K}_{\mathbf{lin}}^{\mathbf{B}}\, \mathbb{D}_{\mathrm{global},l}^{\mathrm{T}}\, \mathrm{d}\overline{\boldsymbol{\epsilon}} \tag{6.50}$$

in terms of the global coordinate matrix (6.36) and the variation of the overall macrostrain $\mathrm{d}\overline{\boldsymbol{\epsilon}}$. Hence, it follows that

$$\frac{\mathrm{d}\mathbf{f}_{\mathrm{b}}^{ext}}{\mathrm{d}\overline{\boldsymbol{\epsilon}}} = \mathbf{K}_{\mathbf{lin}}^{\mathbf{B}}\, \mathbb{D}_{\mathrm{global},l}^{\mathrm{T}} \tag{6.51}$$

which expresses the variation of the external boundary force vector $\mathrm{d}\mathbf{f}_{\mathrm{b}}^{ext}$ with respect to the variation of macroscopic strain $\mathrm{d}\overline{\boldsymbol{\epsilon}}$.

The overall tangent modulus $\overline{\boldsymbol{\mathcal{C}}}_l$ for linear b.c., can be computed in its discretised F.E. matrix form following the general expression given in (6.26) as

$$\overline{\boldsymbol{\mathcal{C}}}_l = \frac{\mathrm{d}\overline{\boldsymbol{\sigma}}}{\mathrm{d}\overline{\boldsymbol{\epsilon}}} = \frac{1}{|\mathbb{V}|}\, \mathbb{D}_{\mathrm{b},l}\, \frac{\mathrm{d}\mathbf{f}_{\mathrm{b}}^{ext}}{\mathrm{d}\overline{\boldsymbol{\epsilon}}}\,. \tag{6.52}$$

Substituting (6.51) into (6.52), the overall tangent modulus representation $\overline{\boldsymbol{\mathcal{C}}}_l$ is obtained

$$\boxed{\overline{\boldsymbol{\mathcal{C}}}_l = \frac{1}{|\mathbb{V}|}\, \mathbb{D}_{\mathrm{b},l}\, \mathbf{K}_{\mathbf{lin}}^{\mathbf{B}}\, \mathbb{D}_{\mathrm{global},l}^{\mathrm{T}}} \tag{6.53}$$

Clearly, the overall tangent modulus $\overline{\boldsymbol{\mathcal{C}}}_l$ is given as a function of the boundary coordinate matrix $\mathbb{D}_{\mathrm{b},l}$ defined in (6.37), the condensed linear stiffness matrix $\mathbf{K}_{\mathbf{lin}}^{\mathbf{B}}$ (6.49) and the global coordinate matrix $\mathbb{D}_{\mathrm{global},l}^{\mathrm{T}}$ outlined in (6.36).

Finally, we remark that by using (6.53) the overall tangent modulus can be computed for heterogeneous material with different microstructures. When using this overall tangent modulus the quadratic rate of convergence is attained at macroscopic level.

6.7.5 Microequilibrium computation for linear b.c.

In Section 6.4.1 a general solution scheme for microequilibrium was given. In this section, the particularisation of the microequilibrium procedure for linear b.c. is given.

The incremental Taylor displacement is given in matrix form as,

$$\triangle\mathbf{u}^{*} = \mathbb{D}_{\mathrm{global},l}^{\mathrm{T}} \triangle\overline{\boldsymbol{\epsilon}}. \tag{6.54}$$

The residual force $\mathbf{r}$ is taken as the difference between the internal and external force vectors for the interior nodes as,

$$\mathbf{r} = \mathbf{f}_{\mathrm{i}}^{int} - \mathbf{f}_{\mathrm{i}}^{ext} \tag{6.55}$$

Assuming that in equilibrium $\mathbf{f}_{\mathrm{i}}^{ext} = \mathbf{0}$ actual residual used for linear b.c. follows as

$$\mathbf{r} = \mathbf{f}_{\mathrm{i}}^{int}. \tag{6.56}$$

Therefore, the differential fluctuation is given by the system (6.17) which now is taking the following form

$$\mathbf{K}_{\mathrm{ii}}\ \delta\widetilde{\mathbf{u}}_{\mathrm{i}} = -\mathbf{f}_{\mathrm{i}}^{int} \quad \rightarrow \quad \delta\widetilde{\mathbf{u}}_{\mathrm{i}} = -\mathbf{K}_{\mathrm{ii}}^{-1}\ \mathbf{f}_{\mathrm{i}}^{int} \tag{6.57}$$

and

$$\delta\widetilde{\mathbf{u}}_{\mathrm{b}} = \mathbf{0} \tag{6.58}$$

The updated incremental fluctuation is then given by

$$\triangle\widetilde{\mathbf{u}}_{\mathrm{i}} \leftarrow \triangle\widetilde{\mathbf{u}}_{\mathrm{i}} + \delta\widetilde{\mathbf{u}}_{\mathrm{i}} \tag{6.59}$$

and

$$\triangle\widetilde{\mathbf{u}}_{\mathrm{b}} = \mathbf{0} \tag{6.60}$$

The incremental displacement used to compute the internal force is updated by

$$\triangle\mathbf{u}_{\mathrm{i}} \leftarrow \triangle\mathbf{u}_{\mathrm{i}} + \delta\widetilde{\mathbf{u}}_{\mathrm{i}} \tag{6.61}$$

and $\triangle\mathbf{u}_{\mathrm{b}}$ does not change.

6.8 Discrete form of the periodic displacements and antiperiodic traction on the boundary condition

In order to discretise the continuum model of the periodic boundary conditions described in Section 5.5.3, the nodes of the mesh are partitioned in four groups outlined in Figure 6.3 :

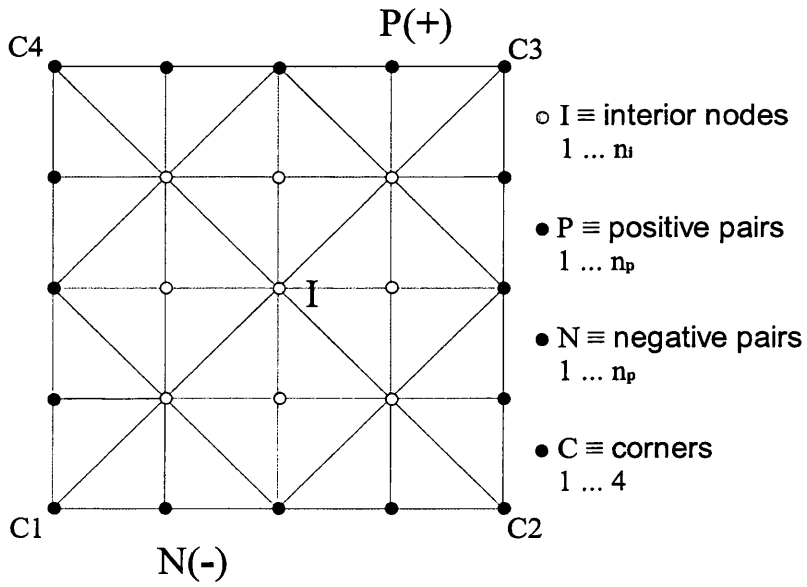

Figure 6.3: Mesh for periodic displacement and antiperiodic traction on the boundary

1. n_i interior nodes are distinguished.
2. n_p positive boundary nodes which are located at the top and right side of the microstructure surface $\partial\mathbb{V}$ of RVE.
3. n_p negative boundary nodes which are located at the bottom and left side of the microstructure surface $\partial\mathbb{V}$ of RVE.
4. n_c node at the corners.

The number of node pairs (positive and corresponding negative nodes) on the boundary $\partial\mathbb{V}$ of RVE are:

$$n_p = \frac{n_b}{2} - 2 \tag{6.62}$$

where n_b is the total number of nodes on the boundary of RVE. Also, the number of corner nodes in a 2D rectangular microstructure is four, i.e.

$$n_c = 4. \tag{6.63}$$

The discrete form of this Periodic constraint was introduced in [20] and [21].

6.8.1 Partitioning of algebraic equations

In this case, the partition of the nodal displacements and forces is as follows

$$\mathbf{u} = \begin{Bmatrix} \mathbf{u}_i \\ \mathbf{u}_p \\ \mathbf{u}_n \\ \mathbf{u}_c \end{Bmatrix} \quad \text{and} \quad \mathbf{f} = \begin{Bmatrix} \mathbf{f}_i \\ \mathbf{f}_p \\ \mathbf{f}_n \\ \mathbf{f}_c \end{Bmatrix} \tag{6.64}$$

where following Figure 6.3 the corresponding contributions are distinguished: (i) the interior contribution, (ii) the contribution of positive boundary nodes, (iii) the contributions from the corresponding negative boundary nodes, and finally (iv) the contribution from the nodes at the corners. In correspondence to (6.64), the tangent stiffness matrix is partitioned in the following way

$$\mathbf{K} = \frac{\mathrm{d}\mathbf{f}^{int}}{\mathrm{d}\mathbf{u}} = \begin{bmatrix} \mathbf{k}_{ii} & \mathbf{k}_{ip} & \mathbf{k}_{in} & \mathbf{k}_{ic} \\ \mathbf{k}_{pi} & \mathbf{k}_{pp} & \mathbf{k}_{pn} & \mathbf{k}_{pc} \\ \mathbf{k}_{ni} & \mathbf{k}_{np} & \mathbf{k}_{nn} & \mathbf{k}_{nc} \\ \mathbf{k}_{ci} & \mathbf{k}_{cp} & \mathbf{k}_{cn} & \mathbf{k}_{cc} \end{bmatrix} \tag{6.65}$$

6.8.2 Periodic displacements and antiperiodic tractions

At each node pair j on the boundary $\partial\mathbb{V}^+ \cup \partial\mathbb{V}^-$, the continuum condition (5.22) induces the discrete constraint

$$\widetilde{\mathbf{u}}_j^+ = \widetilde{\mathbf{u}}_j^- , \qquad j = 1 \cdots n_p \tag{6.66}$$

The link between constraints for each pair of nodes can be compactly represented in a global form as

$$\widetilde{\mathbf{u}}_p = \widetilde{\mathbf{u}}_n \tag{6.67}$$

The displacement fluctuation at the corners is prescribed to zero to avoid the rigid body motion,

$$\widetilde{\mathbf{u}}_{ci} \;=\; \mathbf{0}\,, \qquad i \;=\; 1 \cdots \mathrm{n_c} \tag{6.68}$$

It can easily be proved that (6.68) agrees with the periodic continuum condition (5.22). The relation (6.68) can be represented in a global form

$$\widetilde{\mathbf{u}}_{\mathrm{c}} \;=\; \mathbf{0} \tag{6.69}$$

At each node pair j on the boundary $\partial\mathbb{V}^+ \cup \partial\mathbb{V}^-$, the continuum antiperiodic traction condition (5.21) is discretised as

$$\boldsymbol{f}(\mathbf{y}_{\mathrm{j}}^+) = -\boldsymbol{f}(\mathbf{y}_{\mathrm{j}}^-)\,, \qquad \boldsymbol{f}_{\mathrm{j}}^+ = -\boldsymbol{f}_{\mathrm{j}}^-\,, \qquad \mathrm{j} \;=\; 1 \cdots \mathrm{n_p} \tag{6.70}$$

Again these constraints can be represented in compressed form as

$$\mathbf{f}_{\mathrm{p}}^{ext} = -\mathbf{f}_{\mathrm{n}}^{ext} \tag{6.71}$$

A very important additional equation to take into consideration is equilibrium condition, i.e.

$$\sum_{\mathrm{i}=1}^{4} \mathbf{f}_{\mathrm{ci}}^{ext} = \mathbf{0} \tag{6.72}$$

This vectorial equation agrees with the continuum antiperiodic traction condition (5.21), although, this is not obvious. The underlying idea relies on the antiperiodicity of force in the corners that come from the different continuum distributions as pointed out in Appendix C.

Using the matrix notation introduced in Section 6.3, we redefine the *global coordinate matrix* for periodic b.c. as

$$\mathbb{D}_{\mathrm{global},p} \;\equiv \left[\; \mathbb{D}_{\mathrm{i}} \quad \mathbb{D}_{\mathrm{b},p} \right] \tag{6.73}$$

where $\mathbb{D}_{\mathrm{i}}$ is the *interior coordinate matrix* defined in (6.37) and the $\mathbb{D}_{\mathrm{b},p}$ is the *boundary coordinate matrix* for Periodic b.c. defined as

$$\mathbb{D}_{\mathrm{b},p} \;= \left[\; \mathbb{D}_{\mathrm{p}} \quad \mathbb{D}_{\mathrm{n}} \quad \mathbb{D}_{\mathrm{c}} \;\right] \tag{6.74}$$

where $\mathbb{D}_{\mathrm{p}}$, $\mathbb{D}_{\mathrm{n}}$ and $\mathbb{D}_{\mathrm{c}}$ are the *positive boundary coordinate matrix*, *negative boundary coordinate matrix* and *corner coordinate matrix*, respectively, given by

$$\mathbb{D}_{\mathrm{p}} \equiv \left[\mathbb{D}_1^p \;\; \mathbb{D}_2^p \;\; \ldots \;\; \mathbb{D}_{\mathrm{np}}^p\right]$$

$$\mathbb{D}_{\mathrm{n}} \equiv \left[\mathbb{D}_1^n \;\; \mathbb{D}_2^n \;\; \ldots \;\; \mathbb{D}_{\mathrm{np}}^n\right]$$

$$\mathbb{D}_{\mathrm{c}} \equiv \left[\mathbb{D}_1^c \;\; \mathbb{D}_2^c \;\; \mathbb{D}_3^c \;\; \mathbb{D}_4^c\right]$$

The Taylor displacement $\mathbf{u}^*$ defined as a constant for each node in (6.5), is given in a compact form as

$$\mathbf{u}^* \;=\; \mathbb{D}^{\mathrm{T}}_{\mathrm{global},p}\,\overline{\boldsymbol{\epsilon}} \tag{6.75}$$

where $\mathbb{D}_{\mathrm{global},p}$ is the global coordinate matrix for periodic assumption and $\overline{\boldsymbol{\epsilon}}$ is the matrix representation of the prescribed macroscopic strain tensor. In this model the variation of the Taylor displacement vector $\mathrm{d}\mathbf{u}^*$ is considered as follows

$$\mathrm{d}\mathbf{u}^* = \mathbb{D}^{\mathrm{T}}_{\mathrm{global},p}\,\mathrm{d}\overline{\boldsymbol{\epsilon}}\,, \tag{6.76}$$

i.e. the displacement $\mathrm{d}\mathbf{u}^*$ is a function of the variation of the macroscopic average strain vector $\mathrm{d}\overline{\boldsymbol{\epsilon}}$.

6.8.3 Average macro-stress of periodic b.c.

Following the general procedure to compute average stress given in Section 6.5.1, the average stress is computed, based on the matrix expression for the average stress (6.21), as follows

$$\overline{\boldsymbol{\sigma}} \;=\; \frac{1}{|\mathbb{V}|}\,\Big[\,\sum_{\mathrm{j}\,=\,1}^{\mathrm{n_P}} (\mathbb{D}_{\mathrm{j}}^{+} - \mathbb{D}_{\mathrm{j}}^{-})\;\boldsymbol{f}_{\mathrm{j}}^{+ext} \;+\; \sum_{\mathrm{i}\,=\,1}^{4} \mathbb{D}_{\mathrm{ci}}\;\boldsymbol{f}_{\mathrm{ci}}^{ext}\,\Big] \tag{6.77}$$

By using the boundary coordinate matrix $\mathbb{D}_{\mathrm{b},p}$ defined in (6.74), the expression for the average stress (6.77) is rearranged in a global expression given by

$$\overline{\boldsymbol{\sigma}} \;=\; \frac{1}{|\mathbb{V}|}\;\mathbb{D}_{\mathrm{b},p}\;\mathbf{f}_{\mathrm{b}}^{ext} \tag{6.78}$$

where global matrix notation has been used to gain the compact form (6.78). Note that $\mathbf{f}_{\mathrm{b}}^{ext}$ is the external boundary force vector which is obtained by gathering operation of the

external force vector to extract the positive $\mathbf{f}_{\mathrm{p}}^{ext}$, negative $\mathbf{f}_{\mathrm{n}}^{ext}$ and corner $\mathbf{f}_{\mathrm{c}}^{ext}$ counterpart as in the expression

$$\mathbf{f}_{\mathrm{b}}^{ext} = \begin{Bmatrix} \mathbf{f}_{\mathrm{p}}^{ext} \\ \mathbf{f}_{\mathrm{n}}^{ext} \\ \mathbf{f}_{\mathrm{c}}^{ext} \end{Bmatrix}$$

6.8.4 Tangent modulus of periodic b.c.

After gathering and rearranging the displacement nodal vector $\mathbf{u}$, the external nodal force vector $\mathbf{f}^{ext}$ and finally the stiffness matrix $\mathbf{K}$, as defined in (6.64) and (6.65), respectively, the general system (6.24) that relates the differential $\mathrm{d}\mathbf{u}$ and $\mathrm{d}\mathbf{f}^{ext}$ is rearranged as follows

$$\begin{bmatrix} \mathbf{k}_{\mathrm{ii}} & \mathbf{k}_{\mathrm{ip}} & \mathbf{k}_{\mathrm{in}} & \mathbf{k}_{\mathrm{ic}} \\ \mathbf{k}_{\mathrm{pi}} & \mathbf{k}_{\mathrm{pp}} & \mathbf{k}_{\mathrm{pn}} & \mathbf{k}_{\mathrm{pc}} \\ \mathbf{k}_{\mathrm{ni}} & \mathbf{k}_{\mathrm{np}} & \mathbf{k}_{\mathrm{nn}} & \mathbf{k}_{\mathrm{nc}} \\ \mathbf{k}_{\mathrm{ci}} & \mathbf{k}_{\mathrm{cp}} & \mathbf{k}_{\mathrm{cn}} & \mathbf{k}_{\mathrm{cc}} \end{bmatrix} \begin{Bmatrix} \mathrm{d}\mathbf{u}_{\mathrm{i}} \\ \mathrm{d}\mathbf{u}_{\mathrm{p}} \\ \mathrm{d}\mathbf{u}_{\mathrm{n}} \\ \mathrm{d}\mathbf{u}_{\mathrm{c}} \end{Bmatrix} = \begin{Bmatrix} \mathrm{d}\mathbf{f}_{\mathrm{i}}^{ext} \\ \mathrm{d}\mathbf{f}_{\mathrm{p}}^{ext} \\ \mathrm{d}\mathbf{f}_{\mathrm{n}}^{ext} \\ \mathrm{d}\mathbf{f}_{\mathrm{c}}^{ext} \end{Bmatrix} \quad \equiv \quad \mathbf{K}\ \mathrm{d}\mathbf{u} = \mathrm{d}\mathbf{f}^{ext} \tag{6.79}$$

where $\mathrm{d}\mathbf{f}_{\mathrm{i}}^{ext} = \mathbf{0}$ in equilibrium. Splitting the displacement vector (6.1) and rearranging the system (6.79), leads to

$$\mathbf{K}\ \mathrm{d}\widetilde{\mathbf{u}} = \mathrm{d}\mathbf{f}^{ext} - \mathbf{K}\ \mathrm{d}\mathbf{u}^{*} \tag{6.80}$$

where the variation of Taylor displacement $\mathrm{d}\mathbf{u}^{*}$ is given by (6.76). Again the general procedure of Section 6.5.2 is followed to rearrange the system in the way described in (6.25). In this system the displacement fluctuation variation vector $\mathrm{d}\widetilde{\mathbf{u}}$ is considered as unknown. Applying into the above split system (6.80) the following conditions: (i) periodic displacement condition (6.67), (ii) prescribed corners displacement (6.69), (iii) antiperiodic external force condition (6.71) leads to the following system

$$\begin{bmatrix} \mathbf{k}_{\mathrm{ii}} & \mathbf{k}_{\mathrm{ip}} + \mathbf{k}_{\mathrm{in}} \\ \mathbf{k}_{\mathrm{pi}} + \mathbf{k}_{\mathrm{ni}} & \mathbf{k}_{\mathrm{pp}} + \mathbf{k}_{\mathrm{pn}} + \mathbf{k}_{\mathrm{np}} + \mathbf{k}_{\mathrm{nn}} \end{bmatrix} \begin{Bmatrix} \mathrm{d}\widetilde{\mathbf{u}}_{\mathrm{i}} \\ \mathrm{d}\widetilde{\mathbf{u}}_{\mathrm{p}} \end{Bmatrix} = - \begin{bmatrix} \mathbf{k}_{\mathrm{ii}} & \mathbf{k}_{\mathrm{ip}} & \mathbf{k}_{\mathrm{in}} & \mathbf{k}_{\mathrm{ic}} \\ \mathbf{k}_{\mathrm{pi}} + \mathbf{k}_{\mathrm{ni}} & \mathbf{k}_{\mathrm{pp}} + \mathbf{k}_{\mathrm{np}} & \mathbf{k}_{\mathrm{pn}} + \mathbf{k}_{\mathrm{nn}} & \mathbf{k}_{\mathrm{pc}} + \mathbf{k}_{\mathrm{nc}} \end{bmatrix} \mathrm{d}\mathbf{u}^{*}$$

which is described in the following compact form

$$\mathbf{K}_2 \begin{Bmatrix} \mathrm{d}\widetilde{\mathbf{u}}_{\mathrm{i}} \\ \mathrm{d}\widetilde{\mathbf{u}}_{\mathrm{p}} \end{Bmatrix} = - \mathbf{K}_{\mathrm{F2}}\ \mathrm{d}\mathbf{u}^{*} \tag{6.81}$$

where $\mathrm{d}\widetilde{\mathbf{u}}_{\mathrm{i}}$ and $\mathrm{d}\widetilde{\mathbf{u}}_{\mathrm{p}}$ are the unknowns. Matrices $\mathbf{K}_2$ and $\mathbf{K}_{\mathrm{F2}}$ are defined by

$$\mathbf{K}_2 = \begin{bmatrix} \mathbf{k}_{ii} & \mathbf{k}_{ip} + \mathbf{k}_{in} \\ \mathbf{k}_{pi} + \mathbf{k}_{ni} & \mathbf{k}_{pp} + \mathbf{k}_{pn} + \mathbf{k}_{np} + \mathbf{k}_{nn} \end{bmatrix}$$

$$\mathbf{K}_{F2} = \begin{bmatrix} \mathbf{k}_{ii} & \mathbf{k}_{ip} & \mathbf{k}_{in} & \mathbf{k}_{ic} \\ \mathbf{k}_{pi} + \mathbf{k}_{ni} & \mathbf{k}_{pp} + \mathbf{k}_{np} & \mathbf{k}_{pn} + \mathbf{k}_{nn} & \mathbf{k}_{pc} + \mathbf{k}_{nc} \end{bmatrix}$$

Displacements $\mathrm{d}\widetilde{\mathbf{u}}_\mathrm{i}$ and $\mathrm{d}\widetilde{\mathbf{u}}_\mathrm{p}$ are then obtained by a simple matrix inversion of $\mathbf{K}_2$. Thus, they are obtained in terms of the Taylor displacement variation $\mathrm{d}\mathbf{u}^*$ as

$$\begin{Bmatrix} \mathrm{d}\widetilde{\mathbf{u}}_\mathrm{i} \\ \mathrm{d}\widetilde{\mathbf{u}}_\mathrm{p} \end{Bmatrix} = - \mathbf{K}_2^{-1} \, \mathbf{K}_{F2} \, \mathrm{d}\mathbf{u}^* \tag{6.82}$$

Variation of boundary forces can be computed explicitly in terms of $\mathrm{d}\widetilde{\mathbf{u}}_\mathrm{i}$ and $\mathrm{d}\widetilde{\mathbf{u}}_\mathrm{p}$ and the Taylor displacement variation $\mathrm{d}\mathbf{u}^*$. Firstly, the external positive nodal force vector is

$$\mathrm{df}_\mathrm{p}^{ext} = \begin{bmatrix} \mathbf{k}_{pi} & \mathbf{k}_{pp} + \mathbf{k}_{pn} \end{bmatrix} \begin{Bmatrix} \mathrm{d}\widetilde{\mathbf{u}}_\mathrm{i} \\ \mathrm{d}\widetilde{\mathbf{u}}_\mathrm{p} \end{Bmatrix} + \begin{bmatrix} \mathbf{k}_{pi} & \mathbf{k}_{pp} & \mathbf{k}_{pn} & \mathbf{k}_{pc} \end{bmatrix} \mathrm{d}\mathbf{u}^* \tag{6.83}$$

where using the matrix notation

$$\mathbf{K}_{P1} = \begin{bmatrix} \mathbf{K}_{pi} & \mathbf{k}_{pp} + \mathbf{k}_{pn} \end{bmatrix} \ , \quad \mathbf{k}_{P2} = \begin{bmatrix} \mathbf{k}_{pi} & \mathbf{k}_{pp} & \mathbf{k}_{pn} & \mathbf{k}_{pc} \end{bmatrix} \ ,$$

the following compact expression for $\mathrm{df}_\mathrm{p}^{ext}$ is obtained:

$$\mathrm{df}_\mathrm{p}^{ext} = \mathbf{K}_{P1} \begin{Bmatrix} \mathrm{d}\widetilde{\mathbf{u}}_\mathrm{i} \\ \mathrm{d}\widetilde{\mathbf{u}}_\mathrm{p} \end{Bmatrix} + \mathbf{K}_{P2} \, \mathrm{d}\mathbf{u}^* \tag{6.84}$$

Once the positive nodal force vector variation was computed, the negative nodal force vector variation $\mathrm{df}_\mathrm{n}^{ext}$ is also obtained straight away, since the negative and positive vectors are opposite to each other (6.71). Therefore

$$\mathrm{df}_\mathrm{n}^{ext} = -\mathrm{df}_\mathrm{p}^{ext} \tag{6.85}$$

with $\mathrm{df}_\mathrm{p}^{ext}$ previously obtained in (6.84).

In addition, the external corner node vector variation $\mathrm{df}_\mathrm{c}^{ext}$ is computed as

$$\mathrm{df}_\mathrm{c}^{ext} = \begin{bmatrix} \mathbf{k}_{ci} & \mathbf{k}_{cp} + \mathbf{k}_{cn} \end{bmatrix} \begin{Bmatrix} \mathrm{d}\widetilde{\mathbf{u}}_\mathrm{i} \\ \mathrm{d}\widetilde{\mathbf{u}}_\mathrm{p} \end{Bmatrix} + \begin{bmatrix} \mathbf{k}_{ci} & \mathbf{k}_{cp} & \mathbf{k}_{cn} & \mathbf{k}_{cc} \end{bmatrix} \mathrm{d}\mathbf{u}^* \tag{6.86}$$

which can be represented in a compact form as

$$\mathrm{df}_{\mathrm{c}}^{ext} = \mathbf{K}_{\mathrm{C1}} \begin{Bmatrix} \mathrm{d}\widetilde{\mathbf{u}}_{\mathrm{i}} \\ \mathrm{d}\widetilde{\mathbf{u}}_{\mathrm{p}} \end{Bmatrix} + \mathbf{K}_{\mathrm{C2}}\ \mathrm{d}\mathbf{u}^{*} \tag{6.87}$$

where

$$\mathbf{K}_{\mathrm{C1}} = \begin{bmatrix} \mathbf{k}_{\mathrm{ci}} & \mathbf{k}_{\mathrm{cp}} + \mathbf{k}_{\mathrm{cn}} \end{bmatrix} \quad \mathbf{K}_{\mathrm{C2}} = \begin{bmatrix} \mathbf{k}_{\mathrm{ci}} & \mathbf{k}_{\mathrm{cp}} & \mathbf{k}_{\mathrm{cn}} & \mathbf{k}_{\mathrm{cc}} \end{bmatrix}$$

However, the sum of all the corners force (6.72) there is one condition that has not been taken into consideration so far. This condition implies that one of the corner forces is a dependant variable of the other corner forces. Basically, we can not compute all the corner forces at the same time using (6.87).

Hence, by using (6.72) $\mathrm{df}_{\mathrm{c1}}^{ext}$ is computed as,

$$\mathrm{df}_{\mathrm{c1}}^{ext} = -(\mathrm{df}_{\mathrm{c2}}^{ext} + \mathrm{df}_{\mathrm{c3}}^{ext} + \mathrm{df}_{\mathrm{c4}}^{ext}) \tag{6.88}$$

The new matrices are defined $\hat{\mathbf{K}}_{\mathrm{C1}}$ and $\hat{\mathbf{K}}_{\mathrm{C2}}$, respectively. So that, the expression (6.87) is then reduced to

$$\mathrm{df}_{\mathrm{c}}^{ext} = \hat{\mathbf{K}}_{\mathrm{C1}} \begin{Bmatrix} \mathrm{d}\widetilde{\mathbf{u}}_{\mathrm{i}} \\ \mathrm{d}\widetilde{\mathbf{u}}_{\mathrm{p}} \end{Bmatrix} + \hat{\mathbf{K}}_{\mathrm{C2}}\ \mathrm{d}\mathbf{u}^{*} \tag{6.89}$$

The direct condensation of matrices $\hat{\mathbf{K}}_{\mathrm{C1}}$ and $\hat{\mathbf{K}}_{\mathrm{C2}}$ has been sketched in Appendix D. By using (6.82), the variation external boundary force vectors $\mathrm{df}_{\mathrm{p}}^{ext}$, $\mathrm{df}_{\mathrm{n}}^{ext}$ and $\mathrm{df}_{\mathrm{c}}^{ext}$ can be expressed only in terms of the Taylor displacement variation $\mathrm{d}\mathbf{u}^{*}$

$$\mathrm{df}_{\mathrm{p}}^{ext} = \mathbf{K}^{\mathrm{P}}\ \mathrm{d}\mathbf{u}^{*} \tag{6.90}$$

$$\mathrm{df}_{\mathrm{n}}^{ext} = -\mathbf{K}^{\mathrm{P}}\ \mathrm{d}\mathbf{u}^{*} \tag{6.91}$$

$$\mathrm{df}_{\mathrm{c}}^{ext} = \hat{\mathbf{K}}^{\mathrm{C}}\ \mathrm{d}\mathbf{u}^{*} \tag{6.92}$$

where the matrix $\mathbf{K}^{\mathrm{P}}$ and $\hat{\mathbf{K}}^{\mathrm{C}}$ are defined as

$$\mathbf{K}^{\mathrm{P}} = \mathbf{K}_{\mathrm{P2}} - \mathbf{K}_{\mathrm{P1}}\,\mathbf{K}_{2}^{-1}\,\mathbf{K}_{\mathrm{F2}} \quad \text{and} \quad \hat{\mathbf{K}}^{\mathrm{C}} = \hat{\mathbf{K}}_{\mathrm{C2}} - \hat{\mathbf{K}}_{\mathrm{C1}}\,\mathbf{K}_{2}^{-1}\,\mathbf{K}_{\mathrm{F2}} \tag{6.93}$$

Hence, the boundary force vector variation $\mathrm{df}_{\mathrm{b}}^{ext}$ can now be expressed in terms of the Taylor displacement variation $\mathrm{d}\mathbf{u}^{*}$. By adding (6.90), (6.91) and (6.92) it follows

$$\mathrm{df}_{\mathrm{b}}^{ext} \equiv \left\{ \begin{array}{c} \mathrm{df}_{\mathrm{p}}^{ext} \\ \mathrm{df}_{\mathrm{n}}^{ext} \\ \mathrm{df}_{\mathrm{c}}^{ext} \end{array} \right\} = \mathbf{K}_{\mathbf{per}}^{\mathbf{B}} \, \mathrm{du}^{*} \tag{6.94}$$

where the matrix $\mathbf{K}_{\mathbf{per}}^{\mathbf{B}}$ is defined as

$$\mathbf{K}_{\mathbf{per}}^{\mathbf{B}} = \begin{bmatrix} \mathbf{K}^{\mathrm{P}} \\ -\mathbf{K}^{\mathrm{P}} \\ \hat{\mathbf{K}}^{\mathrm{C}} \end{bmatrix} \tag{6.95}$$

This gives the expression

$$\mathrm{df}_{\mathrm{b}}^{ext} = \mathbf{K}_{\mathbf{per}}^{\mathbf{B}} \; \mathbb{D}_{\mathrm{global},p}^{\mathrm{T}} \, \mathrm{d}\overline{\boldsymbol{\epsilon}} \tag{6.96}$$

where the Taylor displacement variation (6.76) was inserted into the equation (6.94). Therefore, the desired expression is gained as

$$\frac{\mathrm{df}_{\mathrm{b}}^{ext}}{\mathrm{d}\overline{\boldsymbol{\epsilon}}} = \mathbf{K}_{\mathbf{per}}^{\mathbf{B}} \; \mathbb{D}_{\mathrm{global},p}^{\mathrm{T}} \tag{6.97}$$

which gives the variation of external boundary force vector $\mathrm{df}_{\mathrm{b}}^{ext}$ with respect to the variation of macroscopic average strain matrix $\mathrm{d}\overline{\boldsymbol{\epsilon}}$.

The overall tangent modulus $\overline{\boldsymbol{\mathcal{C}}}_p$ for Periodic b.c., can be computed in its discretised F.E. matrix form following the general expression given in (6.26), that is

$$\overline{\boldsymbol{\mathcal{C}}}_p = \frac{\mathrm{d}\overline{\boldsymbol{\sigma}}}{\mathrm{d}\overline{\boldsymbol{\epsilon}}} = \frac{1}{|\mathbb{V}|} \, \mathbb{D}_{\mathrm{b},p} \, \frac{\mathrm{df}_{\mathrm{b}}^{ext}}{\mathrm{d}\overline{\boldsymbol{\epsilon}}} \tag{6.98}$$

where $\mathbb{D}_{\mathrm{b},p}$ was defined in (6.74).

Substituting (6.97) into (6.98), the overall tangent modulus matrix representation $\overline{\boldsymbol{\mathcal{C}}}_p$ is obtained as

$$\boxed{\overline{\boldsymbol{\mathcal{C}}}_p = \frac{1}{|\mathbb{V}|} \, \mathbb{D}_{\mathrm{b},p} \, \mathbf{K}_{\mathbf{per}}^{\mathbf{B}} \, \mathbb{D}_{\mathrm{global},p}^{\mathrm{T}}} \tag{6.99}$$

Clearly, the modulus $\overline{\boldsymbol{\mathcal{C}}}_p$ is a function of the boundary coordinate matrix $\mathbb{D}_{\mathrm{b},p}$ defined in (6.74), the condensed periodic stiffness matrix $\mathbf{K}_{\mathbf{per}}^{\mathbf{B}}$ and the global coordinate matrix $\mathbb{D}_{\mathrm{global},p}$ outlined in (6.73). Finally, we remark that with the above (6.99), the tangent modulus can be computed for heterogeneous material with different microstructures RVE gaining the desired *quadratic rate of convergence*, for the Newton-Raphson solution

procedure applied to solve the homogenized nonlinear macrostructure, under *periodic deformation* and *antiperiodic traction* on the boundary of RVE model.

6.8.5 Microequilibrium computation for periodic b.c.

In Section 6.4.1 a general solution scheme for microequilibrium was given. In this section, the particularisation of the microequilibrium procedure for periodic b.c. is given.

The incremental Taylor displacement is given in matrix form as,

$$\triangle \mathbf{u}^* = \mathbb{D}^{\mathrm{T}}_{\mathrm{global},p} \triangle \overline{\boldsymbol{\epsilon}}. \tag{6.100}$$

The residual force $\mathbf{r}$ is taken as,

$$\mathbf{r} = \begin{Bmatrix} \mathbf{f}_{\mathrm{i}}^{int} \\ \mathbf{f}_{\mathrm{p}}^{int} + \mathbf{f}_{\mathrm{n}}^{int} \end{Bmatrix} - \begin{Bmatrix} \mathbf{f}_{\mathrm{i}}^{ext} \\ \mathbf{f}_{\mathrm{p}}^{ext} + \mathbf{f}_{\mathrm{n}}^{ext} \end{Bmatrix} \tag{6.101}$$

Assuming that in equilibrium $\mathbf{f}_{\mathrm{i}}^{ext} = \mathbf{0}$ and antiperiodicity of the boundary traction in discrete form $\mathbf{f}_{\mathrm{p}}^{ext} + \mathbf{f}_{\mathrm{n}}^{ext} = \mathbf{0}$, the residual for periodic b.c. takes the form,

$$\mathbf{r} = \begin{Bmatrix} \mathbf{f}_{\mathrm{i}}^{int} \\ \mathbf{f}_{\mathrm{p}}^{int} + \mathbf{f}_{\mathrm{n}}^{int} \end{Bmatrix}. \tag{6.102}$$

The differential fluctuation is given by the system (6.17) which takes the following form for periodic b.c.

$$\mathbf{K}_2 \begin{Bmatrix} \delta\widetilde{\mathbf{u}}_{\mathrm{i}} \\ \delta\widetilde{\mathbf{u}}_{\mathrm{p}} \end{Bmatrix} = - \begin{Bmatrix} \mathbf{f}_{\mathrm{i}}^{int} \\ \mathbf{f}_{\mathrm{p}}^{int} + \mathbf{f}_{\mathrm{n}}^{int} \end{Bmatrix} \quad \Rightarrow \quad \begin{Bmatrix} \delta\widetilde{\mathbf{u}}_{\mathrm{i}} \\ \delta\widetilde{\mathbf{u}}_{\mathrm{p}} \end{Bmatrix} = -\mathbf{K}_2^{-1} \begin{Bmatrix} \mathbf{f}_{\mathrm{i}}^{int} \\ \mathbf{f}_{\mathrm{p}}^{int} + \mathbf{f}_{\mathrm{n}}^{int} \end{Bmatrix} \tag{6.103}$$

for differential displacement fluctuation for interior and positive nodes. Also taking into consideration (6.69) and (6.67), the differential displacement fluctuation for negative and corners is computed as,

$$\delta\widetilde{\mathbf{u}}_{\mathrm{n}} = \delta\widetilde{\mathbf{u}}_{\mathrm{p}} \quad \text{and} \quad \delta\widetilde{\mathbf{u}}_{\mathrm{c}} = \mathbf{0} \tag{6.104}$$

The updating of the incremental fluctuation is then given by

$$\begin{array}{rcl} \triangle\widetilde{\mathbf{u}}_{\mathrm{i}} & \leftarrow & \triangle\widetilde{\mathbf{u}}_{\mathrm{i}} + \delta\widetilde{\mathbf{u}}_{\mathrm{i}} \\ \triangle\widetilde{\mathbf{u}}_{\mathrm{p}} & \leftarrow & \triangle\widetilde{\mathbf{u}}_{\mathrm{p}} + \delta\widetilde{\mathbf{u}}_{\mathrm{p}} \\ \triangle\widetilde{\mathbf{u}}_{\mathrm{n}} & \leftarrow & \triangle\widetilde{\mathbf{u}}_{\mathrm{p}} \end{array} \tag{6.105}$$

and $\triangle\widetilde{\mathbf{u}}_c = \mathbf{0}$. Finally, the incremental displacement to compute the internal force is updated as

$$\begin{array}{rcl} \triangle\mathbf{u}_i & \leftarrow & \triangle\mathbf{u}_i + \delta\widetilde{\mathbf{u}}_i \\ \triangle\mathbf{u}_p & \leftarrow & \triangle\mathbf{u}_p + \delta\widetilde{\mathbf{u}}_p \\ \triangle\mathbf{u}_n & \leftarrow & \triangle\mathbf{u}_p \end{array} \tag{6.106}$$

and $\triangle\mathbf{u}_c$ remains constant.

6.9 Conclusions

In this chapter, detailed description of multiscale F.E. analysis of solids undergoing small strains has been given. In the next two chapters 7 and 8 we describe the multiscale homogenization at large strain. In Chapter 9, numerical tests have been performed to validate the models described here.

Chapter 7

Multiscale continuum model at large strains

7.1 Introduction

In this chapter, a general continuum multiscale model at large strain is described. This chapter follows the structure of Chapter 5 for multiscale analysis at small strain. However, this chapter focuses the large strain analysis. Some concepts are repeated from Chapter 5 to facilitate on reading.

7.1.1 Outline

Firstly, a general multiscale continuum description is given. A deformation-driven microstructure analysis is assumed, in which the macroscopic deformation is prescribed over the microstructure as an average. Then, the basic microvariables and macrovariables are introduced. The Hill-Mandel principle links the scales. Finally, three classical conditions are given, to prescribe the macrodeformation over the microstructure:

- Taylor assumption over the microstructure.
- Linear displacement on the boundary (Linear b.c.).
- Periodic displacement and antiperiodic traction on the boundary (Periodic b.c.).

7.2 Continuum macro and microscale at finite deformation

A homogenized macro-continuum, in its deformed configuration, with locally attached microstructures visualized in Figure 7.1 is considered. The microstructure $\mathbb{B} \subset \mathbb{R}^3$ is considered, with overall properties related to the macro-continuum $\overline{\mathbb{B}} \subset \mathbb{R}^3$.

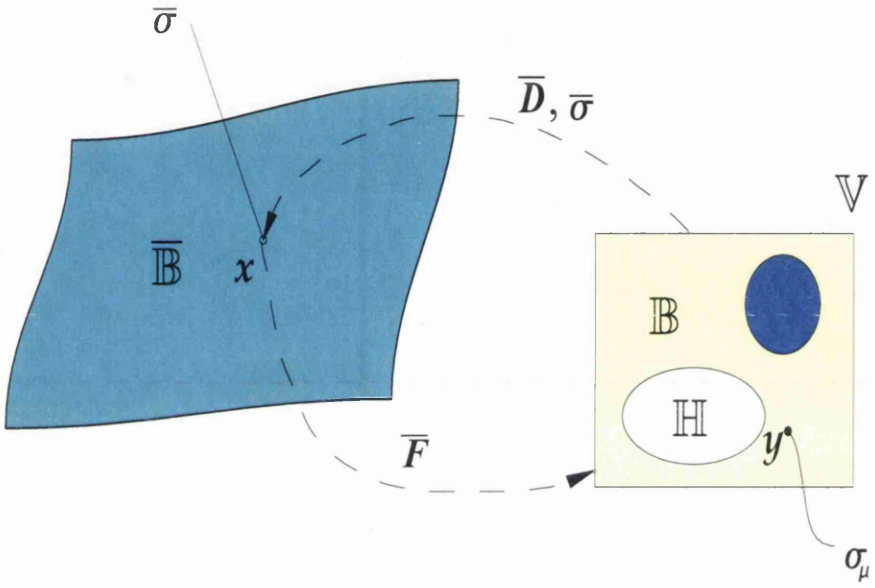

Figure 7.1: Micro to macro transition

For the description of the macro and micro continuum and notation we refer to Section 5.2.

7.3 Basic microvariables

The *microscopic deformation gradient* is defined, following the general definition given in (2.7), by

$$\mathbf{F}_\mu(\mathbf{Y}, t) \equiv \frac{\partial \boldsymbol{\phi}}{\partial \mathbf{Y}} \equiv \frac{\partial \boldsymbol{y}}{\partial \mathbf{Y}} \equiv \nabla_0 \boldsymbol{y} \tag{7.1}$$

where $\boldsymbol{y} \in \mathbb{B}$ is the spatial point, $\mathbb{B}$ is the spatial configuration of the microstructure, and $\boldsymbol{y} \in \mathbb{B}_0$ the corresponding material point of the microstructure in undeformed configuration $\mathbb{B}_0$. Therefore, the microscopic deformation gradient is defined as the material gradient of the spatial coordinates.

The *microscopic small strain tensor* $\boldsymbol{\epsilon}_\mu$ is defined for the finite strain analysis as the symmetric part of the spatial displacement gradient tensor (2.30) i.e.

$$\boldsymbol{\epsilon}_\mu(\mathbf{Y},t) \equiv \text{sym}\{\nabla \mathbf{u}\} \equiv \frac{1}{2}\left[\nabla \mathbf{u} + (\nabla \mathbf{u})^{\text{T}}\right] \tag{7.2}$$

where $\mathbf{u}$ is the displacement field at a material point $\boldsymbol{y} \in \mathbb{B}$.

Microequilibrium state is assumed in its spatial form in the presence of body forces $\mathbf{b}$ per unit of mass (2.56),

$$\nabla \cdot \boldsymbol{\sigma}_\mu + \rho\, \mathbf{b} = \mathbf{0} \quad \text{in } \mathbb{B} \tag{7.3}$$

where $\boldsymbol{\sigma}_\mu$ is the symmetric microscopic Cauchy stress tensor. The material form of the equilibrium is given by

$$\nabla_0 \cdot \mathbf{P}_\mu + \rho_0\, \mathbf{b} = \mathbf{0} \quad \text{in } \mathbb{B}_0 \tag{7.4}$$

The microscopic Kirchhoff symmetric stress tensor $\boldsymbol{\tau}_\mu$ is assumed to be related to the Cauchy stress tensor, as defined in (2.36), by

$$\boldsymbol{\tau}_\mu = J_\mu\, \boldsymbol{\sigma}_\mu \tag{7.5}$$

A constitutive law, as defined in Chapter 4, is assumed, for instance the incremental constitutive law defined as

$$\boldsymbol{\tau}_\mu = \hat{\boldsymbol{\tau}}_\mu(\mathbf{F}_\mu\, ;\boldsymbol{\alpha}\, ;\, \boldsymbol{y}) \quad \text{in } \mathbb{B} \tag{7.6}$$

where $\boldsymbol{\alpha}$ is the set of internal variables. The simplest example is the elastic constitutive model given as

$$\boldsymbol{\tau}_\mu = \frac{\partial \psi(\boldsymbol{\tau}_\mu\, ;\, \boldsymbol{y})}{\partial \mathbf{F}_\mu} \quad \text{in } \mathbb{B} \tag{7.7}$$

where ψ denotes a strain energy function.

Applying Gauss theorem in (7.3) The global microequilibrium condition are obtained

$$\int_{\partial\mathbb{B}} \mathbf{t}\, \mathrm{d}A + \int_{\mathbb{B}} \rho\, \mathbf{b}\, \mathrm{d}V = \mathbf{0} \quad \text{and} \quad \int_{\partial\mathbb{B}} \boldsymbol{y} \times \mathbf{t}\, \mathrm{d}A + \int_{\mathbb{B}} \boldsymbol{y} \times \rho\, \mathbf{b}\, \mathrm{d}V = \mathbf{0} \tag{7.8}$$

where $\mathbf{t} = \boldsymbol{\sigma}_\mu \cdot \mathbf{n}$ on $\partial\mathbb{B}$ denotes the traction field on the surface with outward normal $\mathbf{n}$ at $\boldsymbol{y} \in \partial\mathbb{B}$.

7.4 Basic macrovariables and averaging theorem

7.4.1 Overall Cauchy macrostress

Within the described homogenization technique no constitutive assumptions have been assumed at the macrolevel. Overall macrostress $\boldsymbol{\sigma}_{\mathrm{M}}$ of microstructure $\mathbb{B}$ is defined as average of the microstresses over the unit cell $\overline{\boldsymbol{\sigma}}$. Applying Gauss theorem and micro-quilibrium (7.3), $\overline{\boldsymbol{\sigma}}$ is givenby the expression

$$\boldsymbol{\sigma}_{\mathrm{M}} \equiv \overline{\boldsymbol{\sigma}} = \frac{1}{|\mathbb{V}|}\int_{\partial\mathbb{V}} \mathrm{sym}[\mathbf{t}\otimes\boldsymbol{y}]\,\mathrm{d}A + \frac{1}{|\mathbb{V}|}\int_{\mathbb{V}} \rho\,\mathrm{sym}[\mathbf{b}\otimes\boldsymbol{y}]\,\mathrm{d}V \tag{7.9}$$

in terms of the traction $\mathbf{t}$ at $\boldsymbol{y}\in\partial\mathbb{V}$ and body force vector field $\mathbf{b}$ at $\boldsymbol{y}\in\mathbb{V}$. We refer to the Appendix A.1 for further details of the proof of expression (7.9).

The macro first Piola-Kirchhoff stress tensor can be defined as

$$\mathbf{P}_{\mathrm{M}} = J_{\mathrm{M}}\,\overline{\boldsymbol{\sigma}}\cdot\overline{\mathbf{F}}^{-\mathrm{T}} \tag{7.10}$$

7.4.2 Overall Kirchhoff macrostress

The macroscopic Kirchhoff stress tensor $\boldsymbol{\tau}_{\mathrm{M}}$ is defined in terms of the macroscopic average Cauchy stress tensor

$$\boldsymbol{\tau}_{\mathrm{M}} \equiv J_{\mathrm{M}}\,\boldsymbol{\sigma}_{\mathrm{M}} = J_{\mathrm{M}}\,\overline{\boldsymbol{\sigma}} \tag{7.11}$$

Note that $\boldsymbol{\tau}_{\mathrm{M}}$ is equal to the average Kirchhoff stress tensor over the microstructure

$$\boldsymbol{\tau}_{\mathrm{M}} = \overline{\boldsymbol{\tau}} \tag{7.12}$$

We refer to Appendix A.2 for details of the expression (7.12). In similarity to (7.9), $\overline{\boldsymbol{\tau}}$ is given by the following expression:

$$\boldsymbol{\tau}_{\mathrm{M}} \equiv \overline{\boldsymbol{\tau}} = \frac{1}{|\mathbb{V}_0|}\int_{\partial\mathbb{V}} \mathrm{sym}[\mathbf{t}\otimes\boldsymbol{y}]\,\mathrm{d}A + \frac{1}{|\mathbb{V}_0|}\int_{\mathbb{V}} \rho\,\mathrm{sym}[\mathbf{b}\otimes\boldsymbol{y}]\,\mathrm{d}V \tag{7.13}$$

7.4.3 Overall deformation gradient

The macro deformation gradient $\mathbf{F}_{\mathrm{M}}$ is defined as an average over the undeformed unit cell and denoted by $\overline{\mathbf{F}}$. By applying Green's Lemma the following expression is obtained

$$\mathbf{F}_{\mathrm{M}} \equiv \overline{\mathbf{F}} = \frac{1}{|\mathbb{V}_0|} \int_{\partial \mathbb{V}_0} [\boldsymbol{y} \otimes \mathbf{N}] \, \mathrm{d}A_0 \tag{7.14}$$

in terms of the spatial coordinates at $\boldsymbol{y} \in \partial \mathbb{V}$ and the outward normal vector $\mathbf{N} \in \partial \mathbb{V}_0$. We refer to the Appendix B.2 for further details of the proof of expression (7.14).

7.4.4 Homogenised spatial tangent modulus

The modulus $\overline{\boldsymbol{\mathcal{D}}}^{\tau \mathrm{F}}$, as defined previously in (2.97) in a general continuum form, relates the variations of the overall macro Kirchhoff stress $\overline{\boldsymbol{\tau}}$ and the macro-deformation gradient tensor $\overline{\mathbf{F}}$ in the following form

$$\overline{\boldsymbol{\mathcal{D}}}^{\tau \mathrm{F}} \equiv \frac{\partial \overline{\boldsymbol{\tau}}}{\partial \overline{\mathbf{F}}} \tag{7.15}$$

Homogenised spatial tangent modulus $\overline{\boldsymbol{\mathcal{A}}}$, defined previously for a general continuum media in (2.96) is recalled as,

$$\overline{\boldsymbol{\mathcal{A}}} = \frac{1}{J_{\mathrm{M}}} \overline{\boldsymbol{\mathcal{D}}}^{\tau \mathrm{F}} \diamond \overline{\mathbf{F}} - \overline{\boldsymbol{\sigma}} \star \mathbf{I} \tag{7.16}$$

$$\overline{A}_{ijkl} = \frac{1}{J_{\mathrm{M}}} \frac{\partial \overline{\tau}_{ij}}{\partial \overline{F}_{km}} \overline{F}_{lk} - \overline{\sigma}_{il} \delta_{jk} \tag{7.17}$$

The computation of these fourth-order tensors is one of the goals of this work.

7.4.5 The Hill-Mandel principle

The Hill-Mandel principle or averaging theorem [74], demands that macroscopic stress power must equal the volume average of the microscopic stress power over the RVE correspondent to the macroscopic point $\mathbf{X}$, that is

$$\overline{\mathbf{P}} : \dot{\overline{\mathbf{F}}} = \frac{1}{|\mathbb{V}_0|} \int_{\mathbb{V}_0} \mathbf{P}_\mu : \dot{\mathbf{F}}_\mu \, \mathrm{d}V \tag{7.18}$$

Using (7.1) and integrating by parts the right hand side of (7.18) and then applying microequilibrium in its material form (7.4), the averaging theorem can be expressed in the following

$$\overline{\mathbf{P}} : \dot{\overline{\mathbf{F}}} = \frac{1}{|\mathbb{V}_0|} \int_{\partial \mathbb{V}_0} \mathbf{t}_0 \cdot \dot{\mathbf{u}} \, \mathrm{d}A_0 + \frac{1}{|\mathbb{V}_0|} \int_{\mathbb{V}_0} \rho_0 \, \mathbf{b} \cdot \dot{\mathbf{u}} \, \mathrm{d}V_0 \tag{7.19}$$

We note that the overall deformation at the macroscale have been defined as average deformation gradient on the *undeformed configuration* of the microscale in (7.14). However, in the averaging theorem (7.18) the overall First Piola-Kirchhoff stress tensor $\overline{\mathbf{P}}$ is used as an average of the micro first Piola-Kirchhoff on the *undeformed configuration* of the microscale as follows,

$$\overline{\mathbf{P}} \equiv \frac{1}{|\mathbb{V}_0|} \int_{\mathbb{V}_0} \mathbf{P}_\mu \, \mathrm{d}V_0. \tag{7.20}$$

This seems to be a contradiction because of the definition of our overall Cauchy stress (7.9) suggests that First Piola Kirchhoff stress tensor $\mathbf{P}_{\mathrm{M}}$ should be taken, using (7.10) which in principle differs from the average over the microstructure (7.20).

This problem has been solved by de Souza Neto and Feijóo [19] by proving that, under certain kinematical constraints, for instance Taylor assumption, linear b.c. and periodic b.c. the following is satisfied: the volume averaging of the microscopic first Piola-Kirchhoff stress over the materialconfiguration of the RVE is equivalent to the averaging of the microscopic Cauchy stress tensor over the deformed configuration. This shows the equivalence between material and spatial formulation. Therefore, the first Piola-Kirchhoff tensor $\mathbf{P}_{\mathrm{M}}$, defined as a function of the average deformation gradient and average Cauchy stress tensor in (7.10), and the macro average first Piola-Kirchhoff $\overline{\mathbf{P}}$ over the *undeformed configuration* defined in (7.20) coincide, that is,

$$\overline{\mathbf{P}} = \mathbf{P}_{\mathrm{M}} \tag{7.21}$$

for the Taylor assumption, Linear b.c. and Periodic b.c.

7.5 Definition of the boundary conditions for the small scale

The boundary conditions for the displacement $\mathbf{u}$ and traction $\mathbf{t}$ on the microstructure, are chosen such that condition (7.18) is satisfied. Three classical types of boundary conditions are prescribed on the unit cell: (a) Taylor assumption (b) Linear displacements on the boundary and (c) periodic displacements and antiperiodic tractions on the boundary. A crucial aspect of our approach is the formulation in deformation-driven context, where the macroscopic deformation gradient $\overline{\mathbf{F}}$ is prescribed.

The spatial coordinate field is divided in two parts:

$$\boldsymbol{y}(\mathbf{Y}) \;=\; \mathbf{y}^*(\mathbf{Y}) \;+\; \tilde{\mathbf{u}}(\mathbf{Y}) \;=\; \overline{\mathbf{F}}\,\mathbf{Y} \;+\; \tilde{\mathbf{u}}(\mathbf{Y}) \tag{7.22}$$

where $\mathbf{y}^*$ is the *Taylor spatial coordinate*, which defines a constant deformation gradient

$\overline{\mathbf{F}}$ over the unit cell as

$$\mathbf{y}^* \equiv \overline{\mathbf{F}}\,\mathbf{Y} \tag{7.23}$$

and the component $\widetilde{\mathbf{u}}$ known as the *displacement fluctuation*, which is considered to be the unknown.

Insertion of the rate form of (7.22) into the averaging theorem (7.19) yields in the following new form of the Hill-Mandel principle

$$\frac{1}{|\mathbb{V}_0|}\int_{\partial\mathbb{V}_0} \mathbf{t}_0 \cdot \dot{\widetilde{\mathbf{u}}}\, \mathrm{d}A_0 + \frac{1}{|\mathbb{V}_0|}\int_{\mathbb{V}} \rho_0\, \mathbf{b} \cdot \dot{\widetilde{\mathbf{u}}}\, \mathrm{d}V_0 = 0 \tag{7.24}$$

7.5.1 Taylor assumption on the RVE in large strain

This model was firstly proposed by Taylor [31] and applied to metallic single crystals. The Taylor assumption defines a displacement field over the microstructure as

$$\boldsymbol{y}(\mathbf{Y}) \;=\; \overline{\mathbf{F}}\,\mathbf{Y} \qquad \text{at } \mathbf{Y} \in \mathbb{V}_0 \tag{7.25}$$

with constant deformation gradient $\overline{\mathbf{F}}$ imposed over the whole unit cell RVE. An alternative way to express this condition is to define zero displacement fluctuation over the whole unit cell

$$\widetilde{\mathbf{u}}(\mathbf{Y}) \;=\; \mathbf{0} \qquad \text{at } \mathbf{Y} \in \mathbb{V}_0 \tag{7.26}$$

Insertion of the above condition into (7.24) proves that Taylor assumption satisfies the averaging theorem.

7.5.2 Linear displacements on the boundary of RVE in large strain

The definition of the linear deformation boundary constraint over the microstructure RVE shown in Figure 7.2, in terms of the macroscopic deformation gradient $\overline{\mathbf{F}}$, assumes the following form

$$\boldsymbol{y}(\mathbf{Y}) \;=\; \overline{\mathbf{F}}\,\mathbf{Y} \qquad \text{at } \mathbf{Y} \in \partial\mathbb{V}_0 \tag{7.27}$$

Alternatively, the above statement can be expressed by enforcing zero displacement fluctuation over the boundary of the unit cell

$$\widetilde{\mathbf{u}}(\mathbf{Y}) = \mathbf{0} \qquad \text{at } \mathbf{Y} \in \partial\mathbb{V}_0 \tag{7.28}$$

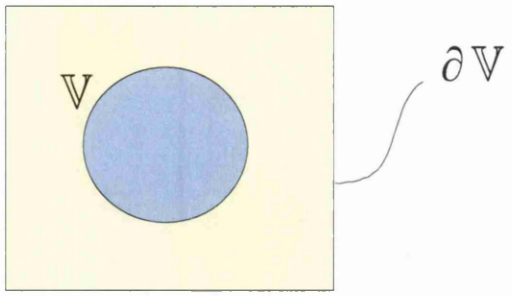

Figure 7.2: Microstructure for linear b.c.

This condition defines a linear deformation $\overline{\mathbf{F}}$ on the boundary $\partial\mathbb{V}$ of the RVE. Insertion of the above condition (7.28) into the new averaging condition form (7.24) confirms that this model satisfies the averaging theorem only when body force effect is negligible.

7.5.3 Periodic deformation and antiperiodic traction on the boundary of RVE in large strain

Another possibility consists of applying periodic deformation and antiperiodic traction on the boundary of the RVE $\partial\mathbb{V}$, which is represented as

$$\boldsymbol{y}(\mathbf{Y}^+) - \boldsymbol{y}(\mathbf{Y}^-) = \overline{\mathbf{F}}\,(\mathbf{Y}^+ - \mathbf{Y}^-) \tag{7.29}$$

$$\mathbf{t}(\mathbf{Y}^+) = -\mathbf{t}(\mathbf{Y}^-) \tag{7.30}$$

By taking into consideration the displacement field division (7.22), the periodic deformation condition above (7.29) can also be imposed by enforcing the displacement fluctuation on the boundary of RVE to be periodic, hence

$$\widetilde{\mathbf{u}}(\mathbf{Y}^+) = \widetilde{\mathbf{u}}(\mathbf{Y}^-) \tag{7.31}$$

In order to apply these conditions the boundary of the unit cell is decomposed in two parts as indicated in Figure 7.3. Thus $\partial\mathbb{V} = \partial\mathbb{V}^+ \cup \partial\mathbb{V}^-$ with outwards normals $\mathbf{n}^+ = -\mathbf{n}^-$ which are associated with the points $\boldsymbol{y}^+ \in \partial\mathbb{V}^+$ and $\boldsymbol{y}^- \in \partial\mathbb{V}^-$.

Body force is not taken into consideration so that this condition satisfy the averaging theorem. This can be proved easily by inserting the periodic displacement fluctuation (7.31) and antiperiodic traction (7.30) into the new form of the averaging theorem (7.24).

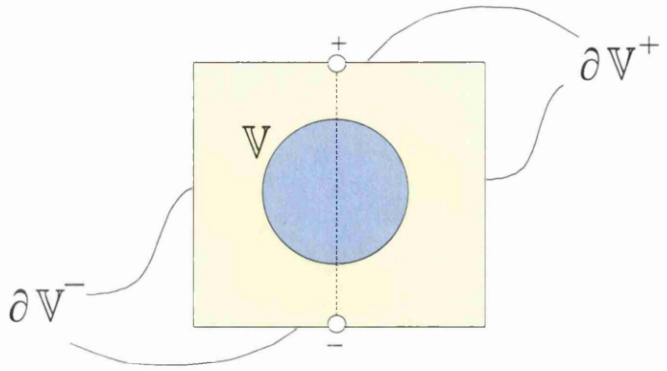

Figure 7.3: Microstructure for periodic b.c.

7.6 Conclusions

In this chapter, the main ingredients of multiscale continuum homogenization of solids undergoing large strains have been given. Chapter 8 describes the multiscale discrete F.E. analysis.

Chapter 8

Multiscale discretised model at large strains

8.1 Introduction

In this chapter, a general discretised multiscale F.E. model at large strain is described. The chapter follows the same structure as Chapter 6 for multiscale F.E. analysis at small strain. However, this chapter focuses on the large strain F.E. analysis. Although many concepts are repeated from Chapter 6, we have described some of them again to facilitate the reading. Chapter 7 gives the continuum mechanics background necessary for this chapter.

8.1.1 Outline

Firstly, a general multiscale F.E. description based on the F.E. discretisation is given. A deformation-driven microstructure analysis is assumed, where the macroscopic deformation at macro Gauss point level is prescribed over the discretised microstructure as an average. Secondly, the partition of the displacement field and a matrix F.E. notation are introduced. Then, a microequilibrium solution procedure is given for the microstructure with the consequent average Kirchhoff macrostress and overall spatial tangent modulus computation. Finally, those computations are particularised for Taylor assumption, Linear b.c. and Periodic b.c.

8.2 Discrete macro and microscale

A discrete model of the macro and microstructure is considered in Figure 8.1.

This work is focussed on deformation-driven microstructures where the value of the

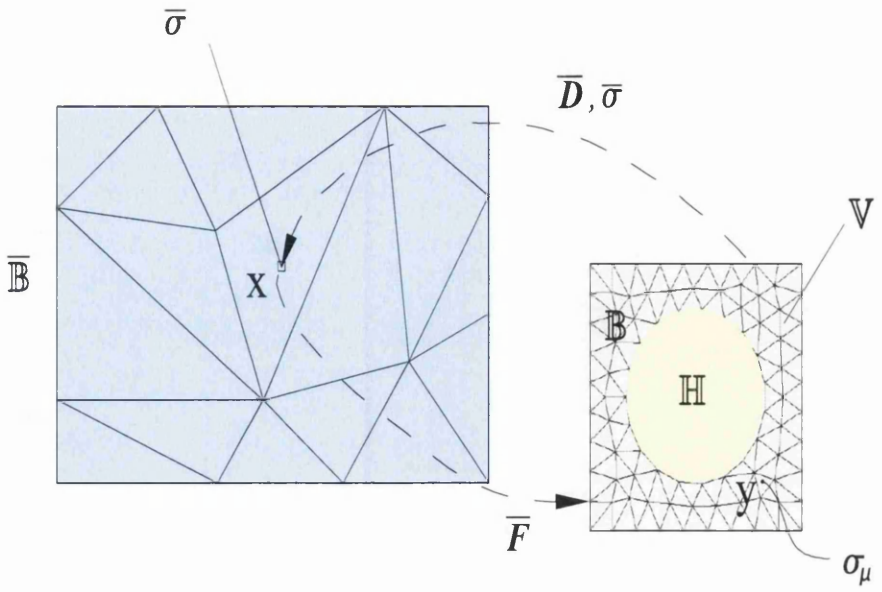

Figure 8.1: Micro to macro transition

overall macroscopic deformation gradient $\overline{\mathbf{F}}$ is prescribed over the discretised RVE. This family of algorithms is considered to be more convenient in comparison with stress-driven microstructures [15].

The main idea of this procedure is based on F.E. discretisation. At every integration Gauss point of the macrostructure, a discrete RVE microstructure is considered as representation of the macro Gauss point.

Based on the Finite Elements discretisation of the microstructure, the goal is to develop a procedure for computing the overall tangent modulus $\overline{\mathcal{A}}$ and macroscopic average Kirchhoff stress $\overline{\tau}$ (or Cauchy $\overline{\sigma}$) at each macroscopic integration point with locally attached microstructure.

8.3 Spatial coordinate field partition and matrix notation

Following the previous Chapter 7, in which the continuum spatial coordinate field partition (7.22) was established, the spatial coordinate field is divided in two parts:

$$\mathbf{y} = \mathbf{y}^* + \widetilde{\mathbf{u}} \tag{8.1}$$

where the *Taylor spatial coordinate* $\mathbf{y}^*$ (previously defined in the continuum form (7.23)) is expressed in its discrete form as,

$$\mathbf{y}_j^* \equiv \overline{\mathbf{F}}\,\mathbf{Y}_j \quad j = 1 \cdots n \tag{8.2}$$

for the n nodes of the microstructure RVE. The *displacement fluctuation* $\tilde{\mathbf{u}}$ is the unknown for every node of the discretised microstructure unit cell.

From now on, the standard Finite Element matrix notation will be used in combination with the tensorial form, where the tensor entities so far used, are represented in the matrix form as

$$\overline{\mathbf{F}} \equiv \left\{ \begin{array}{c} \overline{F}_{11} \\ \overline{F}_{21} \\ \overline{F}_{12} \\ \overline{F}_{22} \end{array} \right\} \quad \text{and} \quad \mathbf{u}_j \equiv \left\{ \begin{array}{c} u_1 \\ u_2 \end{array} \right\}_j \tag{8.3}$$

with $\overline{\mathbf{F}}$ being matrix representation of macro-deformation gradient tensor and $\mathbf{u}_j$ the displacement field at node j of the discretised unit cell $\mathbb{V}$. Moreover, the average Cauchy stress field $\overline{\boldsymbol{\sigma}}$, the macroscopic averaged Kirchhoff stress $\overline{\boldsymbol{\tau}}$ and the force vector $\boldsymbol{f}_j$ associated with the microcell node j, are also defined in this notation as

$$\overline{\boldsymbol{\sigma}} \equiv \left\{ \begin{array}{c} \overline{\sigma}_{11} \\ \overline{\sigma}_{22} \\ \overline{\sigma}_{12} \end{array} \right\} \quad \overline{\boldsymbol{\tau}} \equiv \left\{ \begin{array}{c} \overline{\tau}_{11} \\ \overline{\tau}_{22} \\ \overline{\tau}_{12} \end{array} \right\} \quad \text{and} \quad \boldsymbol{f}_j \equiv \left\{ \begin{array}{c} f_1 \\ f_2 \end{array} \right\}_j \tag{8.4}$$

The *Taylor coordinate* $\mathbf{y}_j^*$ of the node j is computed in the following matrix form

$$\mathbf{y}_j^* = \mathbb{D}_{0j}^T\,\overline{\mathbf{F}} \quad j = 1 \cdots n. \tag{8.5}$$

where $\mathbb{D}_{0j}$ is the *material coordinate matrix* at node j of the microstructure

$$\mathbb{D}_{0j} \equiv \begin{bmatrix} Y_1 & 0 \\ 0 & Y_1 \\ Y_2 & 0 \\ 0 & Y_2 \end{bmatrix}_j \tag{8.6}$$

8.4 Discretised micro-equilibrium state and solution procedure

The solution at macro level is independent of the solution technique used at the micro level. Newton-Raphson solution has been adopted here following the development in [42] and [43].

Following a standard procedure, the *discrete boundary value problem* is formulated as follows: Find the *nodal displacements global vector* $\mathbf{u}$, such that

$$\mathbf{r}(\mathbf{u}) \equiv \mathbf{f}^{int}(\mathbf{u}) - \mathbf{f}^{ext} = \mathbf{0} \tag{8.7}$$

where $\mathbf{f}^{int}$ and $\mathbf{f}^{ext}$ are, respectively, the *internal* and *external global force vectors*, and the difference between them is the *residual* (or *out-of-balance force*) vector $\mathbf{r}$.

An iterative Newton-Raphson procedure for the solution of the nonlinear microscopic equilibrium (8.7) is considered here. Each iteration determines the current fluctuation field assuming frozen macroscopic deformation $\overline{\mathbf{F}}$. At the end of the procedure, when microequilibrium is reached, the averaged macroscopic Kirchhoff stress over the microstructure RVE is updated.

8.4.1 Microstructure equilibrium solution in large strain

In this section an iterative Newton-Raphson procedure for the solution of the nonlinear microscopic equilibrium (8.7) is developed. An iteration determines the current fluctuation field via the update

$$\mathbf{u} \leftarrow \widetilde{\mathbf{u}} + \delta\widetilde{\mathbf{u}} \tag{8.8}$$

It is assumed that the microstructure RVE, corresponding to a macroscopic Gauss point given in Figure 8.1 , has reached equilibrium at time step n. Therefore, all the state variables and stress of the microscopic RVE are known at that stage. The goal is to compute equilibrium at the time step $n+1$ with the incremental strain $\triangle\overline{\mathbf{F}}$ information passed from the macroscale from the global Newton-Raphson iteration to the microscale RVE. From the multiplicative nature of the deformation gradient follows that

$$\overline{\mathbf{F}}_{n+1} = \triangle\overline{\mathbf{F}} \cdot \overline{\mathbf{F}}_n \tag{8.9}$$

The F.E. discrete incremental boundary value problem for the microstructure RVE can be established as follows:

Given: The displacement vector $\mathbf{u}_n$, the Cauchy stress field $\boldsymbol{\sigma}_n$ and the set of internal variables $\boldsymbol{\alpha}_n$ at time step n and the incremental macro deformation gradient $\triangle\overline{\mathbf{F}}$.

Find: The displacement vector $\mathbf{u}_{n+1}$, the Cauchy stress field $\boldsymbol{\sigma}_{n+1}$ and the set of internal variables $\boldsymbol{\alpha}_{n+1}$ at time step $n+1$. In addition, the macroscopic Kirchhoff stress $\overline{\boldsymbol{\tau}}_{n+1}$ is computed, once the microstructure is in equilibrium using (8.23). The macro Cauchy stress $\overline{\boldsymbol{\sigma}}_{n+1}$ is immediately deduced as,

$$\overline{\boldsymbol{\sigma}}_{n+1} = \frac{1}{J_{n+1}} \overline{\boldsymbol{\tau}}_{n+1} \tag{8.10}$$

where $J_{n+1} = \det(\overline{\mathbf{F}}_{n+1})$. The macro Cauchy stress $\overline{\boldsymbol{\sigma}}_{n+1}$ is returned back to the macroscale and used as a macrostress at macro Gauss point level corresponding to the microstructure RVE computed.

The procedure differs depending on the boundary constraint applied over the microstructure RVE. Therefore, linear and periodic constraints have different particularizations of this procedure given later in Sections 8.7.5 and 8.8.5, respectively.

In the following the Newton-Raphson method is used to find the equilibrium at the microstructure RVE at time step $n+1$ assuming the system is already in equilibrium at time step n. The general idea consists in taking the microstructure frozen with macroscopic deformation $\overline{\mathbf{F}} = \textit{constant}$. Therefore, the variation of the Taylor spatial coordinate is zero during the iteration $\mathrm{d}\mathbf{y}^* = \mathbf{0}$.

Before proceeding with the description the scheme, we note that the incremental displacement field, $\triangle\mathbf{u} = \mathbf{u}_{n+1} - \mathbf{u}_n = \triangle\mathbf{y} = \mathbf{y}_{n+1} - \mathbf{y}_n$, can be additively decomposed as,

$$\triangle\mathbf{u} = \triangle\mathbf{u}^* + \widetilde{\mathbf{u}}_{n+1} \tag{8.11}$$

where the notation $\triangle\mathbf{u}^*$ has been used for

$$\triangle\mathbf{u}^* = \mathbf{y}^*_{n+1} - \mathbf{y}_n = \overline{\mathbf{F}}_{n+1}\mathbf{Y} - \mathbf{y}_n. \tag{8.12}$$

The general solution procedure is described as follows:

1. The initial incremental displacement guess $\triangle\mathbf{u}^0$ is given as the incremental Taylor displacement,

$$\triangle\mathbf{u}^0 = \triangle\mathbf{u}^* + \widetilde{\mathbf{u}}_n \tag{8.13}$$

   In other words, the incremental macro deformation $\triangle\overline{\mathbf{F}}$ is fully prescribed at the first pseudo step, so that, the Taylor spatial coordinate is fully prescribed as the initial guess. This means that the initial displacement guess at time step $n+1$ $\mathbf{y}^0_{n+1}$ is given by,

$$\mathbf{y}^0_{n+1} = \mathbf{y}_n + \triangle\mathbf{u}^0 \tag{8.14}$$

   Using the split displacement (8.1) at time step n, the initial guess displacement in then expressed as,

$$\mathbf{y}^0_{n+1} = \mathbf{y}^*_{n+1} + \widetilde{\mathbf{u}}_n \tag{8.15}$$

In the above it can be observed that the incremental Taylor spatial coordinate $\Delta\mathbf{y}^*$ is prescribed entirely at the beginning of the procedure. Moreover, the initial displacement fluctuation is taken as the converged in the previous time step n. Hence,

$$\widetilde{\mathbf{u}}^0_{n+1} = \widetilde{\mathbf{u}}_n \tag{8.16}$$

or in another words, the incremental fluctuation is taken as zero value in the initial guess

$$\Delta\widetilde{\mathbf{u}} = 0 \tag{8.17}$$

2. Computation of the internal forces $\mathbf{f}^{int}$. This is computed with the incremental displacement $\Delta\mathbf{u}$ and the set of state variables $\{\mathbf{F}_{n+1}, \boldsymbol{\alpha}_{n+1}\}$ at microscopic Gauss point level.

3. Check convergence $\|\mathbf{r}\| < \varepsilon_{tolerance}$. This residual force $\mathbf{r}$ depends on the boundary constraint applied on the RVE.

   - IF $\|\mathbf{r}\| < \varepsilon_{tolerance}$. EQUILIBRIUM. The solution is $\mathbf{u}^k_{n+1}$. END OF k ITERATION
   - ELSE GO TO NEXT STEP

4. Computation of the incremental internal fluctuation. Assume that the iterative fluctuation is divided in two parts,

$$\delta\widetilde{\mathbf{u}} = \left\{ \begin{array}{c} \delta\widetilde{\mathbf{u}}_r \\ \delta\widetilde{\mathbf{u}}_d \end{array} \right\} \tag{8.18}$$

where $\delta\widetilde{\mathbf{u}}_r$ are the independent d.o.f. and $\delta\widetilde{\mathbf{u}}_d$ are the dependent d.o.f. displacements of the microstructure. Therefore, $\delta\widetilde{\mathbf{u}}_d$ is known once $\delta\widetilde{\mathbf{u}}_r$ is computed. They are different depending on the micro boundary constraint (linear or periodic b.c.). The Newton-Raphson iteration is defined by,

$$\mathbf{K}_r\ \delta\widetilde{\mathbf{u}}_r = -\mathbf{r} \quad \Rightarrow \quad \delta\widetilde{\mathbf{u}}_r = -\mathbf{K}_r^{-1}\ \mathbf{r} \tag{8.19}$$

where $\mathbf{r}$ is the residual force and $\mathbf{K}_r$ is the reduced matrix of the system. In later Sections 8.7.5 and 8.8.5 particularisations for linear and periodic b.c. are given, respectively.

The updating of the incremental fluctuation is as follows

$$\Delta\widetilde{\mathbf{u}} \leftarrow \Delta\widetilde{\mathbf{u}} + \delta\widetilde{\mathbf{u}} \tag{8.20}$$

and also the incremental displacement

$$\triangle \mathbf{u} \leftarrow \triangle \mathbf{u} + \delta \widetilde{\mathbf{u}} \tag{8.21}$$

GO TO step 2.

Finally, when the microequilibrium is reached, the macro Kirchhoff stress $\overline{\boldsymbol{\tau}}_{n+1}$ is computed from the value of the boundary forces. It is described in the discrete form in Section 8.5. Then, the macro Cauchy stress (obtained from (8.10)) is used for computing the internal forces at the macro level.

8.5 General average Kirchhoff stress and overall spatial tangent modulus computation

8.5.1 Average Kirchhoff stress computation

Assuming no body forces in the expression for the average Kirchhoff stress (7.13), in the discrete setting, $\mathbf{t}\, \mathrm{d}A \rightarrow \boldsymbol{f}_{\mathrm{j}}^{ext}$, that is the infinitesimal force $\mathbf{t}\, \mathrm{d}A$ becomes the finite force $\boldsymbol{f}_{\mathrm{j}}^{ext}$ at nodal position $\mathbf{y}_{\mathrm{j}}$ on the boundary $\partial\mathbb{V}$. Therefore (7.13) degenerates into the discrete sum

$$\overline{\boldsymbol{\tau}} = \frac{1}{|\mathbb{V}_0|} \sum_{\mathrm{j}=1}^{\mathrm{n_b}} \mathrm{sym}[\boldsymbol{f}_{\mathrm{j}}^{ext} \otimes \mathbf{y}_{\mathrm{j}}] \tag{8.22}$$

where $\mathrm{n_b}$ is the number of nodes on the boundary $\partial\mathbb{V}$. Using matrix representation this expression becomes

$$\overline{\boldsymbol{\tau}} = \frac{1}{|\mathbb{V}_0|} \sum_{\mathrm{j}=1}^{\mathrm{n_b}} \mathbb{D}_{\mathrm{j}}\, \boldsymbol{f}_{\mathrm{j}}^{ext} \tag{8.23}$$

where $\mathbb{D}_{\mathrm{j}}$ is the *spatial coordinate matrix* evaluated at node j on the boundary of the discretised microstructure RVE

$$\mathbb{D}_{\mathrm{j}} \equiv \frac{1}{2} \begin{bmatrix} 2\,y_1 & 0 \\ 0 & 2\,y_2 \\ y_2 & y_1 \end{bmatrix}_{\mathrm{j}} \tag{8.24}$$

The above expression can be rearranged in the following global expression

$$\overline{\boldsymbol{\tau}} = \frac{1}{|\mathbb{V}_0|}\,\mathbb{D}_{\mathrm{b}}\,\mathbf{f}_{\mathrm{b}}^{ext}\,, \tag{8.25}$$

where $\mathbf{f}_{\mathrm{b}}^{ext}$ is the external nodal force vector of the boundary nodes, and $\mathbb{D}_{\mathrm{b}}$ is the *boundary coordinate matrix* defined by:

$$\mathbb{D}_{\mathrm{b}} \equiv \left[\, \mathbb{D}_1^b \;\; \mathbb{D}_2^b \;\; \ldots \;\; \mathbb{D}_{\mathrm{n_b}}^b \,\right]. \tag{8.26}$$

8.5.2 Homogenised spatial tangent modulus computation in large strain

In the computational homogenization approach no explicit form of the constitutive behavior on the macro-level is assumed a priori, so that the tangent modulus has to be determined numerically by relations between variations of the macroscopic stress and variations of the macroscopic strain at such integration macro Gauss point. This can be accomplished by numerical differentiation of the numerical macroscopic stress-strain relation, for instance, by using forward difference approximations as suggested in [43]. Another approach is to condense the microstructural stiffness matrix to the macroscopic matrix tangent modulus. This task is achieved by reducing the total RVE system of equations to the relation between the forces acting on the boundary $\partial\mathbb{V}$ and the displacement on the boundary. This procedure has been used in [92], [90], and also in [13], in combination of the Lagrange multiplier method to impose the boundary constraints.

A similar scheme have been used in this work. It employs direct condensation to obtain a relation between the variation of the forces acting on the boundary $\partial\mathbb{V}$ and the variational Taylor spatial coordinate on the boundary nodes array $\mathrm{d}\mathbf{y}^*$ which depends linearly of the macroscopic deformation variation $\mathrm{d}\overline{\mathbf{F}}$.

The total microstructural system of equations that gives the relation between the iterative nodal displacement $\mathbf{du}$ and iterative nodal external force vectors is

$$\mathbf{K}\;\mathrm{d}\mathbf{u} = \mathrm{d}\mathbf{f}^{ext}. \tag{8.27}$$

Due to $\mathrm{d}\mathbf{y} = \mathrm{d}\mathbf{u}$ and the spatial coordinate partition (8.1) we have the following differential relation,

$$\mathrm{d}\mathbf{u} = \mathrm{d}\mathbf{y}^* + \mathrm{d}\widetilde{\mathbf{u}} \tag{8.28}$$

The system (8.27) can be rearranged as follows

$$\mathbf{K}\;\mathrm{d}\mathbf{u} = \mathrm{d}\mathbf{f}^{ext} \;\Rightarrow\; \mathbf{K}\;\mathrm{d}\mathbf{y}^* + \mathbf{K}\;\mathrm{d}\widetilde{\mathbf{u}} = \mathrm{d}\mathbf{f}^{ext} \tag{8.29}$$

The boundary constraints are then applied to this system in the following sections to condense the system. This procedure gives the expression that relates the variation of boundary external forces $\mathrm{d}\mathbf{f}_{\mathrm{b}}^{ext}$ against the variation of the Taylor spatial coordinate $\mathrm{d}\mathbf{y}^{*}$.

Finally, the overall modulus $\overline{\boldsymbol{\mathcal{D}}}^{\tau\mathrm{F}}$ defined in (7.15), can be computed in its discretised F.E. matrix form, using averaged Kirchhoff stress expression (8.25), as follows

$$\overline{\boldsymbol{\mathcal{D}}}^{\tau\mathrm{F}} = \frac{\mathrm{d}\overline{\boldsymbol{\tau}}}{\mathrm{d}\overline{\mathbf{F}}} = \frac{1}{|\mathbb{V}_0|}\,\mathbb{D}_{\mathrm{b}}\,\frac{\mathrm{d}\mathbf{f}_{\mathrm{b}}^{ext}}{\mathrm{d}\overline{\mathbf{F}}} \tag{8.30}$$

The overall spatial tangent modulus (7.16) can be computed in its matrix form for heterogeneous material with different microstructures as,

$$\overline{\boldsymbol{\mathcal{A}}} = \frac{1}{J_{\mathrm{M}}}\overline{\boldsymbol{\mathcal{D}}}^{\tau\mathrm{F}} \diamond \overline{\mathbf{F}} - \overline{\boldsymbol{\sigma}} \star \mathbf{I}. \tag{8.31}$$

This matrix form is obtained by converting the continuous form (7.17) to the matrix form used in the discrete formulation.

Particularisations of the computation average Kirchhoff macrostress and overall spatial tangent modulus are given in the following sections of this chapter, for Taylor assumption, linear b.c. and periodic b.c.

8.6 Taylor assumption in large strain

The *global coordinate matrix* for the Taylor assumption is defined as

$$\mathbb{D}_{0\mathrm{global}} \equiv \left[\, \mathbb{D}_{01} \quad \mathbb{D}_{02} \quad \cdots \quad \mathbb{D}_{0\mathrm{n}} \,\right] \tag{8.32}$$

It is composed of the coordinate matrices of every single node of the RVE. Hence, using this matrix formulation, the Taylor displacement counterpart (6.5), can be expressed in the global form as

$$\mathbf{y}^{*} = \mathbb{D}_{0\mathrm{global}}^{\mathrm{T}}\,\overline{\mathbf{F}} \tag{8.33}$$

In this assumption, zero displacement fluctuation is considered for every single node of the unit cell, therefore,

$$\widetilde{\mathbf{u}}_{\mathrm{j}} = \mathbf{0}\,, \quad \mathrm{j} = 1 \cdots \mathrm{n}$$

or in global notation

$$\widetilde{\mathbf{u}} = \mathbf{0} \tag{8.34}$$

8.6.1 Average Kirchhoff macrostress and homogenised spatial tangent modulus for the Taylor assumption

In order to compute the average Cauchy stress and homogenised tangent modulus for Taylor assumption, the rule of mixtures is used. Then the average Cauchy stress is computed as,

$$\overline{\boldsymbol{\sigma}} = \frac{1}{|\mathbb{V}|}\sum_{i=1}^{n_c} v_i\,\boldsymbol{\sigma}_i \tag{8.35}$$

where n_c is the number of different phases and v_i is the volume of the phase i of the RVE. The stress in each phase $\boldsymbol{\sigma}_i$ is computed separately imposing the global macro-deformation $\overline{\mathbf{F}}$.

The homogenised spatial tangent modulus is also computed in the same way by

$$\overline{\boldsymbol{\mathcal{A}}} = \frac{1}{|\mathbb{V}|}\sum_{i=1}^{n_c} v_i\,\boldsymbol{\mathcal{A}}_i \tag{8.36}$$

where $\boldsymbol{\mathcal{A}}_i$ is the tangent modulus of phase i.

8.7 Linear displacements on the boundary of RVE discrete in large strain

In view of the discrete formulation of the boundary conditions outlined before in Section 7.5.2, the nodes of the mesh are partitioned into those on the surface $\partial\mathbb{V}$ of RVE and those in the interior of $\mathbb{V}$, see Figure 8.2. In this mesh $\mathrm{n_b}$ boundary nodes and $\mathrm{n_i}$ internal nodes are distinguished. The discrete form of this linear constraint was introduced in [20] and [21].

8.7.1 Partitioning of algebraic equations

Partitioning of the current nodal displacements and nodal forces is given as

$$\mathbf{u} = \left\{ \begin{array}{c} \mathbf{u}_\mathrm{i} \\ \mathbf{u}_\mathrm{b} \end{array} \right\} \quad \text{and} \quad \mathbf{f} = \left\{ \begin{array}{c} \mathbf{f}_\mathrm{i} \\ \mathbf{f}_\mathrm{b} \end{array} \right\} \tag{8.37}$$

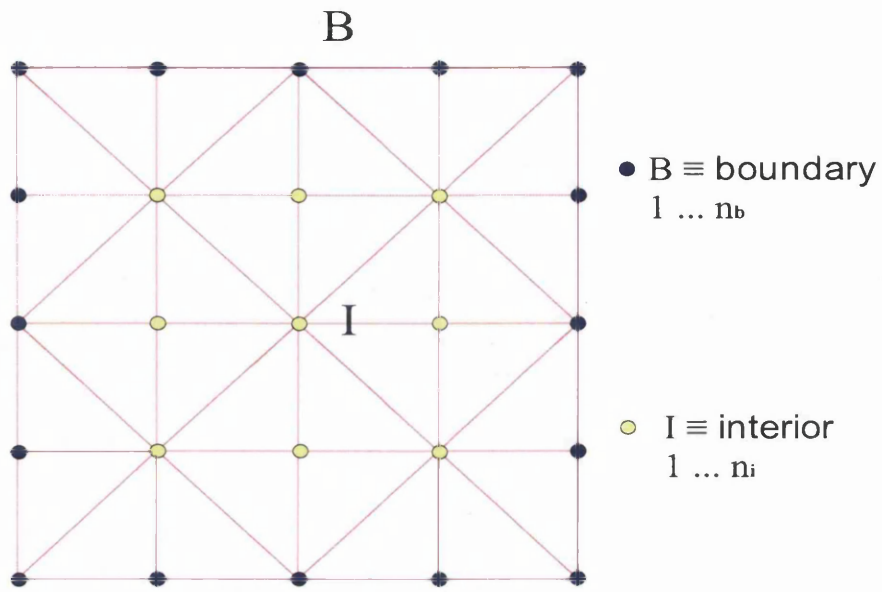

Figure 8.2: Mesh for linear displacement on the boundary

where the contributions for interior and boundary nodes, is given, respectively (see Figure 8.2). The displacement vectors $\mathbf{u}_i$ and $\mathbf{u}_b$ are gathered from $\mathbf{u}$. Using these two vectors we obtain a new $\mathbf{u}$ rearranged as shown in (8.37).

In line with (8.37), the tangent stiffness matrix is rearranged as

$$\mathbf{K} = \frac{\mathrm{d}\mathbf{f}^{int}}{\mathrm{d}\mathbf{u}} = \begin{bmatrix} \mathbf{k}_{ii} & \mathbf{k}_{ib} \\ \mathbf{k}_{bi} & \mathbf{k}_{bb} \end{bmatrix} \tag{8.38}$$

into contributions associated with internal nodes and nodes on the surface of RVE.

8.7.2 Linear displacement

At each node j of the boundary $\partial\mathbb{V}$ condition (7.28) induces the discrete constraint

$$\widetilde{\mathbf{u}}_j \;=\; \mathbf{0} \quad j \;=\; 1 \cdots n_b \tag{8.39}$$

These constraints can be represented as a global boundary displacement vector

$$\widetilde{\mathbf{u}}_b \;=\; \mathbf{0} \tag{8.40}$$

According to the matrix notation introduced in Section 8.3, we define the *global material coordinate matrix*

$$\mathbb{D}_{0\text{global},l} \equiv \left[\mathbb{D}_{0\text{i}} \quad \mathbb{D}_{0\text{b},l} \right] \tag{8.41}$$

where $\mathbb{D}_{0\text{i}}$ and $\mathbb{D}_{0\text{b},l}$ are the *interior material coordinate matrix* and the *boundary material coordinate matrix*, respectively, given as

$$\mathbb{D}_{0\text{i}} \equiv \left[\mathbb{D}^i_{01} \quad \mathbb{D}^i_{02} \quad \dots \quad \mathbb{D}^i_{0\text{n}_\text{i}} \right] \quad \text{and} \quad \mathbb{D}_{0\text{b},l} \equiv \left[\mathbb{D}^b_{01} \quad \mathbb{D}^b_{02} \quad \dots \quad \mathbb{D}^b_{0\text{n}_\text{b}} \right] \tag{8.42}$$

The matrices $\mathbb{D}_{0\text{i}}$ and $\mathbb{D}_{0\text{b},l}$ are defined in terms node material coordinate matrices (8.6) for the interior and boundary nodes, respectively. The Taylor spatial coordinate vector $\mathbf{y}^*$, previously defined in (8.33) for the Taylor assumption, is now represented

$$\mathbf{y}^* = \mathbb{D}^{\text{T}}_{0\text{global},l}\, \overline{\mathbf{F}} \tag{8.43}$$

where $\mathbb{D}_{0\text{global},l}$ is the global material coordinate matrix (8.41) and $\overline{\mathbf{F}}$ is the matrix representation of the prescribed macroscopic deformation gradient (7.14). In this model the variation of the Taylor displacement vector $\text{d}\mathbf{y}^*$ is represented as

$$\text{d}\mathbf{y}^* = \mathbb{D}^{\text{T}}_{0\text{global},l}\, \text{d}\overline{\mathbf{F}} \tag{8.44}$$

that is, as a function of the variation of the macroscopic average deformation gradient vector $\text{d}\overline{\mathbf{F}}$.

8.7.3 Average Kirchhoff macro-stress for the linear b.c.

For this model the average Kirchhoff stress is computed based on the matrix expression for the average stress (8.23). It can be rearranged in the following global expression

$$\overline{\boldsymbol{\tau}} = \frac{1}{|\mathbb{V}_0|}\, \mathbb{D}_{\text{b},l}\, \mathbf{f}^{ext}_{\text{b}} \tag{8.45}$$

where $\mathbf{f}_{\text{b}}$ is the external nodal force vector of the boundary nodes defined in the partition (8.37), and $\mathbb{D}_{\text{b},l}$ is the boundary spatial coordinate matrix

$$\mathbb{D}_{\text{b},l} \equiv \left[\mathbb{D}^b_1 \quad \mathbb{D}^b_2 \quad \dots \quad \mathbb{D}^b_{\text{n}_b} \right] \tag{8.46}$$

where $\mathbb{D}_{\text{b},l}$ is defined in terms node spatial coordinate matrices (8.24) of the boundary nodes.

8.7.4 Homogenised spatial tangent modulus for the linear b.c.

Using partitioning of the algebraic equations (8.37) and (8.38), the system (8.27) can be rewritten as

$$\begin{bmatrix} \mathbf{k}_{ii} & \mathbf{k}_{ib} \\ \mathbf{k}_{bi} & \mathbf{k}_{bb} \end{bmatrix} \begin{Bmatrix} \mathrm{d}\mathbf{u}_i \\ \mathrm{d}\mathbf{u}_b \end{Bmatrix} = \begin{Bmatrix} \mathrm{d}\mathbf{f}_i^{ext} \\ \mathrm{d}\mathbf{f}_b^{ext} \end{Bmatrix} \quad \equiv \quad \mathbf{K}\ \mathrm{d}\mathbf{u} = \mathrm{d}\mathbf{f}^{ext} \tag{8.47}$$

for the case when $\mathrm{d}\mathbf{f}_i^{ext} = \mathbf{0}$. The general procedure explained in Section 8.5.2 where the rearranged system (8.29) was obtained is followed. Therefore, the system (8.47) is then rearranged as,

$$\Rightarrow\ \mathbf{K}\ \mathrm{d}\widetilde{\mathbf{u}} = \mathrm{d}\mathbf{f}^{ext} - \mathbf{K}\ \mathrm{d}\mathbf{y}^* \tag{8.48}$$

where Taylor coordinate variation $\mathrm{d}\mathbf{y}^*$ is given by (8.44) for the linear model. By introducing linear displacement constraint (8.40) into the above split system (8.48), internal nodal displacement fluctuation vector can be computed as,

$$\mathrm{d}\widetilde{\mathbf{u}}_i \ = \ -\mathbf{k}_{ii}^{-1}\ \mathbf{K}_I\ \mathrm{d}\mathbf{y}^* \tag{8.49}$$

where $\mathbf{K}_I$ matrix is defined as

$$\mathbf{K}_I \equiv \left[\ \mathbf{k}_{ii} \quad \mathbf{k}_{ib}\ \right]. \tag{8.50}$$

From the system (8.48), the variation of external boundary force vector is calculated

$$\mathrm{d}\mathbf{f}_b^{ext} = \ \mathbf{k}_{bi}\ \mathrm{d}\widetilde{\mathbf{u}}_i \ + \ \mathbf{K}_B\ \mathrm{d}\mathbf{y}^* \tag{8.51}$$

where $\mathbf{K}_B$ matrix is defined as

$$\mathbf{K}_B \equiv \left[\ \mathbf{k}_{bi} \quad \mathbf{k}_{bb}\ \right]. \tag{8.52}$$

Inserting (8.49) into (8.51), the $\mathrm{d}\mathbf{f}_b$ vector is obtained as

$$\mathrm{d}\mathbf{f}_b^{ext} \ = \ (\ \mathbf{K}_B \ - \ \mathbf{k}_{bi}\ \mathbf{k}_{ii}^{-1}\ \mathbf{K}_I\ )\ \mathrm{d}\mathbf{y}^* \tag{8.53}$$

in terms of the variation of the Taylor spatial coordinate $\mathrm{d}\mathbf{y}^*$. Compacting the right hand side of (8.53), the variation of the external boundary force vector is expressed as

$$\mathrm{d}\mathbf{f}_b^{ext} \ = \ \mathbf{K}_{\mathrm{lin}}^{\mathbf{B}}\ \mathrm{d}\mathbf{y}^* \tag{8.54}$$

where the *condensed linear stiffness matrix* $\mathbf{K}^{\mathbf{B}}_{\mathbf{lin}}$ is defined as follows,

$$\mathbf{K}^{\mathbf{B}}_{\mathbf{lin}} \equiv \mathbf{K}_{\mathrm{B}} - \mathbf{k}_{\mathrm{bi}}\, \mathbf{k}_{\mathrm{ii}}^{-1}\, \mathbf{K}_{\mathrm{I}}\,. \tag{8.55}$$

Finally, insertion of the variation of the Taylor spatial coordinate (8.44) for Linear model, into (8.54) identifies the boundary force vector variation as,

$$\mathrm{d}\mathbf{f}^{ext}_{\mathrm{b}} = \mathbf{K}^{\mathbf{B}}_{\mathbf{lin}}\, \mathbb{D}^{\mathrm{T}}_{0\mathrm{global},l}\, \mathrm{d}\overline{\mathbf{F}}, \tag{8.56}$$

in terms of the global material coordinate matrix (8.41) and the variation of the overall macro deformation gradient $\mathrm{d}\overline{\mathbf{F}}$. Hence, it follows that

$$\frac{\mathrm{d}\mathbf{f}^{ext}_{\mathrm{b}}}{\mathrm{d}\overline{\mathbf{F}}} = \mathbf{K}^{\mathbf{B}}_{\mathbf{lin}}\, \mathbb{D}^{\mathrm{T}}_{0\mathrm{global},l} \tag{8.57}$$

which expresses the variation of the external boundary force vector $\mathrm{d}\mathbf{f}^{ext}_{\mathrm{b}}$ with respect to the variation of macroscopic deformation gradient $\mathrm{d}\overline{\mathbf{F}}$.

The modulus $\overline{\boldsymbol{\mathcal{D}}}^{\tau\mathrm{F}}_{l}$ for linear b.c., can be computed in its discretised F.E. matrix form following the general expression given in (8.30), as

$$\overline{\boldsymbol{\mathcal{D}}}^{\tau\mathrm{F}}_{l} = \frac{\mathrm{d}\overline{\boldsymbol{\tau}}}{\mathrm{d}\overline{\mathbf{F}}} = \frac{1}{|\mathbb{V}_0|}\, \mathbb{D}_{\mathrm{b},l}\, \frac{\mathrm{d}\mathbf{f}^{ext}_{\mathrm{b}}}{\mathrm{d}\overline{\mathbf{F}}}\,. \tag{8.58}$$

Substituting (8.57) into (8.58), the modulus representation $\overline{\boldsymbol{\mathcal{D}}}^{\tau\mathrm{F}}_{l}$ is obtained as

$$\boxed{\overline{\boldsymbol{\mathcal{D}}}^{\tau\mathrm{F}}_{l} = \frac{1}{|\mathbb{V}_0|}\, \mathbb{D}_{\mathrm{b},l}\, \mathbf{K}^{\mathbf{B}}_{\mathbf{lin}}\, \mathbb{D}^{\mathrm{T}}_{0\mathrm{global},l}} \tag{8.59}$$

Clearly the modulus $\overline{\boldsymbol{\mathcal{D}}}^{\tau\mathrm{F}}_{l}$ is given as a function of the boundary spatial coordinate matrix $\mathbb{D}_{\mathrm{b},l}$ defined in (8.42), the condensed linear stiffness matrix $\mathbf{K}^{\mathbf{B}}_{\mathbf{lin}}$ (8.55) and the global material coordinate matrix $\mathbb{D}^{\mathrm{T}}_{0\mathrm{global},l}$ outlined in (8.41). The final step to obtain the overall spatial tangent modulus $\overline{\boldsymbol{\mathcal{A}}}_{l}$ in its discrete form consists in employing expression (8.31), that is

$$\overline{\boldsymbol{\mathcal{A}}}_{l} = \frac{1}{J_{\mathrm{M}}}\overline{\boldsymbol{\mathcal{D}}}^{\tau\mathrm{F}}_{l} \diamond \overline{\mathbf{F}} - \overline{\boldsymbol{\sigma}} \star \mathbf{I}\,. \tag{8.60}$$

Finally, we remark that by using (8.60) the overall spatial tangent modulus can be computed for heterogeneous material with different microstructures. When using this tangent modulus the quadratic rate of convergence is attained at macroscopic level.

8.7.5 Microequilibrium computation for the linear b.c. in large strain

In Section 8.4.1 a general solution scheme for microequilibrium is given for finite strain analysis. In this section, the particularisation of the microequilibrium procedure for linear b.c. is described.

The incremental Taylor displacement is given in global matrix form as,

$$\triangle \mathbf{u}^* = \mathbf{y}^*_{n+1} - \mathbf{y}_n = \mathbb{D}^{\mathrm{T}}_{0\mathrm{global},l} \overline{\mathbf{F}}_{n+1} - \mathbf{y}_n. \tag{8.61}$$

The residual force $\mathbf{r}$ is taken as the difference between the internal and external force vectors for the interior nodes as,

$$\mathbf{r} = \mathbf{f}^{int}_{\mathrm{i}} - \mathbf{f}^{ext}_{\mathrm{i}} \tag{8.62}$$

Assuming that in equilibrium $\mathbf{f}^{ext}_{\mathrm{i}} = \mathbf{0}$ the actual residual used for linear b.c. follows as

$$\mathbf{r} = \mathbf{f}^{int}_{\mathrm{i}}. \tag{8.63}$$

Therefore, the differential fluctuation is given by the system (8.19) which now is taking the following form

$$\mathbf{K}_{\mathrm{ii}}\, \delta\widetilde{\mathbf{u}}_{\mathrm{i}} = -\mathbf{f}^{int}_{\mathrm{i}} \quad \Rightarrow \quad \delta\widetilde{\mathbf{u}}_{\mathrm{i}} = -\mathbf{K}^{-1}_{\mathrm{ii}}\, \mathbf{f}^{int}_{\mathrm{i}} \tag{8.64}$$

and

$$\delta\widetilde{\mathbf{u}}_{\mathrm{b}} = \mathbf{0} \tag{8.65}$$

The updated incremental fluctuation is then given by

$$\triangle\widetilde{\mathbf{u}}_{\mathrm{i}} \leftarrow \triangle\widetilde{\mathbf{u}}_{\mathrm{i}} + \delta\widetilde{\mathbf{u}}_{\mathrm{i}} \tag{8.66}$$

and

$$\triangle\widetilde{\mathbf{u}}_{\mathrm{b}} = \mathbf{0} \tag{8.67}$$

The incremental displacement used to compute the internal force is updated by

$$\triangle\mathbf{u}_{\mathrm{i}} \leftarrow \triangle\mathbf{u}_{\mathrm{i}} + \delta\widetilde{\mathbf{u}}_{\mathrm{i}} \tag{8.68}$$

and $\triangle \mathbf{u}_b$ does not change.

8.8 Periodic displacements and antiperiodic traction on the boundary of RVE discrete in large strain

In order to discretise the continuum model of the periodic boundary conditions described in Section 7.5.3, the nodes of the mesh are partitioned in four groups as outlined in on Figure 8.3 :

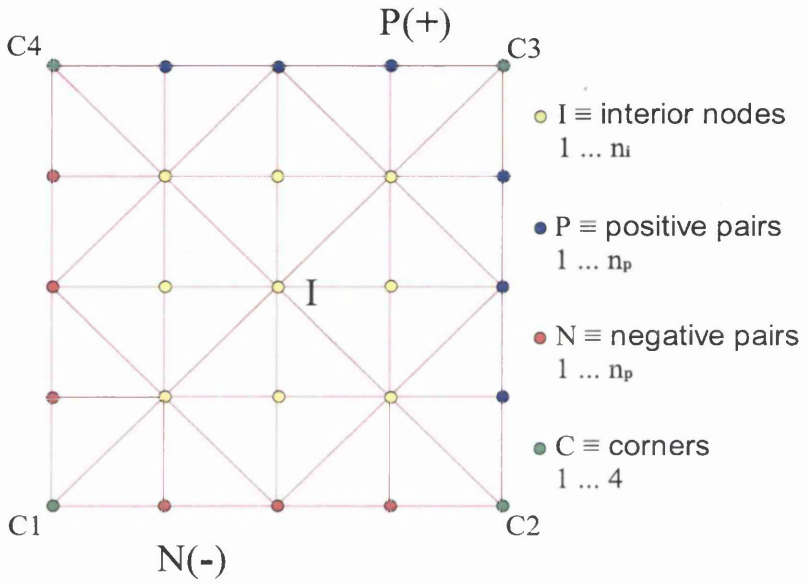

Figure 8.3: Mesh for periodic displacement and antiperiodic traction on the boundary

1. n_i interior nodes are distinguished.
2. n_p positive boundary nodes which are located at the top and right side of the microstructure surface $\partial\mathbb{V}$ of RVE.
3. n_p negative boundary nodes which are located at the bottom and left side of the microstructure surface $\partial\mathbb{V}$ of RVE.
4. n_c node at the corners.

The number of node pairs (positive and corresponding negative nodes) on the boundary $\partial\mathbb{V}$ of RVE are:

$$n_p = \frac{n_b}{2} - 2 \tag{8.69}$$

where n_b is the total number of nodes on the boundary of RVE. Also the number of corner nodes in a 2D rectangular microstructure is four, i.e.

$$n_c = 4. \tag{8.70}$$

We note that the discrete form of this periodic constraint was introduced in [20] and [21].

8.8.1 Partitioning of algebraic equations

The partition of the nodal displacements and forces is as follows

$$\mathbf{u} = \begin{Bmatrix} \mathbf{u}_i \\ \mathbf{u}_p \\ \mathbf{u}_n \\ \mathbf{u}_c \end{Bmatrix} \quad \text{and} \quad \mathbf{f} = \begin{Bmatrix} \mathbf{f}_i \\ \mathbf{f}_p \\ \mathbf{f}_n \\ \mathbf{f}_c \end{Bmatrix} \tag{8.71}$$

where following Figure 8.3 the corresponding contributions are distinguished: : (i) the interior contribution, (ii) the contribution of positive boundary nodes, (iii) the contribution from the corresponding negative boundary nodes, and finally (iv) the contribution form the nodes at the corners. In correspondence to (8.71), the tangent stiffness matrix is partitioned in the following way

$$\mathbf{K} = \frac{\mathrm{d}\mathbf{f}^{int}}{\mathrm{d}\mathbf{u}} = \begin{bmatrix} \mathbf{k}_{ii} & \mathbf{k}_{ip} & \mathbf{k}_{in} & \mathbf{k}_{ic} \\ \mathbf{k}_{pi} & \mathbf{k}_{pp} & \mathbf{k}_{pn} & \mathbf{k}_{pc} \\ \mathbf{k}_{ni} & \mathbf{k}_{np} & \mathbf{k}_{nn} & \mathbf{k}_{nc} \\ \mathbf{k}_{ci} & \mathbf{k}_{cp} & \mathbf{k}_{cn} & \mathbf{k}_{cc} \end{bmatrix} \tag{8.72}$$

8.8.2 Periodic displacements and antiperiodic tractions discrete b.c.

At each node pair j on the boundary $\partial\mathbb{V}^+ \cup \partial\mathbb{V}^-$, the continuum condition (7.31) induces the discrete constraint

$$\widetilde{\mathbf{u}}_j^+ = \widetilde{\mathbf{u}}_j^- , \qquad j = 1 \cdots n_p \tag{8.73}$$

The link between constraints for each pair of nodes can be compactly represented in a global form as

$$\widetilde{\mathbf{u}}_p = \widetilde{\mathbf{u}}_n \tag{8.74}$$

The displacement fluctuation at the corners is prescribed to zero to avoid the rigid body motion, i.e.

$$\widetilde{\mathbf{u}}_{ci} \;=\; \mathbf{0}\,, \qquad i \;=\; 1 \cdots \mathrm{n_c} \tag{8.75}$$

It can easily be proved that (8.75) agrees with the periodic continuum condition (7.31). The relation (8.75) can be represented in a global form

$$\widetilde{\mathbf{u}}_{\mathrm{c}} \;=\; \mathbf{0} \tag{8.76}$$

At each node pair j on the boundary $\partial\mathbb{V}^+ \cup \partial\mathbb{V}^-$, the continuum antiperiodic traction condition (7.30) is discretised as

$$\mathbf{f}(\mathbf{y}_{\mathrm{j}}^{+}) = -\mathbf{f}(\mathbf{y}_{\mathrm{j}}^{-}) \;\text{ or }\; \mathbf{f}_{\mathrm{j}}^{+} = -\mathbf{f}_{\mathrm{j}}^{-}\,, \qquad \mathrm{j} \;=\; 1 \cdots \mathrm{n_p} \tag{8.77}$$

Again these constraints, can be represented in compressed form as

$$\mathbf{f}_{\mathrm{p}}^{ext} = -\mathbf{f}_{\mathrm{n}}^{ext} \tag{8.78}$$

An important additional equation to take into consideration is equilibrium condition given by

$$\sum_{\mathrm{i=1}}^{4} \mathbf{f}_{\mathrm{ci}}^{ext} = \mathbf{0} \tag{8.79}$$

This equation agrees with the continuum antiperiodic traction condition (7.30), although, this is not obvious. The underlying idea relies on the antiperiodicity of force in the corners that come from the different continuum distributions as pointed out Appendix C.

Using the matrix notation introduced in Section 8.3, we redefine the *global material coordinate matrix* for periodic b.c. as

$$\mathbb{D}_{0\mathrm{global},p} \;\equiv \left[\; \mathbb{D}_{0\mathrm{i}} \quad \mathbb{D}_{0\mathrm{b},p} \right] \tag{8.80}$$

where $\mathbb{D}_{0\mathrm{i}}$ is the *interior material coordinate matrix* defined in (8.42) and the $\mathbb{D}_{0\mathrm{b},p}$ and is the *boundary material coordinate matrix* for Periodic b.c. defined as

$$\mathbb{D}_{0\mathrm{b},p} \;= \left[\; \mathbb{D}_{0\mathrm{p}} \quad \mathbb{D}_{0\mathrm{n}} \quad \mathbb{D}_{0\mathrm{c}} \;\right] \tag{8.81}$$

where $\mathbb{D}_{0p}$, $\mathbb{D}_{0n}$ and $\mathbb{D}_{0c}$ are the *positive boundary material coordinate matrix*, *negative boundary material coordinate matrix* and *corner material coordinate matrix*, respectively, given by

$$\mathbb{D}_{0p} \equiv \left[\mathbb{D}^p_{01} \quad \mathbb{D}^p_{02} \quad \dots \quad \mathbb{D}^p_{0np}\right]$$

$$\mathbb{D}_{0n} \equiv \left[\mathbb{D}^n_{01} \quad \mathbb{D}^n_{02} \quad \dots \quad \mathbb{D}^n_{0np}\right]$$

$$\mathbb{D}_{0c} \equiv \left[\mathbb{D}^c_{01} \quad \mathbb{D}^c_{02} \quad \mathbb{D}^c_{03} \quad \mathbb{D}^c_{04}\right]$$

The Taylor spatial coordinate $\mathbf{y}^*$ defined as a constant for each node in (8.5), is given in a compact form as

$$\mathbf{y}^* = \mathbb{D}^{\mathrm{T}}_{0\mathrm{global},p}\,\overline{\mathbf{F}} \tag{8.82}$$

where $\mathbb{D}_{0\mathrm{global},p}$ is the global material coordinate matrix for Periodic b.c. and $\overline{\mathbf{F}}$ is the matrix representation of the prescribed macroscopic deformation gradient tensor. In this model the variation of the Taylor spatial coordinate vector $\mathrm{d}\mathbf{y}^*$ is considered as follows

$$\mathrm{d}\mathbf{y}^* = \mathbb{D}^{\mathrm{T}}_{0\mathrm{global},p}\,\mathrm{d}\overline{\mathbf{F}}\,, \tag{8.83}$$

i.e. the variation of the coordinate $\mathrm{d}\mathbf{y}^*$ is a function of the variation of the macroscopic average deformation gradient vector $\mathrm{d}\overline{\mathbf{F}}$.

8.8.3 Average Kirchhoff macro-stress for the periodic b.c.

Following the general procedure to compute average stress given in Section 8.5.1, the average Kirchhoff stress is computed, based on the matrix expression for the average Kirchhoff stress (8.23), as follows

$$\overline{\boldsymbol{\tau}} = \frac{1}{|\mathbb{V}_0|}\left[\sum_{\mathrm{j}\,=\,1}^{\mathrm{n_p}} (\mathbb{D}^+_{\mathrm{j}} - \mathbb{D}^-_{\mathrm{j}})\,\mathbf{f}^{+ext}_{\mathrm{j}} + \sum_{\mathrm{i}\,=\,1}^{4} \mathbb{D}_{\mathrm{ci}}\,\mathbf{f}^{ext}_{\mathrm{ci}}\right] \tag{8.84}$$

We define the *boundary spatial coordinate matrix* $\mathbb{D}_{\mathrm{b},p}$ as

$$\mathbb{D}_{\mathrm{b},p} = \left[\,\mathbb{D}_{\mathrm{p}} \quad \mathbb{D}_{\mathrm{n}} \quad \mathbb{D}_{\mathrm{c}}\,\right] \tag{8.85}$$

where $\mathbb{D}_{\mathrm{p}}$, $\mathbb{D}_{\mathrm{n}}$ and $\mathbb{D}_{\mathrm{c}}$ are the *positive boundary spatial coordinate matrix*, *negative boundary spatial coordinate matrix* and *corner spatial coordinate matrix*, respectively, given as

$$\mathbb{D}_{\mathrm{p}} \equiv \left[\mathbb{D}_1^p \;\; \mathbb{D}_2^p \;\; \dots \;\; \mathbb{D}_{\mathrm{np}}^p\right]$$

$$\mathbb{D}_{\mathrm{n}} \equiv \left[\mathbb{D}_1^n \;\; \mathbb{D}_2^n \;\; \dots \;\; \mathbb{D}_{\mathrm{np}}^n\right]$$

$$\mathbb{D}_{\mathrm{c}} \equiv \left[\mathbb{D}_1^c \;\; \mathbb{D}_2^c \;\; \mathbb{D}_3^c \;\; \mathbb{D}_4^c\right]$$

Then, the expression for the averaged Kirchhoff stress (8.84) in a global form is given by

$$\overline{\boldsymbol{\tau}} = \frac{1}{|\mathbb{V}_0|}\, \mathbb{D}_{\mathrm{b},p}\, \mathbf{f}_{\mathrm{b}}^{ext} \tag{8.86}$$

where global matrix notation has been used. Note that $\mathbf{f}_{\mathrm{b}}^{ext}$ is the external boundary force vector which is obtained by gathering operation of the external force vector to extract the positive $\mathbf{f}_{\mathrm{p}}^{ext}$, negative $\mathbf{f}_{\mathrm{n}}^{ext}$ and corner $\mathbf{f}_{\mathrm{c}}^{ext}$ counterpart in the expression

$$\mathbf{f}_{\mathrm{b}}^{ext} = \left\{ \begin{array}{c} \mathbf{f}_{\mathrm{p}}^{ext} \\ \mathbf{f}_{\mathrm{n}}^{ext} \\ \mathbf{f}_{\mathrm{c}}^{ext} \end{array} \right\}$$

8.8.4 Homogenised spatial tangent modulus for the periodic b.c.

After gathering and rearranging the displacement nodal vector $\mathbf{u}$, the external nodal force vector $\mathbf{f}^{ext}$ and finally the stiffness matrix $\mathbf{K}$, as defined in (8.71) and (8.72), respectively, the general system (8.27) that relates the variations $\mathrm{d}\mathbf{u}$ and $\mathrm{d}\mathbf{f}^{ext}$ is rearranged as follows

$$\begin{bmatrix} \mathbf{k}_{\mathrm{ii}} & \mathbf{k}_{\mathrm{ip}} & \mathbf{k}_{\mathrm{in}} & \mathbf{k}_{\mathrm{ic}} \\ \mathbf{k}_{\mathrm{pi}} & \mathbf{k}_{\mathrm{pp}} & \mathbf{k}_{\mathrm{pn}} & \mathbf{k}_{\mathrm{pc}} \\ \mathbf{k}_{\mathrm{ni}} & \mathbf{k}_{\mathrm{np}} & \mathbf{k}_{\mathrm{nn}} & \mathbf{k}_{\mathrm{nc}} \\ \mathbf{k}_{\mathrm{ci}} & \mathbf{k}_{\mathrm{cp}} & \mathbf{k}_{\mathrm{cn}} & \mathbf{k}_{\mathrm{cc}} \end{bmatrix} \begin{Bmatrix} \mathrm{d}\mathbf{u}_{\mathrm{i}} \\ \mathrm{d}\mathbf{u}_{\mathrm{p}} \\ \mathrm{d}\mathbf{u}_{\mathrm{n}} \\ \mathrm{d}\mathbf{u}_{\mathrm{c}} \end{Bmatrix} = \begin{Bmatrix} \mathrm{d}\mathbf{f}_{\mathrm{i}}^{ext} \\ \mathrm{d}\mathbf{f}_{\mathrm{p}}^{ext} \\ \mathrm{d}\mathbf{f}_{\mathrm{n}}^{ext} \\ \mathrm{d}\mathbf{f}_{\mathrm{c}}^{ext} \end{Bmatrix} \quad \equiv \quad \mathbf{K}\, \mathrm{d}\mathbf{u} = \mathrm{d}\mathbf{f}^{ext} \tag{8.87}$$

where $\mathrm{d}\mathbf{f}_{\mathrm{i}}^{ext} = \mathbf{0}$ in equilibrium. Splitting the spatial coordinate vector (8.1) and rearranging the system (8.87), leads to

$$\mathbf{K}\, \mathrm{d}\tilde{\mathbf{u}} = \mathrm{d}\mathbf{f}^{ext} - \mathbf{K}\, \mathrm{d}\mathbf{y}^{*} \tag{8.88}$$

where the variation of Taylor coordinate $\mathbf{dy}^*$ is given by (8.83).

By following the procedure described in detail Section 6.8.4 for the small strain conditions (with the only difference is that $\mathbf{du}^*$ is substituted by $\mathbf{dy}^*$), the following expression is obtained

$$\mathrm{df}_{\mathrm{b}}^{ext} \equiv \left\{ \begin{array}{c} \mathrm{df}_{\mathrm{p}}^{ext} \\ \mathrm{df}_{\mathrm{n}}^{ext} \\ \mathrm{df}_{\mathrm{c}}^{ext} \end{array} \right\} = \mathbf{K}_{\mathbf{per}}^{\mathbf{B}} \, \mathbf{dy}^* \tag{8.89}$$

This gives the expression

$$\mathrm{df}_{\mathrm{b}}^{ext} = \mathbf{K}_{\mathbf{per}}^{\mathbf{B}} \; \mathbb{D}_{0\mathrm{global},p}^{\mathrm{T}} \, \mathrm{d}\overline{\mathbf{F}} \tag{8.90}$$

where the Taylor coordinate variation (8.83) was inserted into the equation (8.89). Therefore, the desired expression is obtained as

$$\frac{\mathrm{df}_{\mathrm{b}}^{ext}}{\mathrm{d}\overline{\mathbf{F}}} = \mathbf{K}_{\mathbf{per}}^{\mathbf{B}} \; \mathbb{D}_{0\mathrm{global},p}^{\mathrm{T}} \tag{8.91}$$

which expresses the variation of the external boundary force vector $\mathrm{df}_{\mathrm{b}}^{ext}$ with respect to the variation of macroscopic average deformation gradient matrix $\mathrm{d}\overline{\mathbf{F}}$.

The overall modulus defined in (7.15), can be computed in its discretised F.E. matrix form, using previous averaged stress expression (8.86), in the following way

$$\overline{\boldsymbol{\mathcal{D}}}_p^{\tau \mathrm{F}} = \frac{\mathrm{d}\overline{\boldsymbol{\tau}}}{\mathrm{d}\overline{\mathbf{F}}} = \frac{1}{|\mathbb{V}_0|} \, \mathbb{D}_{\mathrm{b},p} \, \frac{\mathrm{df}_{\mathrm{b}}^{ext}}{\mathrm{d}\overline{\mathbf{F}}} \tag{8.92}$$

where $\mathbb{D}_{\mathrm{b},p}$ was defined in (8.85).

Inserting (8.91) into (8.92), the matrix representation of $\overline{\boldsymbol{\mathcal{D}}}_p^{\tau \mathrm{F}}$ modulus is obtained as

$$\boxed{\overline{\boldsymbol{\mathcal{D}}}_p^{\tau \mathrm{F}} = \frac{1}{|\mathbb{V}_0|} \, \mathbb{D}_{\mathrm{b},p} \, \mathbf{K}_{\mathbf{per}}^{\mathbf{B}} \, \mathbb{D}_{0\mathrm{global},p}^{\mathrm{T}}} \tag{8.93}$$

Clearly, the modulus $\overline{\boldsymbol{\mathcal{D}}}_p^{\tau \mathrm{F}}$ is a function of the boundary spatial coordinate matrix $\mathbb{D}_{\mathrm{b},p}$ defined in (8.85), the condensed periodic stiffness matrix $\mathbf{K}_{\mathbf{per}}^{\mathbf{B}}$ and the global material coordinate matrix $\mathbb{D}_{0\mathrm{global},p}^{\mathrm{T}}$ outlined in (8.80). The final step consists in inserting (8.93) into (8.31) to obtain

$$\overline{\boldsymbol{\mathcal{A}}}_p = \frac{1}{J_{\mathrm{M}}} \overline{\boldsymbol{\mathcal{D}}}_p^{\tau \mathrm{F}} \diamond \overline{\mathbf{F}} - \overline{\boldsymbol{\sigma}} \star \mathbf{I} \tag{8.94}$$

which represents the overall spatial tangent modulus for periodic b.c. in the matrix form. Finally, we remark that with the above expression (8.94), the tangent modulus can be computed for heterogeneous material with different microstructures RVE gaining the desired *quadratic rate of convergence* for the Newton-Raphson solution procedure applied to solve the homogenized nonlinear macrostructure, under *periodic deformation* and *antiperiodic traction* on the boundary of RVE model.

8.8.5 Microequilibrium computation for the periodic b.c. in large strain

In Section 8.4.1 a general solution scheme for microequilibrium is given in finite strain analysis. In this section, the particularisation of the microequilibrium procedure for periodic b.c. is described.

The incremental Taylor displacement is given in global matrix form as,

$$\triangle \mathbf{u}^* = \mathbf{y}^*_{n+1} - \mathbf{y}_n = \mathbb{D}^{\mathrm{T}}_{0\mathrm{global},p}\overline{\mathbf{F}}_{n+1} - \mathbf{y}_n. \tag{8.95}$$

The residual force $\mathbf{r}$ is taken as,

$$\mathbf{r} = \begin{Bmatrix} \mathbf{f}^{int}_{\mathrm{i}} \\ \mathbf{f}^{int}_{\mathrm{p}} + \mathbf{f}^{int}_{\mathrm{n}} \end{Bmatrix} - \begin{Bmatrix} \mathbf{f}^{ext}_{\mathrm{i}} \\ \mathbf{f}^{ext}_{\mathrm{p}} + \mathbf{f}^{ext}_{\mathrm{n}} \end{Bmatrix} \tag{8.96}$$

Assuming that in equilibrium $\mathbf{f}^{ext}_{\mathrm{i}} = \mathbf{0}$ and antiperiodicity of the boundary traction in discrete form $\mathbf{f}^{ext}_{\mathrm{p}} + \mathbf{f}^{ext}_{\mathrm{n}} = \mathbf{0}$, the residual for periodic b.c. takes the form,

$$\mathbf{r} = \begin{Bmatrix} \mathbf{f}^{int}_{\mathrm{i}} \\ \mathbf{f}^{int}_{\mathrm{p}} + \mathbf{f}^{int}_{\mathrm{n}} \end{Bmatrix}. \tag{8.97}$$

The differential fluctuation is given by the system (8.19) which takes the following form for periodic b.c.

$$\mathbf{K}_2 \begin{Bmatrix} \delta\widetilde{\mathbf{u}}_{\mathrm{i}} \\ \delta\widetilde{\mathbf{u}}_{\mathrm{p}} \end{Bmatrix} = - \begin{Bmatrix} \mathbf{f}^{int}_{\mathrm{i}} \\ \mathbf{f}^{int}_{\mathrm{p}} + \mathbf{f}^{int}_{\mathrm{n}} \end{Bmatrix} \quad \Rightarrow \quad \begin{Bmatrix} \delta\widetilde{\mathbf{u}}_{\mathrm{i}} \\ \delta\widetilde{\mathbf{u}}_{\mathrm{p}} \end{Bmatrix} = -\mathbf{K}_2^{-1} \begin{Bmatrix} \mathbf{f}^{int}_{\mathrm{i}} \\ \mathbf{f}^{int}_{\mathrm{p}} + \mathbf{f}^{int}_{\mathrm{n}} \end{Bmatrix} \tag{8.98}$$

for differential displacement fluctuation for interior and positive nodes. Also, taking into consideration (8.76) and (8.74), the differential displacement fluctuation for negative and corners is computed as,

$$\delta\widetilde{\mathbf{u}}_{\mathrm{n}} = \delta\widetilde{\mathbf{u}}_{\mathrm{p}} \quad \text{and} \quad \delta\widetilde{\mathbf{u}}_{\mathrm{c}} = \mathbf{0} \tag{8.99}$$

The updating of the incremental fluctuation is then given by

$$\begin{array}{rcl} \triangle\widetilde{\mathbf{u}}_{\mathrm{i}} & \leftarrow & \triangle\widetilde{\mathbf{u}}_{\mathrm{i}} + \delta\widetilde{\mathbf{u}}_{\mathrm{i}} \\ \triangle\widetilde{\mathbf{u}}_{\mathrm{p}} & \leftarrow & \triangle\widetilde{\mathbf{u}}_{\mathrm{p}} + \delta\widetilde{\mathbf{u}}_{\mathrm{p}} \\ \triangle\widetilde{\mathbf{u}}_{\mathrm{n}} & \leftarrow & \triangle\widetilde{\mathbf{u}}_{\mathrm{p}} \end{array} \tag{8.100}$$

and $\triangle\widetilde{\mathbf{u}}_{\mathrm{c}}^{\cdot} = \mathbf{0}$. Finally, the incremental displacement to compute the internal force is updated as

$$\begin{array}{rcl} \triangle\mathbf{u}_{\mathrm{i}} & \leftarrow & \triangle\mathbf{u}_{\mathrm{i}} + \delta\widetilde{\mathbf{u}}_{\mathrm{i}} \\ \triangle\mathbf{u}_{\mathrm{p}} & \leftarrow & \triangle\mathbf{u}_{\mathrm{p}} + \delta\widetilde{\mathbf{u}}_{\mathrm{p}} \\ \triangle\mathbf{u}_{\mathrm{n}} & \leftarrow & \triangle\mathbf{u}_{\mathrm{p}} \end{array} \tag{8.101}$$

and $\triangle\mathbf{u}_{\mathrm{c}}$ remains constant.

8.9 Conclusions

In this chapter, a detailed description of multiscale F.E. analysis of solids undergoing large strains has been given. In the next chapter, numerical tests have been performed to validate the models described in this chapter.

Chapter 9

Numerical examples

9.1 Introduction

So far, this work has presented a general framework for numerical treatment of multiscale Finite Element analysis. In Chapters 5 and 8 numerical procedures for the first-order multiscale FE homogenization of small and large strain analysis have been presented, respectively. Practical application of these numerical procedure in 2D analysis are presented in this chapter. These numerical examples validate the multiscale FE formulation for the computation of the macro-stress and overall tangent modulus.

The first example given in Section 9.2 is a simple test in which we validate the model in the linear elastic regime. The numerical material properties are compared with analytical solution. The second test given in Section 9.3 gives an illustration of the material nonlinear behaviour for an RVE whose material behaviour is modelling by an elastoplastic law in small strain. Finally, an numerical example of the geometrical nonlinear behaviour for a hyperelastic material in finite deformation is given in Section 9.4.

9.2 Homogenised properties of a linear elastic composite

The first numerical test consists of the computation of the effective material properties of a linear elastic composite. Square microcells are considered composed of epoxy matrix with Young's modulus $E = 3.13\ GPa$ and Poisson's ratio $\nu = 0.34$. Glass fibre is embedded in the matrix with Young's modulus $E = 73\ GPa$ and Poisson's ratio $\nu = 0.2$.

The test has been carried out under plane strain analysis. In Figure 9.1 the ratio of effective shear modulus over the matrix modulus $\overline{\mathrm{G}}/\mathrm{G}_{matrix}$ is compared with analytically obtained properties following Nemat-Nasser [77].

A very similar response can be observed for less than 20% of the fibre volume fraction. Especially, the periodic assumption seems to be very accurate. We note that Nemat-Nasser's analytical model is effective in predicting equivalent material properties for a low volume fraction of the fibre inclusion.

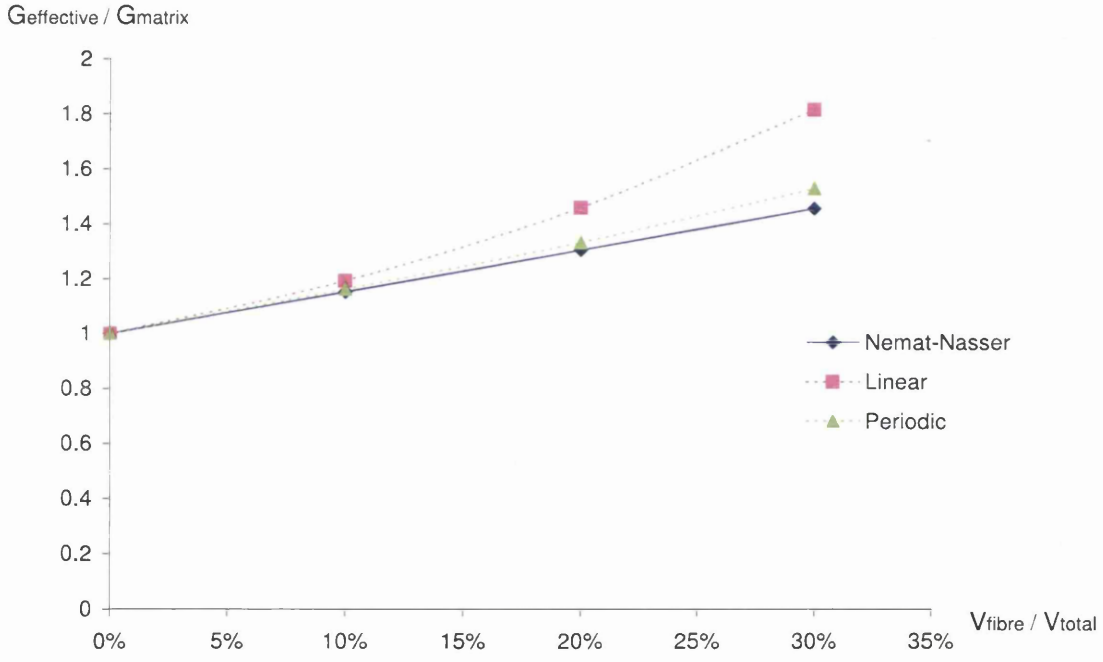

Figure 9.1: Comparison of $\frac{\overline{\mathrm{G}}}{\mathrm{G}_{matrix}}$ for analytical solution of Nemat-Nasser and numerically obtained results.

9.3 Internally pressurised circular plate at small strain

The second numerical test considered is an analysis of nonlinear material behaviour in *small strain*. The test consists of a simulation of the behaviour of an internally pressurised circular metallic plate, see Figure 9.2. We assumed the plate has voids. The analysis is carried out assuming *plane stress* conditions. The von Mises perfect elastoplastic model, introduced in Section 4.5.2, is used to perform the simulation.

The properties of the material are as follows:

- Young's modulus E = 210 GPa.
- Poisson ratio $\nu = 0.3$.
- uniaxial yield stress $\sigma_y = 0.24$ GPa (perfect elastoplastic).

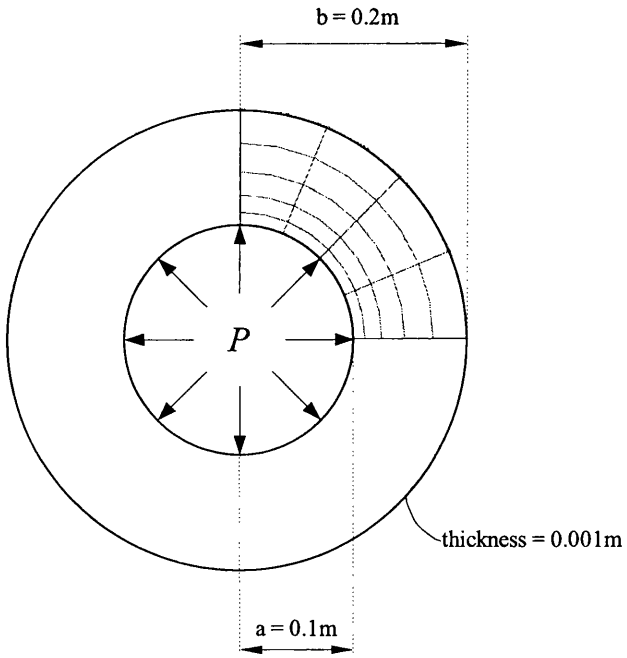

Figure 9.2: Internally pressurised circular plate. Quarter of circular plate mesh

The mesh for the macrostructure is shown in Figure 9.2. Due to symmetry only a quarter of the circular plate is analyzed by employing 20 standard 8-noded quadrilateral elements with reduced integration.

The pressure, P, prescribed on the inner surface, is increased gradually until collapse (limit) load is reached. For the present problem (see Figure 9.3), plastic yielding starts at the inner surface (with radial coordinate $r = a$) and develops gradually, in the from of a circular plastic front (with radius c), towards the outer face ($r = b$). Collapse occurs when the plastic front reaches the outer face (c = b) and the entire cylinder can expand indefinitely without further increase in the applied pressure.

Initially, the pressure is applied during elastic regime until value P_0 is reached at which plastic yielding begins. In this region the radial displacement of the outer surface is a linear function of P, given by:

$$u_b = \frac{2Pb}{E(\frac{b^2}{a^2} - 1)} \quad P < P_0 \tag{9.1}$$

A closed-form in the plastic region, has been derived by Lubliner [41] for the material without voids. It relates the applied pressure to the radius c of the plastic front by means of the expression:

$$\frac{P}{Y} = \ln\left(\frac{c}{a}\right) + \frac{1}{2}\left(1 - \frac{c^2}{b^2}\right), \tag{9.2}$$

where, for the von Mises model (see Section 4.5.2), $Y = 2\sigma_y/\sqrt{3}$. Plastic yielding begins when $c = a$, which corresponds to the yielding pressure:

$$\frac{P_0}{Y} = \frac{1}{2}\left(1 - \frac{a^2}{b^2}\right). \tag{9.3}$$

In the plastic regime ($P \geq P_0$), the radial displacement, u_b, is given by

$$u_b = \frac{Yc^2}{Eb} \quad P < P_0 \tag{9.4}$$

where c can be evaluated as an implicit function of P through (9.2).

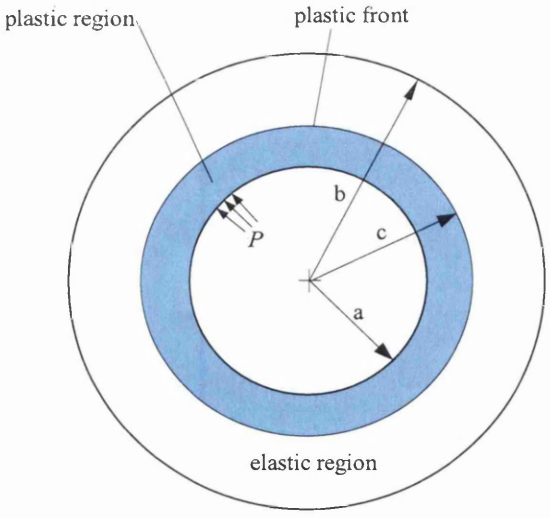

Figure 9.3: Internally pressurised circular plate. Partially plastified cross section

9.3.1 Internal pressure vs outer surface displacement diagrams

In the following figures, diagrams showing the applied pressure P versus radial displacement at the outer face of the plate are plotted together with the closed-form solution [41] described above. The following diagrams are displayed:

- Single scale analysis: Closed form and FEM analysis
- Two multi-scale analyses. RVE: Square microstructure discretized by 8-noded quadrilateral elements with reduced integration. Every cell has a void in the middle with variable shape and volume fraction, as follows:
  - Microstructure 1: Circular void in the middle of the RVE with 5 % volume fraction. $n_{elements} = 126$, $n_{nodes} = 438$.
  - Microstructure 2: Square void in the middle of the RVE with 5 % volume fraction. $n_{elements} = 128$, $n_{nodes} = 448$.
    $n_{elements} = 128$, $n_{nodes} = 448$.
  - Microstructure 3: Circular void in the middle of the RVE with 15 % volume fraction. $n_{elements} = 128$, $n_{nodes} = 448$.
  - Microstructure 4: Square void in the middle of the RVE with 15 % volume fraction. $n_{elements} = 160$, $n_{nodes} = 560$.

These microstructures are depicted in Figure 9.4.

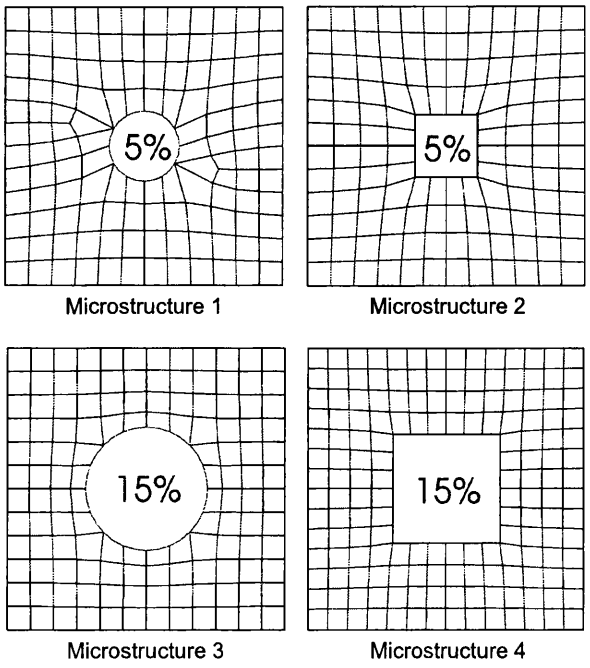

Figure 9.4: Microstructures for analysis of internally pressurised circular plate

In Figures 9.5 and 9.6 results are shown for different constraints on the microcell and 5 and 15% void fraction, respectively. The curve denoted Lubliner-1990 represents the closed-form solution described above and given in [41]. The FEM curve shows a single scale analysis of the problem. The agrement between the closed form and FEM solution is excellent. Furthermore, two scales analysis curves are depicted for the Taylor assumption, linear b.c and periodic b.c. The comments are as follows:

- Taylor assumption gives the stiffest response. Then comes linear b.c. while the softest response is given by periodic b.c. This was expected from the nature of the constraints.
- Taylor assumption and linear b.c. show insensitivity at macroscopic level for different void shape. Diagrams for circular and squared void shape are overlapped.
- Periodic b.c. is the only one which shows sensitivity to the void size. It can be observed that circular void gives slightly stiffer response than the square one, which agrees with the expected response. Moreover, the difference is bigger when the void size is increased.

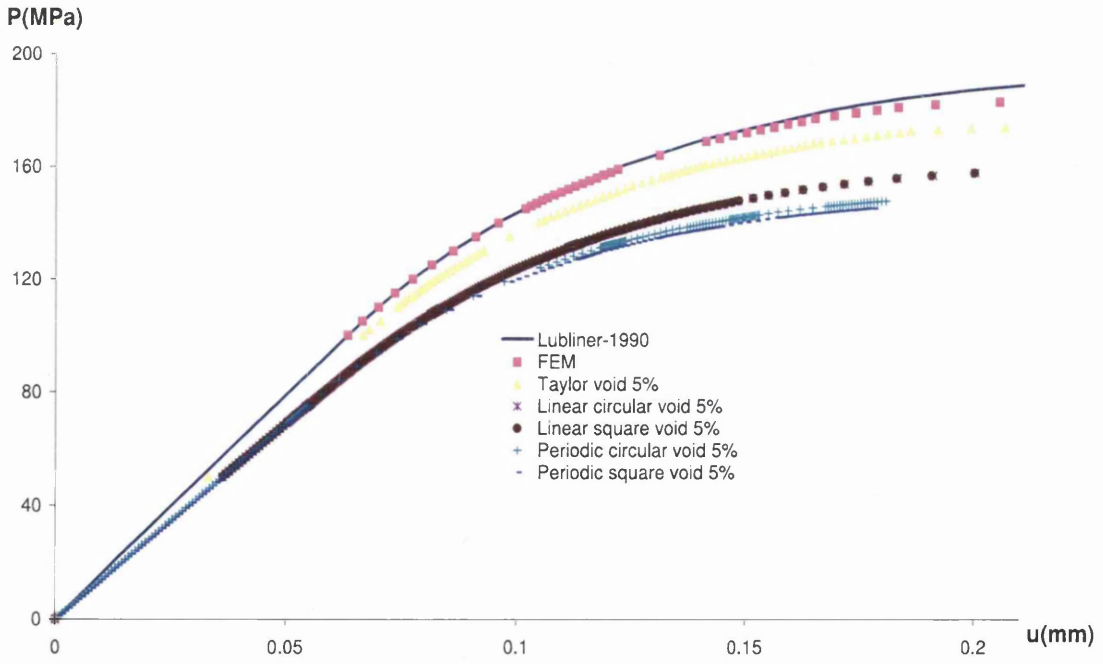

Figure 9.5: Internally pressurised circular plate. Pressure vs displacement diagram for full material and void at 5% volume fraction

The following diagrams 9.7, 9.8 and 9.9 show respectively how the results for each constraint, Taylor assumption, linear b.c. an periodic b.c., with the void volume fraction. It can be observed clearly that the material response softens vary when the void volume fraction increases. The Taylor assumption gives less sensitive results than linear b.c. and periodic b.c..

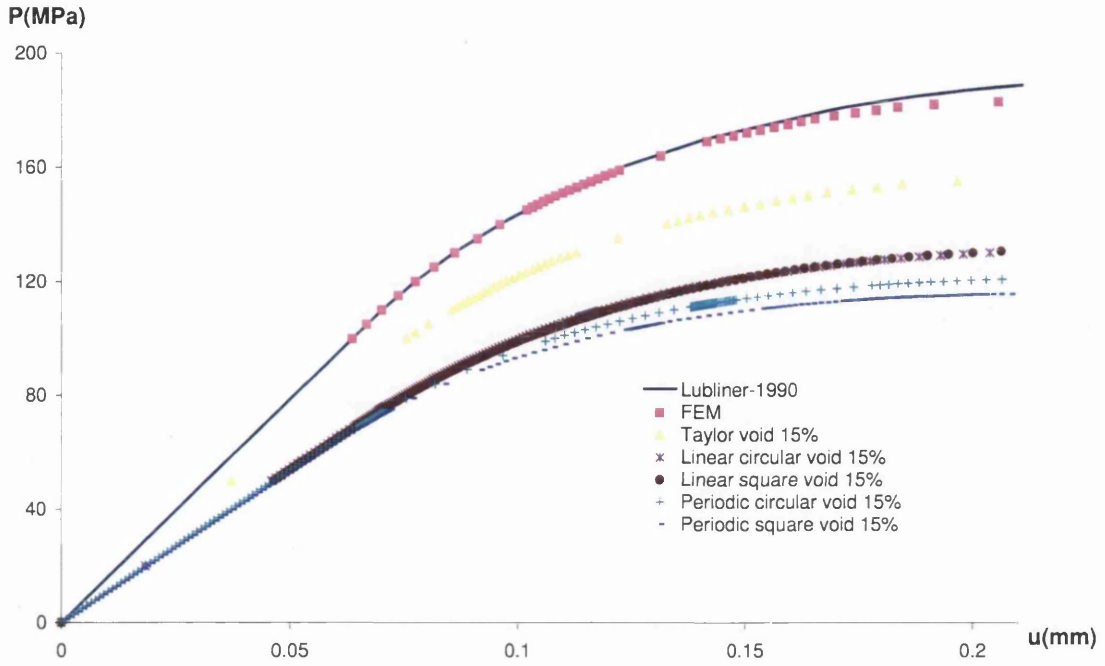

Figure 9.6: Internally pressurised circular plate. Pressure vs displacement diagram for full material and void at 15% volume fraction

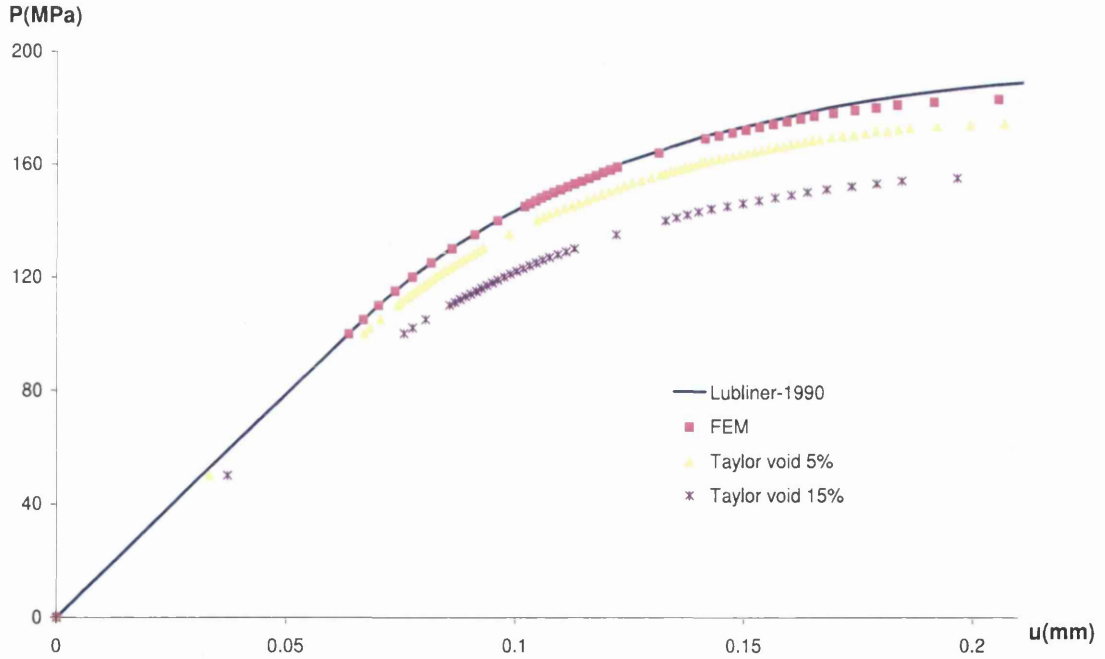

Figure 9.7: Internally pressurised circular plate. Pressure vs displacement diagram for the Taylor assumption

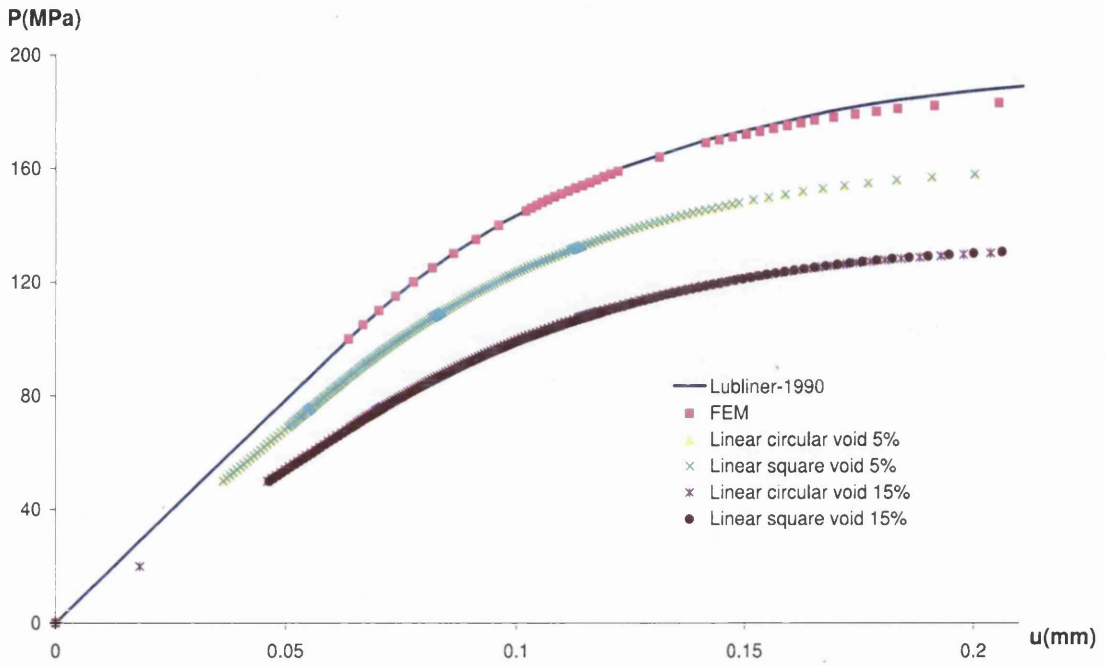

Figure 9.8: Internally pressurised circular plate. Pressure vs displacement diagram for the linear b.c.

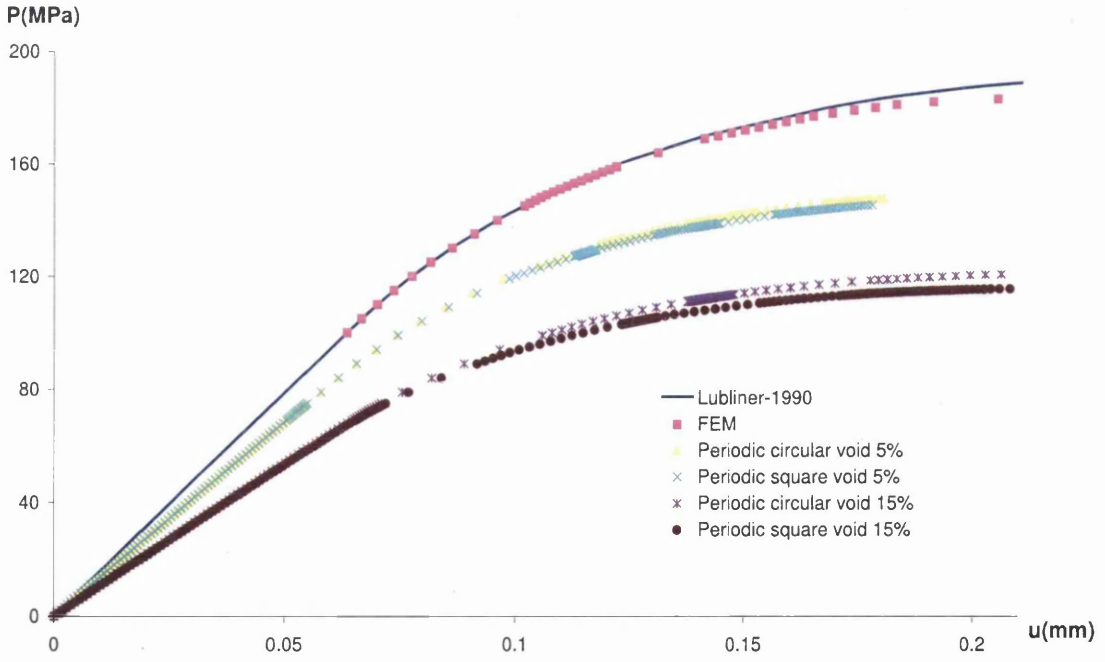

Figure 9.9: Internally pressurised circular plate. Pressure vs displacement diagram for the periodic b.c.

9.3.2 Effective Plastic Strain Distribution

In this section several figures representing effective plastic strain distribution are depicted for a quarter of the cylinder with some representative microstructures. The plastic front evolves in a circular way which agrees with the symmetry of the problem and the analytical solution given earlier [41].

In Figure 9.10 a Microstructure 1 is considered under the Taylor assumption. Two different stages are depicted at different values of internal pressure $P = 140$ and $P = 175$MPa, respectively. We can see the circular evolution of the plastic front at macroscale level. For value of $P = 175$MPa a slight distortion of the plastic front is visible as the load approaches the limit value. This is due to the not perfect axisymmetric distribution of microstructures over the macrostructure.

In Figures 9.11(a) and 9.11(b) the results for the linear b.c. are shown for Microstructure 1 for values of internal pressure of $P = 100$ and $P = 160$MPa, respectively, while Figures 9.12(a) and 9.12(b) give the result for the periodic b.c. for values of internal pressure of $P = 95$ and $P = 150$MPa, respectively. The development of shear bands is observed in these figures.

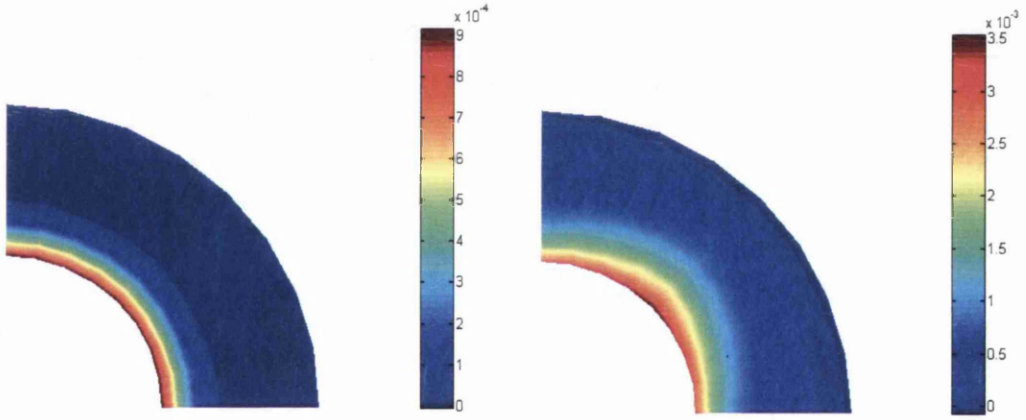

Figure 9.10: Effective plastic strain for the Taylor assumption. Microstructure: circular void at 5% volume fraction

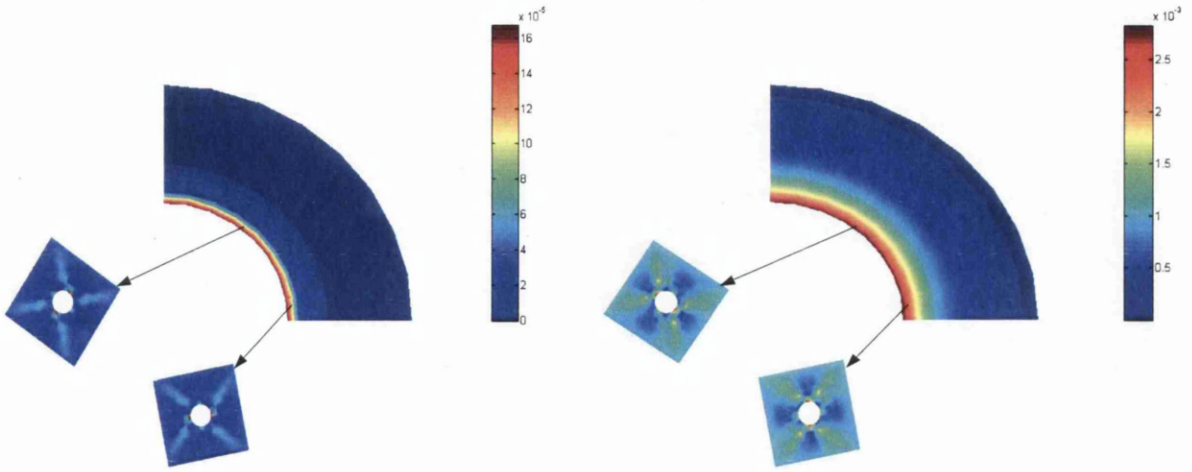

(a) $P = 100$ MPa (b) $P = 160$ MPa

Figure 9.11: Effective plastic strain distribution for the linear b.c. Microstructure 1: circular void at 5% volume fraction

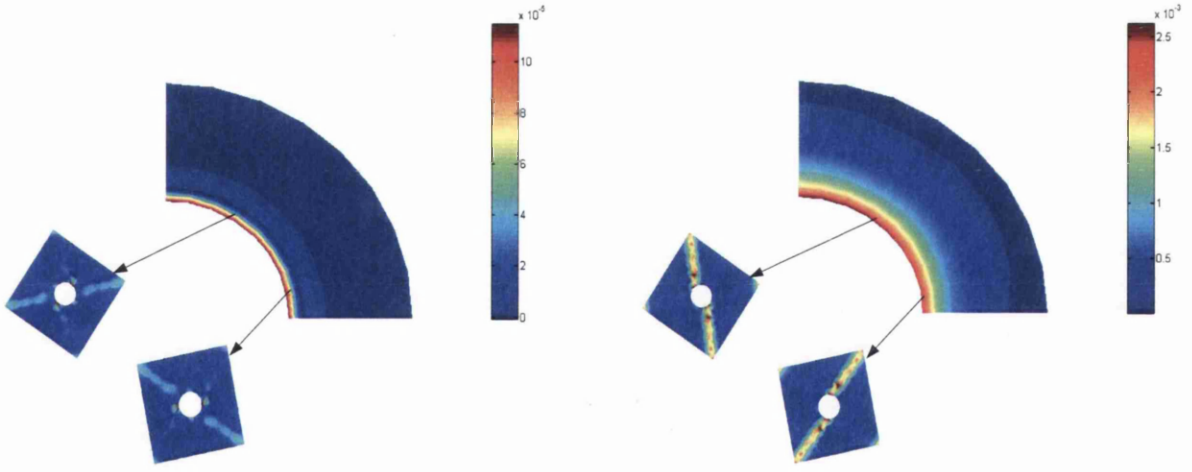

(a) $P = 95$ MPa (b) $P = 150$ MPa

Figure 9.12: Effective plastic strain distribution for the periodic b.c. Microstructure 1: circular void at 5% volume fraction

In Figures 9.13(a) and 9.13(b) the results for the linear b.c. are shown for Microstructure 2 for values of internal pressure of $P = 100$ and $P = 160$MPa, respectively, while Figures 9.14(a) and 9.14(b) give the result for the periodic b.c. for values of internal pressure of $P = 95$ and $P = 150$MPa, respectively. The development of shear bands is observed in these figures.

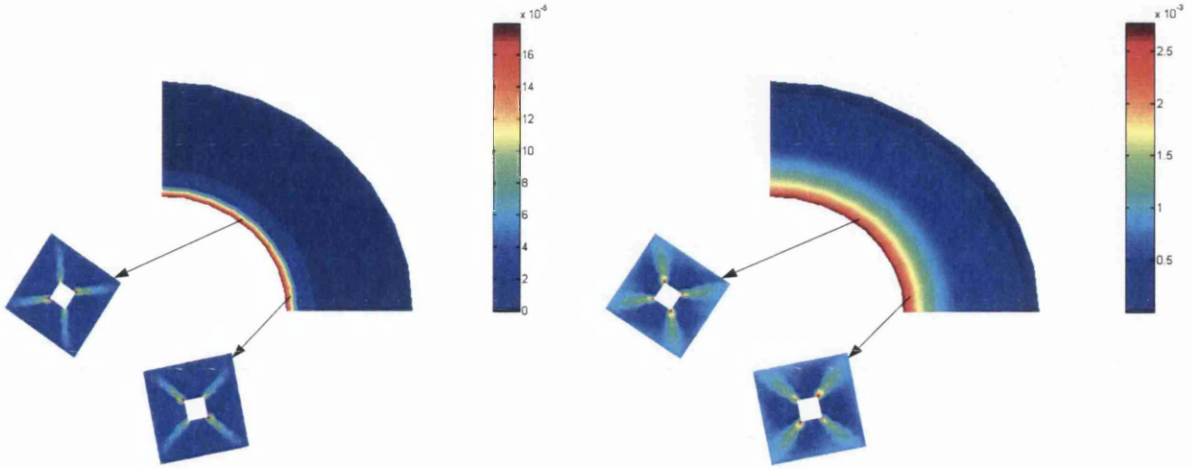

(a) $P = 100$ MPa (b) $P = 160$ MPa

Figure 9.13: Effective plastic strain distribution for the linear b.c. Microstructure 2: square void at 5% volume fraction

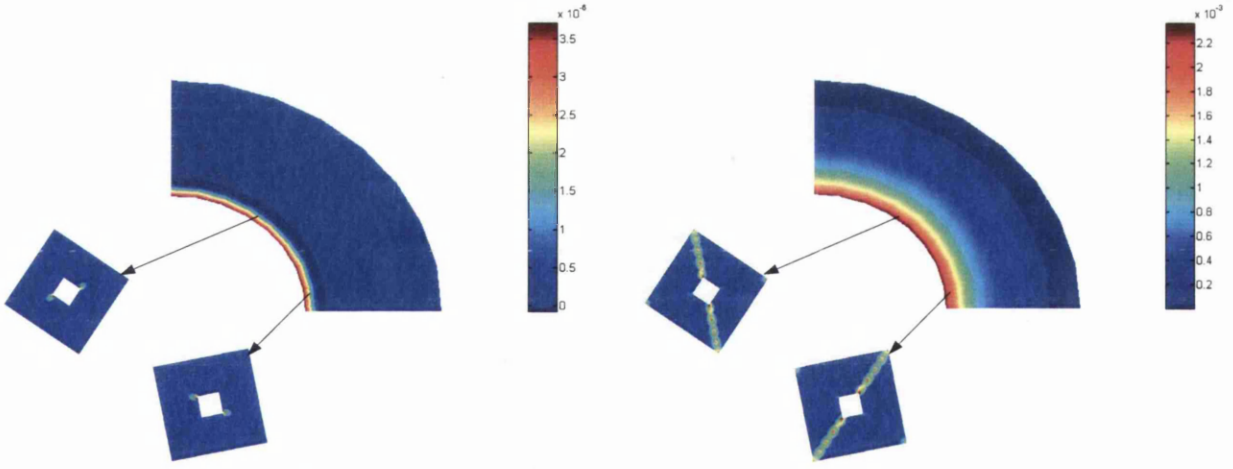

(a) $P = 75$ MPa (b) $P = 145$ MPa

Figure 9.14: Effective plastic strain distribution for the periodic b.c. Microstructure 2: square void at 5% volume fraction

In Figure 9.15 the Microstructure 3 is considered under the Taylor assumption. Two different stages are depicted for different values of internal pressure $P = 115$ and $P = 160$MPa, respectively. We can see the circular evolution of the plastic front at macroscale level. Again, for value of $P = 160$MPa a slight distortion of the plastic front is visible as the load approaches to the limit value. This distortion is due to the non exactly axisymmetric distribution of the microstructures over the quarter of cylinder.

In Figures 9.16(a) and 9.16(b) the results for the linear b.c. are shown for Microstructure 3 for values of internal pressure of $P = 100$ and $P = 130$MPa, respectively, while Figures 9.17(a) and 9.17(b) give the result for the periodic b.c. for values of internal pressure of $P = 100$ and $P = 120$MPa, respectively. The development of shear bands is observed in these figures.

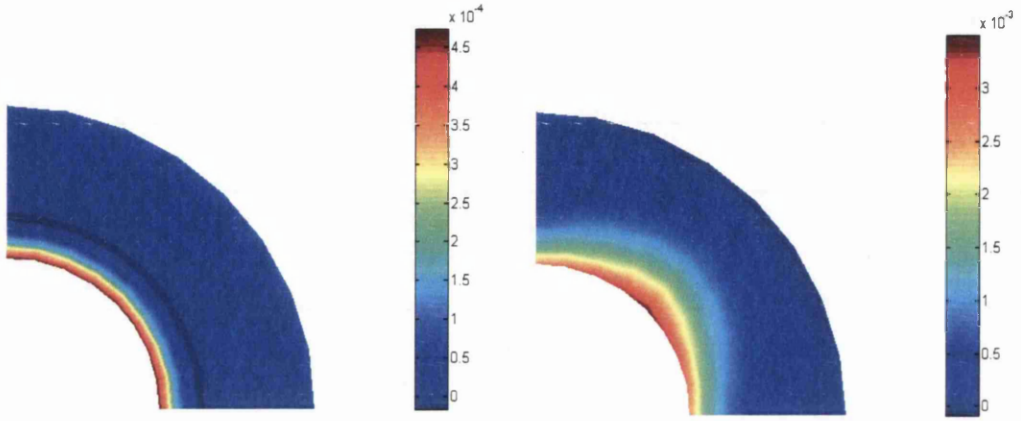

P=115 MPa *P*=160 MPa

Figure 9.15: Effective plastic strain for the Taylor assumption. Microstructure: circular void at 15% volume fraction

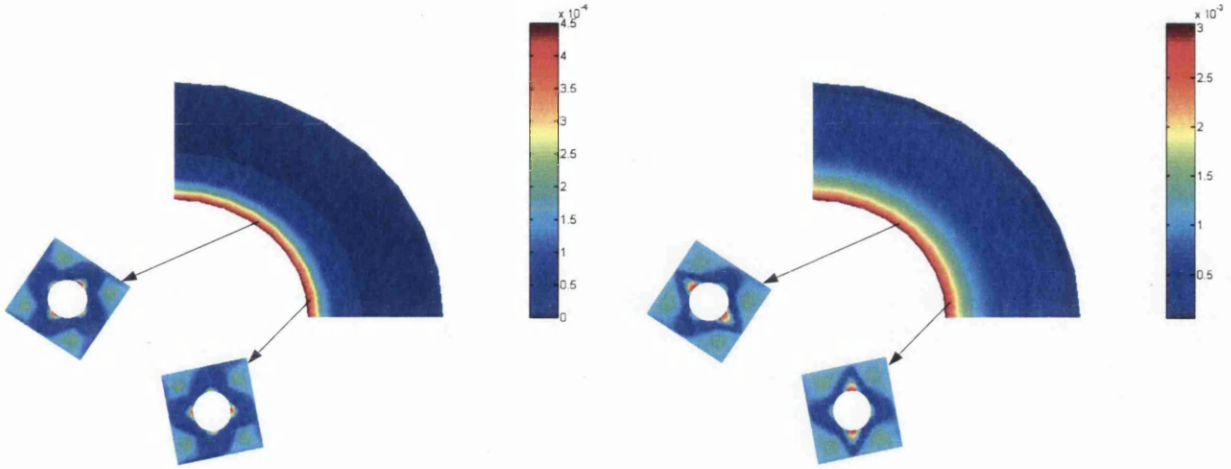

(a) $P = 100$ MPa (b) $P = 130$ MPa

Figure 9.16: Effective plastic strain distribution for the linear b.c. Microstructure 3: circular void at 15% volume fraction

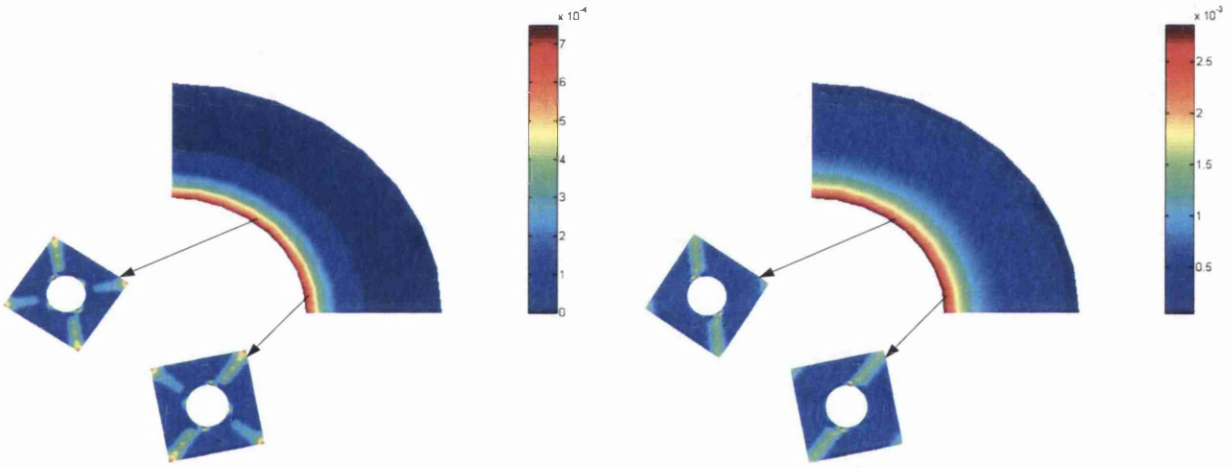

(a) $P = 100$ MPa (b) $P = 120$ MPa

Figure 9.17: Effective plastic strain distribution for the periodic b.c. Microstructure 3: circular void at 15% volume fraction

In Figures 9.18(a) and 9.18(b) the results for the linear b.c. are shown for Microstructure 4 for values of internal pressure of $P = 90$ and $P = 130$MPa, respectively, while Figures 9.19(a) and 9.19(b) give the result for the periodic b.c. for values of internal pressure of $P = 75$ and $P = 115$MPa, respectively. The development of shear bands is observed in these figures.

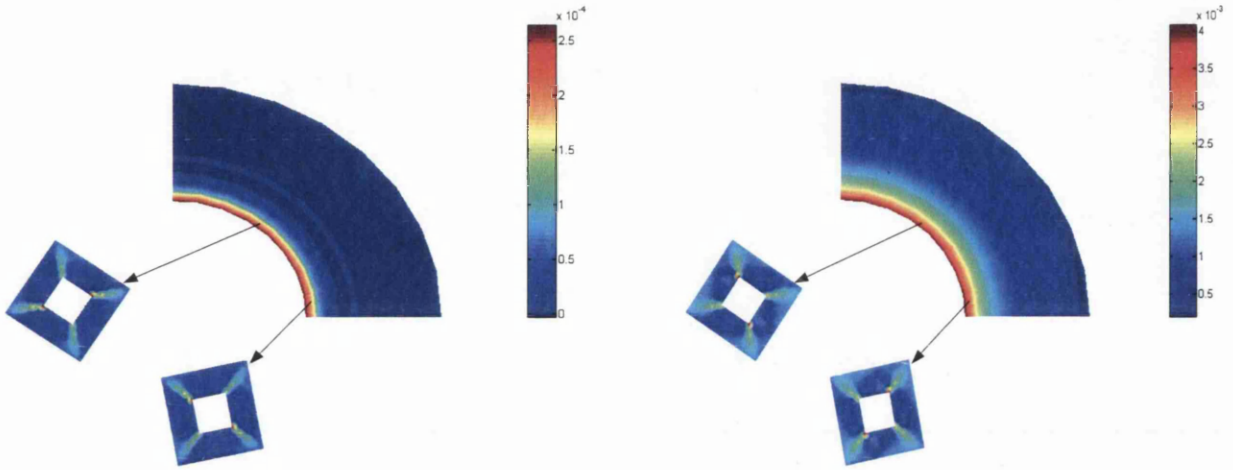

(a) $P = 90$ MPa (b) $P = 130$ MPa

Figure 9.18: Effective plastic strain distribution for the linear b.c. Microstructure 4: square void at 15% volume fraction

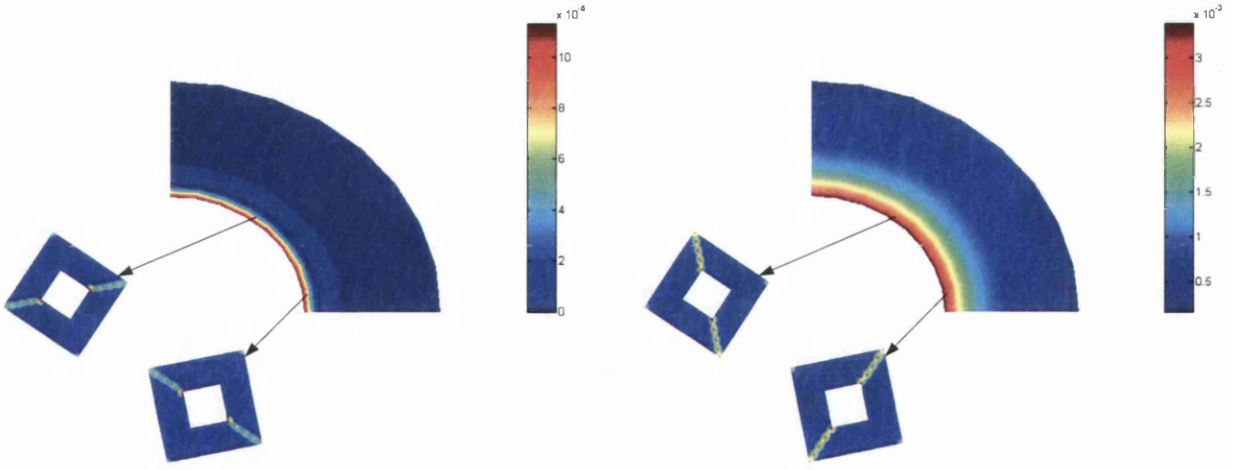

(a) $P = 75$ MPa (b) $P = 115$ MPa

Figure 9.19: Effective plastic strain distribution for the periodic b.c. Microstructure 4: square void at 15% volume fraction

9.3.3 Residuals evolution per iteration in macro and micro levels

In this section tables with the Euclidean norm R_M of the residual are reported associated with the Newton iterations of the macro- and micro-equilibrium. The residual norm evolution is shown for the microstructure that corresponds to the macro Gauss point in the bottom right corner.

In the following tables the Euclidean norm R_M of the residual is reported associated with the Newton iterations of the macro-equilibrium. The macro-residual is normalised and calculated as $R_M = 100 \times \|\mathbf{F}_{int} - \mathbf{F}_{ext}\|/\|\mathbf{F}_{ext}\|$. The micro residual is computed in different ways depending on the constraint. Obviously in Taylor assumption there is no micro BVP so we do not show the residuals.

The residual for linear b.c. is evaluated as $R_\mu = 100 \times \|\mathbf{r}\|/\|\mathbf{f}^{int}\|$ where $\mathbf{r}$ was given in (6.56). The residual for periodic b.c. is evaluated as $R_\mu = 100 \times \|\mathbf{r}\|/\|\mathbf{f}^{int}\|$ where $\mathbf{r}$ was given in (6.102).

Clearly, the quadratic rate of asymptotic convergence can be observed in the macro and microscale for both Linear and Periodic b.c.'s. Also the Taylor assumption shows quatratic rate of convergence in macroequilibrium.

Macro-step	R_M
1	2.049263×10^{-02}
2	1.340442×10^{-06}
3	1.676496×10^{-13}

Table 9.1: Evolution of Residual norm at the Macroscale (R_M) for Taylor constraint assuming Microstructure 3 (15% circular void). Increment of internal pressure P = 115-116 MPa

micro	R_μ	Macro	R_M
1	2.947000×10^{-00}		
2	7.483573×10^{-01}		
3	4.572174×10^{-02}		
4	1.965543×10^{-04}		
5	1.635712×10^{-09}	1	3.569328×10^{-02}
1	2.985146×10^{-00}		
2	1.255292×10^{-00}		
3	8.916588×10^{-02}		
4	6.666795×10^{-04}		
5	7.972844×10^{-09}	2	4.463401×10^{-06}
1	2.985146×10^{-00}		
2	1.255292×10^{-00}		
3	8.916583×10^{-02}		
4	6.666805×10^{-04}		
5	7.972878×10^{-09}	3	4.152282×10^{-12}

a) Linear b.c.

micro	R_μ	Macro	R_M
1	7.570612×10^{-00}		
2	$2.273063\times10^{+01}$		
3	1.220398×10^{-00}		
4	1.857460×10^{-01}		
5	4.258028×10^{-03}		
6	9.028518×10^{-07}		
7	5.974417×10^{-12}	1	6.801729×10^{-02}
1	7.685538×10^{-00}		
2	$2.287550\times10^{+01}$		
3	1.240264×10^{-00}		
4	1.914852×10^{-01}		
5	1.531063×10^{-02}		
6	3.075176×10^{-06}		
7	1.719892×10^{-11}	2	6.902391×10^{-04}
1	7.685065×10^{-00}		
2	$2.287559\times10^{+01}$		
3	1.240250×10^{-00}		
4	1.914694×10^{-01}		
5	1.530919×10^{-02}		
6	3.074341×10^{-06}		
7	1.719583×10^{-11}	3	3.157912×10^{-09}
1	7.685065×10^{-00}		
2	$2.287559\times10^{+01}$		
3	1.240250×10^{-00}		
4	1.914694×10^{-01}		
5	1.530919×10^{-02}		
6	3.074341×10^{-06}		
7	1.718875×10^{-11}	4	1.687747×10^{-13}

b) Periodic b.c.

Table 9.2: Evolution of Residual norm at micro (R_μ) and Macroscale (R_M) for Linear b.c. and Periodicb.c. assuming Microstructure 3 (15% circular void). Increment of internal pressure P = 101.3-101.8 MPa and P = 111.01- 111.51 MPa, respectively.

We have shown the convergence for Microstrucure 3 only. Other microstructures show similar convergence properties, so they are not shown here.

9.4 Internally pressurised hyperelastic cylinder at large deformations

This section describes the simulation of a internally pressurised cylinder, see Figure 9.2 with nonlinear material behaviour, in the *large strain* regime. The analysis is carried out assuming the *plane strain* conditions. The Neo-Hookean model, introduced in Section 4.3.2, is used to perform the simulation.

The properties of the material are as follows:

- Logarithmic bulk modulus K = 2.667 GPa.
- Shear Modulus G = 0.889 GPa.

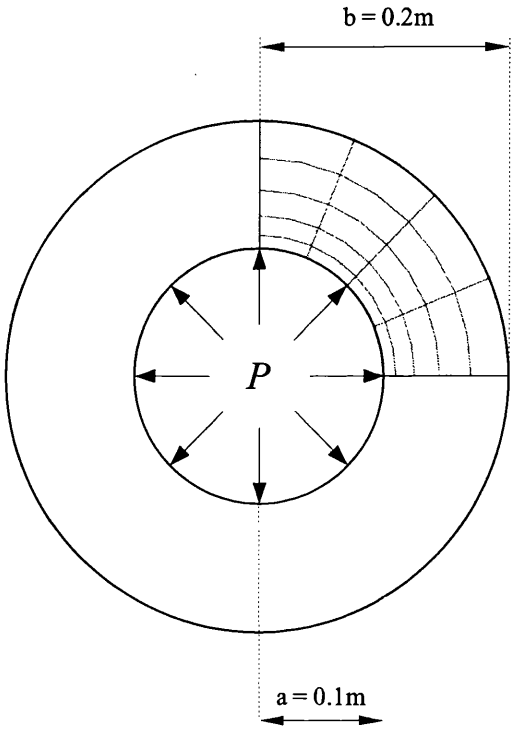

Figure 9.20: Internally pressurised cylinder. Quarter of cylinder is analysed.

The mesh for the macrostructure is shown in Figure 9.20. Due to symmetry, only a quarter of the cylinder is considered, and discretized by 20 standard 8-noded quadrilateral elements with reduced integration.

The pressure, P, is prescribed on the inner surface, and increased gradually.

9.4.1 Internal pressure vs outer surface displacement diagrams

In the following figures, diagrams showing the applied pressure P versus radial displacement at the outer face of the plate are plotted as described earlier.

The diagrams displayed are the same as the one described in Section9.3.1. These Microstructures were depicted in Figure 9.4. For reference we have included a curve in all of them called *Single scale* which corresponds with a material with no voids.

In Figures 9.21 and 9.22 results are shown for different constraints on the microcell and 5 and 15% void fraction, respectively. A full curve shows FE single scale analysis. Two scales results are depicted for Taylor assumption, linear b.c and periodic b.c. The results are as follows:

- Taylor assumption gives the stiffest response.
- For each microstructure linear b.c. shows a slightly stiffer response than periodic.
- In this case the results show larger difference due to the shape of the void than due to different boundary condition.

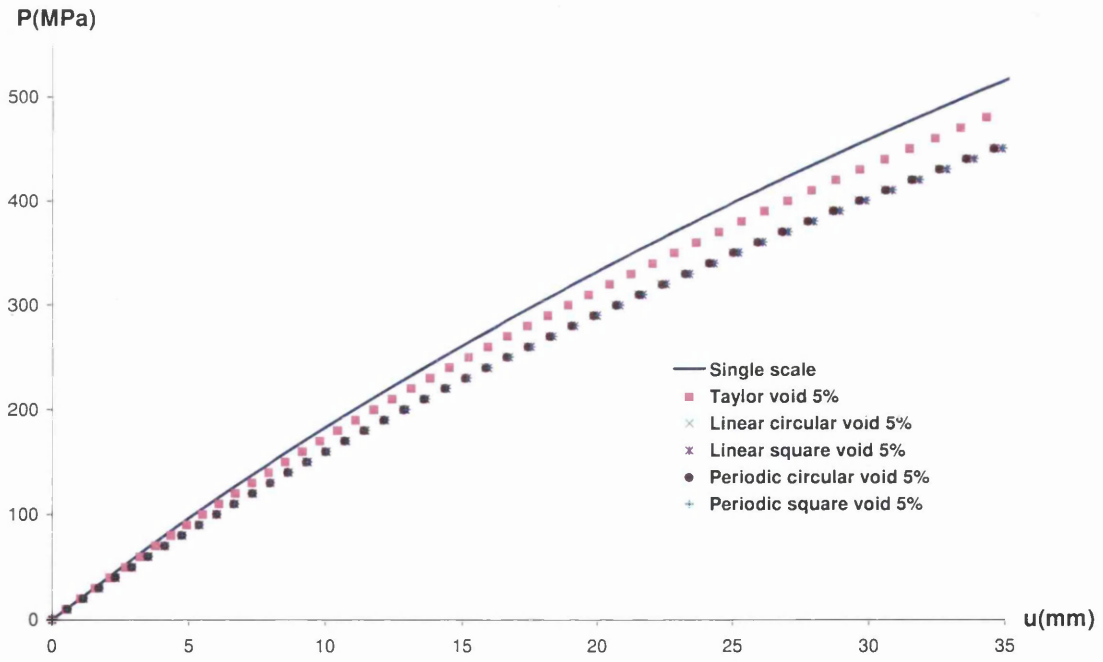

Figure 9.21: Internally pressurised hyperelastic cylinder. Pressure vs displacement diagram for full material and void at 5% volume fraction.

The following diagrams 9.23, 9.24 and 9.25 show respectively how the result vary for each constraint, Taylor assumption, linear b.c. an periodic b.c., with the void volume fraction. It can be observed clearly that the material response softens when the void volume fraction increases. The Taylor assumption shows less sensitive results than linear b.c. and periodic b.c.

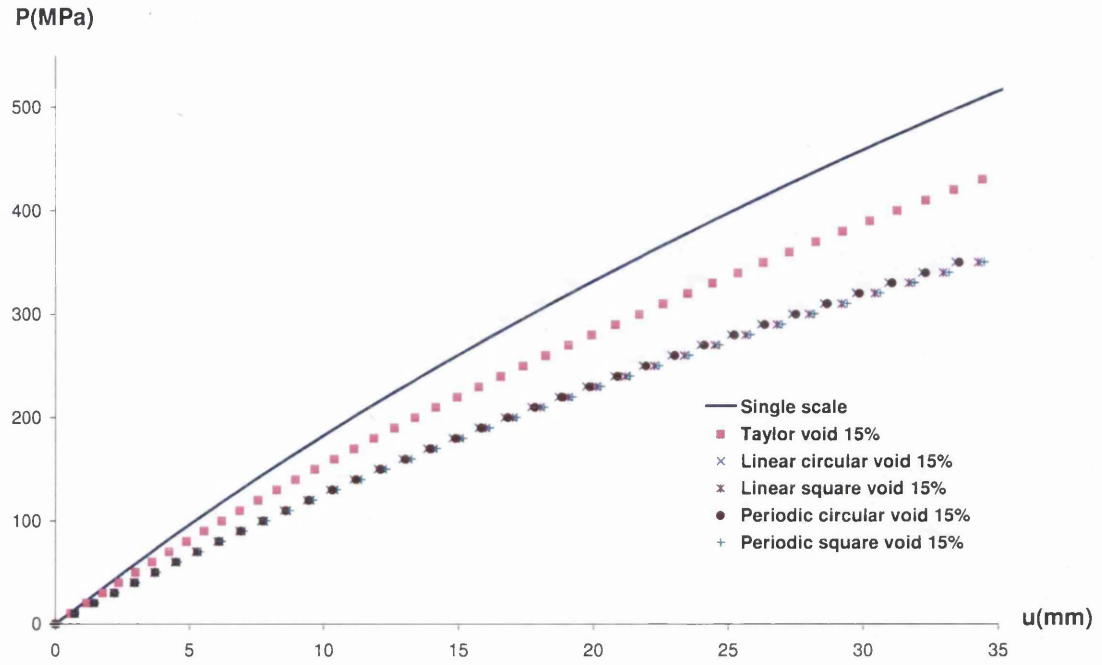

Figure 9.22: Internally pressurised hyperelastic cylinder. Pressure vs displacement diagram for full material and void at 15% volume fraction.

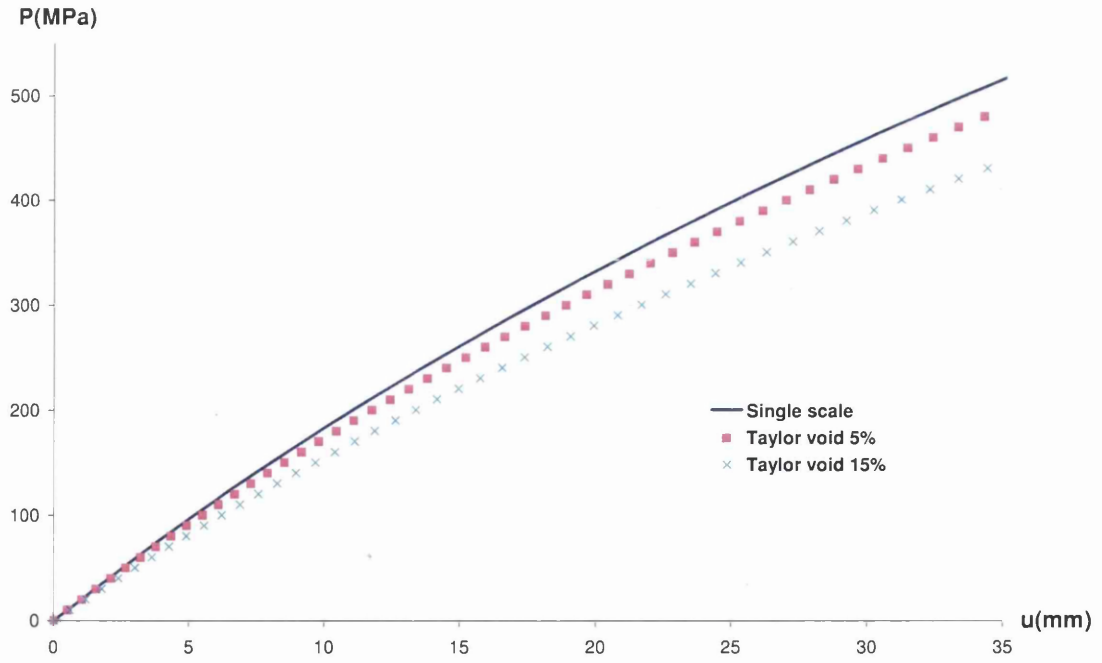

Figure 9.23: Internally pressurised hyperelastic cylinder. Pressure vs displacement diagram for the Taylor assumption

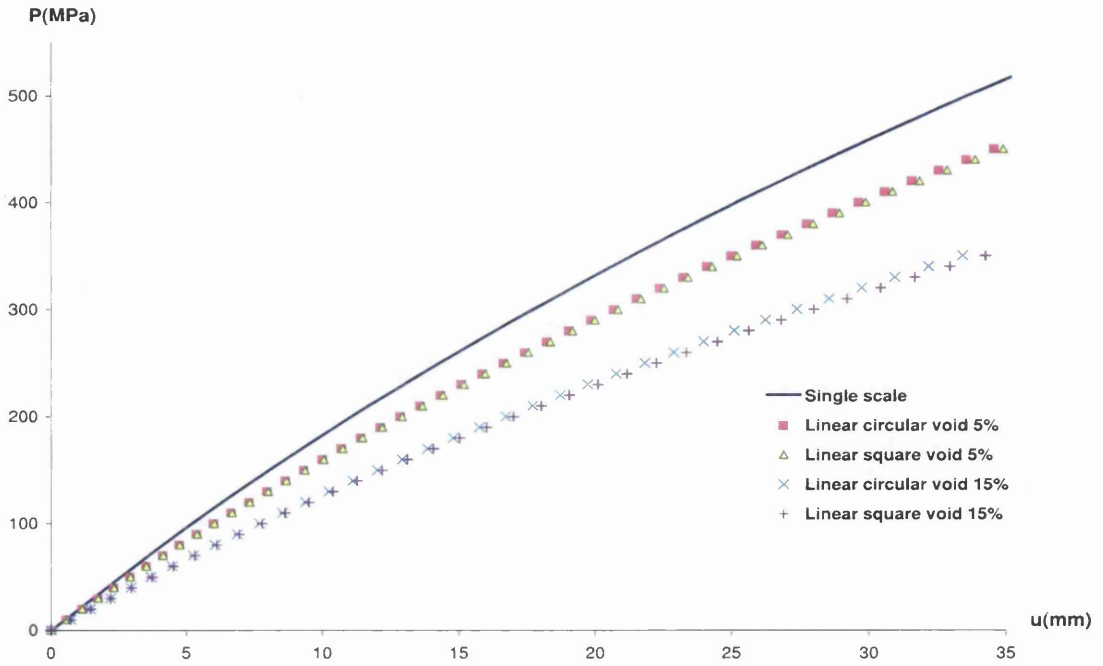

Figure 9.24: Internally pressurised hyperelastic cylinder. Pressure vs displacement diagram for the linear b.c.

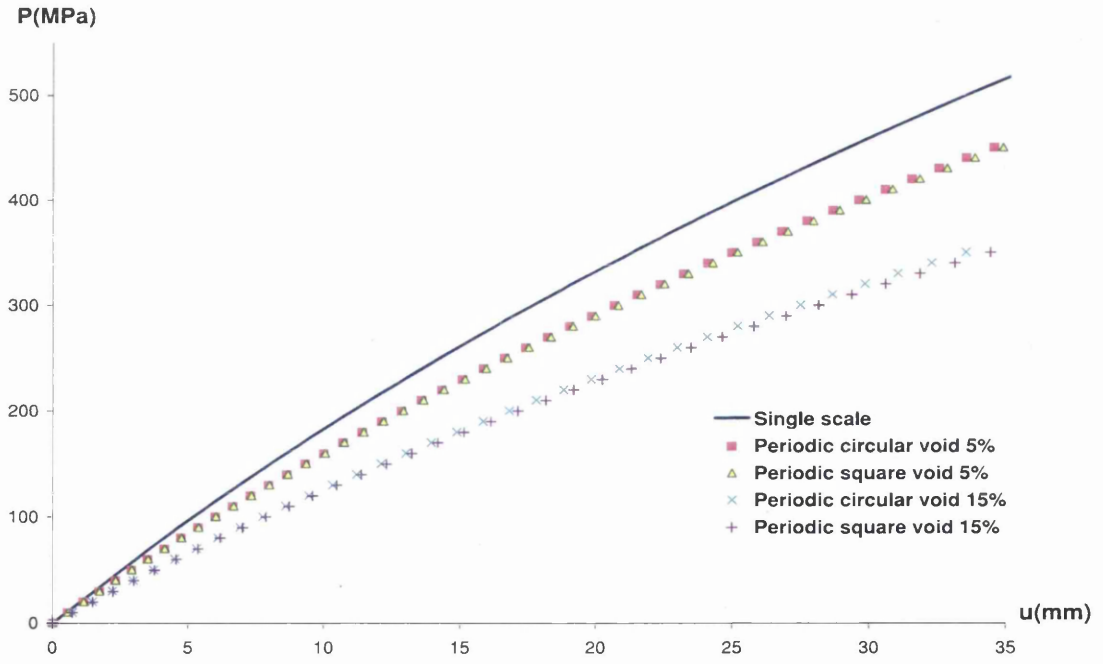

Figure 9.25: Internally pressurised hyperelastic cylinder. Pressure vs displacement diagram for the periodic b.c.

9.4.2 Mesh Evolution

In this section a mesh evolution is depicted to show how the different conditions affect the distortion during the micro-macro analysis. Macro- and micro-meshes are presented in its undeformed and deformed configurations, respectively. At every figure the deformed macro-mesh has been translated radially and the deformed micro-mesh has been translated in order to make the figures more transparent. In this way the strain experienced by both meshes can be observed clearly.

The meshes depicted in the deformed configurations all correspond to a similar outer radial displacement close to 3.5mm. For examples of 5% and 15% void fraction this deformation corresponds to an internal pressure $P = 450$MPa and $P = 350$MPa, respectively.

Figure 9.26(a) and 9.26(b) correspond to a Microstructure 1 (Circular void in the middle of the RVE with 5% volume fraction) for linear b.c. and periodic b.c., respectively. Figure 9.27(a) and 9.27(b) correspond to a Microstructure 2 (Square void in the middle of the RVE with 5% volume fraction) for linear and periodic b.c., respectively. We can observe that due to the small void there is only a small difference between Linear and Periodic b.c.

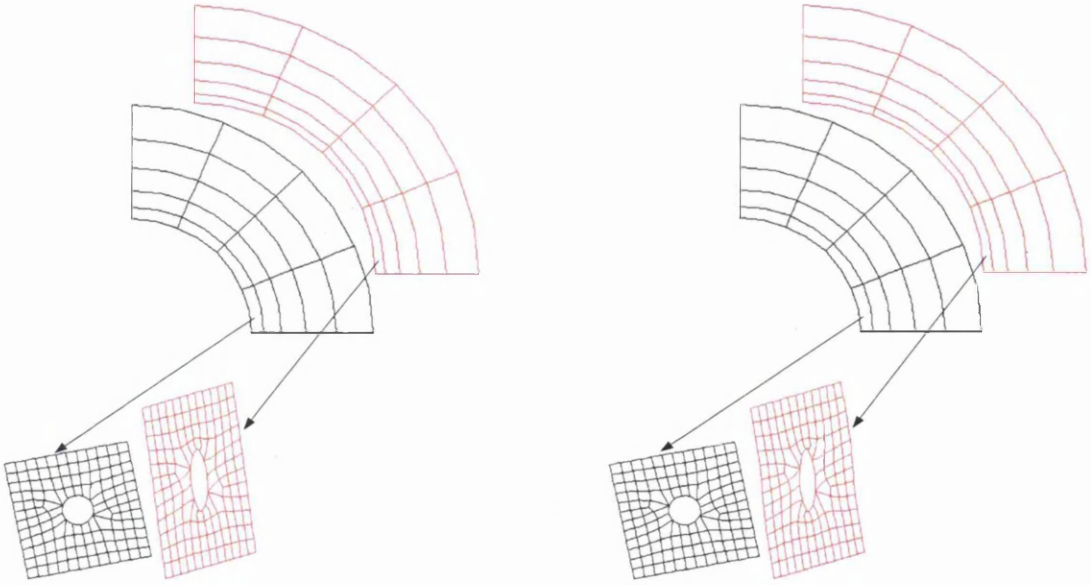

(a) Linear b.c. (b) Periodic b.c.

Figure 9.26: Mesh evolution for P=0-450MPa. Microstructure 1: circular void at 5% volume fraction

Figure 9.28(a) and 9.28(b) corresponds to a Microstructure 3 (Circular void in the middle of the RVE with 15% volume fraction) for Linear and Periodic b.c., respectively. Figure 9.29(a) and 9.29(b) correspond to a Microstructure 4 (Square void in the middle of the RVE with 15% volume fraction) for linear b.c. and periodic b.c., respectively. We can observe that due to a bigger void there is more difference between linear b.c. and periodic b.c. Moreover, the periodicity at periodic b.c. can be observed easily.

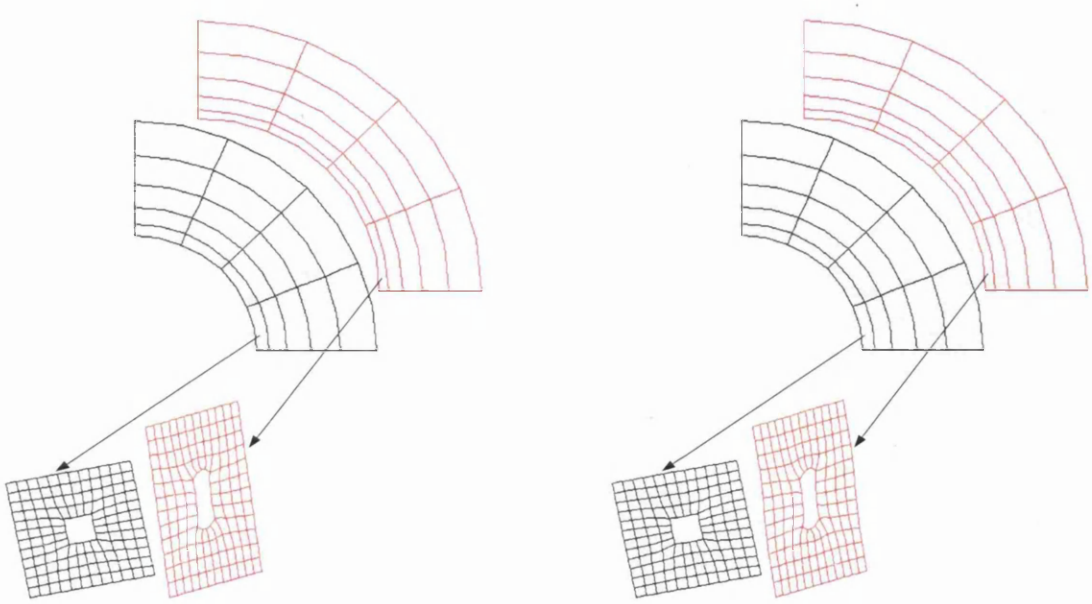

(a) Linear b.c. (b) Periodic b.c.

Figure 9.27: Mesh evolution for P=0-450MPa. Microstructure 2: square void at 5% volume fraction

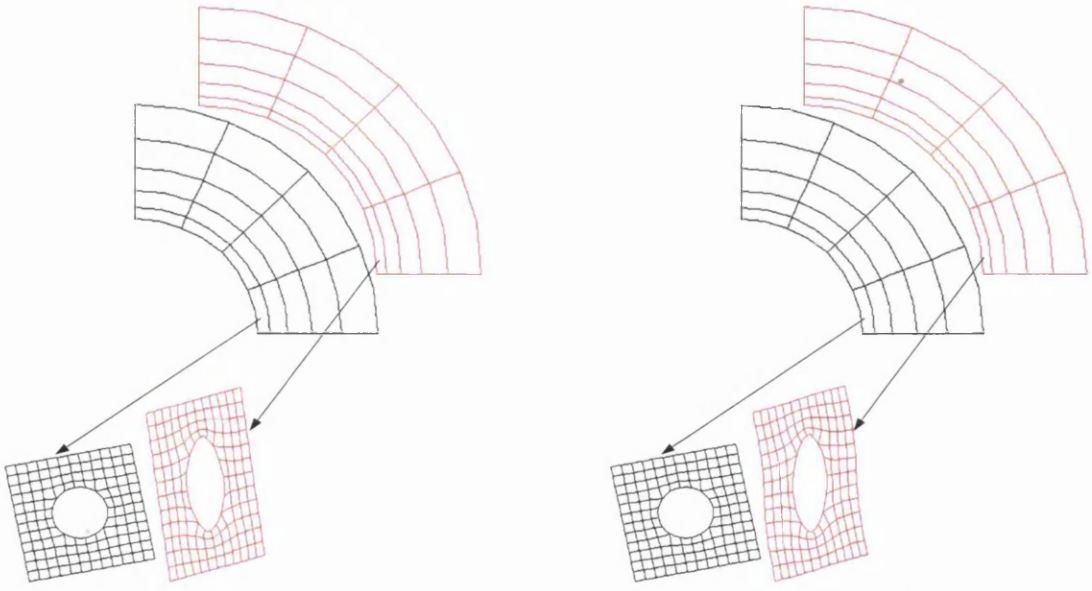

(a) Linear b.c. (b) Periodic b.c.

Figure 9.28: Mesh evolution for P=0-350MPa. Microstructure 3: circular void at 15% volume fraction

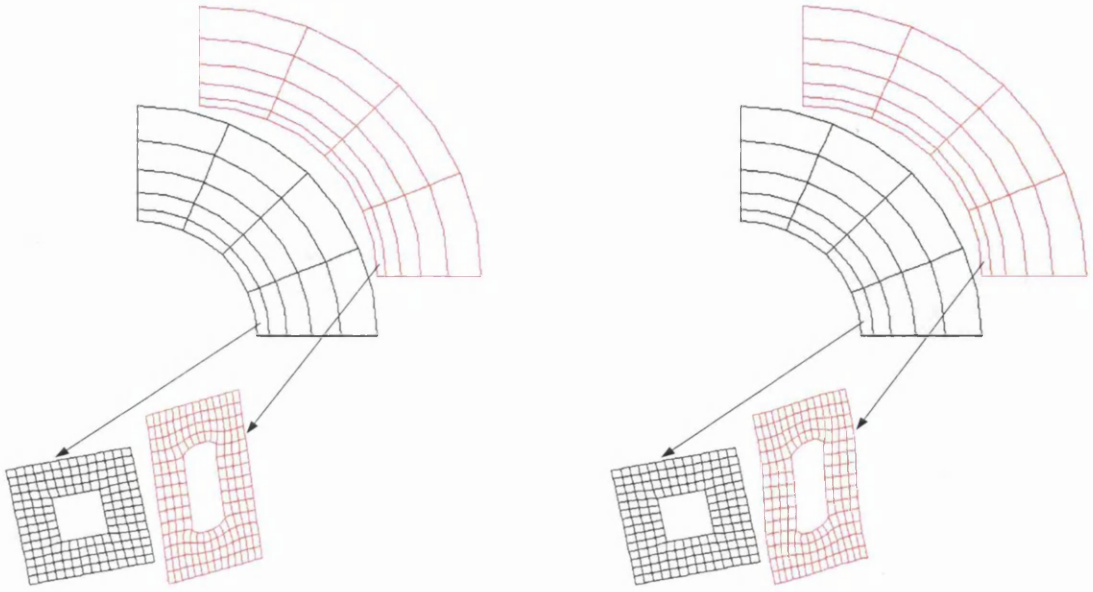

(a) Linear b.c. (b) Periodic b.c.

Figure 9.29: Mesh evolution for P=0-350MPa. Microstructure 4: square void at 15% volume fraction

9.4.3 Strain energy distribution

In this section several figures representing strain energy distributions (in KJ/mm^2) are depicted for a quarter of the cylinder with some representative microstructures. The distributions have been depicted in the deformed configuration. The undeformed mesh has also been depicted to illustrate more clearly deformation of the solid.

In Figure 9.30(a) and 9.30(b) the results for linear b.c. and periodic b.c. are represented for Microstructure 1, respectively, for internal pressure $P = 450$MPa. In Figure 9.31(a) and 9.31(b) the results for linear b.c. and periodic b.c. are represented for Microstructure 2, respectively, for internal pressure $P = 450$MPa. In Figure 9.32(a) and 9.32(b) the effect of linear b.c. and periodic b.c. is represented for Microstructure 3, respectively, for internal pressure $P = 350$MPa. In Figure 9.33(a) and 9.33(b) the effect of linear b.c. and periodic b.c. is represented for Microstructure 4, respectively, for internal pressure $P = 350$MPa. The symmetric evolution of the strain energy can be observed at macroscale level in all figures.

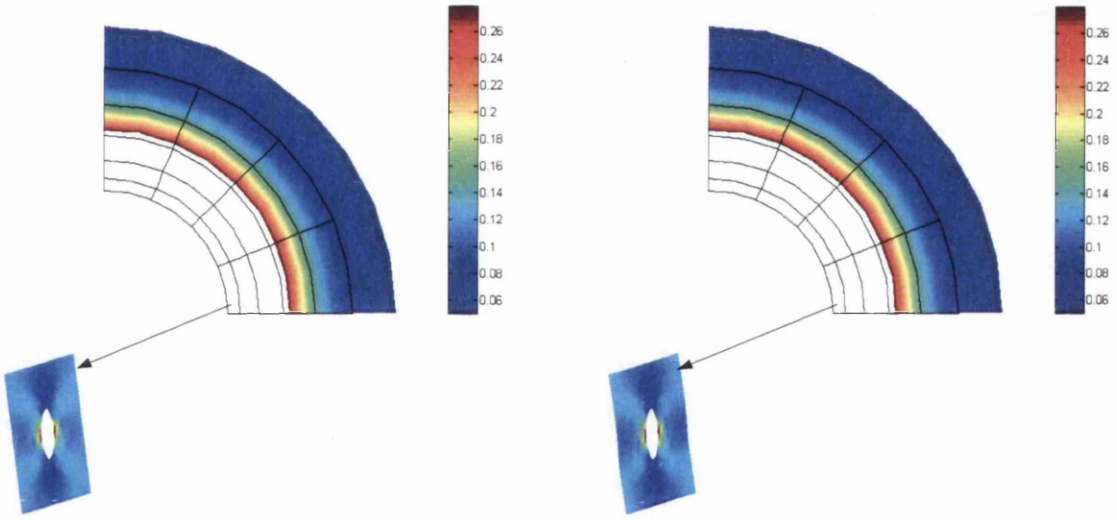

(a) Linear b.c.

(b) Periodic b.c.

Figure 9.30: Strain energy for internal pressure $P = 450$ MPa. Microstructure 1: circular void at 5% volume fraction

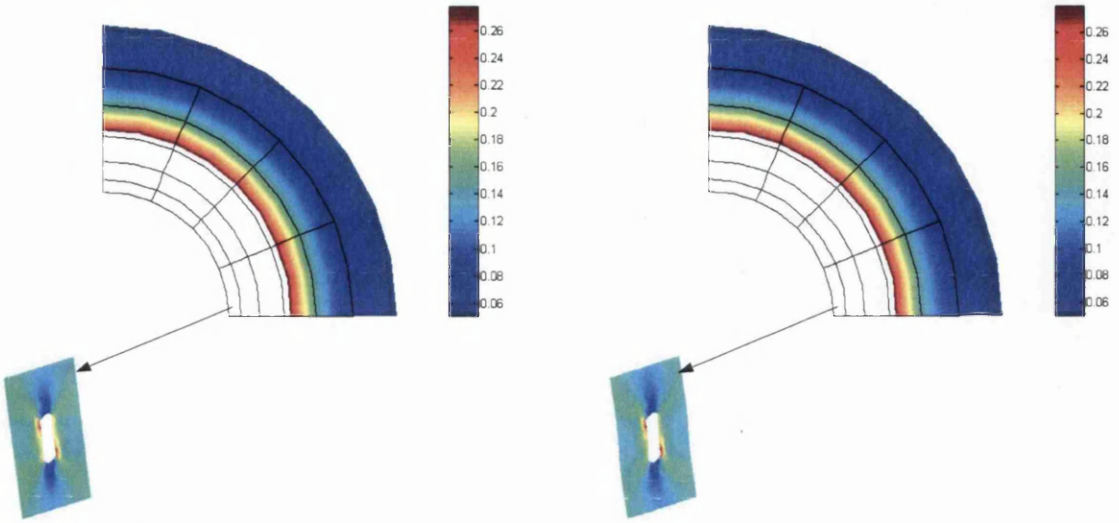

(a) Linear b.c. (b) Periodic b.c.

Figure 9.31: Strain energy for internal pressure $P = 450$ MPa. Microstructure 2: square void at 5% volume fraction

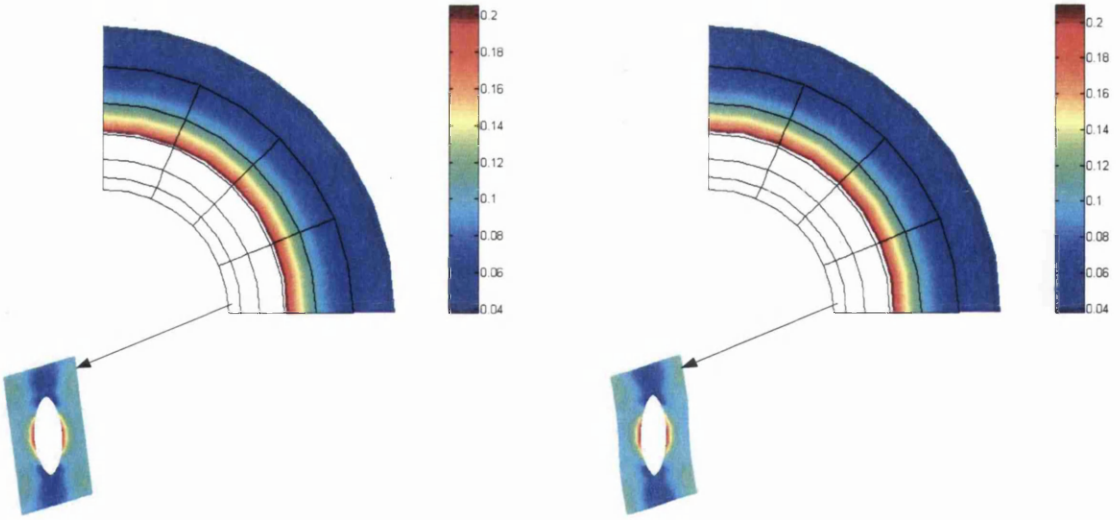

(a) Linear b.c. (b) Periodic b.c.

Figure 9.32: Strain energy for internal pressure $P = 350$ MPa. Microstructure 3: circular void at 15% volume fraction

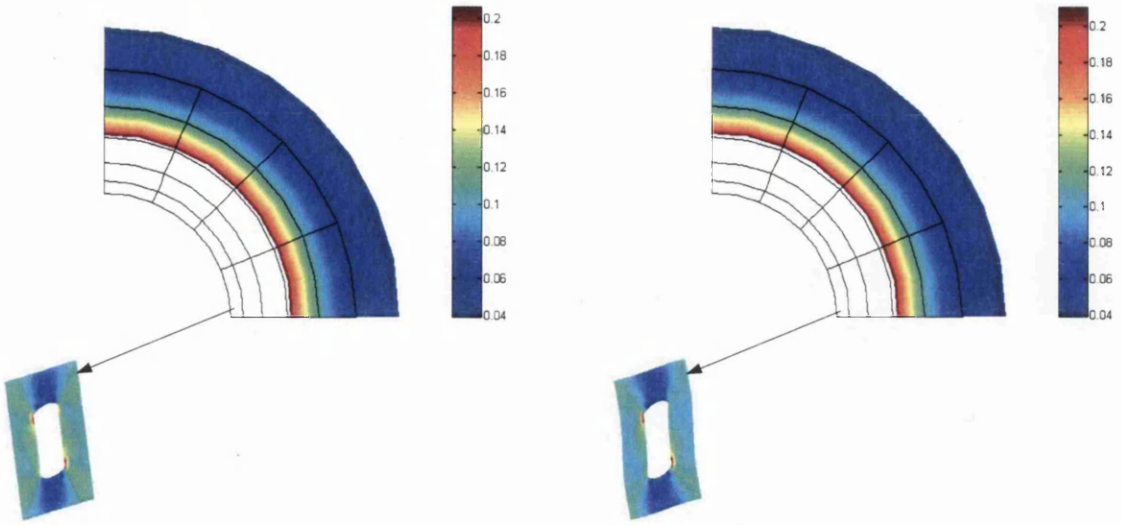

(a) Linear b.c. (b) Periodic b.c.

Figure 9.33: Strain energy for internal pressure $P = 350$ MPa. Microstructure 4: square void at 15% volume fraction

9.4.4 Residuals evolution per iteration in macro and micro levels

In this section tables with the Euclidean norm R_M of the residual are reported associated with the Newton iterations of the macro- and micro-equilibrium. The residual norm evolution is shown for the microstructure that corresponds to the macro Gauss point in the bottom right corner.

In the following tables the Euclidean norm R_M of the residual are reported associated with the Newton iterations of the macro-equilibrium. The macro-residual is normalised and calculated as $R_M = 100 \times \|\mathbf{F}_{int} - \mathbf{F}_{ext}\|/\|\mathbf{F}_{ext}\|$. The micro residual is computed in different ways depending on the constraint.

The residual for linear b.c. is evaluated as $R_\mu = 100 \times \|\mathbf{r}\|/\|\mathbf{f}^{int}\|$ where $\mathbf{r}$ was given in (8.63). The residual for periodic b.c. is evaluated as $R_\mu = 100 \times \|\mathbf{r}\|/\|\mathbf{f}^{int}\|$ where $\mathbf{r}$ was given in (8.97).

Clearly, the quadratic rate of asymptotic convergence can be observed in the macro- and micro-scales for both Linear and Periodic b.c.'s in all the tables.

micro	R_μ	Macro	R_M
1	3.054337×10^{-01}		
2	1.018779×10^{-03}		
3	2.642555×10^{-06}		
4	1.146325×10^{-08}	1	7.386827×10^{-01}
1	2.871463×10^{-01}		
2	4.395136×10^{-04}		
3	6.061724×10^{-07}		
4	1.207273×10^{-09}	2	5.075611×10^{-04}
1	2.870407×10^{-01}		
2	4.393127×10^{-04}		
3	6.059748×10^{-07}		
4	1.206522×10^{-09}	3	2.604021×10^{-07}
1	2.870407×10^{-01}		
2	4.393128×10^{-04}		
3	6.059750×10^{-07}		
4	1.206531×10^{-09}	4	1.912772×10^{-10}

a) Linear b.c.

micro	R_μ	Macro	R_M
1	3.020060×10^{-01}		
2	1.080160×10^{-03}		
3	2.773971×10^{-06}		
4	1.369076×10^{-08}	1	7.484814×10^{-01}
1	2.888288×10^{-01}		
2	4.713476×10^{-04}		
3	6.908600×10^{-07}		
4	1.495429×10^{-09}	2	5.070460×10^{-04}
1	2.887258×10^{-01}		
2	4.711845×10^{-04}		
3	6.907774×10^{-07}		
4	1.495436×10^{-09}	3	2.450213×10^{-07}
1	2.887258×10^{-01}		
2	4.711846×10^{-04}		
3	6.907774×10^{-07}		
4	1.495265×10^{-09}	4	1.739404×10^{-10}

b) Periodic b.c.

Table 9.3: Evolution of Residual norm at micro (R_μ) and Macroscale (R_M) for Linear b.c. and Periodicb.c. assuming Microstructure 2 (5% square void). Increment of internal pressure P = 200-201 MPa.

We have shown the convergence for Microstructure 2 only. Other microstructures show similar convergence properties, so they are not shown here.

9.5 Conclusions

In this chapter, a variety of examples in 2D have been given. They start with a linear small strain analysis, followed by a plastic small strain analysis and finally a hyperelastic finite deformation analysis. In the microstructure RVE the formation of shear bands has been observed. Also, we can say that the macroscale behaves symmetrically in terms of development of effective plastic strain for elasto-plastic material and strain energy for hyperelastic.

The success of the Newton-Raphson procedure to solve the micro and macro equilibrium problems can be observed. We can say that, for elastic behaviour, we can reach convergence with the same increment load for linear b.c. and periodic b.c., despite every iteration takes longer for periodic b.c. However, the load increment necessary to reach convergence can be five times larger in linear b.c. than periodic b.c., during plastic yielding.

Chapter 10

Conclusions and future work

Several approaches are available in order to describe material behaviour. Considering material on the higher (macro) level of observation constitutes the macroscopic approach. However, the key to understand a macro material behaviour lies in its microstructure. As such the microscopic approach can be used which is based on the detailed material description of the lower (micro) observational level. The main focus of this work was the combination of the two approaches called *multiscale* approach. The idea was, by means of a hierarchical multiscale procedure, to bring the homogenized information of the detailed microstructural description to the macro-level in the form of effective properties. Thus, the homogeneous macrostructural behaviour is driven by the heterogeneous microstructure.

This work has presented a general formulation of small and large strain multiscale solid constitutive models based on the volume averaging of the microscopic strain (deformation) and stress fields over a locally attached microstructure RVE. The formulation presented has provided a clearly structured framework within each class of models that is completely defined by a specific choice of kinematical constraints. Three well-known classes of multiscale models, presented in this work, have been cast within this framework: a) The Taylor, or homogeneous microscopic strain (deformation) model; b) the linear boundary displacement model; and finally c) the periodic boundary displacement model.

A Finite Elements formulation for multiscale has been presented. The strain (deformation) was imposed over the RVE as average. We have presented a procedure to compute micro-stress update in RVE. In addition, a macro homogenised constitutive operator have been presented. The operator was computed as a relation between variation of macro-stress with respect to the variation of macro-deformation. The formulation has been developed, for the three constraints.

It is worthy to highlight the success for the computation for linear and periodic b.c. in both (micro-stress update procedure and overall tangent operators). In small strain has been presented this new formulation and then extended to the large strain framework.

Numerical tests have been performed for a material with voids. The quadratic rate of asymptotic convergence, obtained by a Newton-Raphson solution method procedure for the macroscopic and microscopic incremental BVP, has confirmed the success of the microstress update procedure and overall tangent modulus computation and efficient solution of the discrete problem.

The future work will be focussed in include new material models to microstructural behaviour. Moreover, this work will be extended to the second order approach (see [90]). Other issue to take into consideration is the way how we have applied the constraints over the RVE. We have applied the constraints by direct imposition of them over RVE. Applying the constraints in another way could improve the convergence in some cases.

Bibliography

[1] Christman T. Needleman A. and Suresh S. An experimental and numerical study of deformation in metal-ceramic material. *Acta Metallurgica*, 37(11):3029–3050, 1989.

[2] Ibrahimbegović A. and Markovič D. Strong coupling methods in multi-phase and multi-scale modelling of inelastic behaviour of heterogeneous structures. *Computer Methods in Applied Mechanics and Engineering*, 192:3089–3107, 2003.

[3] Taliercio A. Generalized plane strain finite element model for the analysis of elasto-plastic composites. *International Journal of Solids and Structures*, 42:2361–2379, 2005.

[4] Taliercio A. Predicting the macroscopic behaviour of metal-matrix composites embeding an interphase. *In preceedings of the 8^{th} CST2006 Conference, Las Palmas de Gran Canaria Spain*, (269), 2006.

[5] Taliercio A. and Coruzzi R. Mechanical behaviour of brittle matrix composite: a homogenization approach. *International Journal of Solids and Structures*, 36:3591–3615, 1999.

[6] Toledano A. and Murakami H. A high-order mixture model for periodic particulate composites. *International Journal of Solids and Structures*, 23:989–1002, 1987.

[7] Gusev A.A. Representative volume element size for elastic composites: a numerical study. *Journal of Mechaics and Physics of Solids*, 45(9):1149–1459, 1997.

[8] Green A.E. and Zerna W. *Theoretical elasticity.* Oxford University Press, 1954.

[9] Mercatoris B. and Massart T.J. Flexural response of heterogeneous structures using computational homogenization. *In preceedings of the 8^{th} CST2006 Conference, Las Palmas de Gran Canaria Spain*, (287), 2006.

[10] González C. and Llorca J. A self-consistent approach to the elasto-plastic behaviour of two-phase materials including damage. *Journal of the Mechanics and Physics of Solids*, 48:675–692, 2000.

[11] Miehe C. Strain-driven homogenization of inelastic microstructures and composites based on an incremental variational formulation. *International Journal for Numerical Methods in Engineering*, 55:1285–1322, 2002.

[12] Miehe C. Computational micro-to-macro transitions for discretized microstructures of heterogeneous materials at finite strains based on the minimization of averaged incremental energy. *Computer Methods in Applied Mechanics and Engineering*, 192:559–591, 2003.

[13] Miehe C. and Koch A. Computational micro-to-macro transitions of discretized microstructures undergoing small strains. *Archive of Applied Mechanics*, 72:300–317, 2002.

[14] Miehe C. and Dettmar J. A framework for micro-macro transitions in periodic particle aggregates of granular materials. *Computer Methods in Applied Mechanics and Engineering*, 193:225–256, 2004.

[15] Swan C.C. Techniques for stress- and strain-controlled homogenization of inelastic periodic composites. *Computer Methods in Applied Mechanics and Engineering*, 117:249–267, 1994.

[16] Swan C.C. and Cakmak A.S. Homogenization and elastoplasticity models for periodic composites. *Communication in Numerical Methods and Engineering*, 10:257–265, 1994.

[17] Swan C.C. and Kosaka I. Homogenization-based analysis and design of composites. *Computer and Structures*, 64:603–621, 1997.

[18] Nan C.W. and Clarke D.R. The influence of particle size and particle fracture o the elastic/plastic deformation of metal matrix composite. *Acta Materialia*, 44(9):3801–3811, 1996.

[19] de Souza Neto E.A. and Feijóo R.A. Variational foundations multi-scale constitutive models of solids: Small and large strain kinematical formulation. Internal Research & Development Report No. 16/2006, Laboratório Nacional de Computação Científica (LNCC/MCT) Brazil, 2006.

[20] Carneiro Molina A.J. de Souza Neto E.A. and Perić D. Homogeneized tangent moduli for heterogeneous materials. *In preceedings of the* 13^{th} *Association for Computational Mechanics in UK (ACME) Conference, Sheffield U.K.*, 2005.

[21] Carneiro Molina A.J. de Souza Neto E.A. and Perić D. Homogeneized tangent moduli for heterogeneous materials. Internal Research & Development Report No. 13/2005, Laboratório Nacional de Computação Científica (LNCC/MCT) Brazil, May 2005.

[22] de Souza Neto E.A. Perić D. and Owen D.R.J. Computational plasticity: Small and large strain finite element analisys of elastic and inelastic solids. to be published.

[23] Kouznetsova V.G. Brekelmans W.A.M. de Vree J.H.P. and Baaijens F.P.T. A multilevel finite strain analysis for forming. *In preceedings of the ECCM 99 Conference, Munchen, Germany*, 1999.

[24] Owen D.R.J. and Hinton E. *Finite Elements in plasticity: theory and practice.* Pineridge Press. Swansea (UK), 1980.

[25] Hinton E. and Owen D.R.J. *An Introduction to Finite Element Computations.* Pineridge Press, 1979.

[26] Sanchez-Palencia E. *Non-homogeneous media and vibration theory. Lecture notes in physics.* Number 127. Springer-Verlag, Berlin, 1980.

[27] Feyel F. Multiscale fe^2 elastoviscoplastic analysis of composite structures. *Computational Materials Science*, 16:344–354, 1999.

[28] Paris F. *Teoria de la Elasticidad.* Dto. Mecanica de los Medios Continuos ETSII Sevilla, 1996.

[29] Geers M.G.D. Kouznetsova V. G. and Brekelmans W. A. M. Gradient-enhanced computational homogenization for the micro-macro scale transition. *Journal de Physique IV*, 11:145–152, 2001.

[30] Mejak G. Solution of an elastoplastic problem with imperfect bonding using a two scale finite element method. *In preceedings of the* 8^{th} *CST2006 Conference, Las Palmas de Gran Canaria Spain*, (265), 2006.

[31] Taylor G.I. Plastic strain in metals. *Journal of the Institute of Metals*, 62:307–324, 1938.

[32] Zohdi T.I. Oden J.T. Rodin G.J. Hierarchical modelling of heterogeneous bodies. *Computer Methods in Applied Mechanics and Engineering*, 138:273–298, 1996.

[33] Aktaa J. Kiewel H. and Turki J. Modelling of the influence of damage on the deformation behaviour by a self-consistent embedded cell model. *Computational Materials Science*, 12:64–72, 1998.

[34] Gitman I.M. Askes H. and Aifantis E.C. The representative volume size in static and dynamic micro-macro transitions. *Internationa Journal of Fracture*, 135:3–9, 2005.

[35] Gitman I.M. Askes H. and Aifantis E.C. Gradient elasticity with internal length and internal inertia based on the homogenizaton of a representative volume element. *Journal of the Mechanical Behavior of Materials. in Press*, 2006.

[36] Michel J.C. Moulinec H. and Suquet P. Effective properties of composite materials with periodic microstructure: a computational approach. *Computer Methods in Applied Mechanics and Engineering*, 172:109–143, 1999.

[37] Moulinec H. and Suquet P. A numerical method for computing the overall response of nonlinear composites with complex microstrucutres. *Computer Methods in Applied Mechanics and Engineering*, 157:69–94, 1998.

[38] Dye D. Stone H.J. and Reed R.C. A two phase elastic-plastic self-consistent model for the accumulation of the microstrains in waspaloy. *Acta Materialia*, 49:1271–1283, 2001.

[39] Gitman I.M. *Representative Volumes and Multi-scale Modelling of Quasi-brittle Materials.* PhD thesis, Technische Universiteit Delft, 2006.

[40] Bonet J. and Wood R.D. *Nonlinear continuum mechanics for finite element analysis.* Cambridge University Press, 1997.

[41] Lubliner J. *Plasticity theory.* New York: Macmillan, 1990.

[42] Miehe C. Schotte J. and Schroder J. Computational micro-macro transitions and overall tangent moduli in the analysis of polycrystals at large strains. *Computational Material Science*, 16:372–382, 1999.

[43] Miehe C. Schroder J. and Schotte J. Computational homogenization analysis in finite plasticity. simulation of texture development in polycrystalline materials. *Computer Methods in Applied Mechanics and Engineering*, 171:387–418, 1999.

[44] Miehe C. Schroder J. and Becker M. Computational homogenization analysis in finite elasticity: material and structural instabilities on the micro- and macro scales of periodic composites and their interaction. *Computer Methods in Applied Mechanics and Engineering*, 191:4971–5005, 2002.

[45] Yeon J-H. and Youn S-K. Meshfree analysis of softening elastoplastic solids using variational multiscale method. *International journal of Solid and Structures*, 42:4030–4057, 2005.

[46] Simo J.C. and Taylor R.L. Consistent tangent operator for rate independent elastoplaticity. *Computer Methods in Applied Mechanics and Engineering*, 48:101–118, 1985.

[47] Simo J.C. and Hughes T.J.R. *Computational Inelasticity.* New York: Springer-Verlag, 1998.

[48] Eshelby J.D. The determination of the field of an ellipsoidal inclusion and related problems. *Proceeding of the Royal Society of London*, 241:376–396, 1957.

[49] Bensoussan A. Lions J.L. and Papanicolaou G. *Asymptotic analysis for periodic strucutres, in: Studies in Mathematics and its Applications.* North Holland Publishing Company, 1978.

[50] Guedes J.M. and Kikuchi N. Preprocessing and postprocesing for materials based on the homogenization method with adaptative finite element methods. *Computer Methods in Applied Mechanics and Engineering*, 83:143–198, 1990.

[51] Ghosh S. Lee K. and Moorthy S. Multiple scale analisys of heterogeneous elastic structures using homogenization theory and voroni cell finite element method. *International Journal of Solids and Structures*, 32(1):27–62, 1995.

[52] Ghosh S. Lee K. and Moorthy S. Two scale analisys of heterogeneous elastic-plastic materials with asymptotic homogenization and voroni cell finite element method. *Computer Methods in Applied Mechanics and Engineering*, 132:63–116, 1996.

[53] Lee K. and Ghosh S. A microstructure based numrical method for constitutive modelling of composite and porous materials. *Materials Science and Engineering A*, 272:120–133, 1999.

[54] Matsui K. Terada K. and Yuge K. Two-scale finite element analysis of heterogeneous solids with periodic microstructures. *Computers and Structures*, 82:593–606, 2004.

[55] Terada K. and Kikuchi N. *Computational Methods in Micromechanics*, volume 212, chapter Nonlinear homogenization method for practical application, pages 1–16. ASME, 1995.

[56] Terada K. and Kikuchi N. Simulation of the multiscale convergence in computational homogenization approaches. *International Journal of Solids and Structures*, 37:2285–2311, 2000.

[57] Terada K. Siki I. Matsui K. and Yamakawa Y. Two-scale kinematics and linearization for simultaneous two-scale analysis of periodic heterogeneous solids at finite strain. *Computer Methods in Applied Mechanics and Engineering*, 192:3531–3563, 2003.

[58] Bathe K.J. *Finite Element Procedures.* Prentice-Hall. Englewood Cliffs (NJ), 1996.

[59] Chung P.W. Tamma K.K. and Nambutu R.R. Asymptotic expansion homogenization for heterogeneous media: computational issues and applications. *Composites. Part A: applied science and manufacturing*, 32:1291–1301, 2001.

[60] Malvern L.E. *Introduction to the mechanics of a continuous medium.* Prentice-Hall, 1969.

[61] Braccini M. and Wilkinson D.S. A self-consistent approach to modeling strain gradient plasticity. *Scripta Materialia*, 49:53–57, 2003.

[62] Fish J. Shek K. Pandheeradi M. and Shephard M.S. Computational plasticity for composite structures based on mathematical homogenization: Theory and practice. *Computer Methods in Applied Mechanics and Engineering*, 148:53–73, 1997.

[63] Partovi M. *Computational strategies for multiscale analysis of material behaviour.* PhD thesis, University of Wales Swansea, UK, 2007.

[64] Gitman I.M. Gitman M.B. and Askes H. Quantification of the stochastically stable representative volumes for random heterogeneous materials. *Archive of Applied Mechanics*, 75:79–92, 2005.

[65] Gurtin M.E. *An intorduction to continuum mechanics.* Academic Press, 1965.

[66] Kouznetsova V.G. Geers M.G.D. and Brekelmans W.A.M. Multiscale second-order computational homogenization of multi-phase materials: a nested finite element solution strategy. *Computer Methods in Applied Mechanics and Engineering*, 193:5525–5550, 2004.

[67] Kouznetsova V.G. Geers M.G.D. and Brekelmans W.A.M. Size of a representative volume element in a second-order computational homogenization framework. *International Journal for Multiscale Computational Engineering*, 2(4):575–598, 2004.

[68] Oñate E. *Cálculo de Estructuras por el Método de los Elementos Finitos. Análisis estático lineal.* Centro Internacional de Métodos Numéricos en Ingeniería, 1995.

[69] Oñate E. Multiscale computational analysis in mechanics using finite calculus: an introduction. *Computer Methods in Applied Mechanics and Engineering*, 192:3043–3059, 2003.

[70] Ponte Castaneda P. and Suquet P. Nonlinear composites. *Advances in Applied Mechanics*, 34:171–302, 1998.

[71] Suquet P.M. *Local and global aspects in the mathematical theory of plasticity*, pages 279–310. In Sawczuk A. and Bianchi G. editors, Plasticity today: modelling, methods and applications. London. Elsevier Applied Science Publishers, 1985.

[72] Hill R. *The mathematical theory of plasticity.* London: Oxford University Press, 1950.

[73] Hill R. A self-consistent mechanics of composite materials. *Journal of the Mechanics and Physics of Solids*, 13:213–222, 1965.

[74] Hill R. On constitutive macro-variables for heterogeneous solids at finite strain. *Proceeding of the Royal Society of London*, 326:131–147, 1972.

[75] Brockenbrough J.R. Suresh S. and Wienecke H.A. Deformation of metal-matrix composites with continous fibers: geometrical effect of fiber distribution and shape. *Acta Metallurgica et Materialia*, 39(5):735–752, 1991.

[76] Moorthy S. and Ghosh S. A model for analysis of arbitrary composite and porous microstructures with voroni cell finite elements. *International Journal for Numerical Methods in Engineering*, 39:2363–2398, 1996.

[77] Nemat-Nasser S. and Hori M. *Micromechanics: overall properties of heterogeneous materials.* Elsevier, 1999.

[78] Torquato S. *Random Heterogeneous Materials. Microestructure and Macroscopic Properties.* 2002.

[79] Mori T. and Tanaka K. Average stress in the matrix and average elastic energy of materials with misfitting inclusions. *Acta Metallurgica*, 21:571–574, 1973.

[80] Nakamura T. and Suresh S. Effect of thermal stress and fiber packing on deformation of metal-matrix composite. *Acta Metallurgica et Materialia*, 41(6):1665–1681, 1993.

[81] Zohdi T.I. and Wriggers P. Aspects of the computational testing of the mechanical properties of microheterogeneous material samples. *International Journal for Numerical Methods in Engineering*, 50:2573–2599, 2001.

[82] Chandrupatla T.R. and Belegundu A.D. *Introduction to finite elements in engineering.* Prentice Hall, 1991.

[83] Bosso D. Pellegrino C. Galvanetto U. and Schrefler B.A. Macroscopic damage in periodic composite materials. *Communication in Numerical Methods in Engineering*, 16:615–623, 2000.

[84] Pellegrino C. Galvanetto U. and Schrefler B. A. Numerical homogenization of periodic composite materials with non-linear material components. *International Journal for Numerical Methods in Engineering*, 46:1606–1637, 1999.

[85] Carvelli V. and Taliercio A. A micromechanical model for the analysis of unidirectional elastoplastic composites subjected to 3d stresses. *Mechanics Research Communications*, 26(5):547–553, 1999.

[86] Carvelli V. and Pogi C. An homogenization procedure for the numerical analysis of woven fabric composites. *Composites. Part A: applied science and manufacturing*, 32:1425–1432, 2001.

[87] van der Sluis O. Schreurs P.J.G. and Meijer H.E.H. Effective properties of viscosplastic constitutive model obtained by homogenization. *Mechanics of Materials*, 31:743–759, 1999.

[88] van Rens B.J.E. Brekelmans W.A.M. and Baaijens F.P.T. Homogenization of the elastoplastic behavior of perforated plates. *Computer and Structures*, 69:537–545, 1999.

[89] Geers M.G.D. Kouznetsova V.G. and Brekelmans W.A.M. Multiscale first-order and second-order computational homogenization of microstructures towards continua. *International Journal for Multiscale Computational Engineering*, 1(4):371–386, 2003.

[90] Kouznetsova V.G. *Computational homogenization for multiscale analysis of multiphase materials.* PhD thesis, Netherlands Institute for Metals Research (NIMR), 2002.

[91] von Mises R. Mechanik der festen körper im plastische-deformablem zustand. *Nachr. d. gesellsch d. wissench. zu göttingen, math.-phys. klasse.*, 1913.

[92] Kouznetsova V.G. Brekelmans W.A.M. and Baaijens F.P.T. An approach to micro-macro modelling of heterogeneous materials. *Computational Mechanics*, 27:37–48, 2001.

[93] Kouznetsova V.G. Geers M.G.D. Brekelmans W.A.M. Multiscale constitutive modelling of heterogeneous materials with gradient-enhanced computational homogenization scheme. *International Journal for Numerical Methods in Engineering*, 54:1235–1260, 2002.

[94] Smit R.J.M. Brekelmans W.A.M. and Meijer H.E.H. Prediction of the mechanichal behaviour of nonlinear heterogeneous systems by multi-level finite element modeling. *Computer Methods in Applied Mechanics and Engineering*, 155:181–192, 1998.

[95] Smit R.J.M. Brekelmans W.A.M. and Meijer H.E.H. Prediction of the large strain mechanichal response of heterogeneous polymer systems: local and global deformation behaviour of a representative volume elament of voided polycarbonate. *Journal of the Mechanics and Physics of Solids*, 47:201–221, 1999.

[96] Belytschko T. Liu W.K. and Moran B. *Nonlinear Finite Element for Continua and Structures.* Wiley, 2000.

[97] Ohno N. Wu X. and Matsuda T. Homogenized properties of elastic-viscoplastic composites with periodic internal structures. *International Journal of Mechanical Science*, 42:1519–1536, 2000.

[98] Fung Y.C. *Foundations of solid mechanics.* Prentice Hall, 1965.

[99] Hashin Z. The elastic moduli of heterogeneous materials. *Journal of Applied Mechanics*, 29:143–150, 1962.

[100] Hashin Z. Analysis of composite materials. a survey. *Journal of Applied Mechanics*, 50:441–505, 1983.

Appendix A

Average Cauchy and Kirchhoff stress tensors

A.1 Average Cauchy stress tensor

The average Cauchy stress tensor can be computed from the traction forces on the boundary of RVE. We show that as follows

$$\overline{\boldsymbol{\sigma}} \equiv \frac{1}{|\mathbb{V}|}\int_{\mathbb{V}} \boldsymbol{\sigma}_\mu \, \mathrm{d}V$$

We can take into consideration microequilibrium $\nabla \cdot \boldsymbol{\sigma}_\mu + \rho\,\mathbf{b} = \mathbf{0}$, the symmetry of $\boldsymbol{\sigma}_\mu$ and the following identity $\boldsymbol{\sigma}_\mu \cdot \mathbf{I} = \boldsymbol{\sigma}_\mu$ to rewrite the expression as follows

$$\overline{\boldsymbol{\sigma}} = \frac{1}{|\mathbb{V}|}\int_{\mathbb{V}} \mathrm{sym}[(\nabla \cdot \boldsymbol{\sigma}_\mu + \rho\,\mathbf{b}) \otimes \boldsymbol{y} + \boldsymbol{\sigma}_\mu \cdot \mathbf{I}] \, \mathrm{d}V$$

where we can split the left hand side term as,

$$\overline{\boldsymbol{\sigma}} = \frac{1}{|\mathbb{V}|}\int_{\mathbb{V}} \mathrm{sym}[\nabla \cdot \boldsymbol{\sigma}_\mu \otimes \boldsymbol{y} + \rho\,\mathbf{b} \otimes \boldsymbol{y} + \boldsymbol{\sigma}_\mu \cdot \mathbf{I}] \, \mathrm{d}V$$

and then rearrange as

$$\overline{\boldsymbol{\sigma}} = \frac{1}{|\mathbb{V}|}\int_{\mathbb{V}} \mathrm{sym}[\nabla \cdot \boldsymbol{\sigma}_\mu \otimes \boldsymbol{y} + \boldsymbol{\sigma}_\mu \cdot \mathbf{I}] \, \mathrm{d}V + \frac{1}{|\mathbb{V}|}\int_{\mathbb{V}} \mathrm{sym}[\rho\,\mathbf{b} \otimes \boldsymbol{y}] \, \mathrm{d}V$$

Introducing the formula $\nabla \cdot \boldsymbol{\sigma}_\mu \otimes \boldsymbol{y} + \boldsymbol{\sigma}_\mu \cdot \mathbf{I} = \nabla \cdot (\boldsymbol{\sigma}_\mu \otimes \boldsymbol{y})$, we have the following

$$\overline{\boldsymbol{\sigma}} = \frac{1}{|\mathbb{V}|}\int_{\mathbb{V}} \mathrm{sym}[\nabla \cdot (\boldsymbol{\sigma}_\mu \otimes \boldsymbol{y})]\, \mathrm{d}V + \frac{1}{|\mathbb{V}|}\int_{\mathbb{V}} \rho\, \mathrm{sym}[\mathbf{b} \otimes \boldsymbol{y}]\, \mathrm{d}V$$

Finally, applying Gauss theorem, we obtain the following form of the average Cauchy stress over RVE

$$\overline{\boldsymbol{\sigma}} = \frac{1}{|\mathbb{V}|}\int_{\partial\mathbb{V}} \mathrm{sym}[\mathbf{n} \cdot (\boldsymbol{\sigma}_\mu \otimes \boldsymbol{y})]\, \mathrm{d}A + \frac{1}{|\mathbb{V}|}\int_{\mathbb{V}} \rho\, \mathrm{sym}[\mathbf{b} \otimes \boldsymbol{y}]\, \mathrm{d}V$$

where we can substitute $\mathbf{t} = \mathbf{n} \cdot \boldsymbol{\sigma}_\mu$ to have the final form

$$\overline{\boldsymbol{\sigma}} = \frac{1}{|\mathbb{V}|}\int_{\partial\mathbb{V}} \mathrm{sym}[\mathbf{t} \otimes \boldsymbol{y}]\, \mathrm{d}A + \frac{1}{|\mathbb{V}|}\int_{\mathbb{V}} \rho\, \mathrm{sym}[\mathbf{b} \otimes \boldsymbol{y}]\, \mathrm{d}V$$

A.2 Average Kirchhoff stress tensor

The average Kirchhoff stress tensor over the RVE can be computed as follows

$$\overline{\boldsymbol{\tau}} \equiv \frac{1}{|\mathbb{V}_0|}\int_{\mathbb{V}_0} \boldsymbol{\tau}_\mu\, \mathrm{d}V_0$$

where we can use substitute $\boldsymbol{\tau}_\mu = J_\mu\, \boldsymbol{\sigma}_\mu$ to obtain

$$\overline{\boldsymbol{\tau}} = \frac{1}{|\mathbb{V}_0|}\int_{\mathbb{V}_0} J_\mu\, \boldsymbol{\sigma}_\mu\, \mathrm{d}V_0$$

and then using the property (2.13), it can be rewritten as

$$\overline{\boldsymbol{\tau}} = \frac{1}{|\mathbb{V}_0|}\int_{\mathbb{V}} \boldsymbol{\sigma}_\mu\, \mathrm{d}V$$

where we can say that the average Kirchhoff stress can be computed from the average Cauchy stress directly as

$$\overline{\boldsymbol{\tau}} = \frac{|\mathbb{V}|}{|\mathbb{V}_0|}\,\overline{\boldsymbol{\sigma}} = J_{\mathrm{M}}\overline{\boldsymbol{\sigma}}$$

where J_{M} is the macro determinant of the Jacobian ($J_{\mathrm{M}} = \det(\overline{\mathbf{F}})$)

Appendix B

Average small strain and deformation gradient tensors

B.1 Average small strain tensor

The average small strain tensor over RVE can be computed as follows

$$\overline{\boldsymbol{\epsilon}} \equiv \frac{1}{|\mathbb{V}|}\int_{\mathbb{V}} \boldsymbol{\epsilon}_\mu \, \mathrm{d}V = \frac{1}{|\mathbb{V}|}\int_{\mathbb{V}} \mathrm{sym}[\nabla \mathbf{u}] \, \mathrm{d}V$$

where the use of the definition of $\boldsymbol{\epsilon}_\mu = \mathrm{sym}[\nabla \mathbf{u}]$ has been used. Then applying Green's Lemma we obtain the following

$$\overline{\boldsymbol{\epsilon}} = \frac{1}{|\mathbb{V}|}\int_{\partial\mathbb{V}} \mathrm{sym}[\mathbf{u} \otimes \mathbf{n}] \, \mathrm{d}A$$

B.2 Average deformation gradient tensor

The average deformation gradient tensor over RVE can be computed as follows

$$\overline{\mathbf{F}} \equiv \frac{1}{|\mathbb{V}_0|}\int_{\mathbb{V}_0} \mathbf{F}_\mu \, \mathrm{d}V_0 = \frac{1}{|\mathbb{V}_0|}\int_{\mathbb{V}_0} \nabla_0 \mathbf{y} \, \mathrm{d}V_0$$

where the use of the definition of $\mathbf{F}_\mu = \nabla_0 \mathbf{y}$ has been used. Then applying Green's Lemma

$$\overline{\mathbf{F}} = \frac{1}{|\mathbb{V}_0|}\int_{\partial\mathbb{V}_0} [\mathbf{y} \otimes \mathbf{N}] \, \mathrm{d}A_0$$

Appendix C

Antiperiodicity of forces at the corners

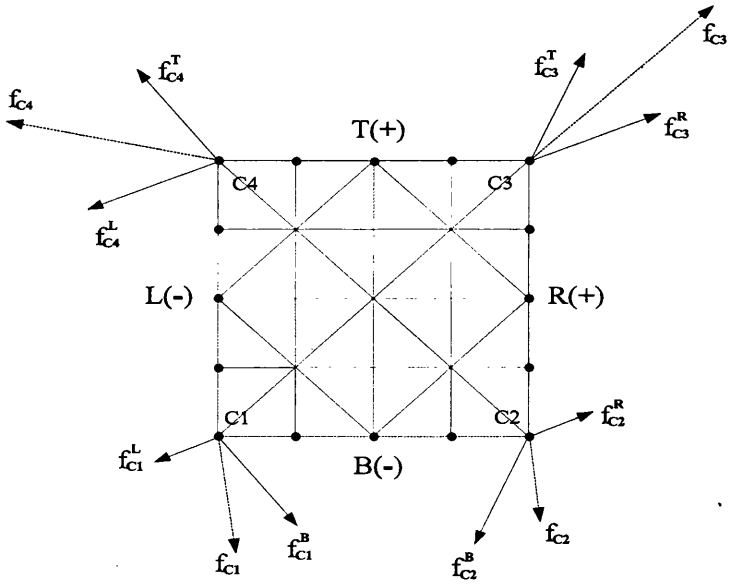

Figure C.1: Discrete forces on the corners

We want to prove how the following equation

$$\sum_{i=1}^{4} \mathbf{f}_{ci} = \mathbf{0} \tag{C.1}$$

which satisfies equilibrium, also satisfies antiperiodicity.

Considering Figure C.1 the forces at the corner nodes are represented as follows: The notation for the forces with superscript indicating:

B Bottom (−)

T Top (+)

L Left (−)

R Right (+)

The forces at the corners that represent the discretization of the traction coming from the continuum distribution that the cell received for the interaction with the next cells are:

- Corner 1 (C1) $\mathbf{f}_{c1}^{B}$ and $\mathbf{f}_{c1}^{L}$
- Corner 2 (C2) $\mathbf{f}_{c2}^{B}$ and $\mathbf{f}_{c2}^{R}$
- Corner 3 (C3) $\mathbf{f}_{c3}^{R}$ and $\mathbf{f}_{c3}^{T}$
- Corner 4 (C4) $\mathbf{f}_{c4}^{T}$ and $\mathbf{f}_{c4}^{L}$

Two forces per corner node (totally 8 at the discretised RVE). This forces must satisfy antiperiodicity, therefore, the following 4 equations for antiperiodicity on the corners are established as,

$$\begin{aligned} \mathbf{f}_{c1}^{B} &= -\mathbf{f}_{c4}^{T} \\ \mathbf{f}_{c2}^{B} &= -\mathbf{f}_{c3}^{T} \\ \mathbf{f}_{c1}^{L} &= -\mathbf{f}_{c2}^{R} \\ \mathbf{f}_{c4}^{L} &= -\mathbf{f}_{c3}^{R} \end{aligned} \tag{C.2}$$

Also the 2 forces per corner are joined in one each to operate in the FE analysis. The resultant on each corner is also described on the Figure C.1. Then the additional 4 relations are obtained as follows,

$$\begin{aligned} \mathbf{f}_{c1}^{B} + \mathbf{f}_{c1}^{L} &= \mathbf{f}_{c1} \\ \mathbf{f}_{c2}^{B} + \mathbf{f}_{c2}^{R} &= \mathbf{f}_{c2} \\ \mathbf{f}_{c3}^{R} + \mathbf{f}_{c3}^{T} &= \mathbf{f}_{c3} \\ \mathbf{f}_{c4}^{L} + \mathbf{f}_{c4}^{T} &= \mathbf{f}_{c4} \end{aligned} \tag{C.3}$$

We are going to reduce the system form by the equations (C.2) and (C.3) to have only one force per corner. As results of this elimination the equation,

$$\mathbf{f}_{c1} + \mathbf{f}_{c2} + \mathbf{f}_{c3} + \mathbf{f}_{c4} = \mathbf{0} \tag{C.4}$$

is obtained. This equation, described before at (C.1), is the additional condition to apply to the system in order to compute the tangent operator. As it has been proved the equation (C.1) (or (C.4)) agrees with the continuum antiperiodicty traction constraint given at (5.21). Moreover, the condition (C.4) makes the system to be in equilibrium.

Appendix D

Direct condensation of the d.o.f. corresponding of f_{C1}

We want to see how the equilibrium and antiperiodicity equation at the corners of discretised RVE

$$\mathbf{f}_{c1} + \mathbf{f}_{c2} + \mathbf{f}_{c3} + \mathbf{f}_{c4} = \mathbf{0} \tag{D.1}$$

has to be imposed to compute the overall tangent modulus (for small starains) and overall spatial tangent modulus (large strains).

The first two rows of $\mathbf{K}_{C1}$ and $\mathbf{K}_{C2}$ (corresponding to the 2 dofs of $\mathbf{f}_{c1}$) have to be removed and then recomputed by adding the other 6 rows (2 by 2) and them multiplied by -1. This process is visually described in Figure D.1.

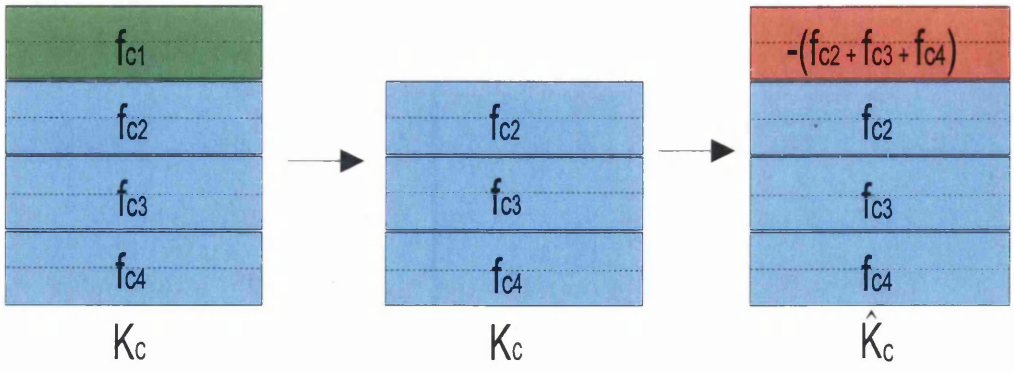

Figure D.1: Elimination and recalculation from $\mathbf{K}_{C1}$ and $\mathbf{K}_{C2}$ to $\hat{\mathbf{K}}_{C1}$ and $\hat{\mathbf{K}}_{C2}$